

1 **Global Methane Budget 2000-2020**

2 Marielle Saunois¹, Adrien Martinez¹, Benjamin Poulter², Zhen Zhang^{3,4}, Peter A. Raymond⁵, Pierre

3 Regnier⁶, Josep G. Canadell⁷, Robert B. Jackson⁸, Prabir K. Patra^{9,10}, Philippe Bousquet¹, Philippe

4 Ciais¹, Edward J. Dlugokencky¹¹, Xin Lan^{11,12}, George H. Allen¹³, David Bastviken¹⁴, David J.

5 Beerling¹⁵, Dmitry A. Belikov¹⁶, Donald R. Blake¹⁷, Simona Castaldi¹⁸, Monica Crippa¹⁹, Bridget R.

6 Deemer²¹, Fraser Dennison²², Giuseppe Etiope^{23,24}, Nicola Gedney²⁵, Lena Höglund-Isaksson²⁶,

7 Meredith A. Holgerson²⁷, Peter O. Hopcroft²⁸, Gustaf Hugelius²⁹, Akihiko Ito³⁰, Atul K. Jain³¹, Rajesh

8 Janardanan³², Matthew S. Johnson³³, Thomas Kleinen³⁴, Paul B. Krummel²², Ronny Lauerwald³⁵,

9 Tingting Li³⁶, Xiangyu Liu³⁷, Kyle C. McDonald³⁸, Joe R. Melton³⁹, Jens Mühle⁴⁰, Jurek Müller⁴¹,

10 Fabiola Murguía-Flores⁴², Yosuke Niwa^{32,43}, Sergio Noce⁴⁴, Shufen Pan⁴⁵, Robert J. Parker⁴⁶, Changhui

11 Peng^{47,48}, Michel Ramonet¹, William J. Riley⁴⁹, Gerard Rocher-Ros⁵⁰, Judith A. Rosentreter⁵¹, Motoki

12 Sasakawa³², Arjo Segers⁵², Steven J. Smith^{53,54}, Emily H. Stanley⁵⁵, Joël Thanwerdas^{56,*}, Hanqin Tian⁵⁷,

13 Aki Tsuruta⁵⁸, Francesco N. Tubiello⁵⁹, Thomas S. Weber⁶⁰, Guido R. van der Werf⁶¹, Douglas E. J.

14 Worthy⁶², Yi Xi¹, Yukio Yoshida³², Wenxin Zhang⁶³, Bo Zheng^{64,65}, Qing Zhu⁴⁹, Qian Zhu⁶⁶, and

15 Qianlai Zhuang³⁷

16

17 ¹Laboratoire des Sciences du Climat et de l'Environnement, LSCE-IPSL (CEA-CNRS-UVSQ), Université

18 Paris-Saclay 91191 Gif-sur-Yvette, France

19 ²NASA Goddard Space Flight Center, Biospheric Science Laboratory, Greenbelt, MD 20771, USA

20 ³National Tibetan Plateau Data Center (TPDC), State Key Laboratory of Tibetan Plateau Earth System,

21 Environment and Resource (TPESER), Institute of Tibetan Plateau Research, Chinese Academy of Sciences,

22 Beijing, 100101, China

23 ⁴Earth System Science Interdisciplinary Center, University of Maryland, College Park, MD 20740, USA

24 ⁵Yale School of the Environment, Yale University, New Haven, CT 06511, USA

25 ⁶Department Geoscience, Environment & Society (BGEOSYS), Université Libre de Bruxelles, 1050 Bruxelles,

26 Belgium

27 ⁷Global Carbon Project, CSIRO Environment, Canberra, ACT 2601, Australia

28 ⁸Department of Earth System Science, Woods Institute for the Environment, and Precourt Institute for Energy,

29 Stanford University, Stanford, CA 94305-2210, USA

30 ⁹Research Institute for Global Change, JAMSTEC, 3173-25 Showa-machi, Kanazawa, Yokohama, 236-

31 0001, Japan

32 ¹⁰Research Institute for Humanity and Nature, Kyoto 6038047, Japan

33 ¹¹NOAA Global Monitoring Laboratory, 325 Broadway, Boulder, CO 80305, USA

34 ¹²Cooperative Institute for Research in Environmental Sciences, University of Colorado Boulder, CO 80303,

35 USA

36 ¹³Department of Geosciences, Virginia Polytechnic Institute and State University, Blacksburg, VA, USA

37 ¹⁴Department of Thematic Studies – Environmental Change, Linköping University, 581 83 Linköping, Sweden

38 ¹⁵School of Biosciences, University of Sheffield, UK

39 ¹⁶Center for Environmental Remote Sensing, Chiba University, Chiba, 263-8522, Japan

40 ¹⁷Department of Chemistry, University of California Irvine, 570 Rowland Hall, Irvine, CA 92697, USA

41 ¹⁸Dipartimento di Scienze Ambientali, Biologiche e Farmaceutiche, Università degli Studi della Campania Luigi

Mis en forme : Français

Mis en forme : Français

Mis en forme : Français

42 Vanvitelli, via Vivaldi 43, 81100 Caserta, Italy
43 ¹⁹European Commission, Joint Research Centre (JRC), Ispra, Italy
44 ²¹U.S. Geological Survey, Southwest Biological Science Center, Flagstaff, AZ, USA
45 ²²CSIRO Environment, Aspendale, Victoria 3195, Australia
46 ²³Istituto Nazionale di Geofisica e Vulcanologia, Sezione Roma 2, via V. Murata 605 00143 Rome, Italy
47 ²⁴Faculty of Environmental Science and Engineering, Babes Bolyai University, Cluj-Napoca, Romania
48 ²⁵Met Office Hadley Centre, Joint Centre for Hydrometeorological Research, Maclean Building, Wallingford
49 OX10 8BB, UK
50 ²⁶Pollution Management Group (PM), International Institute for Applied Systems Analysis (IIASA), 2361
51 Laxenburg, Austria
52 ²⁷Department of Ecology & Evolutionary Biology, Cornell University, Ithaca, NY, USA
53 ²⁸School of Geography, Earth & Environmental Sciences, University of Birmingham, UK
54 ²⁹Department of Physical Geography and Bolin Centre for Climate Research, Stockholm University, 106 91
55 Stockholm, Sweden
56 ³⁰Graduate School of Agricultural and Life Sciences, The University of Tokyo, Tokyo, Japan
57 ³¹Department of Atmospheric Sciences, University of Illinois, Urbana, IL 61821, USA
58 ³²Earth System Division, National Institute for Environmental Studies (NIES), Onogawa 16-2, Tsukuba, Ibaraki
59 305-8506, Japan
60 ³³Earth Science Division, NASA Ames Research Center, Moffett Field, CA USA.
61 ³⁴Max Planck Institute for Meteorology, Bundesstraße 53, 20146 Hamburg, Germany
62 ³⁵Université Paris-Saclay, INRAE, AgroParisTech, UMR EcoSys, Palaiseau, France
63 ³⁶LAPC, Institute of Atmospheric Physics, Chinese Academy of Sciences, Beijing, 100029, China
64 ³⁷Department of Earth, Atmospheric, and Planetary Sciences, Purdue University, West Lafayette, IN, USA
65 ³⁸Department of Earth and Atmospheric Sciences, City College of New York, City University of New York, NY,
66 USA
67 ³⁹Climate Research Division, Environment and Climate Change Canada, Victoria, BC, V8W 2Y2, Canada
68 ⁴⁰Scripps Institution of Oceanography, University of California San Diego, La Jolla, CA, 92037, USA
69 ⁴¹Climate and Environmental Physics, Physics Institute and Oeschger Centre for Climate Change Research,
70 University of Bern, Sidlerstr. 5, 3012 Bern, Switzerland
71 ⁴²Instituto de Investigaciones en Ecología y Sustentabilidad, Universidad Nacional Autónoma de México,
72 Morelia, Mexico
73 ⁴³Department of Climate and Geochemistry Research, Meteorological Research Institute (MRI), Nagamine 1-1, Tsukuba,
74 Ibaraki 305-0052, Japan
75 ⁴⁴CMCC Foundation - Euro-Mediterranean Center on Climate Change, Italy
76 ⁴⁵Department of Engineering and Environmental Studies Program, Boston College, Chestnut Hill, MA 02467,
77 USA
78 ⁴⁶National Centre for Earth Observation, School of Physics and Astronomy, University of Leicester, Leicester,
79 LE1 7RH, UK
80 ⁴⁷Department of Biology Sciences, Institute of Environment Science, University of Quebec at Montreal,
81 Montreal, QC H3C 3P8, Canada
82 ⁴⁸School of Geographic Sciences, Hunan Normal University, Changsha 410081, China
83 ⁴⁹Climate and Ecosystem Sciences Division, Lawrence Berkeley National Lab, 1 Cyclotron Road, Berkeley, CA
84 94720, US
85 ⁵⁰Department of Forest Ecology and Management, Swedish University of Agricultural Sciences, 90183 Umeå,
86 Sweden
87 ⁵Faculty of Science and Engineering, Southern Cross University, Lismore, NSW 2480, Australia
88 ⁵²TNO, dep. of Climate Air & Sustainability, P.O. Box 80015, NL-3508-TA, Utrecht, The Netherlands
89 ⁵³Joint Global Change Research Institute, Pacific Northwest National Lab, College Park, MD, USA
90

Supprimé: ²⁰Unisystems S.A., Milan, Italy

Mis en forme : Français

92 ⁵⁴Center for Global Sustainability, University of Maryland, College Park, MD, USA
93 ⁵⁵Center for Limnology, University of Wisconsin-Madison, Madison, WI, USA
94 ⁵⁶Empa, Swiss Federal Laboratories for Materials Science and Technology, Dübendorf, Switzerland
95 ⁵⁷Center for Earth System Science and Global Sustainability, Schiller Institute for Integrated Science and
96 Society, Department of Earth and Environmental Sciences, Boston College, Chestnut Hill, MA 02467, USA
97 ⁵⁸Finnish Meteorological Institute, P.O. Box 503, FI-00101, Helsinki, Finland
98 ⁵⁹Statistics Division, Food and Agriculture Organization of the United Nations (FAO), Viale delle
99 Terme di Caracalla, Rome 00153, Italy
100 ⁶⁰Department of Earth and Environmental Sciences, University of Rochester, Rochester, NY 14627,
101 USA
102 ⁶¹Meteorology and Air Quality Group, Wageningen University and Research, Wageningen, the Netherlands
103 ⁶²Environment and Climate Change Canada, 4905, Dufferin Street, Toronto, Canada
104 ⁶³Department of Physical Geography and Ecosystem Science, Lund University, Sölvegatan 12, 223 62, Lund, Sweden
105 ⁶⁴Institute of Environment and Ecology, Tsinghua Shenzhen International Graduate School, Tsinghua University,
106 Shenzhen 518055, China
107 ⁶⁵State Environmental Protection Key Laboratory of Sources and Control of Air Pollution Complex, Beijing 100084,
108 China
109 ⁶⁶College of Geography and Remote Sensing, Hohai University, Nanjing, 210098, China

110
111 *formerly at LSCE ¹
112

113 *Correspondence to:* Marielle Sauniois (marielle.sauniois@lsce.ipsl.fr)

114 **Abstract.** Understanding and quantifying the global methane (CH₄) budget is important for assessing realistic pathways to
115 mitigate climate change. CH₄ is the second most important human-influenced greenhouse gas in terms of climate forcing
116 after carbon dioxide (CO₂) and both emissions and atmospheric concentrations of CH₄ continue to increase since 2007 after
117 a temporary pause. The relative importance of CH₄ emissions compared to those of CO₂ for temperature change is related
118 to its shorter atmospheric lifetime, stronger radiative effect, and acceleration in atmospheric growth rate over the past decade,
119 the causes of which are still debated. Two major challenges in quantifying the factors responsible for the observed
120 atmospheric growth rate arise from diverse, geographically overlapping CH₄ sources and from the uncertain magnitude and
121 temporal change in the destruction of CH₄ by short-lived and highly variable hydroxyl radicals (OH). To address these
122 challenges, we have established a consortium of multi-disciplinary scientists under the umbrella of the Global Carbon Project
123 to improve, synthesise and update the global CH₄ budget regularly and to stimulate new research on the methane cycle.
124 Following Sauniois et al. (2016, 2020), we present here the third version of the living review paper dedicated to the decadal
125 CH₄ budget, integrating results of top-down CH₄ emission estimates (based on in-situ and greenhouse gas observing satellite
126 (GOSAT) atmospheric observations and an ensemble of atmospheric inverse-model results) and bottom-up estimates (based
127 on process-based models for estimating land-surface emissions and atmospheric chemistry, inventories of anthropogenic
128 emissions, and data-driven extrapolations). We present a budget for the most recent 2010-2019 calendar decade (the latest
129 period for which full datasets are available), for the previous decade of 2000-2009 and for the year 2020.

Supprimé: Emissions and atmospheric concentrations of CH₄ continue to increase, maintaining

Supprimé:

Supprimé: CH₄ as the second most important human-influenced greenhouse gas in terms of climate forcing after carbon dioxide (CO₂).

Supprimé: of

Supprimé: reducing uncertainties in the factors explaining the well-

139 The revision of the bottom-up budget in this 2024 edition benefits from important progress in estimating inland freshwater
140 emissions, with better accounting of emissions from lakes and ponds, reservoirs, and streams and rivers. This budget also
141 reduces double accounting across freshwater and wetland emissions and, for the first time, includes an estimate of the
142 potential double accounting that may exist (average of 23 Tg CH₄ yr⁻¹). Bottom-up approaches show that the combined
143 wetland and inland freshwater emissions average 248 [159-369] Tg CH₄ yr⁻¹ for the 2010-2019 decade. Natural fluxes are
144 perturbed by human activities through climate, eutrophication, and land use. In this budget, we also estimate, for the first
145 time, this anthropogenic component contributing to wetland and inland freshwater emissions. Newly available gridded
146 products also allowed us to derive an almost complete latitudinal and regional budget based on bottom-up approaches.
147 For the 2010-2019 decade, global CH₄ emissions are estimated by atmospheric inversions (top-down) to be 575 Tg CH₄ yr⁻¹
148 (range 553-586, corresponding to the minimum and maximum estimates of the model ensemble). Of this amount, 369 Tg
149 CH₄ yr⁻¹ or ~65% are attributed to direct anthropogenic sources in the fossil, agriculture and waste and anthropogenic
150 biomass burning (range 350-391 Tg CH₄ yr⁻¹ or 63-68%). For the 2000-2009 period, the atmospheric inversions give a
151 slightly lower total emission than for 2010-2019, by 32 Tg CH₄ yr⁻¹ (range 9-40). The 2020 emission rate is the highest of
152 the period and reaches 608 Tg CH₄ yr⁻¹ (range 581-627), which is 12% higher than the average emissions in the 2000s. Since
153 2012, global direct anthropogenic CH₄ emission trends have been tracking scenarios that assume no or minimal climate
154 mitigation policies proposed by the Intergovernmental Panel on Climate Change (shared socio-economic pathways SSP5
155 and SSP3). Bottom-up methods suggest 16% (94 Tg CH₄ yr⁻¹) larger global emissions (669 Tg CH₄ yr⁻¹, range 512-849)
156 than top-down inversion methods for the 2010-2019 period. The discrepancy between the bottom-up and the top-down
157 budgets has been greatly reduced compared to the previous differences (167 and 156 Tg CH₄ yr⁻¹ in Saunio et al. (2016,
158 2020), respectively), and for the first time uncertainty in bottom-up and top-down budgets overlap. Although differences
159 have been reduced between inversions and bottom-up, the most important source of uncertainty in the global CH₄ budget is
160 still attributable to natural emissions, especially those from wetlands and inland freshwaters.
161 The tropospheric loss of methane, as the main contributor to methane lifetime, has been estimated at 563 [510-
162 663] Tg CH₄ yr⁻¹ based on chemistry climate models. These values are slightly larger than for 2000-2009 due to the impact
163 of the rise in atmospheric methane, and remaining large uncertainty (~25%). The total sink of CH₄ is estimated at 633
164 [507-796] Tg CH₄ yr⁻¹ by the bottom-up approaches and at 554 [550-567] Tg CH₄ yr⁻¹ by top-down approaches. Though
165 most of the top-down models use the same OH distribution, which introduces less uncertainty to the global budget than is
166 likely justified.
167 For 2010-2019, agriculture and waste contributed an estimated 228 [213-242] Tg CH₄ yr⁻¹ in the top-down budget and 211
168 [195-231] Tg CH₄ yr⁻¹ in the bottom-up budget. Fossil fuel emissions contributed 115 [100-124] Tg CH₄ yr⁻¹ in the top-
169 down budget and 120 [117-125] Tg CH₄ yr⁻¹ in the bottom-up budget. Biomass and biofuel burning contributed 27 [26-
170 27] Tg CH₄ yr⁻¹ in the top-down budget and 28 [21-39] Tg CH₄ yr⁻¹ in the bottom-up budget.

Supprimé: still

Supprimé: s

Supprimé:

Supprimé: The latitudinal distribution from atmospheric inversion-based emissions indicates a predominance of tropical and southern hemisphere emissions (~65% of the global budget, <30°N) compared to mid (30°N-60°N, ~30% of emissions) and high-northern latitudes (60°N-90°N, ~4% of global emissions). This latitudinal distribution is similar in the bottom-up budget though the bottom-up budget estimates slightly larger contributions for the mid and high-northern latitudes, and slightly smaller contributions from the tropics and southern hemisphere than the inversions.

Supprimé: still present

Supprimé: [213-242]

Supprimé: [195-231]

Supprimé: [100-124]

Supprimé: [117-125]

Supprimé: [26-27]

Supprimé: [21-39]

Supprimé:

191 We identify five major priorities for improving the CH₄ budget: i) producing a global, high-resolution map of water-saturated
192 soils and inundated areas emitting CH₄ based on a robust classification of different types of emitting ecosystems; ii) further
193 development of process-based models for inland-water emissions; iii) intensification of CH₄ observations at local (e.g.,
194 FLUXNET-CH₄ measurements, urban-scale monitoring, satellite imagery with pointing capabilities) to regional scales
195 (surface networks and global remote sensing measurements from satellites) to constrain both bottom-up models and
196 atmospheric inversions; iv) improvements of transport models and the representation of photochemical sinks in top-down
197 inversions, and v) integration of 3D variational inversion systems using isotopic and/or co-emitted species such as ethane
198 as well as information in the bottom-up inventories on anthropogenic super-emitters detected by remote sensing (mainly oil
199 and gas sector but also coal, agriculture and landfills) to improve source partitioning.
200 The data presented here can be downloaded from <https://doi.org/10.18160/GKQ9-2RHT> (Martinez et al., 2024).

201 **1 Introduction**

202 The average surface dry air mole fraction of atmospheric methane (CH₄) reached 1912 ppb in 2022 (Fig. 1; Lan et
203 al., 2024), 2.6 times greater than its estimated pre-industrial value in 1750. This increase is attributable in large part to
204 increased anthropogenic emissions arising primarily from agriculture (e.g., livestock production, rice cultivation, biomass
205 burning), fossil fuel production and use, waste disposal, and alterations to natural CH₄ fluxes due to increased atmospheric
206 CO₂ concentrations, land use (Woodward et al., 2010, Fluet-Chouinard et al., 2023) and climate change (Ciais et al., 2013;
207 Canadell et al., 2021). **An equal mass of CH₄ emissions have a stronger impact on climate than carbon dioxide (CO₂), which**
208 **is reflected by its global warming potential (GWP) relative to CO₂ on a given time horizon.** For a 100-yr time horizon the
209 GWP of CH₄ **emitted by fossil sources is 29.8 (GWP of CH₄ emitted by microbial sources is 27),** whereas the values reach
210 82.5 over a 20-year horizon for CH₄ **emitted by fossil sources** and 79.7 for CH₄ **emitted by microbial sources** (Forster et al.,
211 2021). Although global anthropogenic emissions of CH₄ are estimated at around 359 Tg CH₄ yr⁻¹ (Saunio et al., 2020),
212 representing around 2.5% of the global CO₂ anthropogenic emissions when converted to units of carbon mass flux for the
213 recent decade, the emissions-based effective radiative forcing of CH₄ concentrations has contributed ~31% (1.19 W m⁻²) to
214 the additional radiative forcing from anthropogenic emissions of greenhouse gases and their precursors (3.84 W m⁻²) over
215 the industrial era (1750-2019) (Forster et al., 2021). Changes in other chemical compounds such as nitrogen oxides (NO_x)
216 or carbon monoxide (CO) also influence atmospheric CH₄ through changes to its atmospheric lifetime. Emissions of CH₄
217 contribute to the production of ozone, stratospheric water vapour, and CO₂, and most importantly affect its own lifetime
218 (Myhre et al., 2013; Shindell et al., 2012). CH₄ has a short lifetime in the atmosphere (about 9 years for the year 2010,
219 Prather et al., 2012; Szopa et al., 2021). Hence a stabilisation or reduction of CH₄ emissions leads to the stabilisation or
220 reduction of its atmospheric concentration (assuming no change in the chemical oxidants), and therefore its radiative forcing,
221 in only a few decades. While reducing CO₂ emissions is necessary to stabilise long-term warming, reducing CH₄ emissions

Supprimé:

Supprimé:

Supprimé:

Supprimé: ,

Supprimé: Atmospheric

Supprimé: is a stronger absorber of Earth's emitted thermal infrared radiation

Supprimé: as assessed

Mis en forme : Non Exposant/ Indice

Supprimé: and without considering climate feedbacks

Supprimé: -fossil

Supprimé: CH₄-non fossil

Mis en forme : Indice

Supprimé: -fossil

Supprimé: -non fossil

235 is recognized as an effective option to limit climate warming in the near-term (Shindell et al., 2012; Jackson et al., 2020;
236 Ocko et al., 2021; UNEP, 2021), because of its shorter lifetime compared to CO₂.

237 The momentum around the potential of CH₄ to limit near-term warming has led to the launch of the Global Methane
238 Pledge at the November 2021 Conference of the Parties (COP 26). Signed by 158 countries (update on October 2024), this
239 collective effort aims at reducing global CH₄ anthropogenic emissions at least 30 percent from 2020 levels by 2030 (Global
240 Methane Pledge, 2023). Given that global baseline CH₄ emissions are expected to grow through 2030 (by an additional 20-
241 50 Million tons (Mt) of CH₄, UNEP 2022), the CH₄ emission reductions currently needed to reach the Global Methane
242 Pledge objective (UNEP, 2022) correspond to 36% of the projected baseline emissions in 2030 (ie. if no further emission
243 reductions were implemented). This implies that large reductions of CH₄ emissions are needed to meet the Global Methane
244 Pledge that is consistent also with the 1.5-2°C target of the Paris Agreement (UNEP, 2022). Moreover, because CH₄ is a
245 precursor of important air pollutants such as ozone, CH₄ emissions reductions are required by two international conventions:
246 the United Nations Framework Convention on Climate Change (UNFCCC) and the Convention on Long Range Transport
247 of Air Pollution (CLRTAP), making this global CH₄ budget assessment all the more critical.

248 Changes in the magnitude and temporal variation (annual to interannual) of CH₄ sources and sinks over the past
249 decades are characterised by large uncertainties (e.g., Kirschke et al., 2013; Sauniois et al., 2017; Turner et al., 2019). Also,
250 the decadal budget suggests relative uncertainties (hereafter reported as min-max ranges) of 20-35% for inventories of
251 anthropogenic emissions in specific sectors (e.g., agriculture, waste, fossil fuels (Tibrewal et al., 2024)), 50% for biomass
252 burning and natural wetland emissions, and up to 100% for other natural sources (e.g., inland waters, geological sources).
253 The uncertainty in the chemical loss of CH₄ by OH, the predominant sink of atmospheric CH₄, has been estimated using
254 Prather et al. (2012) and Rigby et al. (2017). The former study estimated this uncertainty at ~10% from the uncertainty in
255 the reaction rate between CH₄ and OH, and the latter study was based on methyl-chloroform measurements. Bottom-up
256 approaches (chemistry transport models) estimate the uncertainty of the chemical loss by OH at around 15-20% (Sauniois et
257 al., 2016, 2020). This uncertainty on the OH induced loss translates, in the top-down methods, into the minimum relative
258 uncertainty associated with global CH₄ emissions, as other CH₄ sinks (atomic oxygen and chlorine oxidations, soil uptake)
259 are much smaller and the atmospheric growth rate is well-defined (Dlugokencky et al., 2009). Globally, the contribution of
260 natural CH₄ emissions to total emissions can be quantified by combining lifetime estimates with reconstructed pre-industrial
261 atmospheric CH₄ concentrations from ice cores (assuming natural emissions have not been perturbed during the
262 anthropocene) (e.g., Ehhalt et al., 2001). Regionally or nationally, uncertainties in emissions may reach 40-60% (e.g., for
263 South America, Africa, China, and India; see Sauniois et al., 2016). Another difficulty of the CH₄ budget lies in the necessity
264 to also match the isotopic signal and in particular reflect the decreasing methane isotopic signal ¹³C (Nisbet et al., 2016;
265 2019). The previous budgets were tested against the isotopic observations (Sauniois et al., 2017) and follow an exhaustive
266 assessment (Zhang et al., 2021b). To date only a couple of atmospheric inverse systems are able to assimilate both CH₄
267 mixing ratios and stable isotopic signal to retrieve fluxes at the global scale (Thanwerdas et al., 2024; Basu et al., 2022), but

Supprimé: 150

Supprimé: -

Supprimé: s

Supprimé: or

Supprimé: using

Supprimé: ,

Supprimé: balance

Supprimé: 2

276 these systems still need improvements in terms of configuration set-up and computing time resources, in addition to
277 characterisation of source signatures and chemical kinetic effect (Chandra et al., 2024). We hope to be able to report isotopic
278 constrained budgets in the coming years, or at least test the budget against the isotopic balance.

Supprimé: s

Supprimé: .

279 To monitor emission reductions, for example to help conduct the Paris Agreement's stocktake, sustained and long-
280 term monitoring of anthropogenic emissions per sector is needed in particular for hotspots of emissions that may be missed
281 in inventories (Bergamaschi et al., 2018a; Pacala, 2010; Lauvaux et al., 2022). At the same time, reducing uncertainties in
282 all individual CH₄ sources, and thus in the overall CH₄ budget remains challenging for at least four reasons. First, CH₄ is
283 emitted by multiple processes, including natural and anthropogenic sources, point and diffuse sources, and sources
284 associated with at least three different production origins (i.e., microbial, thermogenic, and pyrogenic). These multiple
285 sources and processes require the integration of data from diverse scientific communities and across multiple temporal and
286 spatial scales. The production of accurate bottom-up estimates is complicated by the fact that anthropogenic emissions result
287 from leakage from fossil fuel production with large differences between countries depending on technologies and practices,
288 the fact that many large leak events are sporadic, and the location of many emissions hotspots is not well known, and from
289 uncertain emission factors used to summarise complex microbial processes in the agriculture and waste sectors. For the
290 latter, examples include difficulties in upscaling methane emissions from livestock without considering the variety of animal
291 weight, diet and environment, and difficulties in assessing emissions from landfills depending on waste type and waste
292 management technology. Second, atmospheric CH₄ is removed mainly by chemical reactions in the atmosphere involving
293 OH and other radicals that have very short lifetimes (typically ~1s). Due to the short lifetime of OH, the spatial and temporal
294 distributions of OH are highly variable. While OH can be measured locally, calculating global CH₄ loss through OH
295 measurements requires high-resolution global OH measurements (typically half an hour to integrate cloud cover, and 1 km
296 spatially to consider OH high reactivity and heterogeneity) which is impossible from direct OH observations. As a result,
297 OH can only be calculated through large scale atmospheric chemistry modelling. Those simulated OH concentrations from
298 transport-chemistry models prescribed with emissions of precursor species affecting OH still show uncertain spatio-temporal
299 distribution from regional to global scales (Zhao et al., 2019). Third, only the net CH₄ budget (sources minus sinks) is well
300 constrained by precise observations of atmospheric growth rates (Dlugokencky et al., 2009), leaving the sum of sources and
301 the sum of sinks uncertain. One distinctive feature of CH₄ sources compared to CO₂ fluxes is that the oceanic contribution
302 to the global CH₄ budget is small (~1-3%), making CH₄ source estimation predominantly a terrestrial endeavour (USEPA,
303 2010b). Finally, we lack comprehensive observations to constrain 1) the areal extent of different types of wetlands and
304 inland freshwater (Kleinen et al., 2012, 2020, 2021, 2023; Stocker et al., 2014; Zhang et al., 2021), 2) models of wetland
305 and inland freshwater emission rates (Melton et al., 2013; Poulter et al., 2017; Wania et al., 2013; Bastviken et al., 2011;
306 Wik et al., 2016a; Rosentreter et al., 2021; Bansal et al., 2023; Lauerwald et al., 2023a; Stanley et al. 2023), 3) inventories
307 of anthropogenic emissions (Höglund-Isaksson et al., 2020; Crippa et al., 2023; USEPA, 2019), and 4) atmospheric
308 inversions, which aim to estimate CH₄ emissions from global to regional scales (Houweling et al., 2017; Jacob et al., 2022).

311 The global CH₄ budget inferred from atmospheric observations by atmospheric inversions relies on regional
312 constraints from atmospheric sampling networks, which are relatively dense for northern mid-latitudes, with various high-
313 precision and high-accuracy surface stations, but are sparser at tropical latitudes and in the Southern Hemisphere
314 (Dlugokencky et al., 2011). Recently, the density of atmospheric observations has increased in the tropics due to satellite-
315 based platforms that provide column-average CH₄ mixing ratios. Despite continuous improvements in the precision and
316 accuracy of space-based measurements (e.g., Buchwitz et al., 2016), systematic errors greater than several ppb on total
317 column observations can still limit the usage of such data to constrain surface emissions (e.g., Jacob et al., 2022). The
318 development of robust bias corrections on existing data can help overcome this issue (e.g., Inoue et al., 2016, [Lorente et al.,](#)
319 [2023; Balasu et al., 2023](#)) and satellite data are now widely used in atmospheric inversions where they provide more global
320 information on the distribution of fluxes and highly complement the surface networks (e.g., Lu et al., 2021).

321 In this context, the Global Carbon Project (GCP) seeks to develop a complete picture of the carbon cycle by
322 establishing common, consistent scientific knowledge to support policy development and actions to mitigate greenhouse gas
323 emissions to the atmosphere (www.globalcarbonproject.org). The objective of this paper is to analyse and synthesise the
324 current knowledge of the global CH₄ budget, by gathering results of observations and models to better understand and
325 quantify the main robust features of this budget, its remaining uncertainties, and to make recommendations for improvement.
326 We combine results from a large ensemble of bottom-up approaches (e.g., process-based models for natural wetlands, data-
327 driven approaches for other natural sources, inventories of anthropogenic emissions and biomass burning, and atmospheric
328 chemistry models), and top-down approaches (including CH₄ atmospheric observing networks, atmospheric inversions
329 inferring emissions and sinks from the assimilation of atmospheric observations into models of atmospheric transport and
330 chemistry). The focus of this work is to update the previous assessment made for the period 2000-2017 (Saunois et al., 2020)
331 to the more recent 2000-2020 period. More in-depth analyses of trends and year-to-year changes are left to future
332 publications. Our current paper is a living review, published at about four-year intervals, to provide an update and new
333 synthesis of available observational, statistical, and model data for the overall CH₄ budget and its individual components.

334 Kirschke et al. (2013) was the first CH₄ budget synthesis followed by Saunois et al. (2016) and Saunois et al.
335 (2020), with companion papers by Stavert et al. (2021) on regional CH₄ budgets and Jackson et al. (2020) focusing on the
336 last year of the budget (2017). Saunois et al. (2020) covered 2000-2017 and reported CH₄ emissions and sinks for three time
337 periods: 1) the latest calendar decade at that time (2000-2009), 2) data for the latest available decade (2008-2017), and 3)
338 the latest available year (2017) at the time. Here, the Global Methane Budget (GMB) covers 2000-2020 split into the 2000-
339 2009 decade, the 2010-2019 decade (where data are available), the year 2020 affected by COVID induced changes in human
340 activity, and briefly for 2021-2023 as per data availability (Section 6). The CH₄ budget is presented at global, latitudinal,
341 and regional scales and data can be downloaded from <https://doi.org/10.18160/GKQ9-2RHT> (Martinez et al., 2024). A
342 global, regional and sectoral assessment of methane emission changes over the last two decades is discussed in Jackson et
343 al. (2024) based on the data of Martinez et al. (2024).

Supprimé: si

Supprimé:

346 Six sections follow this introduction. Section 2 presents the methodology used in the budget: units, definitions of
347 source categories, regions, data analysis; and discusses the delay between the period of study of the budget and the release
348 date. Section 3 presents the current knowledge about CH₄ sources and sinks based on the ensemble of bottom-up approaches
349 reported here (models, inventories, data-driven approaches). Section 4 reports atmospheric observations and top-down
350 atmospheric inversions gathered for this paper. Section 5, based on Sections 3 and 4, provides the updated analysis of the
351 global CH₄ budget by comparing bottom-up and top-down estimates and highlighting differences. Section 6 discusses the
352 recent changes in atmospheric CH₄ in relation with changes in CH₄ sources and sinks. Finally, Section 7 discusses future
353 developments, missing components, and the most critical remaining uncertainties based on our update to the global CH₄
354 budget. [For easier reading, the list of Contents of this manuscript is presented in the first section of the Supplementary](#)
355 [Material.](#)

356 2 Methodology

357 2.1 Units used

358 Unless specified, fluxes are expressed in teragrams of CH₄ per year ($1 \text{ Tg CH}_4 \text{ yr}^{-1} = 10^{12} \text{ g CH}_4 \text{ yr}^{-1}$), while atmospheric
359 mixing ratios are expressed as dry air mole fractions, in parts per billion (ppb), with atmospheric CH₄ annual increases,
360 G_{ATM} , expressed in ppb yr⁻¹. In the tables, we present mean values and ranges for the two decades 2000-2009 and 2010-
361 2019, together with results for the most recent available year (2020). Results obtained from previous syntheses (i.e., Saunois
362 et al., 2020 and Saunois et al., 2016) are also given for the decade 2000-2009. Following Saunois et al. (2016) and
363 considering that the number of studies is often relatively small for many individual source and sink estimates, uncertainties
364 are reported as minimum and maximum values of the available studies, given in brackets. In doing so, we acknowledge that
365 we do not consider the uncertainty of the individual estimates, and we express uncertainty as the range of available mean
366 estimates, i.e., differences across measurements/methodologies considered. These minimum and maximum values are those
367 presented in Section 2.5 and exclude identified outliers.

368 The CH₄ emission estimates are provided with up to three significant digits, for consistency across all budget flux
369 components and to ensure the accuracy of aggregated fluxes. Nonetheless, given the values of the uncertainties in the CH₄
370 budget, we encourage the reader to consider not more than two digits as significant for the global total budget.

371 2.2 Period of the budget and availability of data

372 The bottom-up estimates rely on global anthropogenic emission inventories, an ensemble of process-based models for
373 wetlands emissions, and published estimates in the literature for other natural sources. The global gridded anthropogenic
374 inventories (see Section (3.1.1)) are updated irregularly, generally every 3 to 5 years. The last reported years of available
375 inventories were 2018 or 2019 when we started the top-down modelling activity. In order to cover the period 2000-2020, it

376 was necessary to extrapolate the anthropogenic inventory EDGARv6 (Crippa et al., 2021) to 2020 to use it as prior
377 information for the anthropogenic emissions in the atmospheric inversion systems as explained in the supplementary
378 material. Though EDGARv7 (EDGAR, 2022; Crippa et al., 2023) spanning until 2021 was then released, and was used for
379 the bottom-up budget. EDGARv8 (EDGAR, 2023; Crippa et al., 2023) spanning until 2022 and released in 2024, was used
380 in Section 6 to discuss the post 2020 methane budget. The land surface (wetland) models were run over the full period 2000-
381 2020 using dynamical wetland areas, derived by remote sensing data or other models of flooded area variability (Sect. 3.2.1).
382 The atmospheric inversions run until mid-2021, but the last year of reported inversion results is 2020, which represents a
383 three-year lag with the present. This is due to the long time period it takes to acquire atmospheric in-situ data and integrate
384 models. Even though satellite observations are processed operationally and are generally available with a latency of days to
385 weeks, by contrast surface observations can lag from months to years because of the time for flask analyses and data quality
386 checks in (mostly) non-operational chains. In addition, the final six months of inversions must be generally ignored because
387 the estimated fluxes are not constrained by as many observations as the previous periods. Lastly, this budget presents an
388 extended synthesis of the most recent development regarding inland water emissions (Sect. 3.2.2) and corrections associated
389 with double counting with wetlands.

390 2.3 Definition of regions

391 Geographically, emissions are reported globally and for three latitudinal bands (90°S-30°N, 30-60°N, 60-90°N, only for
392 gridded products). When extrapolating emission estimates forward in time (see Sect. 3.1.1), and for the regional budget
393 presented by Stavert et al. (2021), a set of 19 regions (oceans and 18 continental regions, see supplementary Fig. S3) were
394 used. As anthropogenic emissions are often reported by country, we define these regions based on a country list (Table S1).
395 This approach was compatible with all top-down and bottom-up approaches considered. The number of regions was chosen
396 to be close to the widely used TransCom inter-comparison map (Gurney et al., 2004) but with subdivisions to separate the
397 contribution from important countries or regions for the CH₄ cycle (China, South Asia, Tropical America, Tropical Africa,
398 United States of America, and Russia). The resulting region definition is the same as that used for the Global Carbon Project
399 (GCP) N₂O budget (Tian et al., 2020). Compared to Sauniois et al. (2020), the Oceania region has been replaced by
400 Australasia including only Australia and New Zealand. Other territories formerly in Oceania were included in Southeast
401 Asia.

402 2.4 Definition of source and sink categories

403 CH₄ is emitted by different processes (i.e., biogenic, thermogenic, or pyrogenic) and can be of anthropogenic or natural
404 origin. Biogenic CH₄ is the final product of the decomposition of organic matter by methanogenic *Archaea* in anaerobic
405 environments, such as water-saturated soils, swamps, rice paddies, marine and freshwater sediments, landfills, sewage and
406 wastewater treatment facilities, or inside animal digestive systems. Thermogenic methane is formed on geological time

Supprimé:

scales by the breakdown of buried organic matter due to heat and pressure deep in the Earth's crust. Thermogenic CH₄ reaches the atmosphere through marine and land geological gas seeps. These CH₄ emissions are increased by human activities, for instance, the exploitation and distribution of fossil fuels. Pyrogenic CH₄ is produced by the incomplete combustion of biomass and other organic materials. Peat fires, biomass burning in deforested or degraded areas, wildfires, and biofuel burning are the largest sources of pyrogenic CH₄. CH₄ hydrates, ice-like cages of frozen CH₄ found in continental shelves and slopes and below sub-sea and land permafrost, can be of either biogenic or thermogenic origin. Each of these three process categories has both anthropogenic and natural components.

In the following, we present the different CH₄ sources depending on their anthropogenic or natural origin, which is relevant to climate policy. Compared to the previous budgets, marginal changes have been made regarding source categories (naming and grouping), to reflect the improved estimates for inland water sources and their indirect anthropogenic component. In the previous Global Methane Budgets (Saunio et al., 2016, 2020), natural and anthropogenic emissions were split in a way that did not correspond exactly to the definition used by the UNFCCC following the IPCC guidelines (IPCC, 2006), where, for pragmatic reasons, all emissions from managed land are typically reported as anthropogenic. For instance, we considered all wetlands as natural emissions, despite some wetlands being on managed land and their emissions being partly reported as anthropogenic in UNFCCC national communications. Separating natural from anthropogenic sources could be quite challenging, especially over regions where sources overlap, as over heavily human-dominated floodplain deltas for example. The human induced perturbation of climate, atmospheric CO₂, and nitrogen and sulfur deposition may also cause changes in wetland sources we classified as natural. Following our previous definition, emissions from wetlands, inland freshwaters, thawing permafrost, or geological leaks are accountable for "natural" emissions, even though we acknowledge that climate change and other human perturbations (e.g., eutrophication) may cause changes in those emissions. CH₄ emissions from reservoirs were also considered as natural even though reservoirs are human-made. Indeed, since the 2019 refinement to the IPCC guidelines (IPCC, 2019) emissions from reservoirs and other flooded lands are considered to be anthropogenic by the UNFCCC and should be reported as such. However, these estimates are not provided by inventories and not systematically reported by all countries (especially non Annex-I countries). In this budget we rename "natural sources" to "natural and indirect anthropogenic sources" to acknowledge that CH₄ emissions from reservoirs, as well as from water bodies that were perturbed by agricultural activities (drainage, eutrophication, land use change) are indirect anthropogenic emissions. As a result, here, "natural and indirect anthropogenic sources" refer to "emissions that do not directly originate from fossil, agricultural, waste, and biomass burning sources" even if they are perturbed by anthropogenic activities and climate change. Natural and indirect anthropogenic emissions are split between "Wetlands and Inland Freshwaters" and "Other natural" emissions (e.g., wild animals, termites, land geological sources, oceanic geological and biogenic sources, and terrestrial permafrost). "Anthropogenic direct sources" are caused by direct human activities since pre-industrial/pre-agricultural time (3000-2000 BC, Nakazawa et al., 1993) including agriculture, waste management, fossil fuel-related activities and biofuel and biomass burning (yet we acknowledge that a small fraction of wildfires are naturally ignited). Direct anthropogenic

Supprimé:

emissions are split between: “Agriculture and waste emissions”, “Fossil fuel emissions”, and “Biomass and biofuel burning emissions”, assuming that all types of fires are caused by anthropogenic activities. To conclude, this budget reports “direct anthropogenic”, and “natural and indirect anthropogenic” methane emissions for the five main source categories explained above for both bottom-up and top-down approaches.

The sinks of methane are split into the soil uptake that can be derived from land-surface models in the bottom-up budget, and the chemical sinks. The chemical sinks are estimated by either chemistry climate or chemistry transport models in the bottom-up budget, and are further detailed in terms of vertical distribution (troposphere and stratosphere) and oxidants.

Bottom-up estimates of CH₄ emissions for some processes are derived from process-oriented models (e.g., biogeochemical models for wetlands, models for termites), inventory models (agriculture and waste emissions, fossil fuel emissions, biomass and biofuel burning emissions), satellite-based models (large scale biomass burning), or observation-based upscaling models for other sources (e.g., inland water, geological sources). From these bottom-up approaches, it is possible to provide estimates for more detailed source subcategories inside each main category described above (see budget in Table 3). However, the total CH₄ emission derived from the sum of independent bottom-up estimates remains unconstrained.

For atmospheric inversions (top-down approach), atmospheric methane concentration observations provide a constraint on the global methane total source if we assume the global sink is known (OH and other oxidant prescribed), or inversions are optimising also for the chemical sink. OH estimates are constrained by methyl chloroform-inversion (Montzka et al., 2011; Rigby et al., 2017; Patra et al., 2021). The inversions reported in this work solve for the total net CH₄ flux at the surface (sum of sources minus soil uptake) (e.g., Pison et al., 2013), or a limited number of source categories (e.g., Bergamaschi et al., 2013). In most of the inverse systems the atmospheric oxidant concentrations were prescribed with pre-optimized or scaled OH fields, and thus the atmospheric sink is not optimised. The assimilation of CH₄ observations alone, as reported in this synthesis, can help to separate sources with different locations or temporal variations but cannot fully separate individual sources where they overlap in space and time in some regions. Top-down global and regional CH₄ emissions per source category were nevertheless obtained from gridded optimised fluxes, for the inversions that separated emissions into the five main GCP categories. Alternatively, for the inversion that only solved for total emissions (or for other categories other than the five described above), the prior contribution of each source category at the spatial resolution of the inversion was scaled by the ratio of the total (or embedding category) optimised flux divided by the total (or embedding category) prior flux (Kirschke et al., 2013). In other words, the prior relative mix of sources at model resolution is kept in each grid cell while total emissions are given by the atmospheric inversions. The soil uptake was provided separately to report total gross surface emissions instead of net fluxes (sources minus soil uptake).

In summary, bottom-up models and inventories emissions are presented for all relevant source processes and grouped if needed into the five main categories defined above. Top-down inversion emissions are reported globally and for the five main emission categories.

474 **2.5 Processing of emission maps and box-plot representation of emission budgets**

475 Common data analysis procedures have been applied to the different bottom-up models, inventories and atmospheric
476 inversions whenever gridded products exist. Gridded emissions from atmospheric inversions, land-surface models for
477 wetland or biomass burning were provided at the monthly scale. Emissions from anthropogenic inventories are usually
478 available as yearly estimates. These monthly or yearly fluxes were provided on a 1°x1° grid or re-gridded to 1°x1°, then
479 converted into units of Tg CH₄ per grid cell. Inversions with a resolution coarser than 1° were downscaled to 1° by each
480 modelling group. Land fluxes in coastal pixels were reallocated to the neighbouring land pixel according to our 1° land-sea
481 mask, and vice-versa for ocean fluxes. Annual and decadal means used for this study were computed from the monthly or
482 yearly gridded 1°x1° maps.
483 Budgets are presented as boxplots with quartiles (25%, median, 75%), outliers, and minimum and maximum values without
484 outliers. Outliers were determined as values below the first quartile minus three times the interquartile range, or values above
485 the third quartile plus three times the interquartile range. Mean values reported in the tables are represented as “+” symbols
486 in the corresponding figures.

487 **3 Methane sources and sinks: bottom-up estimates**

488 For each source category, a short description of the relevant processes, original data sets (measurements, models) and related
489 methodology are given. More detailed information can be found in original publication references, in Annex A2 where the
490 sources of data used to estimate the different sources and sinks are summarised and compared with those used in Saunio et
491 al. (2020) and in the Supplementary Material of this study when specified in the text. The emission estimates for each source
492 category are compared with Saunio et al. (2020) in Table 3 and with Saunio et al. (2016) in Table S12 for the decade 2000-
493 2009.

494 **3.1 Anthropogenic direct sources**

495 **3.1.1 Global inventories**

496 The main bottom-up global inventory datasets covering direct anthropogenic emissions from all sectors (Table 1) are from
497 the United States Environmental Protection Agency (USEPA, 2019), the Greenhouse gas and Air pollutant Interactions and
498 Synergies (GAINS) model developed by the International Institute for Applied Systems Analysis (IIASA) (Höglund-
499 Isaksson et al., 2020) and the Emissions Database for Global Atmospheric Research (EDGARv6 and v7, Crippa et al., 2021,
500 2023) compiled by the European Commission Joint Research Centre (EC-JRC) and Netherlands Environmental Assessment
501 Agency (PBL). We also used the Community Emissions Data System for historical emissions (CEDS) (Hoesly et al., 2018)
502 developed for climate modelling and the Food and Agriculture Organization (FAO) FAOSTAT emission database (Tubiello

et al., 2022), which covers emissions from agriculture and land use (including peatland fires and biomass fires). These inventories are not independent as they may use the same activity data or emission factors, as discussed below.

These inventory datasets report emissions from fossil fuel production, transmission, and distribution; livestock enteric fermentation; manure management and application; rice cultivation; solid waste and wastewater. Since the level of detail provided by country and by sector varies among inventories, the data were reconciled into common categories according to Table S2. For example, agricultural waste-burning emissions treated as a separate category in EDGAR, GAINS and FAO, are included in the biofuel sector in the USEPA inventory and in the agricultural sector in CEDS. The GAINS, EDGAR and FAO estimates of agricultural waste burning were excluded from this analysis (these amounted to 1-3 Tg CH₄ yr⁻¹ in recent decades) to prevent any potential overlap with separate estimates of biomass burning emissions (e.g., GFEDv4.1s; Giglio et al. (2013); van der Werf et al (2017)). In the inventories used here, emissions for a given region/country and a given sector are usually calculated following IPCC methodology (IPCC, 2006), as the product of an activity factor and its associated emission factor. An abatement coefficient may also be used, to account for any regulations implemented to control emissions (see e.g., Höglund-Isaksson et al., 2015). These datasets differ in their assumptions and data used for the calculation; however, they are not completely independent because they often use the same activity data and some of them follow the same IPCC guidelines (IPCC, 2006). While the USEPA inventory adopts emissions reported by the countries to the UNFCCC, other inventories (FAOSTAT, EDGAR and the GAINS model) produce their own estimates using a consistent approach for all countries, typically IPCC Tier 1 methods or deriving IPCC Tier 2 emission factors from country-specific information using a consistent methodology. These other inventories compile country-specific activity data and emission factor information or, if not available, adopt IPCC default factors (Tibrewal et al., 2024; Oreggioni et al., 2021; Höglund-Isaksson et al., 2020; Tubiello, 2019). CEDS takes a different approach (Hoesly et al., 2018) and combines data from GAINS, EDGAR and FAO depending on the sector. Then their first estimates are scaled to match other individual or region-specific inventory values when available. This process maintains the spatial information in the default emission inventories while preserving consistency with country level data. The FAOSTAT dataset (hereafter FAO-CH₄) provides estimates at the country level and is limited to agriculture (CH₄ emissions from enteric fermentation, manure management, rice cultivation, energy usage, burning of crop residues, and prescribed burning of savannahs) and land-use (peatland fires and biomass burning). FAO-CH₄ uses activity data mainly from the FAOSTAT crop and livestock production database, as reported by countries to FAO (Tubiello et al., 2013), and applies mostly the Tier 1 IPCC methodology for emissions factors (IPCC, 2006), which depends on geographic location and development status of the country. For manure, the country-scale temperature was obtained from the FAO global agro-ecological zone database (GAEZv3.0, 2012). Although country emissions are reported annually to the UNFCCC by annex I countries, and episodically by non-annex I countries, data gaps of those national inventories do not allow the inclusion of these estimates in this analysis.

In this budget, we use the following versions of these inventories that were available at the start and during the analysis (see Table 1):

- EDGARv6 which provides yearly gridded emissions by sectors from 1970 to 2018 (Crippa et al., 2021; Oreggioni et al., 2021; EDGARv6 website https://edgar.jrc.ec.europa.eu/dataset_ghg60; Monforti Ferrario et al., 2021),
- EDGARv7, which provides yearly gridded emissions by sectors from 1970 to 2020 (monthly for some sectors), but emissions from fossil fuel energy are not separated (oil and gas, and coal are lumped together - see Table S2) (EDGARv7 website https://edgar.jrc.ec.europa.eu/dataset_ghg70; Crippa et al., 2023).
- GAINS model scenario version 4.0 (Höglund-Isaksson et al., 2020) which provides an annual sectorial gridded product from 1990 to 2020 both by country and gridded. USEPA (USEPA, 2019), which provides 5-year sectorial totals by country from 1990 to 2020 (estimates from 2015 onward are a projection), with no gridded distribution available. The USEPA dataset was linearly interpolated to provide yearly values from 1990-2020.
- CEDS version v_2021_04_21 which provides gridded monthly and annual country-based emissions by sectors from 1970 to 2019 (Hoesly et al., 2018; O'Rourke et al., 2021). Fossil fuel emissions for 2020 have been updated using the methodology described for CO in Zheng et al. (2023).
- FAO-CH₄ (database accessed in December 2022, FAO, 2022) containing annual country level data for the period 1961-2020, for rice, manure, and enteric fermentation; and 1990-2020 for burning savannah, crop residue and non-agricultural biomass burning.

3.1.2 Total anthropogenic direct emissions

We calculated separately the total anthropogenic emissions for each inventory by adding its values for “Agriculture and waste”, “Fossil fuels” and “Biofuels” with additional large-scale biomass burning emissions data (Sect. 3.1.5). This method avoids double counting and ensures consistency within each inventory. This approach was used for the EDGARv6 and v7, CEDS and GAINS inventories, but we kept the USEPA inventory as originally reported because it includes its own estimates of biomass burning emissions. FAO-CH₄ was only included in the range reported for the “Agriculture and waste” category. For the latter, we calculated the range and mean value as the sum of the mean and range of the three anthropogenic subcategory estimates “Enteric fermentation and Manure”, “Rice”, and “Landfills and Waste”. The values reported for the upper-level anthropogenic categories (“Agriculture and waste”, “Fossil fuels” and “Biomass burning & biofuels”) are therefore consistent with the sum of their subcategories, although there might be small percentage differences between the reported total anthropogenic emissions and the sum of the three upper-level categories. This approach provides a more accurate representation of the range of emission estimates, avoiding an artificial expansion of the uncertainty attributable to subtle differences in the definition of sub-sector categorisations between inventories.

Based on the ensemble of databases detailed above, total direct anthropogenic emissions were 358 [329-387] Tg CH₄ yr⁻¹ for the decade 2010-2019 (Table 3, including biomass and biofuel burning) and 331 [305-365] Tg CH₄ yr⁻¹ for the decade 2000-2009. Our estimate for the 2000-2009 decade is within the range of Saunio et al. (2020) (334 [321-358]), Saunio et al. (2016) (338 Tg CH₄ yr⁻¹ [329-342]) and Kirschke et al. (2013) (331 Tg CH₄ yr⁻¹ [304-368]) for the same period. The

568 slightly larger range reported herein with respect to previous estimates is due to the USEPA lower estimate for agriculture,
569 waste and fossil emissions associated with the lowest estimate of biomass burning.

570 Figure 2 (left) summarises or projects global CH₄ emissions of anthropogenic sources (including biomass and biofuel
571 burning) by different datasets between 2000 and 2050. The datasets consistently estimate total anthropogenic emissions of
572 ~300 Tg CH₄ yr⁻¹ in 2000. For the Sixth Assessment Report of the IPCC, seven main Shared Socioeconomic Pathways
573 (SSPs) were defined for future climate projections in the Coupled Model Intercomparison Project 6 (CMIP6) (Gidden et al.,
574 2019; O'Neill et al., 2016) ranging from 1.9 to 8.5 W m⁻² radiative forcing by the year 2100 (as shown by the number in the
575 SSP names). For the 1970-2015 period, historical emissions used in CMIP6 (Feng et al., 2019) combine anthropogenic
576 emissions from CEDS (Hoesly et al., 2018) and a climatological value from the GFEDv4.1s biomass burning inventory (van
577 Marle et al., 2017). The harmonised scenarios used for CMIP6 activities start in 2015 at 388 Tg CH₄ yr⁻¹, which corresponds
578 to the higher range of our estimates. Since CH₄ emissions continue to track scenarios that assume no or minimal climate
579 policies (SSP5 and SSP3), it may indicate that climate policies, when present, have not yet produced sufficient results to
580 change the emissions trajectory substantially (Nisbet et al., 2019). After 2015, the SSPs span a range of possible outcomes,
581 but current emissions appear likely to follow the higher-emission trajectories over the past decade in terms of trend, and the
582 peak year has not yet been reached. High or medium emission reduction rates as suggested by scenarios SSP1 and SSP2
583 have not yet happened. This illustrates the challenge of methane mitigation that lies ahead to help reach the goals of the
584 Paris Agreement (Nisbet et al., 2020; Shindell et al., 2024). In addition, estimates of methane atmospheric concentrations
585 (Meinshausen et al., 2017, 2020) from the harmonised scenarios (Riahi et al., 2017) indicate that observations of global CH₄
586 concentrations fall well within the range of scenarios in absolute values but their trend over the past few years is closest to
587 those of scenario SSP5-8.5 (Fig. 2 right). The CH₄ concentrations are estimated using a simple exponential decay with
588 inferred natural emissions (Meinshausen et al., 2011), and the emergence of any trend between observations and scenarios
589 needs to be confirmed in the following years. However, the current observed concentrations and emissions estimates lie in
590 the upper range of the former RCPs scenarios starting in 2005 (Fig. S1). In the future, it will be important to monitor the
591 trends from 2015 (the Paris Agreement) and from 2020 (Global Methane Pledge) estimated in inventories and from
592 atmospheric observations, and compare them to various scenarios.

593 **3.1.3 Fossil fuel production and use**

594 Most anthropogenic CH₄ emissions related to fossil fuels come from the exploitation, transportation, and usage of coal, oil,
595 and natural gas. Additional emissions reported in this category include small industrial contributions such as the production
596 of chemicals and metals, fossil fuel fires (e.g., underground coal mine fires and the Kuwait oil and gas fires), and transport
597 (road and non-road transport). CH₄ emissions from the oil processing industry (e.g., refining) and production of charcoal
598 are estimated to be a few Tg CH₄ yr⁻¹ only, and are included in the transformation industry sector in the inventory. Fossil
599 fuel fires are included in the subcategory “Oil & Gas”. Emissions from industries, road and, non-road transport are reported

Supprimé: next

Supprimé: .

Supprimé: s

Supprimé:

Supprimé:

605 apart from the two main subcategories “Oil & Gas” and “Coal”, as in Sauniois et al. (2020) and contrary to Sauniois et al.
606 (2016); each of these amounts to about 2 to 5 Tg CH₄ yr⁻¹ (Table 3). The large range (1-9 Tg CH₄ yr⁻¹) is attributable to
607 difficulties in allocating some sectors to these sub-sectors consistently among the different inventories (See Table S2). The
608 spatial distribution of CH₄ emissions from fossil fuels is presented in Fig. 3 based on the mean gridded maps provided by
609 CEDS, EDGARv6, and GAINS for the 2010-2019 decade; USEPA lacks a gridded product.
610 Global mean emissions from fossil fuel-related activities, other industries and transport are estimated from the four global
611 inventories (Table 1) to be of 120 [117-125] Tg CH₄ yr⁻¹ for the 2010-2019 decade (Table 3), but with large differences in
612 the rate of change during this period across inventories. The sector accounts on average for 34% (range 31-42%) of total
613 global anthropogenic emissions in 2010-2019. This contribution has slightly increased from 32% on average in 2000-2009.

Supprimé:

615 Coal mining.

616 During mining, CH₄ is emitted primarily from ventilation shafts, where large volumes of air are pumped in and out of the
617 mine to keep the CH₄ mixing ratio below 0.5% to avoid accidental ignition, and from dewatering operations. In countries of
618 the Organization for Economic Co-operation and Development (OECD), coalbed CH₄ is often extracted as fuel up to ten
619 years before the coal mine starts operation, thereby reducing the CH₄ channelled through ventilation shafts during mining.
620 In many countries, large quantities of ventilation air CH₄ are still released to the atmosphere or flared, despite efforts to
621 extend coal mine gas recovery under the UNFCCC Clean Development Mechanisms (<http://cdm.unfccc.int>). CH₄ leaks also
622 occur during post-mining handling, processing, and transportation. Some CH₄ is released from coal waste piles and
623 abandoned mines; while emissions from these sources were believed to be low (IPCC, 2000), recent work has estimated
624 these at 22 billion m³ (compared to 103 billion m³ from functioning coal mines) in 2010 with emissions projected to increase
625 into the future (Kholod et al., 2020).

626 In 2020, more than 35% (IEA, 2023a) of the world’s electricity is still produced from coal. This contribution grew in the
627 2000s at the rate of several percent per year, driven by Asian economic growth where large reserves exist, but global coal
628 consumption declined between 2014 and 2020. In 2020, the top ten largest coal producing nations accounted for ~90% of
629 total world CH₄ emissions from coal mining; among them, the top three producers (China, United States of America, and
630 India) produced almost two-thirds (66%) of the world’s coal (IEA, 2021).

631 Global estimates of CH₄ emissions from coal mining show a reduced range of 37-44 Tg CH₄ yr⁻¹ for 2010-2019 (Table 3),
632 compared to the previous estimate for 2008-2017 in Sauniois et al. (2020) reporting a range of 29-61 Tg CH₄ yr⁻¹ for 2008-
633 2017. This reduced range probably results from using similar activity data (mostly from IEA statistics) in the different
634 inventories. The highest value of the range in Sauniois et al. (2020) came from the CEDS inventory while the lowest came
635 from USEPA. CEDS seems to have revised downward their estimate compared to the previous version used in Sauniois et
636 al. (2020). There were previously large discrepancies in Chinese coal emissions, with a large overestimation from
637 EDGARv4.2 on which CEDS was based. As highlighted by Liu et al. (2021a), a county-based inventory of Chinese methane

emissions also confirms the overestimation of previous EDGAR inventories and estimated total anthropogenic Chinese emissions at 38.2 ± 5.5 Tg CH₄ yr⁻¹ for 2000-2008 (Liu et al., 2021a). Coal mining emission factors depend strongly on the type of coal extraction (underground mining emits up to 10 times more than surface mining), the geological underground structure (region-specific), history (basin uplift), and the quality of the coal (brown coal (lignite) emits more than hard coal (anthracite)). Finally, the different emission factors derived for coal mining is the main reason for the differences between inventories globally (Fig. 2).

For the 2010-2019 decade, methane emissions from coal mining represent 33% of total fossil fuel-related emissions of CH₄ (40 [37-44] Tg CH₄ yr⁻¹, Table 3). An additional assumed very small source corresponds to fossil fuel fires, which are mostly underground coal fires. This source is estimated at around 0.15 Tg yr⁻¹ in EDGARv7, though this value remains the same across EDGAR versions and for all years despite the changes in coal production, which could influence this estimate. However, to date, insufficient data is available to better estimate this largely unknown source.

Oil and natural gas systems.

This sub-category includes emissions from both conventional and shale oil and gas exploitation. Natural gas is composed primarily of CH₄, so both fugitive and planned emissions during the drilling of wells in gas fields, extraction, transportation, storage, gas distribution, end use, and incomplete combustion in gas flares emit CH₄ (Lamb et al., 2015; Shorter et al., 1996). Persistent fugitive emissions (e.g., due to leaky valves and compressors) should be distinguished from intermittent emissions due to maintenance (e.g., purging and draining of pipes) or incidents. During transportation, fugitive emissions can occur in oil tankers, fuel trucks and gas transmission pipelines, attributable to corrosion, manufacturing, and welding faults. According to Lelieveld et al. (2005), CH₄ fugitive emissions from gas pipelines should be relatively low, however, old distribution networks in some cities may have higher rates, especially those with cast-iron and unprotected steel pipelines (Phillips et al., 2013). Measurement campaigns in cities within the USA (e.g., McKain et al., 2015) and Europe (e.g., Defratyka et al., 2021) revealed that significant emissions occur in specific locations (e.g., storage facilities, city natural gas fueling stations, well and pipeline pressurisation/depressurisation points, sewage systems, and furnaces of buildings) along the distribution networks (e.g., Jackson et al., 2014a; McKain et al., 2015; Wunch et al., 2016). However, CH₄ emissions vary significantly from one city to another depending, in part, on the age of city infrastructure and the quality of its maintenance, making urban emissions difficult to scale-up from measurement campaigns, although attempts have been made (e.g., Defratyka et al., 2021). In many facilities, such as gas and oil fields, refineries, and offshore platforms, most of the associated and other waste gas generated will be flared for security reasons with almost complete conversion to CO₂, however, due to the large quantities of waste gas generated, small fractions of gas still being vented make up relatively large quantities of methane. These two processes are usually considered together in inventories of oil and gas industries. In addition, single-point failure of natural gas infrastructure can leak CH₄ at high rate for months, such as at the Aliso Canyon blowout in the Los Angeles, CA (Conley et al., 2016) or the shale gas well blowout in Ohio (Pandey et al., 2019), thus

Supprimé:

Supprimé: (

Supprimé: ,

Supprimé: ~

Supprimé:)

677 hampering emission control strategies. Production of natural gas from the exploitation of hitherto unproductive rock
678 formations, especially shale, began in the 1970s in the US on an experimental or small-scale basis, and then, from the early
679 2000s, exploitation started at a large commercial scale. The shale gas contribution to total dry natural gas production in the
680 United States reached 82% in 2023, growing rapidly from 48% in 2013 (IEA, 2023b). The possibly larger emission factors
681 from shale gas compared to conventional gas, have been widely debated (e.g., Cathles et al., 2012; Howarth, 2019; Lewan,
682 2020). The latest studies tend to infer emission factors from the oil gas production chain of about 1% to 6% (e.g., Schneising
683 et al., 2020; Varon et al., 2023; Zhang et al., 2020), but loss rate could be as high as more than 10% in low producing well
684 sites (e.g., Omara et al., 2022, Williams et al., 2024).
685 CH₄ emissions from oil and natural gas systems vary greatly in different global inventories (67 to 80 Tg yr⁻¹ in 2020, Table
686 3). The inventories generally rely on the same sources and magnitudes for activity data, with the derived differences
687 therefore resulting primarily from different methodologies and parameters used, including emission factors. Those factors
688 are country- or even site-specific and the few field measurements available often combine oil and gas activities (Brandt et
689 al., 2014), resulting in high uncertainty in emission estimates for many major oil and gas producing countries. Depending
690 on the region, the IPCC 2006 default emission factors may vary by two orders of magnitude for oil production and one order
691 for gas production. For instance, the GAINSv4.0 estimate of CH₄ emissions from US oil and gas systems in 2015 is 16
692 Tg, which is almost twice as high as EDGARv8.0 (EDGAR, 2024) at 8.4 Tg and USEPA (UNFCCC, 2023) at 9.5 Tg. The
693 difference can partly be explained by GAINS using a bottom-up methodology to derive country- and year-specific flows of
694 associated petroleum gas and attributing these to recovery/reinjection, flaring or venting (Höglund-Isaksson, 2017), and
695 partly to GAINS using a higher emission factor for unconventional gas production (Höglund-Isaksson et al., 2020). Recent
696 quantifications using satellite observations and inversion estimate a relatively stable trend for US oil and gas systems
697 emissions since 2010, with Lu et al. (2023) estimating 14.6 Tg for 2010, 15.9 Tg for 2014 and 15.6 Tg for 2019, Shen et al.
698 (2022) estimating a mean of 12.6 Tg for 2018-2020, and Maasakkers et al (2021) a mean of 11.1 Tg for 2010 to 2015. The
699 stable top-down trend for the US appears not well captured in the bottom-up inventories from GAINS and EDGAR, which
700 tend to show an increasing trend driven by increase in production volumes.
701 Most recent studies (e.g., Zhang et al., 2020 ; Shen et al., 2023; Li et al., 2024, Tibrewal et al., 2024; Sherwin et al., 2024)
702 still suggest that the methane emissions from oil and gas industry are underestimated by inventories, industries, and agencies,
703 including the USEPA and UNFCCC reporting. Lauvaux et al. (2022) showed that emissions from a few high-emitting
704 facilities, i.e., super-emitters (> 20 t hr⁻¹), which are usually sporadic in nature, and not accounted for in the inventories,
705 could represent 8-12% of global oil & gas emissions, or around 8 Tg CH₄ yr⁻¹. These high emitting points, located on the
706 conventional part of the facilities, could be avoided through better operating conditions and repair of malfunctions. Over the
707 last decade, absolute CH₄ emissions almost certainly increased, since USA crude oil production doubled and natural gas
708 production rose by about 50% (IEA, 2023a). However, global implications of the rapidly growing shale gas activity in the
709 US remain to be determined precisely.

Supprimé: However, t

Supprimé: infer similar

Supprimé: in a narrow range of 1-3% (Alvarez et al., 2018; Peischl et al., 2015; Zavala-Araiza et al., 2015), different from the widely spread rates of 3-17% from previous studies (e.g., Caulton et al., 2014; Schneising et al., 2014).

Supprimé: Alvarez et al., 2018; Brandt et al., 2014; Jackson et al., 2014b; Karion et al., 2013; Moore et al., 2014; Olivier and Janssens-Maenhout, 2014; Pétron et al., 2014; Zavala-Araiza et al., 2015), albeit not all (Allen et al., 2013; Cathles et al., 2012; Peischl et al., 2015)

Supprimé: ,

Supprimé:

723 For the 2010-2019 decade, CH₄ emissions from upstream and downstream oil and natural gas sectors are estimated to
724 represent about 56% of total fossil CH₄ emissions (67 [57-74] Tg CH₄ yr⁻¹, Table 3) based on global inventories, with a
725 lower uncertainty range than for coal emissions for most countries. However, it is worth noting that 8 Tg CH₄ yr⁻¹ should
726 be added on top of this estimate to acknowledge the ultra-emitters contribution, as done in Tibrewal et al (2024).

727 **3.1.4 Agriculture and waste sectors**

728 This main category includes CH₄ emissions related to livestock production (i.e., enteric fermentation in ruminant animals
729 and manure management), rice cultivation, landfills, and wastewater handling. Of these activities, globally and in most
730 countries, livestock is by far the largest source of CH₄, followed by waste handling and rice cultivation. Conversely, field
731 burning of agricultural residues is a minor source of CH₄ reported in emission inventories (a few Tg at the global scale).
732 The spatial distribution of CH₄ emissions from agriculture and waste handling is presented in Fig. 3 based on the mean
733 gridded maps provided by CEDS, EDGARv6 and GAINS over the 2010-2019 decade.

734 Global emissions from agriculture and waste for the period 2010-2019 are estimated to be 211 [195-231] Tg CH₄ yr⁻¹ (Table
735 3), representing 60% of total direct anthropogenic emissions. Agriculture emissions amount to 144 Tg CH₄ yr⁻¹, 40% of the
736 direct anthropogenic emissions, with the rest coming from the fossil fuel sector (34%), waste (19%) and biomass (5%) and
737 biofuel (3%) burning .

738 **Livestock: Enteric fermentation and manure management.** Domestic ruminants such as cattle, buffalo, sheep, goats, and
739 camels emit CH₄ as a by-product of the anaerobic microbial activity in their digestive systems (Johnson et al., 2002). The
740 very stable temperatures (about 39°C) and pH (6.5-6.8) within the rumen of domestic ruminants, along with a constant plant
741 matter flow from grazing (cattle graze many hours per day), allow methanogenic *Archaea* residing within the rumen to
742 produce CH₄. CH₄ is released from the rumen mainly through the mouth of multi-stomached ruminants (eructation, ~90%
743 of emissions) or absorbed in the blood system. The CH₄ produced in the intestines and partially transmitted through the
744 rectum is only ~10% (Hill et al. 2016).

745 The total number of livestock continues to grow steadily. There are currently (2020) about 1.5 billion cattle globally, almost
746 1.3 billion sheep, and nearly as many goats (<http://www.fao.org/faostat/en/#data/GE>). Livestock numbers are linearly related
747 to CH₄ emissions in inventories using the Tier 1 IPCC approach such as FAOSTAT. In practice, some non-linearity may
748 arise due to dependencies of emissions on the total weight of the animals and their diet, which are better captured by Tier 2
749 and higher approaches. Cattle, due to their large population, large individual size, and particular digestive characteristics,
750 account for the majority of enteric fermentation CH₄ emissions from livestock worldwide (Tubiello, 2019; FAO, 2022),
751 particularly in intensive agricultural systems in wealthier and emerging economies, including the United States (USEPA,
752 2016). CH₄ emissions from enteric fermentation also vary from one country to another as cattle may experience diverse
753 living conditions that vary spatially and temporally, especially in the tropics (Chang et al., 2019).

754 Anaerobic conditions often characterise manure decomposition in a variety of manure management systems globally (e.g.,
 755 liquid/slurry treated in lagoons, ponds, tanks, or pits), with the volatile solids in manure producing CH₄. In contrast, when
 756 manure is handled as a solid (e.g., in stacks or dry-lots) or deposited on pasture, range, or paddock lands, it tends to
 757 decompose aerobically and to produce little or no CH₄. However aerobic decomposition of manure tends to produce nitrous
 758 oxide (N₂O), which has a larger global warming impact than CH₄. Ambient temperature, moisture, energy contents of the
 759 feed, manure composition, and manure storage or residency time affect the amount of CH₄ produced. Despite these
 760 complexities, most global datasets used herein apply a simplified IPCC Tier 1 approach, where amounts of manure treated
 761 depend on animal numbers and simplified climatic conditions by country.

762 Global CH₄ emissions from enteric fermentation and manure management are estimated in the range of 114-124 Tg CH₄ yr⁻¹
 763 ¹, for the year 2020, in the GAINS model and CEDS, USEPA, FAO-CH₄ and EDGARv7 inventories ([Table 3](#)). Using the
 764 Tier 2 method adopted from the 2019 Refinement to 2006 IPCC guidelines, a recent study (Zhang et al., 2022) estimated
 765 that global CH₄ emissions from livestock increased from 31.8 [26.5–37.1] (mean
 766 [minimum–maximum of 95% confidence interval) Tg CH₄ yr⁻¹ in 1890 to 131.7 [109.6–153.7] Tg CH₄
 767 yr⁻¹ in 2019, a fourfold increase in the past 130 years. Chang et al. (2021) estimates enteric fermentation and manure
 768 management emissions based on mixed Tier 1&2 and Tier1 approaches and calculate livestock emissions being 120±13 and
 769 136±15 Tg CH₄ yr⁻¹ respectively for 2018. Chang et al. (2021) and Zhang et al. (2022) estimates for 2018 or 2019 are on
 770 average a bit higher than the inventories estimates but in agreement considering the uncertainties. [It is worth recalling here](#)
 771 [that the ranges provided in this study correspond to the minimum-maximum of the existing estimates and do not include the](#)
 772 [uncertainty of the individual estimate; these uncertainties could be larger than the range proposed here.](#)

773 For the period 2010-2019, we estimated total emissions of 112 [107-118] Tg CH₄ yr⁻¹ for enteric fermentation and manure
 774 management, about one third of total global anthropogenic emissions ([Table 3](#)).

775 **Rice cultivation.** Most of the world's rice is grown in flooded paddy fields (Baicich, 2013). The water management systems,
 776 particularly flooding, used to cultivate rice are one of the most important factors influencing CH₄ emissions and one of the
 777 most promising approaches for CH₄ emission mitigation: periodic drainage and aeration not only cause existing soil CH₄ to
 778 oxidise, but also inhibit further CH₄ production in soils (Simpson et al., 1995; USEPA, 2016; Zhang, 2016). Upland rice
 779 fields are not typically flooded, and therefore are not a significant source of CH₄. Other factors that influence CH₄ emissions
 780 from flooded rice fields include fertilisation practices (i.e., the use of urea and organic fertilisers), soil temperature, soil type
 781 (texture and aggregated size), rice variety and cultivation practices (e.g., tillage, seeding, and weeding practices) (Conrad et
 782 al., 2000; Kai et al., 2011; USEPA, 2011; Yan et al., 2009). For instance, CH₄ emissions from rice paddies increase with
 783 organic amendments (Cai et al., 1997) but can be mitigated by applying other types of fertilisers (mineral, composts, biogas
 784 residues) or using wet seeding (Wassmann et al., 2000).

785 The geographical distribution of rice emissions has been assessed by global (e.g., Janssens-Maenhout et al., 2019; Tubiello,
 786 2019; USEPA, 2012) and regional (e.g., Castelán-Ortega et al., 2014; Chen et al., 2013; Chen and Prinn, 2006; Peng et al.,

2016; Yan et al., 2009; Zhang and Chen, 2014) inventories and land surface models (Li et al., 2005; Pathak et al., 2005; Ren et al., 2011; Spahni et al., 2011; Tian et al., 2010, 2011; Zhang, 2016). The emissions show a seasonal cycle, peaking in the summer months in the extra-tropics associated with monsoons and land management. Emissions from rice paddies are influenced not only by the extent of rice field area, but also by changes in the productivity of plants (Jiang et al., 2017) as these alter the CH₄ emission factor used in inventories. However, the inventories considered herein are largely based on IPCC Tier 1 methods, which mainly scale with cultivated areas and include regional specific emission factors but do not account for changes in plant productivity and detailed cultivation practices.

The largest emissions from rice cultivation are found in Asia accounting for 30 to 50% of global emissions (Fig. 3). The decrease of CH₄ emissions from rice cultivation over recent decades is confirmed in most inventories, because of the decrease in rice cultivation area, changes in agricultural practices, and a northward shift of rice cultivation since the 1970s, as in China (e.g., Chen et al., 2013).

Based on the global inventories considered in this study, global CH₄ emissions from rice paddies are estimated to be 32 [25-37] Tg CH₄ yr⁻¹ for the 2010-2019 decade (Table 3), or about 9% of total global anthropogenic emissions of CH₄. These estimates are consistent with the 29 Tg CH₄ yr⁻¹ estimated for the year 2000 by Carlson et al. (2017).

Waste management. This sector includes emissions from managed and non-managed landfills (solid waste disposal on land), and wastewater handling, where all kinds of waste are deposited. CH₄ production from waste depends on the pH, moisture, and temperature of the material. The optimum pH for CH₄ emission is between 6.8 and 7.4 (Thorneloe et al., 2000). The development of carboxylic acids leads to low pH, which limits methane emissions. Food or organic waste, such as leaves and grass clippings, ferment quite easily, while wood and wood products generally ferment slowly, and cellulose and lignin even more slowly (USEPA, 2010a).

Waste management was responsible for about 11% of total global direct anthropogenic CH₄ emissions in 2000 (Kirschke et al., 2013). A recent assessment of CH₄ emissions in the USA found landfills to account for almost 26% of total USA anthropogenic CH₄ emissions in 2014, the largest contribution of any single CH₄ source in the United States of America (USEPA, 2016). In Europe, gas control has been mandatory on all landfills since 2009, and more importantly for CH₄ emissions, the EU Landfill Directive (1999) with subsequent amendments, has diverted most biodegradable waste away from landfills towards source separation, recycling, composting and energy recovery, and with a legally binding target not to landfill more than 10% of municipal solid waste by 2035.

Wastewater from domestic and industrial sources is treated in municipal sewage treatment facilities and private effluent treatment plants. The principal factor in determining the CH₄ generation potential of wastewater is the amount of degradable organic material in the wastewater. Wastewater with high organic content is treated anaerobically, which leads to increased emissions (André et al., 2014). Excessive and rapid urban development worldwide, especially in Asia and Africa, could enhance methane emissions from waste unless adequate mitigation policies are designed and implemented rapidly.

819 The GAINS model and CEDS and EDGAR inventories give robust emission estimates from solid waste in the range of 37-
820 42 Tg CH₄ yr⁻¹ for the year 2019, and more uncertain wastewater emissions in the range 20-45 Tg CH₄ yr⁻¹.
821 In our study, the global emission of CH₄ from waste management is estimated in the range of 56-80 Tg CH₄ yr⁻¹ for the
822 2010-2019 period with a mean value of 69 Tg CH₄ yr⁻¹, about 19% of total global anthropogenic emissions (Table 3).

823 3.1.5 Biomass and biofuel burning

824 This category includes CH₄ emissions from biomass burning in forests, savannahs, grasslands, peats, agricultural residues,
825 as well as, from the burning of biofuels in the residential sector (stoves, boilers, fireplaces). Biomass and biofuel burning
826 emit CH₄ under incomplete combustion conditions (i.e., when oxygen availability is insufficient for complete combustion),
827 for example in charcoal manufacturing and smouldering fires. The amount of CH₄ emitted during the burning of biomass
828 depends primarily on the amount of biomass, burning conditions, fuel moisture and the specific material burned.

829 In this study, we use large-scale biomass burning (forest, savannah, grassland, and peat fires) from five biomass burning
830 inventories (described below) and the biofuel burning contribution from anthropogenic emission inventories (EDGARv6
831 and v7, CEDS, GAINS and USEPA). The spatial distribution of emissions from the burning of biomass and biofuel over
832 the 2010-2019 decade is presented in Fig. 3 based on data listed in Table 1.

833 At the global scale, during the period of 2010-2019, biomass and biofuel burning generated CH₄ emissions of 28 [21-39] Tg
834 CH₄ yr⁻¹ (Table 3), of which 30-50% is from biofuel burning.

835
836 **Biomass burning.** Fire is an important disturbance event in terrestrial ecosystems globally (van der Werf et al., 2010), and
837 can be of either natural (typically ~10% of fires, ignited by lightning strikes or started accidentally) or anthropogenic origin
838 (~90%, human initiated fires) (USEPA, 2010b, chapter 9.1). As previously noted all fires are accounted as anthropogenic in
839 Table 3. Anthropogenic fires are concentrated in the tropics and subtropics, where forests, savannahs and grasslands may
840 be burned to clear land for agricultural purposes or to maintain pastures and rangelands. Small fires associated with
841 agricultural activity, such as field burning and agricultural waste burning, are often not detected by moderate resolution
842 remote sensing methods and are instead estimated based on cultivated area or through in-situ measurements such as
843 dedicated airborne campaigns (e.g., Barker et al., 2023).

844 Emission rates of biomass burning vary with biomass loading (depending on the biomes) at the location of the fire, the
845 efficiency of the fire (depending on the vegetation type), the fire type (smouldering or flaming) and emission factor (mass
846 of the considered species / mass of biomass burned). Depending on the approach, these parameters can be derived using
847 satellite data and/or biogeochemical model, or through simpler IPCC default approaches.

848 In this study, we use five products to estimate biomass burning emissions. The Global Fire Emission Database (GFED) is
849 the most widely used global biomass burning emission dataset and provides estimates from 1997 onwards. Here, we use
850 GFEDv4.1s (van der Werf et al., 2017), based on the Carnegie-Ames-Stanford-Approach (CASA) biogeochemical model

Supprimé: well

(van der Werf et al., 2010) driven by satellite derived vegetation characteristics and burned area mostly from the MODerate resolution Imaging Sensor, MODIS (Giglio et al., 2013). GFEDv4.1s (with small fires) is available at a 0.25° resolution and on a daily basis from 1997 to 2020. One characteristic of the GFEDv4.1s burned area is that small fires are better accounted for compared to GFEDv4.1 (Randerson et al., 2012), increasing carbon emissions by approximately 35% at the global scale. The latest version GFEDv5 (Chen et al., 2023) suggest 61% higher burned area than GFEDv4.1s, in closer agreement with burned area products from higher resolution satellite sensors. The next budget would benefit from GFEDv5 to revisit the estimates of biomass burning emissions (which would likely go up) based on more specific comparison studies.

The Quick Fire Emissions Dataset (QFED) is calculated using the fire radiative power (FRP) approach, in which the thermal energy emitted by active fires (detected by MODIS) is converted to an estimate of CH₄ flux using biome specific emissions factors and a unique method of accounting for cloud cover. Further information related to this method and the derivation of the biome specific emission factors can be found in Darnenov and da Silva (2015). Here we use the historical QFEDv2.5 product available daily on a 0.1x0.1 grid for 2000 to 2020.

The Fire INventory from the National Center for Atmospheric Research (FINNv2.5, Wiedinmyer et al., 2023) provides daily, 1 km resolution estimates of gas and particle emissions from open burning of biomass (including wildfire, agricultural fires and prescribed burning) over the globe for the period 2002-2020. FINNv2.5 uses MODIS and VIIRS satellite observations for active fires, land cover and vegetation density.

We use v1.3 of the Global Fire Assimilation System (GFAS, Kaiser et al., 2012), which calculates emissions of biomass burning by assimilating Fire Radiative Power (FRP) observations from MODIS at a daily frequency and 0.5° resolution and is available for 2000-2020.

The FAO-CH₄ yearly biomass burning emissions are based on the most recent MODIS 6 burned area products (Prosperi et al., 2020), coupled with a pixel level (500 m) implementation of the IPCC Tier 1 approach, and are available from 1990 to 2020 (Table 1).

The differences in emission estimates for biomass burning arise from specific geographical and meteorological conditions and fuel composition, which strongly impact combustion completeness and emission factors. The latter vary greatly according to fire type, ranging from 2.2 g CH₄ kg⁻¹ dry matter burned for savannah and grassland fires up to 21 g CH₄ kg⁻¹ dry matter burned for peat fires (van der Werf et al., 2010). Biomass burning emissions encountered large interannual variability related to meteorological conditions, with generally higher emissions during El-Nino periods as in 2019 (20 [14-28] Tg CH₄ yr⁻¹), 2015 (22 [15-28] Tg CH₄ yr⁻¹) and 2010 to a lesser extent (18 [15-29] Tg CH₄ yr⁻¹).

In this study, based on the five aforementioned products, biomass burning emissions are estimated at 17 Tg CH₄ yr⁻¹ [12-24] for 2010-2019, representing about 5% of total global anthropogenic CH₄ emissions (Table 3).

Biofuel burning. Burning of biomass to produce energy for domestic, industrial, commercial, or transportation purposes is hereafter called biofuel burning. A largely dominant fraction of CH₄ emissions from biofuel burning comes from domestic

Supprimé:

886 cooking or heating in stoves, boilers, and fireplaces, mostly in open cooking fires where wood, charcoal, agricultural
887 residues, or animal dung are burned. It is estimated that more than two billion people, mostly in developing countries, use
888 solid biofuels to cook and heat their homes daily (André et al., 2014), and yet CH₄ emissions from biofuel combustion have
889 received relatively little attention. Biofuel burning estimates are gathered from the CEDS, USEPA, GAINS and EDGAR
890 inventories. Due to the sectoral breakdown of the EDGAR and CEDS inventories the biofuel component of the budget has
891 been estimated as equivalent to the “RCO - Energy for buildings” sector as defined in Worden et al. (2017) and Hoesly et
892 al. (2018) (Table S2). This is equivalent to the sum of the IPCC 1A4a_Commercial-institutional, 1A4b_Residential,
893 1A4c_Agriculture-forestry-fishing and 1A5_Other-unspecified reporting categories. This definition is consistent with that
894 used in Saunio et al. (2016) and Kirschke et al. (2013). While this sector incorporates biofuel use, it also includes the use
895 of other combustible materials (e.g., coal or gas) for small-scale heat and electricity generation within residential and
896 commercial premises. Data provided by the GAINS inventory suggests that this approach may overestimate biofuels
897 emissions by between 5 and 50%. Further study into this category would be needed to better disentangle biofuels from fossil
898 combustibles.
899 In our study, biofuel burning is estimated to contribute 11 [8-14] Tg CH₄ yr⁻¹ to the global CH₄ budget, about 3% of total
900 global anthropogenic CH₄ emissions for 2010-2019 (Table3).

901 **3.1.6 Other anthropogenic sources (not explicitly included in this study)**

902 Other anthropogenic sources not included in this study are related to agriculture and land-use management. In particular,
903 increases in agricultural areas (such as global palm oil production) have led to the clearing of natural peat forests, reducing
904 natural peatland area and associated natural CH₄ emissions. Peatlands planted to forests (like in Northern Europe) also lead
905 to reduced CH₄ emissions. While studies have long suggested that CH₄ emissions from peatland drainage ditches are likely
906 to be significant (e.g., Minkinen and Laine, 2006, Peacock et al., 2021), CH₄ emissions related to palm oil plantations have
907 yet to be properly quantified (e.g., Manning et al, 2019). Taylor et al. (2014) have quantified global palm oil wastewater
908 treatment fluxes to be 4 ± 32 Tg CH₄ yr⁻¹ for 2010-2013. This currently represents a small and highly uncertain source of
909 methane but one potentially growing in the future.

910 **3.2 Natural and indirect anthropogenic sources**

911 As introduced in section 2.4, natural and indirect anthropogenic sources refer to pre-agricultural CH₄ emissions even if they
912 are perturbed by anthropogenic climate change or other global change factors (e.g., eutrophication), and indirect emissions
913 resulting from anthropogenic perturbation of the landscape (reservoirs) and the biogeochemical characteristics of soil. They
914 include vegetated wetland emissions and inland freshwater systems (lakes, small ponds, reservoirs, and rivers), land
915 geological sources (gas-oil seeps, mud volcanoes, microseepage, geothermal manifestations, and volcanoes), wild animals,
916 wildfires, termites, thawing terrestrial and marine permafrost, and coastal and oceanic sources (biogenic, geological and

hydrate). In water-saturated or flooded ecosystems, the decomposition of organic matter gradually depletes most of the oxygen in the soil or the sediment zone, resulting in anaerobic conditions and CH₄ production. Once produced, CH₄ can reach the atmosphere through a combination of three processes: (1) diffusive loss of dissolved CH₄ across the air-water boundary; (2) ebullition flux from sediments; and (3) flux mediated by emergent aquatic macrophytes and terrestrial plants (plant transport). On its way to the atmosphere, in the soil or water columns, CH₄ can be partly or completely oxidised by microorganisms, which use CH₄ as a source of energy and carbon (USEPA, 2010b). Concurrently, methane from the atmosphere can diffuse into the soil column and be oxidised (See Sect. 3.3.4 on soil uptake).

3.2.1 Wetlands

Wetlands are generally defined as ecosystems in which mineral or peat soils are water-saturated at some depth or where surface inundation (permanent or not) has a dominating influence on the soil biogeochemistry and determines the ecosystem species composition (USEPA, 2010b). To refine such an overly broad definition for CH₄ emissions, we define wetlands as ecosystems with inundated or saturated soils or peats where anaerobic conditions below the water table lead to CH₄ production (Matthews and Fung, 1987; USEPA, 2010b). Brackish water emissions are discussed separately in Sect. 3.2.6. Our definition of wetlands includes ombrotrophic and minerotrophic peatlands (i.e., bogs and fens), mineral soil wetlands (swamps and marshes), and seasonal or permanent floodplains. It excludes exposed water surfaces without emergent macrophytes, such as lakes, rivers, estuaries, ponds, and reservoirs (addressed in the next section), as well as rice agriculture (see Sect. 3.1.4, rice cultivation paragraph), and wastewater ponds. It also excludes coastal vegetated ecosystems (mangroves, seagrasses, salt marshes) with salinities usually >0.5 (See Sect. 3.2.6). Even with this definition, some wetlands could be considered as anthropogenic systems, being affected by human land-use changes such as impoundments, drainage, or restoration (Woodward et al., 2012). In the following, we retain the generic denomination “wetlands” for natural and human-influenced wetlands, as discussed in Sect. 2.2.

The three most important factors influencing CH₄ production in wetlands are the spatial and temporal extent of anoxia (linked to water saturation), temperature, and substrate availability (Valentine et al., 1994; Wania et al., 2010; Whalen, 2005; Delwiche et al., 2021; Knox et al., 2021).

Land surface models estimate CH₄ emissions through a series of processes, including CH₄ production, oxidation, and transport. The models are then forced with inputs accounting for changing environmental factors (Melton et al., 2013; Poulter et al., 2017; Tian et al., 2010; Wania et al., 2013; Xu et al., 2010). CH₄ emissions from wetlands are computed as the product of an emission flux density and a CH₄ producing area or surface extent (see Supplementary Material; Bohn et al., 2015; Melton et al., 2013). The areal extent of different wetland types (having large differences in areal CH₄ emission rates) appears to be a primary contributor to uncertainties in the absolute flux of CH₄ emissions from wetlands, with meteorological response being the main source of uncertainty for seasonal and interannual variability (Poulter et al., 2017; Kuhn et al., 2021; Parker et al., 2022; McNicol et al., 2023; Karlson and Bastviken 2023). However, large uncertainty

949 remains in both spatial and temporal emission distributions, especially over tropical wetlands where data are lacking to
950 evaluate the models but are nevertheless a key region for climate feedbacks (Nisbet, 2023; Zhang et al., 2023). Direct
951 measurement campaigns and remote sensing are providing key insights where to improve the land surface models (e.g.,
952 France et al., 2022; Shaw et al., 2022).

953 In this work, sixteen land surface models computing net CH₄ emissions (Table 2) were run under a common protocol with
954 a spin-up using repeated climate data from 1901-1920 to pre-industrial conditions followed by a transient simulation through
955 the end of 2020. Of the 16 models, 13 previously contributed to Saunio et al. (2020), and three models were new to this
956 release (CH4MOD_{wetland} (Li et al., 2010), ISAM (Shu et al., 2020; Xu et al., 2021), and SDGVM (Beerling and Woodward,
957 2001; Hopcroft et al., 2011; Hopcroft et al., 2020)) (Table 2, see also in the Supplementary Material Table S3 for a history
958 of the contributing models). Climatic forcing uncertainties are considered in the ensemble estimate by using two climate
959 datasets, CRU/CRU-JRA55 (Harris, 2014) and GSWP3-W5E5 (Dirmeyer et al., 2006; Kim 2017; Lange, 2019; Cuccchi et
960 al., 2020). Atmospheric CO₂ was also prescribed in the models. For all models, two wetland area dynamic schemes were
961 applied: a diagnostic scheme using a remote sensing-based wetland area and dynamics dataset called WAD2M (Wetland
962 Area Dynamics for Methane Modeling; Zhang et al., 2021a; 2021b) available at 0.25 degree of horizontal resolution, as in
963 Saunio et al. (2020), and a prognostic scheme using internal model-specific hydrologic models.

964 The diagnostic wetland extent product WAD2Mv1.0 (Zhang et al., 2021a) has been updated since Saunio et al. (2020) to
965 WAD2Mv2.0 (Zhang et al., 2021b) and extended to 2020. It uses the same Surface Water Microwave Product Series
966 (SWAMPSv3.2) for capturing inundation dynamics (Jenson and McDonald, 2019), which was extended to 2020. To reduce
967 potential double-counting with the freshwater budget, the surface areas of rivers/streams and lakes/ponds are excluded by
968 using the products Global River Widths from Landsat (GRWL) database v01.01 (Allen and Pavelsky, 2018) and HydroLakes
969 v1.0 (Messenger et al., 2016), instead of the Global Surface Water (GSW) product (Pekel et al., 2016) used in WAD2Mv1.0.
970 The GRWL and Hydrolakes are also the datasets used separately in the upscaling of the freshwater budget allowing for a
971 more consistent approach between the wetland and freshwater CH₄ budgets (Sect. 3.2.2). This update in WAD2M leads to
972 a downward revised annual average wetland extent by 0.5 Mkm² for the mid-high latitudes (mainly due to larger lake extent
973 in HydroLakes than in the GSW dataset) with small impacts in other regions. However, since HydroLakes includes only
974 vectorized lakes larger than 0.1 km², smaller lakes/ponds under 0.1 km² are implicitly still included as wetlands in
975 WAD2Mv2.0. For the high-latitude region, the recent peatland extent product from Hugelius et al. (2020) is applied, which
976 indicates a slightly higher peatland area by 0.2 Mkm² primarily in regions above 60°N, compared to the Northern
977 Circumpolar Soil Carbon Database (NCSCD) product (Hugelius et al., 2013) used in WAD2Mv1.0. Rice agriculture was
978 removed using the Monthly Irrigated and Rainfed Crop Areas (MIRCA2000, Portmann et al. (2010)) dataset from circa
979 2000, as a fixed distribution.

980 The combined remote-sensing and inventory WAD2Mv2.0 product leads to a maximum wetland area of 13.6 Mkm² during
981 the peak season (7.9 Mkm² on annual average, with a range of 7.5 to 8.4 Mkm² from 2000-2020, about 5.2% of the global

Supprimé:

land surface). The largest wetland areas in WAD2Mv2.0 are in Amazonia, the Congo Basin, and the Western Siberian Lowlands, which in previous studies were underestimated by inventories (Bohn et al., 2015). However, the SWAMPS v3.2 dataset which serves as a proxy of temporal variations of wetland extent, has discontinuity issues over a few tropical hotspots since 2015 and hence affects the temporal variations of WAD2M. Consequently, this affects CH₄ emissions estimates for a subset of land surface models that are particularly sensitive to inundation in these hotspots. Meanwhile, prognostic estimates show moderate consistency in capturing the spatial distribution of wetland area with WAD2M, with an annual average wetland area of 8.0 ± 2.0 Mkm² during the peak season for 2000-2020. The ensemble mean of annual wetland area anomaly by the prognostic models show reasonable agreement with satellite-based estimates in capturing the response of wetland area to climate variations (Zhang et al., in review), with higher agreement over temperate and boreal regions than in the tropics.

For the wetland methane emissions estimate, we use the decadal mean from the prognostic runs and adjust these flux estimates for double counting from inland waters (described in next section) given the reliance of the prognostic models on satellite flooded area data like WAD2Mv2 to parameterize maximum wetland extent (Zhang et al., in review). The average emission from wetlands for 2010-2019 for the 16 models is plotted in Fig. 3. The zones with the largest emissions are the Amazon basin, equatorial Africa and Asia, Canada, western Siberia, eastern India, and Bangladesh. Regions where CH₄ emissions have high inter-model agreement (defined as regions where mean flux is larger than the standard deviation of the models, on a decadal mean) represent 72% of the total CH₄ flux due to natural wetlands. The different sensitivities of the models to temperature, vapour pressure, precipitation, and radiation can generate substantially different patterns, such as in India. Emission estimates over regions with lower emissions (in total) are also consistently inferred between models (e.g., Scandinavia, Continental Europe, Eastern Siberia, Central United States of America, and Southern Africa).

The resulting global flux range for vegetated wetland emissions from the prognostic runs is 117-195 Tg CH₄ yr⁻¹ for the 2000-2020 period, with an average of 157 Tg CH₄ yr⁻¹ and a one-sigma standard deviation of 24 Tg CH₄ yr⁻¹. Using the prognostic set of simulations, the average ensemble emissions were 159 [119-203] Tg CH₄ yr⁻¹ for the 2010-2019 period (Table 3). The estimated average ensemble annual total from the two sets of simulations by CRU/CRU-JRA55 and GSWP3-W5E5 are 158 [126-193] and 158 [118-203] for 2010-2019, respectively. Generally, the magnitude and interannual variability agree between these two sets of simulations (Zhang et al., 2024). Wetland emissions represent about 25% of the total (natural plus anthropogenic) CH₄ sources estimated by bottom-up approaches. The large range in the estimates of wetland CH₄ emissions results from difficulties in defining wetland CH₄ producing areas as well as in parameterizing terrestrial anaerobic conditions that drive sources and the oxidative conditions leading to sinks (Melton et al., 2013; Poulter et al., 2017; Wania et al., 2013). The ensemble mean emission using the same simulation setup (i.e., diagnostic wetland extent and CRU/CRU-JRA55) in the models is 163 [117-195] Tg CH₄ yr⁻¹, higher by ~22 Tg CH₄ yr⁻¹ than the one previously reported (see Table 3, for 2000-2009 with comparison to Saunio et al., 2020). This difference is mainly due to the updated

1015 model structure and parameterizations in the wetland CH₄ models compared to the versions in the previous budget and the
1016 inclusion of three new land surface models.
1017 For the last decade 2010-2019, we report in this budget an average ensemble estimate of 159 Tg CH₄ yr⁻¹ with a range of
1018 119-203 (based on prognostic wetland extent runs, [Table 3](#)).

Supprimé:)

1019 **3.2.2 Inland freshwater [ecosystems](#) (lakes, ponds, reservoirs, streams, rivers)**

1020 This category includes CH₄ emissions from freshwater systems (lakes, ponds, reservoirs, streams, and rivers). Numerous
1021 advances have been made in the freshwater greenhouse gases knowledge base in the last few years (Lauerwald et al., 2023a).
1022 These advances include improvements in the underlying databases used to estimate inland water surface areas and model
1023 their dynamics, a rapidly growing number of direct measurements of methane fluxes, and improvements in our process-
1024 based understanding of methane biogeochemistry. Despite this, aspects of global freshwater methane estimates remain rather
1025 crude and continue to have large uncertainties. This includes the overall temperature dependency of methane emissions, the
1026 relative role of ebullition (i.e., bubble flux, which may represent the most important, but most difficult-to-capture emission
1027 path in many standing water bodies), fluxes from the smallest standing water bodies (sometimes referred to as ponds) having
1028 large emissions per m² but uncertain area extent, and the magnitude of anthropogenic influence on emissions, all which are
1029 discussed below.

1030
1031 **Streams and rivers.** The last global CH₄ budget used an estimate of 27 Tg CH₄ yr⁻¹ for global streams and rivers based
1032 largely on a data compilation by Stanley et al. (2016). This estimate was scaled from a simple data compilation without a
1033 spatial component or an estimate of ebullition. More recently, Rosentreter et al. (2021) performed a new data compilation
1034 of 652 flux estimates, including diffusive and ebullitive fluxes, coupled to an ice corrected surface area estimate of ~625,000
1035 km² that was aggregated to 5 latitudinal bands to come up with a global estimate of 6 and 31± 17 Tg CH₄ yr⁻¹ (respectively
1036 for the median and mean ± c.i. 95%). We believe, due to better data representation in underlying datasets, that the mean
1037 estimate of Rosentreter et al. (2021) is more representative statistically because the median does not capture hotspots and
1038 hot moments of intense ebullitive fluxes. Finally, Rocher-Ros et al. (2023) used a new Global River Methane (GRiMeDB)
1039 database (Stanley et al., 2023) with > 24,000 observations of CH₄ concentrations to predict ~28±17 Tg CH₄ yr⁻¹ (±c.i. 95%)
1040 river emissions globally. This approach used machine learning methods coupled to the latest spatially and temporally explicit
1041 mapping of monthly stream surface area (the smallest streams are still extrapolated) which incorporates drying and freezing
1042 effects (yearly average 672,000 km², Liu et al., 2022) and includes an ebullitive flux estimated from a correlation between
1043 measured diffusive and ebullitive emissions in the GRiMeDB database (Stanley et al., 2023). Thus, for this study we use an
1044 estimate of 29±17 (±c.i. 95%) Tg CH₄ yr⁻¹ for streams and rivers ([Figure 4](#)), which averages the mean estimate of Rosentreter
1045 et al. (2021) and Rocher-Ros et al. (2023). Currently, ebullitive fluxes remain a major unknown quantity in streams and
1046 rivers but appear to be coarsely linearly correlated in a log-space to diffusive fluxes and of similar magnitude (Rocher-Ros

et al., 2023). Methodologically, the high-water velocity of many streams and rivers make measurement of ebullitive fluxes challenging (Robison et al., 2021). Effluxes are also linked to hydrology (Aho et al., 2021) although very few studies have sampled over a representative hydrograph. Plant-mediated effluxes of CH₄ in running waters also remain difficult to constrain, with a recent compilation highlighting very few measurements (Bodmer et al. 2024). Connected adjacent wetlands is a common source of CH₄ to streams and rivers (Borges et al., 2019) which may be important for the regulation of running water emissions but is currently difficult to assess at the global scale. Overall, the poor representation of sites and deficient mechanistic understanding make it difficult to model and predict methane evasion from streams and rivers using process-based models.

Lakes and ponds. The previous global CH₄ budget used an estimate of 71 Tg CH₄ yr⁻¹ for lakes and 18 Tg CH₄ yr⁻¹ for reservoirs. These estimates were based on an early study by Bastviken et al. (2011) coupled with a newer estimate for lakes north of 50°N (Wik et al., 2016b). There have been three new lake studies that have published their data with global estimates of 56 and 151± 73 (Rosentreter et al. (2021); ~~respectively for the median and mean ± c.i. 95%~~), 22±8 (Zhuang et al., 2023; ~~±lake-area-weighted normalised RMSE for all parameterized lake types~~), process-based model), and 41±36 Tg CH₄ yr⁻¹ (Johnson et al., 2022, mean ±c.i. 95%). This large range in estimated emissions can be attributed to the differences in the datasets and methods used to calculate the surface area of small waterbodies, as well as the differences between how the flux data were analyzed and extrapolated between studies. For instance, total surface areas of all lakes and ponds of 3712-5688 × 10³ km² (Rosentreter et al., 2021) and 2806 × 10³ km² (Johnson et al., 2022) were used along with measurement data from 198 and 575 individual lake systems, respectively. In contrast, Zhuang et al. (2023) generated estimates using higher temporal resolution data from just 54 lakes to build a process-based model, which generated much lower flux estimates from tropical lakes than previously implemented statistical approaches, but in line with the most recent assessments by Borges et al. (2022). For this study, we explicitly excluded lakes <0.1 km² which are treated separately (see below). If we re-assess these three studies for only lakes greater than 0.1 km², we obtain global effluxes of 17 and 42.9±20.8 Tg CH₄ yr⁻¹ (Rosentreter et al. (2021); median and mean ~~± c.i. 95%~~ of global flux), 21.9±8.0. (Zhuang et al., 2023, ~~±lake-area-weighted normalised RMSE for all parameterized lake types~~), and 35.3±31.0 Tg CH₄ yr⁻¹ (Johnson et al. 2022, ~~±95% C.I.~~) (with areas of 2556-3468 x10³, 2640x10³, and 2676x10³ km² respectively). Thus, for lakes >0.1 km², we propose an efflux of ~~33±26~~ Tg CH₄ yr⁻¹ (an average of the mean from Rosentreter et al., 2021 Zhuang et al., 2023, and Johnson et al., 2022, with the average ~~c.i. 95%~~ from Rosentreter et al., 2021 and Johnson et al. 2022) ~~as represented in Figure 4.~~

Small waterbody emissions, hereafter small lakes and ponds<0.1 km², remain difficult to assess. Evidence is emerging that there is a lower limit to the power scaling laws that early studies used to extrapolate the surface area of these small systems (Bastviken et al., 2023; Kyzivat et al., 2022). Thus, for small lakes and ponds < 0.1 km² (and >0.001 km²), we disregard the higher end surface area used in Rosentreter et al., 2021 which relied on these earlier estimates and scale their numbers to the evasion estimates to the lower end surface area of 1,002x10³ to obtain a mean flux of 33 Tg CH₄ yr⁻¹ (Rosentreter et al.,

Supprimé: (±c.i. 95%)

Supprimé: ;

Supprimé: (±95% C.I.)

Supprimé: ~

Supprimé: 95% C.I.

2021). Johnson et al. (2022) estimated a surface area of only 166x103 km² for this size class to obtain an efflux of 6.3 Tg CH₄ yr⁻¹, which we acknowledge as a lower limit. Averaging these two values provide a conservative estimate of 20 [6-33] Tg CH₄ yr⁻¹, which is close to the number proposed by Holgerson and Raymond (2016) for diffusion effluxes only for this size class. The experts involved in this assessment have low confidence in this estimate. This estimate also does not include artificial ponds, which we discuss below. As a result, combined CH₄ emissions from large lakes (>0.1 km²) and small lakes and ponds (<0.1 km²) are estimated at 53 [19-86] Tg CH₄ yr⁻¹ (Figure 4), which is lower than the 71 Tg estimated in the previous budget.

Reservoirs. New mean estimates of diffusive + ebullitive CH₄ emissions from reservoirs include 15 and 24±8 (the median and mean±c.i. 95% from Rosentreter et al., 2021), 10±4 (Johnson et al., 2021, mean±95% C.I.), 10 (Harrison et al., 2021, low and high c.i. 95% 7 and 22, respectively), and 2.1 Tg CH₄ yr⁻¹ (Zhuang et al., 2023). We compile the first three estimates to a direct efflux of ~14 Tg CH₄ yr⁻¹ (with ±c.i. 95% of 9 and 23). We note the fourth estimate as a lower bound, but exclude it from this budget given that it was generated via a model that only included data from six reservoir systems (Zhuang et al., 2023). We also add in an additional 12 Tg CH₄ yr⁻¹ (c.i. 95% 7 and 37) that is estimated to degas in dam turbines (Harrison et al., 2021), which was not addressed in the studies by Rosentreter et al. (2021), Zhuang et al. (2023), or Johnson et al. (2021). Rocher-Ros et al. (2023) also excluded river observations below dams when executing their statistical model, and so did not capture downstream dam emissions. Thus, we use a direct reservoir emission here of ~13 [6-28] Tg CH₄ yr⁻¹ and estimate an additional ~12 [7-37] Tg CH₄ yr⁻¹ from dam turbine degassing fluxes, giving a total of 25 [13-65] Tg CH₄ yr⁻¹ from reservoirs (Figure 4).

Uncertainties and confidence levels. The emission estimates of lakes, reservoirs and ponds described above are limited by several uncertainties. First, a major unknown for lakes remains the size cut off and the representation of small lakes and ponds (Deemer and Holgerson, 2021), which are also more variable than larger water bodies in their CH₄ concentrations and fluxes (Rosentreter et al. 2021, Ray et al., 2023). Interestingly, there is also a lack of methane data representation from large lakes that are a large component of global lake surface area (Deemer and Holgerson, 2021; Messenger et al., 2016). There is also a growing knowledge base on the importance of high CH₄ fluxes from lake littoral zones that is not yet well incorporated into global scaling efforts (e.g., Grinham et al., 2011; Natchimuthu et al., 2016), and emergent vegetation (Bastviken et al., 2023; Kyzivat et al., 2022). Ebullition is more constrained in lakes/reservoirs compared to streams/rivers but is still difficult to measure and model accurately. Finally, for all inland water systems a greater scrutiny for the limiting factors (including the impact of ice-cover and seasonality, stratification of the water column) of different CH₄ production, consumption and transport pathways is needed. In addition, a better understanding of the climatic, environmental and geomorphological controls on key CH₄ processes (e.g., sedimentary diffusive and ebullitive production, bubble dissolution, CH₄ oxidation) on the large-scale remains critically needed. For instance, the consistently lower global emissions determined

Supprimé: ,000

Supprimé: ~

Supprimé: both

Mis en forme : Non Exposant/ Indice

Supprimé: on average

Supprimé: ±95% C.I.

Supprimé:

Supprimé: 95% CI

Supprimé: ±95% C.I.

Supprimé: 95% C.I.

Mis en forme : Français

Supprimé: aquatic

Supprimé: of the regulation

Supprimé: emission

1131 by the process-based model of Zhuang et al. (2023) compared to observations, suggest that current datasets are too limited
1132 to fully capture the spatio-temporal variability in CH₄ dynamics and their key control factors, possibly leading to biased-
1133 high estimates.

1134 The majority of the inland water CH₄ estimates are from a limited number of studies, some without spatial representation or
1135 reported statistical uncertainties. Furthermore, as mentioned above the knowledge base of the surface area of these
1136 ecosystems is new and rapidly expanding, but not standardised between studies leading to uncertainty (but see Lauerwald
1137 et al. 2023b), particularly for ponds. For this study, we are able to provide confidence intervals from the original studies for
1138 all fluxes except the smallest lake/pond size class.

1139
1140 **The Surface Area of Inland Freshwaters.** For all of these ecosystems, determining their surface area remains a central
1141 challenge. Since the last GMB, several methodological advances have reduced the uncertainty associated with the surface
1142 area estimates of rivers, streams, lakes, and reservoirs. Using a single geospatial dataset that includes both lakes and
1143 reservoirs (Messenger et al., 2016) has decreased double counting of lakes and reservoirs (Johnson et al., 2022; Rosentreter
1144 et al., 2021). For rivers and streams, high-resolution global streamflow simulations, informed by satellite observations,
1145 enabled a much finer scale estimate of surface areas for rivers with a new temporal component (Allen and Pavelsky, 2018;
1146 Lin et al., 2019; Liu et al., 2022), although the surface for the smaller streams are still estimated indirectly, and mapping of
1147 human-created drainage ditches and canals is lacking. Seasonal ice cover and melt turnover corrections also have been newly
1148 incorporated into rivers, streams, lakes, and reservoirs (Harrison et al., 2021; Johnson et al., 2022; Lauerwald et al., 2023b;
1149 Rocher-Ros et al., 2023; Rosentreter et al., 2021; Zhuang et al., 2023). Finally, removing open water body surface areas
1150 from wetland surface areas based on geographic location has reduced double counting between these two land cover types,
1151 as described in the wetlands section of the GMB. Yet, the surface area of small lakes and ponds (<0.1 km²) is still highly
1152 uncertain, and new techniques for counting these systems and determining the overlap with wetland data bases is paramount.

1153
1154 **Anthropogenic Contributions to Inland Freshwater Emissions.** We argue that all reservoirs should be categorised as a
1155 direct anthropogenic source of emissions. Most of the surface area of reservoirs are human-made and reservoir construction
1156 leads to anoxic sediments and/or bottom waters with labile organic matter sourced from the watershed and to in-situ nutrient
1157 augmented phytoplankton production (Deemer et al., 2016; Maavara et al., 2017; Prairie et al., 2018). It is also clear that the
1158 cultural eutrophication of natural lakes driven by run-off of agricultural nitrogen fertilizer and manure is augmenting
1159 CH₄ emissions (DelSontro et al., 2018; Li et al., 2021), with shallow lakes particularly likely to experience eutrophication
1160 (Qin et al., 2020). For instance, Beaulieu et al. (2019) modelled a 15% reduction in lake CH₄ with a 25% reduction in lake
1161 phosphorus concentrations. Several recent studies have estimated that anywhere between 30 and 50% of lakes are eutrophic
1162 (Cael et al., 2022; Qin et al., 2020; Sayers et al., 2015; Wu et al., 2022). These studies estimate numerical percentages (one
1163 by depth class: Qin et al., 2020), but none have estimated the percent of lake surface area that is eutrophic nor have any

Supprimé: n

1165 determined the extent of anthropogenic vs. natural eutrophication. Still, numerous studies have noted widespread increases
 1166 in eutrophication indicators across lakes due to nutrient loading and warming (Griffiths et al., 2022; Ho et al., 2019; Taranu
 1167 et al., 2015), thus we estimate that $\frac{1}{3}$, or 11 Tg CH₄ yr⁻¹ of CH₄ emissions from lakes >0.1 km² could be anthropogenic
 1168 (Figure 4). Similarly, CH₄ emissions from small lakes and ponds are influenced by human factors, with emissions increasing
 1169 with eutrophication (Deemer and Holgerson, 2021), erosion and runoff in agricultural landscapes (Heathcote et al., 2013),
 1170 and warming, the latter likely to have a disproportionately greater effect in small, shallow systems (Woolway et al., 2016).
 1171 Thus, we adopt the same $\frac{1}{3}$ number as for lakes for the proportion of anthropogenic emissions in small lakes and ponds
 1172 (<0.1 km²), which amounts to 6 Tg CH₄ yr⁻¹ (Figure 4).
 1173 There are also human-made small lakes and ponds, notably for agriculture, aquaculture, and recreation, that generally have
 1174 conditions favourable for high CH₄ emissions (Downing, 2010; Holgerson and Raymond, 2016; Malerba et al., 2022;
 1175 Ollivier et al., 2019; Zhao et al., 2021; Dong et al., 2023). Downing (2010) estimated that farm ponds comprise a global
 1176 surface area of ~77,000 km²; using a conservative emission rate of 265 mg CH₄ m⁻² d⁻¹ and an ice correction factor of 0.6
 1177 leads to an emission of 4.5 Tg yr⁻¹ that is anthropogenically sourced from farm ponds. Here the value is rounded to 5 Tg yr⁻¹
 1178 (Figure 4). Clearly, more work is required to assess the anthropogenic component of CH₄ emissions from lakes and ponds.
 1179 It remains difficult to parse out an anthropogenic component to stream and river CH₄ fluxes. Although some studies have
 1180 noticed a temperature dependence with stream sediments (Comer-Warner et al., 2018; Zhu et al., 2020), Rocher-Ros et al.
 1181 (2023) noted a small temperature dependence of CH₄ emissions in streams and rivers compared to other freshwater
 1182 ecosystems, potentially due to the many other external processes affecting fluxes in these dynamic flowing ecosystems.
 1183 Urbanisation can lead to elevated river CH₄ emissions, particularly in regions with elevated organic matter and nutrient
 1184 loading due to limited wastewater treatment (Begum et al., 2021; Nirmal Rajkumar et al., 2008; Wang et al., 2021a). Some
 1185 studies have found agricultural streams and ditches can have higher effluxes due to inputs of fine sediments (Comer-Warner
 1186 et al., 2018; Crawford and Stanley, 2016), organic carbon, and nutrients (Borges et al., 2018) that lead to in-situ methane
 1187 production. Furthermore, the creation of drainage ditches in organic soils tap CH₄ rich waters from water-logged horizons
 1188 and heighten emissions from ex-situ sources (Peacock et al., 2021), although limitations in both the geographic scope of
 1189 existing ditch emission estimates our ability to estimate global surface area of ditches precludes their inclusion in this budget.
 1190 Finally, extremely high rates of CH₄ emission have been linked to ongoing permafrost thaw in Asia's Qinghai-Tibet Plateau
 1191 (Zhang et al., 2020). However, the loss and disconnection of wetlands to rivers may have resulted in a decrease in the input
 1192 of dissolved CH₄ from this source. A recent expert elicitation (Rosentreter, et al. 2024) reported that 35% of all inland
 1193 freshwater sources were anthropogenic and given that some of the river flux is from upstream reservoirs, we assign a 30%
 1194 anthropogenic contribution to the stream and river flux (9 Tg CH₄ yr⁻¹, Figure 4), which approximates the expert elicitation
 1195 via the impact of eutrophication and urban influences.
 1196

Supprimé: submitted

1198 **Combination (lakes, ponds, reservoirs, streams and rivers, farm ponds).** Combining the aforementioned emissions from
1199 lakes $>0.1 \text{ km}^2$ (33 [13-53] $\text{Tg CH}_4 \text{ yr}^{-1}$), small lakes and ponds $<0.1 \text{ km}^2$ (20 [6-33] $\text{Tg CH}_4 \text{ yr}^{-1}$), reservoirs (25 [13-65]
1200 $\text{Tg CH}_4 \text{ yr}^{-1}$), streams and rivers (29 [12-46] $\text{Tg CH}_4 \text{ yr}^{-1}$) and farm ponds (5 $\text{Tg CH}_4 \text{ yr}^{-1}$), leads to a total of $\sim 112 \text{ Tg CH}_4$
1201 yr^{-1} from freshwater systems, with a range of [49-202] $\text{Tg CH}_4 \text{ yr}^{-1}$. This estimate is about 50 Tg lower than in Sauniois et
1202 al. (2020) and is broadly consistent with the recent regionalized estimate by Lauerwald et al. (2023b) compiled for the
1203 Regional Carbon Cycle Assessment and Processes (RECCAP2, <https://www.globalcarbonproject.org/reccap/>; 103 Tg CH_4
1204 yr^{-1} , IQR= 82.1–134.8). The updated budget from these ecosystems and their anthropogenic components are represented in
1205 Fig. 4. The gridded products for emissions from lakes and ponds by Johnson et al. (2022), from reservoirs by Johnson et al.
1206 (2021) and from streams and rivers by Rocher-Ros et al. (2023) have been combined into a single map presented in Fig. 5.
1207
1208 **Double-counting inland freshwater ecosystems in the bottom-up estimates.** To address the differences found between
1209 bottom-up and top-down CH_4 budgets, and to acknowledge advances in addressing the central issue of double counting CH_4
1210 emissions for inland freshwater ecosystems, we introduce here a new correction term. Historically, the bottom-up estimate
1211 of global CH_4 emissions has been higher than the top-down estimate, first recognized in Kirschke et al. (2013) and confirmed
1212 in Sauniois et al. (2016, 2020). The larger bottom-up emissions estimate has been partly attributed to double-counting
1213 vegetated wetland emissions with inland freshwater emissions (including lakes, ponds, rivers, streams, and reservoirs) and
1214 also the emissions of CH_4 produced in vegetated wetlands and then transported via aquatic processes and emitted from
1215 inland freshwaters (Pangala et al., 2017; Kirk and Cohen, 2023). The Sauniois et al. (2020) CH_4 budget addressed the issue
1216 of double counting through the use of a revised vegetated wetland area dataset, WAD2M v1.0 (Zhang et al., 2021), that
1217 removed inland waters from the SWAMPS (Jenson and McDonald, 2019) surface-inundation dataset, allowing for
1218 independent vegetated wetlands and inland freshwater CH_4 emissions to be compiled. Yet, the Sauniois et al. (2020) CH_4
1219 budget still had a $\sim 150 \text{ Tg CH}_4 \text{ yr}^{-1}$ difference between bottom-up and top-down estimates. In this budget, we refined the
1220 vegetated wetland area dataset with WAD2M v2.0 (see section 3.2.1, where HydroLakes is used to remove lakes and ponds
1221 $>0.1 \text{ km}^2$). Additionally, we applied numbers from peer-reviewed publications and expert elicitation to account for lateral
1222 CH_4 flux emissions. This most recent bottom-up budget estimates 159 [119-203] $\text{Tg CH}_4 \text{ yr}^{-1}$ from vegetated wetlands for
1223 2010-2019 and 112 $\text{Tg CH}_4 \text{ yr}^{-1}$ from inland freshwaters that includes 83 $\text{Tg CH}_4 \text{ yr}^{-1}$ from lakes, ponds, and reservoirs and
1224 29 $\text{Tg CH}_4 \text{ yr}^{-1}$ from rivers and streams, leading to a combined wetland and inland freshwater flux of 271 $\text{Tg CH}_4 \text{ yr}^{-1}$. Here,
1225 we propose a correction of 20 $\text{Tg CH}_4 \text{ yr}^{-1}$ to account for double counting of small lakes and ponds ($<0.1 \text{ km}^2$) that are
1226 likely included in our vegetated wetlands estimate, and removing 1-3 $\text{Tg CH}_4 \text{ yr}^{-1}$ from river emissions due to lateral
1227 transport of CH_4 originating in adjacent vegetated wetlands. The river flux correction arises from assuming that for
1228 catchments with $>10\%$ wetlands, rivers provide 5-10% of vegetated CH_4 emissions. The total double-counting correction
1229 term of 23 Tg CH_4 reduces the bottom-up budget for combined wetlands and inland waters from 271 $\text{Tg CH}_4 \text{ yr}^{-1}$ to 248 Tg
1230 $\text{CH}_4 \text{ yr}^{-1}$ (see Fig. 4 and Table 3). Comparing the 2000-2009 decadal emissions from wetlands and inland freshwater

Supprimé: ~

Supprimé: o

Supprimé: aquatic

Supprimé: BU

Supprimé: BU

ecosystems across the last three previous assessments of the budget shows a significant downward revision with 305 (183+122) Tg CH₄ yr⁻¹, 356 (147+209) Tg CH₄ yr⁻¹ and 248 (159+112-23) Tg CH₄ yr⁻¹ (respectively from Saunio et al. (2016; 2020) and this work).

Finally, it is worth noting that inland freshwater ecosystems can overlap with geological seepage systems in some areas, i.e., they may occur in correspondence with geological structures that emit fossil (microbial, thermogenic, or abiotic) CH₄ generated in the Earth's crust. Examples have been documented in the Fisherman Lake in Canada (Smith et al., 2005), in the Baikal lake (Schmid et al, 2007), and in rice paddies in Japan (Etiope et al., 2011). Thus, some gas emissions in freshwater environments, particularly as bubble plumes, can be incorrectly attributed to modern biological (ecosystem) activities if appropriate isotopic and molecular analyses are not performed.

3.2.3 Onshore and offshore geological sources

Significant amounts of CH₄, produced within the Earth's crust, naturally migrate to the atmosphere through tectonic faults and fractured rocks. Major emissions are related to hydrocarbon formation in sedimentary basins (microbial and thermogenic methane), through continuous or episodic exhalations from onshore and shallow marine hydrocarbon seeps and through diffuse soil microseepage (Etiope, 2015). Specifically, five source categories have been considered. Four are onshore sources: gas-oil seeps, mud volcanoes, diffuse microseepage, and geothermal manifestations including volcanoes. One source is offshore: submarine seepage, which may include the same types of gas manifestations occurring on land. Etiope et al. (2019) have produced the first gridded maps of geological CH₄ emissions and their isotopic signature for these five categories, with a global total of 37.4 Tg CH₄ yr⁻¹ (reproduced in Fig. 5). However, these maps are based on incomplete data on geological sites due to missing information and difficulties in defining all current geological emitting sites. Combining the best estimates for the five categories of geological sources (from grid maps or from previous statistical and process-based models), the breakdown by category reveals that onshore microseepage dominate (24 Tg CH₄ yr⁻¹), the other categories having similar smaller contributions: as mean values, 4.7 Tg CH₄ yr⁻¹ for geothermal manifestations, about 7 Tg CH₄ yr⁻¹ for submarine seepage and 9.6 Tg CH₄ yr⁻¹ for onshore seeps and mud volcanoes. These values lead to a global bottom-up geological emission mean of 45 [27-63] Tg CH₄ yr⁻¹ (Etiope and Schwietzke, 2019).

While all bottom-up and some top-down estimates, following different and independent techniques from different authors, consistently suggest a global geo-CH₄ emission in the order of 40-50 Tg yr⁻¹, the radiocarbon (¹⁴C-CH₄) data in ice cores reported by Hmiel et al. (2020) appear to give a much lower estimate, with a minimum of about 1.6 Tg CH₄ yr⁻¹ and a maximum value of 5.4 Tg CH₄ yr⁻¹ (95 percent confidence) for the pre-industrial period. [Dyonisius et al. \(2020\) also suggest a low range of geological emissions over the last deglaciation period and for the late Holocene \(0-10 Tg CH₄ yr⁻¹\)](#). The discrepancy between Hmiel et al. (2020) and all other estimates has been discussed in Thornton et al. (2021), which demonstrated that the global near-zero geologic CH₄ emission estimate in Hmiel et al. (2020) is incompatible with the sum of multiple independent bottom-up estimates, based on a wide variety of methodologies, from individual natural geological

Supprimé:

1269 seepage areas: for example, from the Black Sea (up to 1 Tg CH₄ yr⁻¹), the Eastern Siberian Arctic Shelf (ESAS, up to 4.6
1270 Tg CH₄ yr⁻¹, referring mostly to thermogenic gas), onshore Alaska (up to 1.4 Tg CH₄ yr⁻¹) and a single seepage site in
1271 Indonesia (releasing 0.1 Tg CH₄ yr⁻¹ as estimated by satellite measurement) (see Thornton et al. (2021) and references
1272 therein). Jackson et al. (2020) expressed doubt about the low Hmiel et al. (2020) estimates, noting that they are difficult to
1273 reconcile with the results of many other researchers and with bottom-up approaches in general. This discrepancy highlights
1274 another main unresolved uncertainty in the methane budget and calls for further investigations to reconcile the different
1275 estimates, and reduce the uncertainty on geological emissions. ~~Waiting for further investigation to better understand~~
1276 discrepancies between radiocarbon approaches and other studies, we decided to keep the estimates from Etiope and
1277 Schwiethzke (2019) for the mean values, and associate it to the lowest estimates reported in Etiope et al. (2019), as in Saunio
1278 et al. (2020). Thus, we report a total global geological emission of 45 [18-63] Tg CH₄ yr⁻¹, with a breakdown between
1279 offshore emissions of 7 [5-10] Tg CH₄ yr⁻¹ and onshore emissions of 38 [13-53] Tg CH₄ yr⁻¹ (Table 3), similar to Saunio et
1280 al. (2020). This bottom-up estimate is slightly lower than in the Saunio et al. (2016) budget mostly due to a reduction of
1281 estimated emissions of onshore and offshore seeps (see Sect. 3.2.6 for more offshore contribution explanations).

1282 **3.2.4 Termites**

1283 Termites are decomposers playing a central role in ecosystem nutrient fluxes at tropical and subtropical latitudes, in
1284 particular (Abe et al., 2000). Termites represent a natural CH₄ source due to methanogenesis occurring in their hindgut
1285 during the symbiotic metabolic breakdown of lignocellulose (Sanderson, 1996; Brune, 2014). The upscaling of CH₄
1286 emissions from termites from site to global level is characterised by high uncertainty (Sanderson, 1996; Kirschke et al.,
1287 2013; Saunio et al., 2016) due to the combination of factors that need to be considered and the scarcity of information for
1288 each of these factors for global upscaling. Needed data include termite biomass density (Sanderson, 1996), species
1289 distribution within and among ecosystems (Sugimoto et al., 1998), variation of termite CH₄ emission rates per species and
1290 dietary group (Sanderson, 1996), the role played by the termite mound structure in affecting the fraction of produced CH₄
1291 that is effectively released into the atmosphere (Sugimoto et al., 1998; Nauer et al., 2018). In Kirschke et al. (2013) and
1292 Saunio et al. (2016) a global upscaling of termite CH₄ emissions was proposed, where CH₄ emissions, E_{CH₄} (kg CH₄ ha⁻¹yr⁻¹),
1293 were estimated as the product of three terms: termite biomass (Bi_{TERM} g fresh weight m⁻²), a scalar correction factor
1294 (LU) expressing the effect of land use/cover change on termite biomass density, a termite CH₄ emission factor (EF_{TERM}, µg
1295 CH₄ g⁻¹ Bi_{TERM} h⁻¹). The approach between the two re-analyses of CH₄ emissions varied only for the data sources of gross
1296 primary productivity (GPP) and land use which were used to attribute biomass values of termite per ecosystem surface unit,
1297 in order to cover different time spans, 1980s, 1990s and 2000s in Kirschke et al. (2013) and 2000-2007 and 2010-2016 in
1298 Saunio et al. (2016). For the present update, additional changes have been introduced compared with the previous versions.
1299 Here we summarise the key data used for the new upscaling. CH₄ fluxes were modelled between 45°S and 45°N and within
1300 35°S and 35°N. The termite biomass density, Bi_{TERM}, for tropical ecosystems was estimated as function (Kirschke et al.,

Supprimé: community

Supprimé:

Mis en forme : Non Exposant/ Indice

1303 2013; $\text{BioTERM} = 1.21 \cdot e^{0.0008 \cdot \text{GPP}}$ of the gross primary production (GPP, $\text{g C m}^{-2} \text{ yr}^{-1}$) using the 0.25° native resolution
 1304 VODCA2GPP dataset covering the period 2001-2020 (Wild et al., 2022). Wetlands, barren areas, water bodies and artificial
 1305 surfaces were excluded from this estimation and set as no data (no emissions). The scalar correction factor LU of 0.4 (60%)
 1306 for agricultural areas (i.e., croplands) (Kirschke et al., 2013) was applied to the GPP value of the nearest natural areas to
 1307 account for anthropic disturbance. The annual (2001-2020) land cover information was obtained from the MODIS
 1308 Terra+Water Combined Land Cover product (MCD12C1v006; <https://lpdaac.usgs.gov/products/mcd12c1v006/>), using the
 1309 International Geosphere-Biosphere Programme (IGBP) classification with a 0.05° spatial resolution. For desert and arid lands,
 1310 within 35°S and 35°N , a fixed BioTERM value of 1.56 g m^{-2} was instead used (Sanderson, 1996; Hedě́nec et al., 2022).
 1311 Similarly, fix values from the few available studies reported in literature were used to estimate BioTERM between 35° - 45° N
 1312 and 35° - 45° S as follows: 1.83 g m^{-2} for temperate forests and grasslands (Wood and Sands, 1978; Petersen and Luxton,
 1313 1982; Sanderson, 1996; Bignell and Eggleton, 2000; King et al., 2013; conversion factor from dry to fresh biomass is 0.27
 1314 from Petersen and Luxton, 1982), 5.3 g m^{-2} for scrublands and Mediterranean areas of Australia (Sanderson, 1996), 1.09 g
 1315 m^{-2} for the other Mediterranean shrubland ecosystems (Hedě́nec et al., 2022). Other climates and land covers were set as no
 1316 data. Climate zoning was defined using the Climate Zones Köppen-Geiger dataset (Beck et al., 2018), this product is
 1317 representative for the 1980-2016 time period and has a 0.0083° native resolution. The EF_{TERM} was revised compared with
 1318 previous estimates (Kirschke et al., 2013; Saunio et al., 2016), in order to consider the different distribution of termite
 1319 families and subfamilies in the different continents and ecosystems, characterised by different feeding habits and nest
 1320 typologies, as reported by Sugimoto et al. (1998), which might influence the EF. The species of each family and subfamily
 1321 of the two major groups of lower and higher termites, listed by Sugimoto et al. (1998) were associated with EF values based
 1322 on emissions from in-vitro experiments as reported by Sanderson (1996) and Eggleton et al. (1999), to which a correction
 1323 factor (cf_{MOUND}) of 0.5 (Nauer et al., 2018; Chiri et al., 2020; 2021) was applied in order to take into account the mound
 1324 effect on the CH_4 produced by termites, once inside the nest. The average EF_{TERM} for tropical and temperate areas was hence
 1325 estimated as the weighted EF_{TERM} derived from the product of the percentage weight of each family or subfamily of termites
 1326 in the “community composition” in each geographical area and ecosystem (Sugimoto et al. (1998, Table 6), the respective
 1327 calculated EF of each family or subfamily, a scalar or correction factor which considers the nest type (as in Table 5 from
 1328 Sugimoto et al. 1998). For desert and arid lands and temperate areas, which were not reported in Sugimoto et al. (1998), EF
 1329 rates were calculated directly from data reported in literature for the most representative species which were the genus
 1330 *Amitermes* for the former (EF from data by Sanderson 1996, Eggleton et al. 1999, Jamali et al. 2011) and the genus
 1331 *Reticulitermes* (family Rhinotermitidae) for the latter (EF from data by Odelson and Breznak, 1983; Sanderson, 1996;
 1332 Eggleton et al., 1999; Myer et al., 2021). The following EF_{TERMS} were hence obtained to scale up emissions: $3.26 \pm 1.79 \mu\text{g}$
 1333 $\text{CH}_4 \text{ g}^{-1} \text{ termite h}^{-1}$ ($28.56 \text{ mg CH}_4 \text{ g}^{-1} \text{ termite year}^{-1}$) for tropical ecosystems, $1.82 \pm 1.54 \mu\text{g CH}_4 \text{ g}^{-1} \text{ termite h}^{-1}$ for temperate
 1334 forests, grasslands, and Mediterranean areas, $1.24 \pm 1.22 \mu\text{g CH}_4 \text{ g}^{-1} \text{ termite h}^{-1}$ for deserts and arid lands (warm climate).
 1335 Annual CH_4 fluxes were computed for all the years from 2001 to 2020 producing 20 global maps at 0.05° resolution of

1336 yearly total emissions. A further map of the estimated error representative of the entire time period was elaborated at the
1337 same resolution as the emissions dataset.

1338 Termite CH₄ emissions over the period 2001-2020 varied between 9.7-10.8 Tg CH₄ yr⁻¹, with an average of 10.2 ± 6.2 Tg
1339 CH₄ yr⁻¹. Considering a 20-year average, tropical and subtropical moist broadleaf forests contributed to 46% of the total
1340 average flux, while tropical and subtropical grasslands, savannas, and shrublands to another 36%. In terms of regional
1341 contribution, 37.2% of fluxes were attributed to South America, 31.5% to Africa, 18.1% to Asia, 5.5% to Australia, 7.4%
1342 to North America and less than 1% to Europe. The present estimate value is within the range of previous up-scaling studies,
1343 spanning from 2 to 22 Tg CH₄ yr⁻¹ (Ciais et al., 2013). In this study, we report a decadal value of 10 Tg CH₄ yr⁻¹ with a
1344 range of [4-16] (Table 3).

1345 **3.2.5 Wild animals**

1346 Wild ruminants emit CH₄ through microbial fermentation that occurs in their rumen, similarly to domesticated livestock
1347 species (USEPA, 2010b). Using a total animal population of 100-500 million, Crutzen et al. (1986) estimated the global
1348 emissions of CH₄ from wild ruminants to be in the range of 2-6 Tg CH₄ yr⁻¹. More recently, Pérez-Barbería (2017) lowered
1349 this estimate to 1.1-2.7 Tg CH₄ yr⁻¹ using a total animal population estimate of 214 million (range of 210-219), arguing that
1350 the maximum number of animals (500 million) used in Crutzen et al. (1986) was poorly justified. Moreover Pérez-Barbería
1351 (2017) also stated that the value of 15 Tg CH₄ yr⁻¹ found in the last IPCC reports is much higher than their estimate because
1352 this value comes from an extrapolation of Crutzen's work for the last glacial maximum when the population of wild animals
1353 was much larger, as originally proposed by Chappellaz et al. (1993). Recently, based on the modelling of grassland extent,
1354 Kleinen et al. (2023) also suggest that the population of wild animal during the last glacial maximum proposed by Crutzen
1355 et al. (1986) and further used by Chappellaz et al. (1993) were overestimated. However, the estimate of 1-3 Tg CH₄ yr⁻¹
1356 seems underestimated when considering that Hempson et al. (2017) found actual CH₄ emissions from African wildlife alone
1357 to be around 9 Tg CH₄ yr⁻¹ but without discussing the uncertainty of this value. As a result, high uncertainty remains and
1358 recalls the need for further investigation of this natural source of CH₄.

1359 Based on these findings and waiting for further global estimates, the range adopted in this updated CH₄ budget is 2 [1-3] Tg
1360 CH₄ yr⁻¹ (Table 3).

1361 **3.2.6 Coastal and oceanic sources**

1362 Coastal and oceanic sources comprise CH₄ release from estuaries, coastal vegetated habitats, as well as marine waters
1363 including seas and oceans. Possible sources of coastal and oceanic CH₄ include (1) in-situ biogenic production through
1364 various pathways in oxygenated sea-surface waters (Oremland, 1979; Karl et al., 2008; Lenhart et al., 2016; Repeta et al.,
1365 2016), a flux that can be enhanced in the coastal ocean because of submarine groundwater discharge (USEPA, 2010b); (2)
1366 production from shallow and marine (bare and vegetated) sediments including free gas or destabilised hydrates and thawing

Mis en forme : Non Exposant/ Indice

1367 subsea permafrost containing modern (¹⁴C-bearing) microbial gas; (3) geological marine seepage (see also Sect. 3.2.3),
1368 including hydrates, containing fossil (¹⁴C-free) microbial or thermogenic CH₄. CH₄ produced in marine sediments and
1369 seabed CH₄ seepage can be transported across the water column to the sea-surface by upwelling waters (once at the surface
1370 methane can cross the sea-air interface via diffusion) and gas bubble plumes (for instance from geological marine seeps;
1371 e.g., Judd, 2004; Etiope et al., 2019). Gas bubble plumes generally reach the atmosphere in relatively shallow waters (<400
1372 m) of continental shelves depending on the intensity of the events (e.g., Westbrook et al., 2009); however massive deep-
1373 water seepage events could contribute a significant amount of CH₄ to the atmosphere, even from depths > 1000 m (e.g.,
1374 Schmale et al., 2005.; Greinert et al., 2006; Solomon et al., 2009). In coastal vegetated habitats, CH₄ can also be transported
1375 to the atmosphere through the aerenchyma of emergent aquatic plants (Purvaja et al., 2004).
1376 We distinguish between coastal and oceanic “geological” and “modern biogenic” CH₄ sources. Coastal and oceanic
1377 “geological” emissions refer to CH₄ seepage from the Earth’s crust (mostly in hydrocarbon-rich sedimentary basins), which
1378 is typically evaluated by combining geochemical analyses (isotopic and molecular, including radiocarbon, ¹⁴C, analyses)
1379 and geological observations (degassing along faults, seeps, mud volcanoes). Geological emissions do not contain modern
1380 biogenic gas that is fossil (¹⁴C-free). Coastal and oceanic “biogenic” CH₄ refers to CH₄ formed *in situ* in coastal and marine
1381 sediments and in the water column by recent or modern microbial activity (therefore with measurable amounts of
1382 radiocarbon (¹⁴C)). To avoid double-counting, we assume that all diffusive CH₄ emissions outside of geological seepage
1383 regions (identified in global grid maps; Etiope et al., 2019) are fuelled by biogenic CH₄. Finally, we briefly discuss the case
1384 of CH₄ hydrates, which can be considered either a “geological” source when they host fossil CH₄ or a “biogenic” source
1385 when they host modern CH₄.
1386 **Coastal and oceanic modern biogenic methane emissions.** Area-integrated diffusive modern biogenic CH₄ emissions
1387 from coastal ecosystems are 1-2 magnitudes lower than from inland freshwaters but significantly higher than biogenic
1388 emissions from the open ocean (Rosentreter et al., 2021; Rosentreter et al., 2023; Weber et al., 2019). Particularly the shallow
1389 vegetated coastline fringed by mangroves, salt marshes, and seagrasses is a CH₄ hotspot in the coastal ocean, characterised
1390 by significantly higher flux densities than other coastal settings such as estuaries or the continental shelves (Rosentreter et
1391 al., 2021; Rosentreter et al., 2023). Coastal ecosystems are thus being increasingly recognized as weak global sources to the
1392 atmosphere (Weber et al., 2019; Saunio et al., 2020; Rosentreter et al., 2021). Hydrogenotrophic and acetoclastic
1393 methanogenesis are largely outcompeted by sulphate reduction in coastal/marine sediments, which is often shown by a
1394 decreasing trend of CH₄ concentrations with increasing salinity from upper tidal (low salinity) to marine (high salinity)
1395 regions. Much of the CH₄ produced below the sulfate-reduction zone is indeed re-oxidized by sedimentary anaerobic
1396 methane oxidation or re-oxidized in the water column, leading to small emissions despite much larger production (Knittel
1397 and Boetius 2009; Regnier et al., 2011). Methylated compounds such as methylamines and methyl sulphides are non-
1398 competitive substrates that are exclusively used by methanogens, therefore methylated methanogenesis can occur in coastal
1399 regions with high sulphate concentrations, for example, in organic-rich (Maltby et al., 2018), vegetated (Schorn et al., 2022),

Supprimé: can

Supprimé: (but not exclusively, as described below)

Supprimé: and coastal zones

1403 and hypersaline coastal sediments (Xiao et al., 2018). Coastal CH₄ can be driven by the exchange of pore water or
1404 groundwater (high in CH₄) with coastal surface waters in tidal systems, referred to as tidal pumping (Ovalle et al., 1990;
1405 Call et al., 2015). Anthropogenic impacts such as wastewater pollution and land-use change can increase CH₄ fluxes in
1406 estuaries (Wells et al., 2020). A large increase of CH₄ emissions follows the conversion of natural coastal habitats to
1407 aquaculture farms (Yuan et al., 2019; Yang et al., 2022).

1408 Currently available global modern biogenic CH₄ flux data show high spatiotemporal variability within and between coastal
1409 systems, but also because of the overall global paucity of data. Therefore, global estimates have high uncertainties and show
1410 large ranges in both empirical (Rosentreter et al., 2021) and machine-learning based approaches (Weber et al., 2019).
1411 According to a recent data-driven meta-data analysis, global estuaries, including tidal systems and deltas, lagoons, and
1412 fjords, are estimated to emit median (Q1-Q3) 0.25 (0.07-0.46) Tg CH₄ yr⁻¹ (Rosentreter et al., 2023). Coastal vegetation,
1413 including mangrove forests, salt marshes, and seagrasses are estimated to emit 0.77 (0.47-1.41) Tg CH₄ yr⁻¹, which is 3
1414 times more than global estuaries (Rosentreter et al., 2023). The combined median (Q1-Q3) emission of 1.01 (0.54-1.87) Tg
1415 CH₄ yr⁻¹ for coastal vegetation and estuaries by Rosentreter et al. (2023) is lower than the recent observation-based global
1416 synthesis including tidal flats and aquaculture ponds (median 1.49 (0.22-6.48) Tg CH₄ yr⁻¹) by Rosentreter et al. (2021).
1417 Total shallow coastal modern biogenic CH₄ emissions based on existing data including emissions from estuaries, coastal
1418 vegetation (Rosentreter et al., 2023), tidal flats, and man-made coastal aquaculture ponds (Rosentreter et al., 2021) amount
1419 to median (Q1-Q3) 1.8 (0.59-5.57) Tg CH₄ yr⁻¹. This range is about 3-4 times lower than the earlier global assessment by
1420 Borges and Abril (2011) and also lower than the value of 4-5 Tg CH₄ yr⁻¹ reported in the previous CH₄ budget for inner and
1421 outer estuaries including marshes and mangroves (Saunois et al., 2020), which was based on a significantly smaller dataset
1422 (n=80) and larger estuarine surface areas (Laruelle et al., 2013) than used here (Laruelle et al., 2023).

1423 The near-shore (0-50 m), inner shelf diffusive modern biogenic CH₄ flux of median (Q1-Q3) 1.33 (0.93-2.10) Tg CH₄ yr⁻¹
1424 by Weber et al. (2019) based on machine-learning is similar to the combined shallow coastal (estuaries and coastal
1425 vegetation) median by Rosentreter et al. (2021, 2023). Adding the diffusive modern biogenic CH₄ flux for the outer shelf
1426 (50-200 m) (median (Q1-Q3) of 0.54 (0.40-0.73) Tg CH₄ yr⁻¹) and for the slope (200-2000m) (median (Q1-Q3) of 0.28
1427 (0.22-0.37) Tg CH₄ yr⁻¹) (Weber et al., 2019), and excluding geological seepage regions (Etiope et al., 2019; see below),
1428 gives a total median (Q1-Q3) of 3.95 (2.14-8.77) Tg CH₄ yr⁻¹ for combined coastal shallow, near-shore, outer shelf and
1429 slope diffusive modern biogenic CH₄ emissions. The previous budget by Saunois (2020) also included poorly constrained
1430 emissions (upper bound value: 1-2 Tg CH₄ yr⁻¹) from large river plumes protruding onto the shelves. However, here we
1431 assume that emissions from large river plumes are accounted for in the near-shore and outer shelf estimates by Weber et al.
1432 (2019). Area-integrated diffusive CH₄ emissions from the open ocean and deep seas (>2000 m) are much lower than from
1433 other coastal systems but amount to median (Q1-Q3) 0.91 (0.75-1.12) Tg CH₄ yr⁻¹ because of the large surface area of the
1434 open ocean (>300 x 10⁶ km²) (Weber et al., 2019). Overall, these marine biogenic emissions are sustained by a mixture of
1435 sedimentary production and in-situ production in the sea-surface layers (including the methylphosphonate pathway), e.g.,

Supprimé: 3

Supprimé: , as shown by,

1438 Karl et al., 2008, Repeta et al., 2016, Resplandy et al., 2024). The total coastal and ocean diffusive modern biogenic
1439 emissions retained here amount to 5 (3-10) Tg CH₄ yr⁻¹ (Table 3).
1440
1441 **Coastal and oceanic geological methane emissions** Submarine geological CH₄ emission is the offshore component of the
1442 general geological emissions of natural gas from the Earth's crust (Judd, 2004; Etiope, 2009; Etiope et al., 2019). The
1443 onshore components include terrestrial seeps, mud volcanoes, microseepage, and geothermal manifestations, addressed in
1444 Sect. 3.2.3. Natural gas seeping at the seabed as bubble plumes can reach the surface in relatively shallow waters (<400 m),
1445 but CH₄-rich bubble plumes reaching the atmosphere from depths >500 m have been observed in some cases (e.g., Solomon
1446 et al., 2009), and upwelling of bottom marine waters can, in theory, transport geological CH₄ (dissolved) to the surface from
1447 any depth. This represents, however, a small and poorly known fraction of geological CH₄ emission. Geological CH₄ can be
1448 either microbial or thermogenic, produced throughout diverse geological periods in hydrocarbon source rocks in
1449 sedimentary basins (therefore it is always fossil, ¹⁴C-free). The seepage at the seafloor is typically related to tectonic faults,
1450 sometimes forming mud diapirs and mud volcanoes (Mazzini and Etiope, 2017). Published estimates of geological CH₄
1451 submarine emissions range from 3 to 20 Tg yr⁻¹, with a best guess of 7 Tg yr⁻¹ (Etiope and Schwietzke, 2019; Etiope et al.,
1452 2019 and references therein).
1453 Here, the diffusive geological CH₄ emissions are estimated at 0.16 (0.11-0.24) Tg CH₄ yr⁻¹ for near-shore (0-50 m), 0.03
1454 (0.02-0.05) Tg CH₄ yr⁻¹ for outer shelf (50-200 m), and 0.02 (0.01-0.03) Tg CH₄ yr⁻¹ for slope (200-2000 m) by calculating
1455 the fraction of the Weber et al. (2019) diffusive fluxes that occur within the identified geological seepage regions from
1456 Etiope et al. (2019). No geological seepage regions were identified in the open ocean and deep seas (> 2000 m).
1457 In this study, we consider the ebullitive flux as geologically sourced CH₄. While modern biogenic CH₄ gas production
1458 appears ubiquitous in shallow sediments (Fleischer et al., 2001; Best et al., 2006), no global dataset is currently available to
1459 estimate the biogenic ebullitive CH₄ flux to the atmosphere. Omission of this flux thus constitutes a significant knowledge
1460 gap in the coastal and oceanic CH₄ budget. Global geological CH₄ ebullition from continental shelf and slope, referring only
1461 to depths <200 m, were estimated at 5.06 (1.99-8.16) Tg CH₄ yr⁻¹ (Weber et al., 2019). This estimate is based on prior
1462 estimates of the geological flux from the seafloor (Hovland et al., 1993) and bubble transfer efficiency to the ocean surface
1463 (McGinnis et al., 2006). Etiope et al. (2019) estimated a partial fraction of geological emissions in the form of gas bubbles
1464 of 3.9 (1.8-6) Tg CH₄ yr⁻¹, only referring to the sum of published estimates from 15 geological seepage regions, which are
1465 also deeper than 200 m. Global extrapolation including other 16 identified seepage zones (where flux data are not available)
1466 was suggested to be at least 7 (3-10) Tg CH₄ yr⁻¹ (Etiope et al., 2019), and this value coincides with the mean emission value
1467 (best guess) derived by combining literature data, see Etiope and Schwietzke (2019) for further details. It is worth noting
1468 that the Weber et al. (2019) estimate of 5.06 (1.99-8.16) Tg CH₄ yr⁻¹, which considers only the continental shelf at depths
1469 <200 m, is compatible with the overall submarine emission of 7 (3-10) Tg CH₄ yr⁻¹ (including seeps > 200 m deep) indicated
1470 in Etiope and Schwietzke (2019) and Etiope et al. (2019). Although 300-400 m is considered a general depth limit for

Supprimé: (
Supprimé:)
Supprimé: and
Supprimé: (

Supprimé: , generally occurs

1476 efficient transport (with limited oxidation and dissolution) of CH₄ bubbles to the atmosphere (e.g., Judd, 2004; Schmale et
1477 al., 2005; Etiope et al., 2019), in some cases oil coatings on bubbles inhibit gas dissolution so that CH₄-rich bubbles can
1478 reach the atmosphere from depths >500 m (e.g., Solomon et al., 2009). As mentioned above, a fraction of geological CH₄
1479 released in deep seas (such as in the areas with gas-charged sediments inventoried in Fleischer et al., 2001) can also be
1480 transported to the surface by upwelling bottom waters. Further research is needed to better evaluate the atmospheric impact
1481 of such deep seeps.

1482 Geological submarine emissions, thus, would amount to 0.21 (0.14-0.32) Tg CH₄ yr⁻¹ in the form of a diffusive flux while
1483 the ebullitive flux would be 5.06 (3.01-7.88) Tg CH₄ yr⁻¹, considering only < 200 m deep seepage, and 7 (3-10) Tg CH₄ yr⁻¹
1484 ¹ considering all data available (Etiope and Schwietzke, 2019). Here, we select the Etiope and Schwietzke (2019) assessment
1485 in order to account for all potential seepage areas, including those located at water depths > 200m. While we use the estimate
1486 by Etiope and Schwietzke (2019) estimate, we acknowledge that high uncertainty remains and other studies suggest a lower
1487 ranges of emissions based on radiocarbon (¹⁴C-CH₄) data in ice cores (e.g., Hmiel et al., 2020). The suggested estimate may
1488 overestimate this source and be part of the top-down bottom-up discrepancy as discussed in Section 5.1.2.
1489 As a result, here we report a (rounded) median of 12 Tg CH₄ yr⁻¹ with a range of 6-20 Tg CH₄ yr⁻¹ for all coastal and oceanic
1490 sources (Table 3).

1491

1492 **Methane emissions from gas hydrates.** Among the different origins of coastal and oceanic CH₄, hydrates have attracted a
1493 lot of attention. CH₄ hydrates (or clathrates) are ice-like crystals formed under specific temperature and pressure conditions
1494 (Milkov, 2005). Hydrates may host either modern microbial CH₄, containing ¹⁴C and formed *in situ* in shallow sediments
1495 (this type of hydrates is also called “autochthonous”) or fossil, microbial or thermogenic CH₄, migrated from deeper
1496 sediments, generally from reservoirs in hydrocarbon-rich sedimentary basins (this type of hydrates is also called
1497 “allochthonous”; Milkov, 2005; Foschi et al., 2023). The total stock of marine CH₄ hydrates is large but uncertain, with
1498 global estimates ranging from hundreds to thousands of Pg CH₄ (Klauda and Sandler, 2005; Wallmann et al., 2012). Note
1499 that the highly climate-sensitive subsea permafrost reservoir beneath Arctic Ocean shelves also contributes to the hydrate
1500 inventory (Ruppel and Kassler, 2017).

1501 Concerning more specifically atmospheric emissions from marine hydrates, Etiope (2015) points out that current estimates
1502 of CH₄ air-sea flux from hydrates (2–10 Tg CH₄ yr⁻¹ in Ciais et al., 2013, or Kirschke et al., 2013) originate from the
1503 hypothetical values of Cicerone and Oremland (1988). No experimental data or estimation procedures have been explicitly
1504 described along the chain of references since then (Denman et al., 2007; IPCC, 2001; Kirschke et al., 2013; Lelieveld et al.,
1505 1998). It was estimated that ~473 Tg CH₄ has been released into the water column over 100 years (Kretschmer et al., 2015).
1506 Those few teragrams per year become negligible once consumption within the water column has been accounted for. While
1507 events such as submarine slumps may trigger local releases of considerable amounts of CH₄ from hydrates that may reach

Supprimé: ¶

1509 the atmosphere (Etiope, 2015; Paull et al., 2002), on a global scale, present-day atmospheric CH₄ emissions from hydrates
1510 do not appear to be a significant source to the atmosphere, and at least formally, we should consider 0 (< 0.1) Tg CH₄ yr⁻¹
1511 emissions.

1512 **3.2.7 Terrestrial permafrost**

1513 Permafrost is defined as frozen soil, sediment, or rock having temperatures at or below 0°C for at least two consecutive
1514 years (Harris et al., 1988). The total extent of permafrost in the Northern Hemisphere is about 14 million km² or 15% of the
1515 exposed land surface (Obu et al., 2019). As the climate warms, a rise in soil temperatures has been observed across the
1516 permafrost region, and permafrost thaw occurs when temperatures pass 0°C, often associated with melting of ice in the
1517 ground (Biskaborn et al., 2019). Permafrost thaw is most pronounced in southern and spatially isolated permafrost zones,
1518 but also occurs in northern continuous permafrost (Obu et al., 2019). Thaw occurs either as a gradual, often widespread,
1519 deepening of the active layer (surface soils that thaw every summer) or as more rapid localised thaw associated with loss of
1520 massive ground ice (thermokarst) (Turetsky et al., 2020). A total of 1000 ± 200 Pg of carbon can be found in the upper 3
1521 meters of permafrost region soils, or 1400-2000 Pg C for all permafrost (Hugelius et al., 2014; Strauss et al., 2021).

1522 The thawing permafrost can generate direct and indirect CH₄ emissions. Direct CH₄ emissions are from the release of
1523 CH₄ contained within the thawing permafrost. This flux to the atmosphere is small and estimated to be a maximum of 1 Tg
1524 CH₄ yr⁻¹ at present (USEPA, 2010b). Increased release of CH₄ from deep geogenic sources that occurs as seepage along
1525 permafrost boundaries and lake beds may also be considered a direct, and this is estimated to be 2±0.4 Tg CH₄ yr⁻¹ (Walter
1526 Anthony et al., 2012). Indirect CH₄ emissions are probably more important. They are caused by 1) methanogenesis induced
1527 when the organic matter contained in thawing permafrost becomes available for microbial decomposition; 2) thaw induced
1528 soil wetting and changes in land surface hydrology possibly enhancing CH₄ production (McCalley et al., 2014; Schuur et
1529 al., 2022); and 3) the landscape topography changes driven by abrupt thaw processes and loss of ground ice, including the
1530 formation of thermokarst lakes, hill-slope thermokarst, and wetland thermokarst (Turetsky et al., 2020). Such
1531 CH₄ production is probably already significant today and is likely to become more important in the future associated with
1532 climate change and strong positive feedback from thawing permafrost (Schuur et al., 2022). However, indirect
1533 CH₄ emissions from permafrost thawing are difficult to estimate at present, with very few data to refer to, and in any case
1534 largely overlap with wetland and freshwater emissions occurring above or around thawing areas. In a recent synthesis of
1535 full permafrost region CH₄ budgets for the period 2000-2017, Hugelius et al. (2023) compared CH₄ budgets from bottom-
1536 up and top-down (atmospheric inversion models) approaches. They estimate an integrated bottom-up budget of 50 (23, 53;
1537 mean upper and lower 95% CI) Tg CH₄ yr⁻¹ while the top-down estimate is 19 (15, 24) Tg CH₄ yr⁻¹. The bottom-up estimate
1538 is based on a combination of data-driven upscaling reported by Ramage et al. (2023) and process-based model estimates for
1539 wetland CH₄ flux calculated from model ensembles used in Saunio et al. (2020). The top-down estimate is calculated from
1540 ensembles of atmospheric inversion models used in Saunio et al. (2020). Although it is difficult with direct process-

Supprimé:

Supprimé:

Mis en forme : Indice

Supprimé: Increased seepage of geogenic CH₄ gas seeps along permafrost boundaries and lake beds may also be considered a direct flux

1546 attribution, fluxes of ca. 20-30 Tg CH₄ yr⁻¹ in the bottom-up budget are caused by land cover types affected by previous
1547 permafrost thaw (thermokarst lakes, wetlands, hillslope). Because pre-thaw land cover types often have near neutral CH₄
1548 balances (Ramage et al. 2023), these fluxes can largely be seen as driven by permafrost thaw, however the thaw may have
1549 occurred decades, or even centuries, before today.
1550 Here, we choose to report only the direct emission range of 0-1 Tg CH₄ yr⁻¹ (Table 3), keeping in mind that current wetland,
1551 thermokarst lakes and other freshwater methane emissions already likely include a significant indirect contribution
1552 originating from thawing permafrost.

1553 **3.2.8 Vegetation**

1554 Three distinct pathways for the production and emission of CH₄ by living vegetation are considered here (see Covey and
1555 Megonigal (2019) and Bastviken et al. (2023) for extensive reviews). Firstly, plants produce CH₄ through an abiotic
1556 photochemical process induced by stress (Keppler et al., 2006). This pathway was initially questioned (e.g., Dueck et al.,
1557 2007; Nisbet et al., 2009), and although numerous studies have since confirmed aerobic emissions from plants and better
1558 resolved its physical drivers (Fraser et al., 2015), global estimates still vary by two orders of magnitude (Liu et al., 2015).
1559 This plant source has not been confirmed in-field however, and although the potential implication for the global CH₄ budget
1560 remains unclear, emissions from this source are certainly much smaller than originally estimated in Keppler et al. (2006)
1561 (Bloom et al., 2010; Fraser et al., 2015). Second, and of clearer significance, plant stems act as “straws”, drawing up and
1562 releasing microbially produced CH₄ from anoxic soils (Cicerone and Shetter, 1981; Rice et al., 2010; Nisbet et al., 2009).
1563 For instance, in the forested wetlands of Amazonia, tree stems are the dominant ecosystem flux pathway for soil-produced
1564 CH₄, therefore, including stem emissions in ecosystem budgets can reconcile regional bottom-up and top-down estimates
1565 (Pangala et al., 2017; Gauci et al., 2022). Third, the stems of both living trees (Covey et al., 2012) and dead wood (Covey
1566 et al., 2016) provide an environment suitable for microbial methanogenesis. Static chambers demonstrate locally significant
1567 through-bark flux from both soil- (Pangala et al., 2013, 2015), and tree stem-based methanogens (Pitz and Megonigal, 2017;
1568 Wang et al., 2016). A synthesis indicates stem CH₄ emissions significantly increase the source strength of forested wetlands,
1569 and modestly decrease the sink strength of upland forests (Covey and Megonigal, 2019). Recently, field-work suggested
1570 that trees may also act as a CH₄ sink (Machacova et al., 2021; Gorgolewski et al., 2023; Gauci et al., 2024). The scientific
1571 activity covering CH₄ emissions in forested ecosystems reveals a far more complex story than previously thought, with an
1572 interplay of productive/consumptive, aerobic/anaerobic, and biotic/abiotic processes occurring between upland/wetland
1573 soils, trees, and atmosphere. Understanding the complex processes that regulate CH₄ source–sink dynamics in forests and
1574 estimating their contribution to the global CH₄ budget requires cross-disciplinary research, more observations, and new
1575 models that can overcome the classical binary classifications of wetland versus upland forest and of emitting versus uptaking
1576 soils (Barba et al., 2019; Covey and Megonigal, 2019). Although we recognize these emissions are potentially large

Supprimé: s

Supprimé: 2021

Supprimé: recent

Supprimé:

(particularly tree transport from inundated soil), global estimates for each of these pathways remain highly uncertain and/or are currently included here within other flux category sources (e/g. inland waters, wetlands, upland soils).

3.3 Methane sinks and lifetime

CH₄ is the most abundant reactive trace gas in the troposphere and its reactivity is important to both tropospheric and stratospheric chemistry. The main atmospheric sink of CH₄ (~90% of the total sink mechanism) is oxidation by the hydroxyl radical (OH), mostly in the troposphere (Ehhalt, 1974). Other losses are by photochemistry in the stratosphere (reactions with chlorine atoms (Cl) and excited atomic oxygen (O(¹D))), oxidation in soils (Curry, 2007; Dutaur and Verchot, 2007), and by photochemistry in the marine boundary layer (reaction with Cl; Allan et al. (2007), Thornton et al. (2010)). Uncertainties in the total sink of CH₄ as estimated by atmospheric chemistry models are in the order of 20-40% (Saunio et al., 2016). It is much less (10-20%) when using atmospheric proxy methods (e.g., methyl chloroform, see below) as in atmospheric inversions (Saunio et al., 2016). In the present release of the global CH₄ budget, we estimate bottom-up CH₄ chemical sinks and lifetime mainly based on global model results from the Chemistry Climate Model Initiative (CCMI) 2022 activity (Plummer et al., 2021) and CMIP6 simulations (Collins et al., 2017).

3.3.1 Tropospheric OH oxidation

OH radicals are produced following the photolysis of ozone (O₃) in the presence of water vapour. OH is destroyed by reactions with carbon monoxide (CO), CH₄, and non-methane volatile organic compounds. Following the Atmospheric Chemistry and Climate Model Intercomparison Project (ACCMIP), which studied the long-term changes in atmospheric composition between 1850 and 2100 (Lamarque et al., 2013), a new series of experiments was conducted by several chemistry-climate models and chemistry-transport models participating in the Chemistry-Climate Model Initiative (CCMI) (Plummer et al., 2021). Mass-weighted OH tropospheric concentrations do not directly represent CH₄ loss, as the spatial and vertical distributions of OH affect this loss through, in particular, the temperature dependency and the distribution of CH₄ (e.g., Zhao et al., 2019). However, estimating OH concentrations and, spatial and vertical distributions is a key step in estimating methane loss through OH. Over the period 2000-2010, the global mass-weighted OH tropospheric concentration is estimated at 13.3 [11.7-18.2] x 10⁵ molecules cm⁻³ by 8 CCMI-2022 models and at 11.8 [9.4-13.5] x 10⁵ molecules cm⁻³ by 9 models contributing CMIP6 historical run (Collins et al., 2021) (see supplementary Table S4). The ranges calculated here are similar to the ones proposed previously in Saunio et al. (2020), where the multi-model mean (11 models) global mass-weighted OH tropospheric concentration was 11.7±1.0 x 10⁵ molecules cm⁻³ (range 9.9-14.4 x 10⁵ molecules cm⁻³, Zhao et al. (2019)) consistent with the previous estimates from ACCMIP (11.7±1.0 x 10⁵ molecules cm⁻³, with a range of 10.3-13.4 x 10⁵ molecules cm⁻³, Voulgarakis et al. (2013) for year 2000) and the estimates of Prather et al. (2012) of 11.2±1.3 x 10⁵ molecules cm⁻³. Nicely et al. (2017) attribute the differences in OH simulated by different chemistry transport models to, in decreasing order of importance, different chemical mechanisms,

- Supprimé: 5
- Supprimé: 7.9
- Supprimé: 10
- Supprimé: larger than

1616 various treatments of the photolysis rate of O₃, and modelled O₃ and CO. Besides the uncertainty on global OH
1617 concentrations, there is an uncertainty in the spatial and temporal distribution of OH. Models often simulate higher OH in
1618 the northern hemisphere (NH) than in the southern hemisphere (SH), leading to a NH/SH OH ratio greater than 1 (e.g., Zhao
1619 et al., 2019). However, there is evidence for parity in inter-hemispheric OH concentrations (Patra et al., 2014), which needs
1620 to be confirmed by other observational and model-derived estimates. The analysis of the latest CCMI (Plummer et al., 2021)
1621 and CMIP6 (Collins et al., 2021) model outputs show that structural uncertainties in the atmospheric chemistry models
1622 remain large, probably due to inherent biases in OH precursors. Such biases have been highlighted in the OH 3D fields
1623 simulated by two atmospheric chemistry models (Zhao et al., 2023), and were corrected using OH precursors observations.
1624 Such corrections resulted in tropospheric OH mean concentrations lowered by 2. 10⁵ molecules cm⁻³, leading to around 10
1625 x 10⁵ molecules cm⁻³, and a NH/SH OH ratio closer to 1, in better agreement with methyl chloroform (MCF)-based
1626 approaches. This study highlights the need for further improvement of the atmospheric chemistry model.

1627 OH concentrations and their changes can be sensitive to climate variability (e.g., Nicely et al., 2018; Anderson et al., 2021),
1628 biomass burning (e.g., Anderson et al., 2024), and anthropogenic emissions of precursors (Peng et al., 2022; Stevenson et
1629 al., 2020). OH distributions calculated by chemistry climate models show large regional differences and various vertical
1630 profiles (Zhao et al., 2019). OH changes present also regional differences over the long term (Stevenson et al., 2020). Despite
1631 large regional changes, the global mean OH concentration was suggested to have changed only slightly from 1850 to 1980,
1632 but followed by strong (9 %) increases up to the present day (Stevenson et al., 2020). This increase simulated by models
1633 over 2000-2015 are however not in agreement with observation-based approaches (Thompson et al., 2024; Patra et al., 2020;
1634 Nicely et al., 2018; Rigby et al., 2017; Turner et al., 2017) where OH decreases or remain constant over the period. CCMI
1635 and CMIP6 models show OH interannual variability ranging from 0.9% to 1.8% over 2000-2010 (Table S4), in agreement
1636 with the values of IAV derived from some observationally constrained studies (e.g., Thompson et al., 2024; Montzka et al.,
1637 2011) but lower than value deduced from methyl chloroform measurements (Patra et al., 2021; Naus et al., 2021). However,
1638 chemistry climate simulations consider meteorology variability but not fully emission interannual variability (e.g., from
1639 biomass burning) and thus are expected to simulate lower OH interannual variability than in reality. Using an empirical
1640 model constrained by global observations of O₃, water vapour, CH₄, and temperature as well as the simulated effects of
1641 changing NO_x emissions and tropical expansion, Nicely et al. (2017) found an interannual variability in OH of about 1.3-
1642 1.6% between 1980 and 2015, in agreement with methyl chloroform based estimates (Montzka et al., 2011).

1643 Over 2000-2009, the tropospheric loss (tropopause height at 200 hPa) of CH₄ by OH oxidation derived from the ten and
1644 CCMI modelling activities (see supplementary Table S5) is estimated at of 546 [446-663] Tg CH₄ yr⁻¹ (Table 3), which is
1645 similar to the one reported previously in Saunio et al. (2020) from CCMI model (553 [476-677] Tg CH₄ yr⁻¹) and still
1646 slightly higher than the one from the ACCMIP models (528 [454-617] Tg CH₄ yr⁻¹ reported in Kirschke et al. (2013) and
1647 Saunio et al. (2016).

- Supprimé: Naik et al., 2013;
- Supprimé: Based on OH precursor observations and a chemical box model,
- Supprimé: (
- Supprimé: the OH 3D fields simulated by two atmospheric chemistry models,
- Supprimé: resulting
- Supprimé: Dlugokencky et al., 1996; Holmes et al., 2013; Turner et al., 2018
- Supprimé: Voulgarakis
- Supprimé: 2015
- Supprimé: activities
- Supprimé: For instance, the increase of the oxidizing capacity of the troposphere in South and East Asia associated with increasing NO_x emissions (Mijling et al., 2013) and decreasing CO emissions (Yin et al., 2015), possibly enhances CH₄ oxidation and therefore limits the atmospheric impact of increasing emissions (Dalsøren et al., 2009).
- Supprimé: such
- Supprimé: over the past 150 years
- Supprimé: (Naik
- Supprimé: 2013
- Supprimé: This is due to the compensating effects of the concurrent increases of positive influences on OH (water vapour, tropospheric ozone, nitrogen oxides (NO_x) emissions, and UV radiation due to decreasing stratospheric O₃), and of OH sinks (CH₄ burden, CO and non-CH₄ volatile organic compound emissions and burden).
- Supprimé: -
- Supprimé: 4
- Supprimé: 8
- Supprimé: (Zhao et al., 2019)
- Supprimé: similar values are derived in the latest CCMI and CMIP6 activities - see supplementary
- Supprimé: the
- Supprimé: proxy, top-down approach
- Supprimé: these
- Supprimé:
- Supprimé: -

For the recent 2010-2019 decade, we report a climatological value based on only five models that contributed to CMIP6 runs (historical run followed by SSP3-7.0 projections starting in 2015, Collins et al. (2021)) to acknowledge the impact of the rise in atmospheric methane on the methane chemical sink. Hence, for 2010-2019, we report the climatological value of 563 [462-663] Tg CH₄ yr⁻¹ (Table 3).

Supprimé: 510

3.3.2 Stratospheric loss

In the stratosphere, CH₄ is lost through reactions with excited atomic oxygen O(¹D), atomic chlorine (Cl), atomic fluorine (F), and OH (Brasseur and Solomon, 2005; le Texier et al., 1988). Uncertainties in the chemical loss of stratospheric CH₄ are large, due to uncertain interannual variability in stratospheric transport (Zhang et al., 2023) as well as its chemical interactions and feedbacks with stratospheric O₃ (Morgenstern et al., 2018). Particularly, the fraction of stratospheric loss due to the different oxidants is still uncertain, with possibly 20-35% due to halons, about 25% due to O(¹D) mostly in the high stratosphere and the rest due to stratospheric OH (McCarthy et al., 2003).

Supprimé: -

Supprimé: Portmann et al., 2012

In this study, six chemistry climate models that contributed to CMIP6 modelling activities (Table S5) provided estimates of CH₄ chemical loss, including reactions with OH, O(¹D), and Cl; CH₄ photolysis is also included but occurs only above the stratosphere. Considering a 200 hPa tropopause height, these six CMIP6 simulations suggest an estimate of 34 [10-51] Tg CH₄ yr⁻¹ for the CH₄ stratospheric sink for the 2000-2009 decade (Table S5), similar to the value derived from the previous CCMI activity reported in Saunois et al. (2020) (31 [12-41] Tg CH₄ yr⁻¹). The lowest estimate provided by a model (10 Tg CH₄ yr⁻¹) is quite unrealistic and would yield a methane stratospheric lifetime of several hundreds of years. As a result, this outlier is excluded and we prefer to report a mean of 39 Tg CH₄ yr⁻¹ associated with a range of [27-51] for 2000-2009.

Supprimé: ten

Supprimé: and CCMI

Supprimé: are used to provide

Supprimé:

Supprimé: and CCMI results

For 2010-2019, we report here a climatological range of 28-43 Tg CH₄ yr⁻¹ associated with a mean value of 37 Tg CH₄ yr⁻¹ (Table 3) based on five models that contributed to CMIP6 runs (historic followed by SSP3-7.0 projections starting in 2015; Table S5).

Supprimé: 11

Supprimé: 3

3.3.3 Tropospheric reaction with Cl

Halogen atoms can also contribute to the oxidation of CH₄ in the troposphere. Allan et al. (2005) measured mixing ratios of methane and δ¹³C-CH₄ at two stations in the southern hemisphere from 1991 to 2003, and found that the apparent kinetic isotope effect (KIE) of the atmospheric CH₄ sink was significantly larger than that explained by OH alone. A seasonally varying sink due to Cl in the marine boundary layer of between 13 and 37 Tg CH₄ yr⁻¹ was proposed as the explanatory mechanism (Allan et al., 2007; Platt et al., 2004). This sink was estimated to occur mainly over coastal and marine regions, where sodium chloride (NaCl) from evaporated droplets of seawater react with NO₂ to eventually form Cl₂, which then UV-dissociates to Cl. However significant production of nitryl chloride (ClNO₂) at continental sites has been recently reported (Riedel et al., 2014) and suggests the broader presence of Cl, which in turn would expand the significance of the Cl sink in the troposphere. Recently, Hossaini et al. (2016), Sherwen et al. (2016), and Wang et al. (2019b, 2021b) have made

significant improvements in tropospheric chemistry modelling and they conclude to an oxidation contribution of 2.6%, 2%, 1% and 0.8%, respectively. These values correspond to a tropospheric CH₄ loss of around 12-13 Tg CH₄ yr⁻¹, 9 Tg CH₄ yr⁻¹, 5 Tg yr⁻¹, and 3 Tg CH₄ yr⁻¹ respectively, much lower than the first estimates by Allan et al. (2007). The recent work of Wang et al. (2021b) is the most comprehensive modelling study and based upon Sherwen et al. (2016) and Wang et al. (2019b). Both the KIE approach and chemistry transport model simulations carry uncertainties (extrapolations based on only a few sites and use of indirect measurements, for the former and missing sources, coarse resolution, underestimation of some anthropogenic sources for the latter). However, Gromov et al. (2018) found that Cl can contribute only 0.23% the tropospheric sink of CH₄ (about 1 Tg CH₄ yr⁻¹) in order to balance the global ¹³C(CO) budget (see their Table S1). While tropospheric Cl has a marginal impact on the total CH₄ sink (few percents), it influences more significantly the atmospheric isotopic δ¹³C-CH₄ signal and improved estimates of the tropospheric Cl amount should be used for isotopic CH₄ modelling studies (Strode et al., 2020; Thanwerdas et al., 2022b).

Each recent Cl estimate suggests a reduced contribution to the methane loss than previously reported by Allan et al. (2007). As a result, we suggest here to use the mean, minimum and maximum of the last five estimates published since 2016, leading to a climatological value of 6 [1-13] Tg CH₄ yr⁻¹ (Table 3), thus reducing both the magnitude and the uncertainty range compared to Saunois et al. (2020).

Supprimé: Allen

3.3.4 Soil uptake

Unsaturated oxic soils are sinks of atmospheric CH₄ due to the presence of methanotrophic bacteria, which consume CH₄ as a source of energy. Dutaur and Verchot (2007) conducted a comprehensive meta-analysis of field measurements of CH₄ uptake spanning a variety of ecosystems. Extrapolating to the global scale, they reported a range of 36 ± 23 Tg CH₄ yr⁻¹, but also showed that stratifying the results by climatic zone, ecosystem, and soil type led to a narrower range (and lower mean estimate) of 22 ± 12 Tg CH₄ yr⁻¹. Modelling studies, employing meteorological data as external forcing, have also produced a considerable range of estimates. Using a soil depth-averaged formulation based on Fick's law with parameterizations for diffusion and biological oxidation of CH₄, Ridgwell et al. (1999) estimated the global sink strength at 38 Tg CH₄ yr⁻¹, with a range 20-51 Tg CH₄ yr⁻¹ reflecting the model structural uncertainty in the base oxidation parameter. Curry (2007) improved on the latter by employing an exact solution of the one-dimensional diffusion-reaction equation in the near-surface soil layer (i.e., exponential decrease in CH₄ concentration below the surface), a land surface hydrology model, and calibration of the oxidation rate to field measurements. This resulted in a global estimate of 28 Tg CH₄ yr⁻¹ (9-47 Tg CH₄ yr⁻¹), the result reported by Zhuang et al. (2013), Kirschke et al. (2013) and Saunois et al. (2016). Ito and Inatomi (2012) used an ensemble methodology to explore the variation in estimates produced by these parameterizations and others, which spanned the range 25-35 Tg CH₄ yr⁻¹. For the period 2000-2020, as part of the wetland emissions modelling activity, JSBACH (Kleinen et al., 2020) and VISIT (Ito and Inatomi, 2012) models compute a global CH₄ soil uptake to 18 and 35 Tg CH₄ yr⁻¹, respectively.

Murguia-Flores et al. (2018) further refined the Curry (2007) model's structural and parametric representations of key drivers of soil methanotrophy, demonstrating good agreement with the observed latitudinal distribution of soil uptake (Dutaur and Verchot, 2007). Their model (MeMo) simulates a CH₄ soil sink of 37.5 Tg CH₄ yr⁻¹ for the period 2010-2019 (Fig. S4), compared to 39.5 and 31.3 Tg CH₄ yr⁻¹ using the Ridgwell et al. (1999) and Curry (2007) parameterizations, respectively, under the same meteorological forcing, run specifically for this study. For the 2000s period, the simulations estimate the soil uptake at 30.4, 36.7 and 38.3 Tg CH₄ yr⁻¹ based on the parameterization of Curry, MeMo, and Ridgwell, respectively. As part of a more comprehensive model accounting for a range of CH₄ sources and sinks, Tian et al. (2010, 2015, 2016) computed vertically-averaged CH₄ soil uptake including the additional mechanisms of aqueous diffusion and plant-mediated (*aerenchyma*) transport, arriving at the estimate 30±19 Tg CH₄ yr⁻¹ (Tian et al., 2016) for the 2000s. The still more comprehensive biogeochemical model of Riley et al. (2011) included vertically resolved representations of the same processes considered by Tian et al. (2016), in addition to grid cell fractional inundation and, importantly, the joint limitation of uptake by both CH₄ and O₂ availability in the soil column. Riley et al. (2011) estimated a global CH₄ soil sink of 31 Tg CH₄ yr⁻¹ with a structural uncertainty of 15-38 Tg CH₄ yr⁻¹ (a higher upper limit resulted from an elevated gas diffusivity to mimic convective transport; as this is not usually considered, we adopt the lower upper bound associated with no limitation of uptake at low soil moisture). A model of this degree of complexity is required to explicitly simulate situations where the soil water content increases enough to inhibit the diffusion of oxygen, and the soil becomes a methane source (Lohila et al., 2016). This transition can be rapid, thus creating areas (for example, seasonal wetlands) that can be either a source or a sink of methane depending on the season.

The previous Curry (2007) estimate can be revised upward slightly based on subsequent work and the increase in CH₄ concentration since that time. Indeed, Murguia-Flores et al. (2021) estimated that the global soil-uptake doubled between 1900 and 2015 and could further increase due to enhanced diffusion of CH₄ into soil as a result of increases in atmospheric CH₄ mole fraction. Further investigation of the soil uptake is required to better constrain this process at the global scale while it is highly dependent on local scale microbial activity and environmental conditions (e.g., D'Imperio et al., 2023; Fest et al., 2017).

Considering the latest estimates (based on VISIT, JSBACH, and Memo models, Table S6 in the supplementary) we report here a mean estimate of 31 [17-39] Tg CH₄ yr⁻¹ for 2000-2009 and 32 [18-40] for 2010-2019 Tg CH₄ yr⁻¹ (Table 3).

3.3.5 CH₄ lifetime

The atmospheric lifetime of a given gas in steady state may be defined as the global atmospheric burden (Tg) divided by the total sink (Tg yr⁻¹) (IPCC, 2001). This value is different from what is called perturbation lifetime. Perturbation lifetime is used to determine how a one-time pulse emission may decay as a function of time as needed for the calculation of Global Warming Potentials (GWPs), and as a result is related to a theoretical concept. For CH₄, the corresponding perturbation lifetime that should be used in the GWP calculation is 11.8 ± 1.8 years (Forster et al., 2021). In this section, we discuss the

Mis en forme : Indice

Mis en forme : Indice

Mis en forme : Indice

1794 global atmospheric lifetime (also called ‘burden lifetime’ or ‘turnover lifetime’) that characterises the time required to turn
1795 over the global atmospheric burden and defined as the burden divided by the removal flux.

1796 Global models provide an estimate of the loss of the gas due to individual sinks, which can then be used to derive lifetime
1797 due to a specific sink. For example, the tropospheric lifetime of CH₄ is determined as the global atmospheric CH₄ burden
1798 divided by the loss from OH oxidation in the troposphere, sometimes called “chemical lifetime”. The total lifetime of
1799 CH₄ corresponds to the global burden divided by the total loss including tropospheric loss from OH oxidation, stratospheric
1800 chemistry and soil uptake. The CCMI (Plummer et al., 2021) and CMIP6 (Collins et al., 2021) runs estimate the tropospheric
1801 methane lifetime at about 9.2 years (average over years 2000-2009), with a range of 7.5-11 years (see Table S5). This range
1802 agrees with previous values found in ACCMIP and CCMI (9.3 [7.1-10.6] years, Voulgarakis et al. (2013), 9 [7.2-10.1] years,
1803 Saunio et al. (2020)). Adding 31 Tg to account for the soil uptake to the total chemical loss of the CMIP6 and CCMI
1804 models, we derive a total CH₄ lifetime of 8.2 years (average over 2000-2009 with a range of 6.8-9.7 years). The lifetime
1805 calculated over 2010-2019 based on CMIP6 simulations is similar (Table S5). These updated model estimates of total
1806 CH₄ lifetime agree with the previous estimates from ACCMIP (8.2 [6.4-9.2] years for year 2000, Voulgarakis et al. (2013))
1807 and Saunio et al. (2020) based CCMI models. Reducing the large spread in CH₄ lifetime (between models, and between
1808 models and observation-based estimates) would 1) bring an improved constraint on global total methane emissions, and 2)
1809 ensure an accurate forecast of future climate.

1810 **4 Atmospheric observations and top-down inversions**

1811 **4.1 Atmospheric observations**

1812 Systematic atmospheric CH₄ observations began in 1978 (Blake et al., 1982) with infrequent measurements from discrete
1813 air samples collected in the Pacific at a range of latitudes from 67°N to 53°S. Because most of these air samples were from
1814 well-mixed oceanic air masses and the measurement technique was precise and accurate, they were sufficient to establish
1815 an increasing trend and the first indication of the latitudinal gradient of methane. Spatial and temporal coverage was greatly
1816 improved soon after (Blake and Rowland, 1986) with the addition of the Earth System Research Laboratory from US
1817 National Oceanic and Atmospheric Administration (NOAA/GML) flask network (Steele et al. (1987); Lan et al. (2024), Fig.
1818 1), and the Advanced Global Atmospheric Gases Experiment (AGAGE) (Cunnold et al., 2002; Prinn et al., 2018), the
1819 Commonwealth Scientific and Industrial Research Organisation (CSIRO, Francey et al. (1999)), the University of California
1820 Irvine (UCI, Simpson et al., 2012) and in situ and flask measurements from regional networks, such as ICOS (Integrated
1821 Carbon Observation System) in Europe (<https://www.icos-ri.eu/>). The combined datasets provide the longest time series of
1822 globally averaged CH₄ abundances. Since the early-2000s, CH₄ column-averaged mole fractions have been retrieved through
1823 passive remote sensing from space (Buchwitz et al., 2005a, 2005b; Butz et al., 2011; Crevoisier et al., 2009; Frankenberg et
1824 al., 2005; Hu et al., 2018). Ground-based Fourier transform infrared (FTIR) measurements at fixed locations also provide

1825 time-resolved CH₄ column observations during daylight hours, and a validation dataset against which to evaluate the satellite
1826 measurements such as the Total Carbon Column Observing Network (TCCON) network (e.g., Pollard et al., 2017; Wunch
1827 et al., 2011), or Network for Detection of Atmospheric Composition Change (NDACC) (e.g., Bader et al., 2017).
1828 In this budget, in-situ observations from the different networks were used in the top-down atmospheric inversions to estimate
1829 CH₄ sources and sinks over the period 2000-2020. Satellite observations from the TANSO/FTS instrument on board the
1830 satellite GOSAT were used to estimate CH₄ sources and sinks over the period 2010-2020. Other atmospheric data (FTIR,
1831 airborne measurements, AirCore, isotopic measurements, etc.) have been used for validation by some groups, but not
1832 specifically in this study. However, further information is provided in Tables S7, S8, S9, S10, and S11 and a more
1833 comprehensive validation of the inversions is planned to use some of these data.

1834 4.1.1 In situ CH₄ observations and atmospheric growth rate at the surface

1835 We use globally averaged CH₄ mole fractions at the Earth's surface from the four observational networks (NOAA/GML,
1836 AGAGE, CSIRO and UCI). The data are archived at the World Data Centre for Greenhouse Gases (WDCGG) of the WMO
1837 Global Atmospheric Watch (WMO-GAW) program (<https://gaw.kishou.go.jp/>), including measurements from other sites
1838 that are not operated as part of the four networks. The CH₄ in-situ monitoring network has grown significantly over the last
1839 decade due to the emergence of laser diode spectrometers which are robust and accurate enough to allow deployments with
1840 low maintenance enabling the development of denser networks in developed countries (Stanley et al., 2018; Yver Kwok et
1841 al., 2015), and new stations in remote environments (Bian et al., 2015; Nisbet et al., 2019).
1842 The networks differ in their sampling strategies, including the frequency of observations, spatial distribution, and methods
1843 of calculating globally averaged CH₄ mole fractions. Details are given in the supplementary material of Kirschke et al.
1844 (2013). The global average values of CH₄ abundances at Earth's surface presented in Fig. 1 are computed using long-term
1845 measurements from background conditions with minimal influence from immediate emissions. All measurements are
1846 calibrated against gas standards either on the current WMO reference scale or on independent scales with well-estimate
1847 differences from the WMO scale. The current WMO reference scale, maintained by NOAA/ESRL, WMO-X2004A
1848 (Dlugokencky et al., 2005) was updated in July 2015. NOAA and CSIRO global means are on this scale. AGAGE uses an
1849 independent standard scale (based on work by Tohoku University (Aoki et al., 1992) and maintained at Scripps Institution
1850 of Oceanography (SIO)), but direct comparisons of standards and indirect comparisons of atmospheric measurements show
1851 that differences are well below 5 ppb (Tans and Zwellberg, 2014; Vardag et al., 2014) and the TU-1987 scale used for
1852 AGAGE measurements is only 0.5 ppb difference from WMO-X2004A at 1900 ppb level. UCI uses another independent
1853 scale that was established in 1978 and is traceable to NIST (Flores et al., 2015; Simpson et al., 2012), but has not been
1854 included in standard exchanges with other networks so differences with the other networks cannot be quantitatively defined.
1855 Additional experimental details are presented in the supplementary material from Kirschke et al. (2013) and references
1856 therein.

In Fig. 1 (a) globally averaged CH₄ and (b) its growth rate (derivative of the deseasonalized trend curve) through to 2022 are plotted for the four measurement programs using a procedure of signal decomposition described in Thoning et al. (1989). We define the annual G_{ATM} as the increase in the atmospheric concentrations from Jan. 1 in one year to Jan. 1 in the next year. Agreement among the four networks is good for the global growth rate, especially since ~1990. The large differences observed mainly before 1990 probably reflect the different spatial coverage of each network. The long-term behaviour of globally averaged atmospheric CH₄ shows a positive growth rate (defined as the derivative of the deseasonalized mixing ratio) that is slowing down from the early-1980s through 1998, a near-stabilisation of CH₄ concentrations from 1999 to 2006, and a renewed period with positive persistent overall accelerating growth rates since 2007, slightly larger after 2014. From 1999 to 2006, the annual increase of atmospheric CH₄ was remarkably small at 0.6±0.1 ppb yr⁻¹. After 2006, the atmospheric growth rate has increased to a level similar to that of the mid-1990s (~5 ppb yr⁻¹), and for 2014 and 2015 even to that of the 1980s (>10 ppb yr⁻¹). In the two recent years 2020 and 2021, the highest growth rates of 15 ppb yr⁻¹ and 18 ppb yr⁻¹ (see Sect. 6) were unprecedented since the 1980s. On decadal timescales, the annual increase is on average 2.2±0.3 ppb yr⁻¹ for 2000-2009, 7.6±0.3 ppb yr⁻¹ for 2010-2019 and 15.2±0.4 ppb yr⁻¹ for the year 2020 (Table 3). Both climate variability and anthropogenic emission changes are responsible for variations in atmospheric CH₄ growth rates. Indeed, climate variation such as El Nino Southern Oscillation induce changes in emissions such as biomass burning or wetland emission but also impact OH oxidation (e.g., Rowlinson et al., 2019; Zhao et al., 2020b; Peng et al., 2022).

4.1.2 Satellite data of column average CH₄

In this budget, we use satellite data from the JAXA satellite Greenhouse Gases Observing SATellite (GOSAT) launched in January 2009 (Butz et al., 2011; Morino et al., 2011) containing the TANSO-FTS instrument, which observes in the shortwave infrared (SWIR). Different retrievals of CH₄ based on TANSO-FTS/GOSAT products are made available to the community: from NIES (Yoshida et al., 2013), from SRON (Scheepers et al., 2012) and from University of Leicester (Parker et al., 2020; Parker and Boesch, 2020). The three retrievals are used by the top-down systems (Table 4 and S6). Although GOSAT retrievals still show significant unexplained biases and limited sampling in cloud covered regions and in the high latitude winter, it represents an important improvement compared to the first satellite measuring CH₄ from space, SCIAMACHY (Scanning Imaging Absorption spectrometer for Atmospheric Cartography) both for random and systematic observation errors (see Table S2 of Buchwitz et al. (2016)). Here, as in Saunio et al. (2020), only inversions using GOSAT retrievals are used.

4.2 Top-down inversions used in the budget

An atmospheric inversion is the optimal combination of atmospheric observations, of a model of atmospheric transport and chemistry, of a prior estimate of CH₄ sources and sinks, and of their uncertainties, to provide improved estimates of the

Supprimé: When a constant atmospheric lifetime is assumed, the decreasing growth rate from 1983 through 2006 may imply that atmospheric CH₄ was approaching steady state, leading to no trend in emissions. The NOAA global mean CH₄ concentration was fitted with a function that describes the approach to a first-order steady state (ss index): $[CH_4](t) = [CH_4]_{ss} - ([CH_4]_{ss} - [CH_4]_0)e^{-t/\tau}$, solving for the lifetime, τ , gives 9.3 years, which is very close to current literature values (e.g., Prather et al. (2012), 9.1 ± 0.9 years). Such an approach includes uncertainties, especially due to the strong assumption of no trend in lifetime. The result of constant emissions does not agree with some study explaining the stabilisation period by decreasing emissions associated with increasing sink (e.g., Bousquet et al., 2006). However, this value seems consistent albeit higher than the chemistry climate estimates (8.2 years, see Sect. 3.3.5)

Mis en forme : Non Exposant/ Indice

Supprimé:

sources and sinks, and their uncertainty. The theoretical principle of CH₄ inversions is detailed in the Supplementary Material and an overview of the different methods applied to CH₄ is presented in Houweling et al. (2017).

We consider an ensemble of inversions gathering various chemistry transport models, differing in vertical and horizontal resolutions, meteorological forcing, advection and convection schemes, and boundary layer mixing. Including these different systems is a conservative approach that allows us to cover different potential uncertainties of the inversion, among them: model transport, set-up issues, and prior dependency. General characteristics of the inversion systems are provided in Table 4. Further details can be found in the referenced papers and in the Supplementary Material. Each group was asked to provide gridded flux estimates for the period 2000-2020, using either surface or satellite data, but no additional constraints were imposed so that each group could use their preferred inversion setup. Two sets of prior emission distributions were built from the most recent inventories or model-based estimates (see Supplementary Material), but its use was not mandatory (see Table S8 to S11 for the inversion characteristics). This approach corresponds to a flux assessment, but not to a model inter-comparison as the protocol was not too stringent. Estimating posterior uncertainty is time and computer resource consuming, especially for the 4D-var approaches and Monte Carlo methods. Posterior uncertainties have not been requested for this study, but they were found to be lower than the ensemble spread in Sauniois et al. (2020). Indeed, chemistry transport models differ in inter-hemispheric transport, stratospheric CH₄ profiles, and OH distribution, limitations which are not fully considered in the individual posterior uncertainty. As a result, we report the minimum-maximum range among the different top-down approaches.

Seven atmospheric inversion systems using global Eulerian transport models were used in this study; they contributed to the previous budgets that included eight atmospheric inversion systems in Sauniois et al. (2016) and nine in Sauniois et al. (2020). Each inversion system provided one or several simulations, including sensitivity tests varying the assimilated observations (surface or satellite), the OH interannual variability, or the prior fluxes ensemble. This represents a total of 24 inversion runs with different time coverage: generally, 2000-2020 for surface-based observations, and 2010-2020 for GOSAT-based inversions (Table 4 and Table S7). In poorly observed regions, top-down surface inversions may rely on the prior estimates and bring little or no additional information to constrain (often) spatially overlapping emissions (e.g., in India, China). Also, we recall that many top-down systems solve for the total fluxes at the surface only or for some categories that may differ from the GCP categories. When multiple sensitivity tests were performed the mean of this ensemble was used not to overweight one particular inverse system. It should also be noticed that some satellite-based inversions are in fact combined satellite and surface inversions as they use surface-based inversions to correct the latitudinal bias of the satellite retrievals against the optimised atmosphere measurements to correct for errors in the transport model especially in the stratosphere (e.g., Segers et al., 2022; Maasakkers et al., 2019). Nevertheless, these inversions are still referred to as satellite-based inversions. Most of the top-down models use the OH distribution from the TRANSCOM experiment (Patra et al., 2011) either as fixed over the period or with the interannual variability derived by Patra et al. (2021).

Supprimé: -

Supprimé: -

1936 Each group provided gridded monthly maps of emissions for both their prior and posterior total and for sources per category
1937 (see the categories Sect. 2.3). Results are reported in Sect. 5. Atmospheric sinks from the top-down approaches have been
1938 provided for this budget, and are compared with the values reported in Saunois et al. (2020). Not all inverse systems report
1939 their chemical sink; as a result, the global mass imbalance for the top-down budget is derived as the difference between total
1940 sources and total sinks for each model when both fluxes were reported.

1941 **5 Methane budget: top-down and bottom-up comparison**

1942 **5.1 Global methane budget**

1943 **5.1.1 Global total methane emissions**

1944 **Top-down estimates.** At the global scale, the total annual emissions inferred by the ensemble of 24 inversions is 575 [553-
1945 586] Tg CH₄ yr⁻¹ for the 2010-2019 decade (Table 3), with the highest ensemble mean emission of 608 [581-627] Tg CH₄
1946 yr⁻¹ for 2020. Global emissions for 2000-2009 (543 Tg CH₄ yr⁻¹) are consistent with Saunois et al. (2016, 2020) and the
1947 range for global emissions, 526-558 Tg CH₄ yr⁻¹ falls within the range in Saunois et al. (2016) (535-569) and Saunois et al.
1948 (2020) (524-560), although the ensemble of inverse systems contributing to this budget is different from Saunois et al. (2016,
1949 2020). Changes in ensemble members contributing to the different budgets are a feature of each new GMB release and,
1950 therefore, introduce a source of variation (Table S7). The range reported gives the minimum and maximum values among
1951 studies and does not reflect the individual full uncertainties. In addition, most of the top-down models use the same OH
1952 distribution from the TRANSCOM experiment (Patra et al., 2011), which introduces less variability to the global budget
1953 than is likely justified, and so contributes to the rather low range (10%) compared to bottom-up estimates (see below). We
1954 recall here that Zhao et al. (2020a) found an uncertainty of about 17% in global methane emissions (518 to 611 Tg CH₄ yr⁻¹
1955 for the early 2000s) due to changes in OH burden and distribution (OH ranging from 10.3 to 12.6 10⁵ molec cm⁻³)

1956 **Bottom-up estimates.** The bottom-up estimates considered here differ substantially from the top-down results, with annual
1957 global emissions being about 15% larger at 669 [512-849] Tg CH₄ yr⁻¹ for 2010-2019 (Table 3). Yet, thanks to the double
1958 counting corrections in this budget, bottom-up and top-down budgets are in better agreement compared to previous GMB
1959 releases. For the period 2000-2009, the discrepancy between bottom-up and top-down was about 30% of the top-down
1960 estimates in Saunois et al. (2016, 2020) (167 and 156 Tg CH₄ yr⁻¹, respectively), a value that has been reduced significantly
1961 in this budget (now 95 Tg CH₄ yr⁻¹ (<17%) for the same 2000-2009 period). This reduction is due to improvements from an
1962 important decrease in the estimate of emissions from natural and indirect anthropogenic emissions from bottom-up
1963 approaches, and more specifically inland freshwater emissions. From the previous budget, the estimate for inland freshwater
1964 emissions (lakes, ponds, reservoirs, rivers, and streams) has decreased from 159 Tg CH₄ yr⁻¹ to 112 Tg CH₄ yr⁻¹ (47 Tg
1965 decrease). Then, 23 Tg have been removed in the total freshwater ecosystem emissions due to double counting between
1966 vegetated wetlands and mostly small ponds and lakes (Sect. 3.2.2). As a result, the combined wetland and inland freshwater

Supprimé: -

Supprimé: [553-586]

Supprimé: [581-627]

Mis en forme : Exposant

Mis en forme : Exposant

Supprimé: [512-849]

emissions are estimated to be 242 Tg CH₄ yr⁻¹ for 2000-2009 (Table 3), compared with 306 Tg CH₄ yr⁻¹ in Sauniois et al. (2020). This budget is the first that reconciles bottom-up and top-down total emissions within the uncertainty ranges. However, the uncertainty in the global budget remains high because of the large range reported for emissions from freshwater systems. Still, the upper bound of global emissions from bottom-up approaches is not consistent with top-down estimates that rely on OH burden constrained by methyl chloroform atmospheric observations and is still likely overestimated.

5.1.2 Global methane emissions per source category

The global CH₄ emissions from natural and anthropogenic sources (see Sect. 2.3) for 2010-2019 are presented in Fig. 6, Fig. 7, and Table 3. Top-down estimates attribute about 65% of total emissions to anthropogenic activities (range of 55-70%), and 35% to natural emissions. Bottom-up estimates attribute 57% of emissions to direct anthropogenic and the rest to natural plus indirect anthropogenic emissions. A current predominant role of direct anthropogenic sources of CH₄ emissions is consistent with and strongly supported by available ice core and atmospheric CH₄ records. These data indicate that atmospheric CH₄ varied around 700 ppb during the last millennium before increasing by a factor of 2.6 to ~1800 ppb since pre-industrial times. Accounting for the decrease in mean-lifetime over the industrial period, Prather et al. (2012) estimated from these data a total source of 554±56 Tg CH₄ in 2010 of which about 64% (352±45 Tg CH₄) was of direct anthropogenic origin, consistent with the range in our top-down estimates.

Natural and indirect anthropogenic emissions. Although smaller than in previous Global Methane Budget releases, the main remaining discrepancy between top-down and bottom-up budgets is found for the natural and indirect anthropogenic emission total (105 Tg), with 311 [183-462] Tg CH₄ yr⁻¹ for bottom-up and only 206 [188-225] Tg CH₄ yr⁻¹ for top-down over the 2010-2019 decade (Table 3). In the bottom-up estimates, this discrepancy comes first from the estimates in both inland freshwater sources (64 Tg) and second from other natural sources (20 Tg from geological sources, termites, oceans, and permafrost). The top-down approaches may be biased due to missing fluxes (mainly inland freshwaters) in their prior estimates.

For 2010-2019, the top-down and bottom-up derived estimates for wetlands emissions of 165 [145-214] Tg CH₄ yr⁻¹ and 159 [119-203] Tg CH₄ yr⁻¹ (Table 3), respectively, are comparable within their range. Based on diagnostic wetland area values (see notes in Table 3), bottom-up mean wetland emissions for the 2000-2009 period are smaller in this study than those of Sauniois et al. (2016) but larger than in Sauniois et al. (2020). The changes in wetland emissions from bottom-up models may be related to updates on the wetland extent data set (WAD2M), the use of two different meteorological forcings for this study and a different set of models (see Sect. 3.2.1). Conversely, the current 2000-2009 mean top-down wetland estimates are lower than those of Sauniois et al. (2016) and Sauniois et al. (2020) (Table 3). In the bottom-up estimates, the amplitude of the range of emissions of 116-189 is roughly similar to Sauniois et al. (2016) (151-222) and Sauniois et al.

Supprimé:

Supprimé: s

(2020) (102-179) for 2000-2009. Here, the larger range in bottom-up estimates of wetland emissions is due to the use of GSWP3-W5E5 and greater sensibilities of some models to the climate parameters, as discussed in Sect. 3.2.1. Bottom-up and top-down estimates for wetland emissions agree better in this study ($\sim 5 \text{ Tg yr}^{-1}$ for 2000-2009) than in Saunio et al. (2016, 2020) ($\sim 17 \text{ Tg yr}^{-1}$ and $\sim 30 \text{ Tg yr}^{-1}$, respectively). Natural emissions from inland freshwater systems were not included in the prior fluxes used in the top-down approaches, due to unavailable or uncertain gridded products at the start of the modelling activity. However, emissions from these inland freshwater systems may be implicitly included in the posterior estimates of the top-down models, as these two sources are close and probably overlap at the rather coarse resolution of the top-down models. This is the reason why the ‘wetland emissions’ in the top-down budget in fact **better** correspond to the sum of combined wetland and inland freshwaters emissions in the bottom-up budget. The double-counting of 23 Tg CH_4 reduces the bottom-up budget for combined wetland and inland freshwaters from $271 \text{ Tg CH}_4 \text{ yr}^{-1}$ to $248 \text{ Tg CH}_4 \text{ yr}^{-1}$ (Sect. 3.2.2). Comparing the 2000-2009 decadal emissions from wetlands and inland freshwater ecosystems estimated by the bottom-up approaches across the last three Global Methane Budgets shows an upward and then a downward revision with $305 (183+122) \text{ Tg CH}_4 \text{ yr}^{-1}$, $356 (147+209) \text{ Tg CH}_4 \text{ yr}^{-1}$ and $248 (159+112-23) \text{ Tg CH}_4 \text{ yr}^{-1}$ (respectively from Saunio et al. (2016, 2020) and this work; the sum in bracket corresponds to the sum of vegetated wetland emissions and inland water emissions estimated through the different budgets). The combined wetland and inland freshwater emissions discrepancy between bottom-up and top-down approaches amount to $105 \text{ Tg CH}_4 \text{ yr}^{-1}$ for the 2010-2019 decade. From a top-down point of view, the sum of all the natural sources is more robust than the partitioning between wetlands, inland waters, and other natural sources. Including all known spatio-temporal distributions of natural emissions in top-down prior fluxes would be a step forward to consistently compare natural versus anthropogenic total emissions between top-down and bottom-up approaches.

In the top-down budget, wetlands represent 28% on average of the total methane emissions but only 24% in the bottom-up budget (because of higher total emissions inferred) (see Table 3). Given the large uncertainties, neither bottom-up nor top-down approaches included in this study point to significant changes in wetland emissions between the two decades 2000-2009 and 2010-2019 at the global scale.

For the 2010-2019 decade, top-down inversions infer “Other natural emissions” (Table 3) at $43 [40-46] \text{ Tg CH}_4 \text{ yr}^{-1}$, whereas the sum of the individual bottom-up emissions is $63 [24-93] \text{ Tg CH}_4 \text{ yr}^{-1}$, contributing to a 20 Tg discrepancy between bottom-up and top-down approaches. Atmospheric inversions infer the same amount over the decade 2000-2009 as over 2010-2019, which is almost half of the value reported in Saunio et al. (2016) ($68 [21-130] \text{ Tg CH}_4 \text{ yr}^{-1}$). This reduction in magnitude and uncertainty is due to 1) a more consistent way of considering other natural emissions in the various inverse systems (same prior estimate as in this budget) and 2) a difference in the ensemble of top-down inversions reported here compared to previous releases. It is worth noting that, most of the top-down models include about the same ocean and onshore geological emissions and termite emissions in their prior scenarios. **However**, none include freshwater or permafrost emissions in their prior fluxes, and thus in their posterior estimates.

Supprimé: [40-46]

Supprimé: [24-93]

Supprimé: However

2041 Geological emissions are associated with relatively large uncertainties, and marine seepage emissions are still widely
2042 debated (Thornton et al., 2020). However, summing up all bottom-up fossil-CH₄ related sources (including anthropogenic
2043 emissions) leads to a total of 165 [135-190] Tg CH₄ yr⁻¹ in 2010-2019, which is about 29% of the top-down global
2044 CH₄ emissions, and 25% of the bottom-up total global estimate. These results agree with the value inferred from ¹⁴C
2045 atmospheric isotopic analyses of 30% contribution of fossil-CH₄ to global emissions (Etiope et al., 2008; Lassey et al.,
2046 2007b). This total fossil fuel emissions from bottom-up approaches agrees well with the ¹³C-based estimate of Schwietzke
2047 et al. (2016) of 192 ± 32 Tg CH₄ yr⁻¹. In the bottom-up budget, the larger total emissions (due to uncertainties in bottom-up
2048 estimates of natural emissions) leads to a lower fossil fuel contribution compared to Lassey et al. (2007b).

2049 **Anthropogenic direct emissions.** Total anthropogenic direct emissions for the period 2010-2019 were assessed to be
2050 statistically consistent between top-down (369 Tg CH₄ yr⁻¹, range 350-391) and bottom-up approaches (358 Tg CH₄ yr⁻¹,
2051 range 329-387), albeit top-down approaches infer direct anthropogenic emissions larger by 11 Tg CH₄ yr⁻¹ on average
2052 compared to bottom-up approaches (Table 3). The partitioning of anthropogenic direct emissions between agriculture and
2053 waste, fossil fuels extraction and use, and biomass and biofuel burning, also shows good consistency between top-down and
2054 bottom-up approaches, though top-down approaches still suggest less fossil fuel and more agriculture and waste emissions
2055 than bottom-up estimates (Table 3 and Fig. 6 and 7). For 2010-2019, agriculture and waste contributed an estimated
2056 228 [213-242] Tg CH₄ yr⁻¹ in the top-down budget and 211 [195-231] Tg CH₄ yr⁻¹ in the bottom-up budget. Fossil fuel
2057 emissions contributed 115 [100-124] Tg CH₄ yr⁻¹ in the top-down budget and 120 [117-125] Tg CH₄ yr⁻¹ in the bottom-up
2058 budget. Biomass and biofuel burning contributed 27 [26-27] Tg CH₄ yr⁻¹ in the top-down budget and 28 [21-39] Tg CH₄ yr⁻¹
2059 in the bottom-up budget. Biofuel CH₄ emissions rely on very few estimates currently (Wuebbles and Hayhoe, 2002).
2060 Although biofuel is a small source globally (~12 Tg CH₄ yr⁻¹), more estimates are needed to allow a proper uncertainty
2061 assessment. Overall for top-down inversions the global fraction of total emissions for the different source categories is 40%
2062 for agriculture and waste, 20% for fossil fuels, and 5% for biomass and biofuel burning. With the exception of biofuel
2063 emissions, the uncertainty associated with global anthropogenic emissions appears to be smaller than that of natural sources
2064 but with an asymmetric uncertainty distribution (mean significantly different than median). The relative agreement between
2065 top-down and bottom-up approaches may indicate a limited capability of the inversion to separate emissions and a
2066 dependency to their prior fluxes; this agreement should therefore be treated with caution. Indeed, in poorly observed regions,
2067 top-down inversions rely on the prior estimates and bring little or no additional information to constrain (often) spatially
2068 overlapping emissions (e.g., in India, China). Also, as many top-down systems solve for the total fluxes at the surface or for
2069 some categories that may differ from the GCP categories, their posterior partitioning relies on the prior ratio between
2070 categories that are prescribed using bottom-up inventories.

Supprimé: [135-190]

Supprimé: [213-242]

Supprimé: [195-231]

Supprimé: [100-124]

Supprimé: [117-125]

Supprimé: [26-27]

Supprimé: [21-39]

2078 **5.1.3 Global budget of total methane sinks**

2079 **Top-down estimates.** The annual CH₄ chemical removal from the atmosphere is estimated to be 521 Tg CH₄ yr⁻¹ averaged
2080 over the period 2010-2019, with an uncertainty of about ±2% (range 485-532 Tg CH₄ yr⁻¹) (Table 3). All the inverse models
2081 account for CH₄ oxidation by OH and O(¹D), and some include stratospheric Cl oxidation (Table S8 to S11). Most of the
2082 top-down models use the OH distribution from the TRANSCOM experiment (Patra et al., 2011) either as fixed over the
2083 period or including interannual variability from Patra et al. (2021). This study shows no trend in OH and IAV below ±4%,
2084 in agreement with Thompson et al. (2024) (no significant OH trend and IAV < 2%). As a result, the range of the top-down
2085 sink estimates is rather low compared to bottom-up estimates (see below). Differences between transport models affect the
2086 chemical removal of CH₄, leading to different chemical loss rates, even with the same OH distribution. However,
2087 uncertainties in the OH distribution and magnitude (around ±10% at the global scale, Zhao et al., 2019) are not considered
2088 in our study, while they could contribute to a significant change in the chemical sink, and then in the derived posterior
2089 emissions through the inverse process ((Zhao et al., 2020), around ±17% at the global scale, much larger than the model
2090 spread derived here. The chemical sink represents more than 90% of the total sink, the rest being attributable to soil uptake
2091 (35 [35-36] Tg CH₄ yr⁻¹). The rather narrow range is due to the use of the same climatological soil sink provided within the
2092 modelling protocol which is based on Murgia-Flores et al. (2018). This sink estimate used as prior in the inversions is a bit
2093 higher than the mean estimate of the soil sink calculated by bottom-up models (30 Tg CH₄ yr⁻¹, Sec. 3.3.4).
2094 **Bottom-up estimates.** The total chemical loss for the 2010s reported here is 602 Tg CH₄ yr⁻¹ with an uncertainty of 21%
2095 (~125 Tg CH₄ yr⁻¹). Differences in chemistry schemes in the models (especially in the stratosphere) and in the volatile
2096 organic compound treatment probably explain most of the discrepancies among models (Zhao et al., 2019).

2097 **5.2 Latitudinal and regional methane budgets**

2098 The latitudinal and regional breakdown of the bottom-up budget is based on crude assumptions that we acknowledge here.
2099 Natural and indirect anthropogenic emissions are based on wetland gridded products from land surface models and the
2100 combination of the maps from lakes and ponds from Johnson et al. (2022), reservoirs from Johnson et al. (2022) and streams
2101 and rivers from Rocher-Ros et al. (2023), the sum of those three scaled to 89 Tg CH₄ yr⁻¹ (shown in Fig. 5) to artificially
2102 include the double counting (estimated only at the global scale) and match the global estimate. However, we acknowledge
2103 that this procedure distributes the double counting relatively to the final emission distribution and not according to the
2104 freshwater ecosystems where the double counting probably occurs. Wild animal and permafrost maps do not exist and are
2105 missing from the calculation, leading to at least 3 Tg CH₄ yr⁻¹ of discrepancy. However, as aforementioned (Sections 3.2.5
2106 and 3.2.7) this 3 Tg CH₄ yr⁻¹ estimate is probably underestimated in the bottom-up budget. Geological and ocean sources
2107 are based on Etiope et al. (2019) and Weber et al. (2019) gridded products scaled to 50 Tg CH₄ yr⁻¹ to be consistent to the
2108 reported global values. Finally, we use the termite emission map produced for this budget and used in the global budget.

Supprimé:

Supprimé: s

Supprimé: around

2112 The latitudinal budget does not include the estimates from FAO and USEPA for the direct anthropogenic emissions as they
2113 are only provided at country scale.

2114 **5.2.1 Latitudinal budget of total methane emissions**

2115 The latitudinal breakdown of emissions inferred from atmospheric inversions reveals a dominance of emissions in the
2116 latitudinal band 90°S-30°N of 364 [337-390] Tg CH₄ yr⁻¹, representing 64% of the global total (Table 5 and 6). As emissions
2117 in the Tropics (30°S-30°N) dominate this latitudinal contribution, we may refer to 90°S-30°N as the Tropics in the following
2118 32% of the emissions are from the mid-latitudes (187 [160-204] Tg CH₄ yr⁻¹) and 4% from high latitudes (above 60°N).
2119 While the amounts of emissions depend on the surface area of the regions, the relative contribution of the emissions is much
2120 larger (12 points of percent) than the relative importance of the surface areas for the 90°S-30°N region, on the contrary the
2121 boreal regions (60°N-90°N) emissions contribute significantly less than the relative importance of their surface areas (9
2122 points of percent). The ranges around the mean latitudinal emissions are larger than for the global CH₄ sources. While the
2123 top-down uncertainty is less than ±5% at the global scale, it increases to ±7% for the tropics, to ±12% the northern mid-
2124 latitudes and to more than ±20% in the northern high-latitudes (for 2010-2019, Table 5). Both top-down and bottom-up
2125 approaches consistently show that CH₄ decadal emissions have increased by +21-27 Tg CH₄ yr⁻¹ in the tropics, and by +5-
2126 16 Tg CH₄ yr⁻¹ in the northern mid-latitudes between 2000-2009 and 2010-2019 using the mean ensemble estimate.
2127 Over 2010-2019, at the global scale, satellite-based inversions infer almost identical emissions to ground-based inversions
2128 (difference of +1 [-3-9] Tg CH₄ yr⁻¹, with GOSAT based inversion a bit higher than surface measurements-based inversions),
2129 when comparing consistently surface versus satellite-based inversions for each system, similar to Saunio et al. (2020). This
2130 difference is much lower than the range derived between the different systems (range of 20 Tg CH₄ yr⁻¹ using surface- or
2131 satellite-based inversions). This result reflects that differences in atmospheric transport among the systems probably have
2132 more impact on the estimated global emissions than the types of observations assimilated.
2133 As expected, considering the different coverage of observation datasets, regional distributions of inferred emissions differ
2134 depending on the nature of the observations used (satellite or surface). The largest differences (satellite-based minus surface-
2135 based inversions) are observed over the tropical region, between -10 and +43 Tg CH₄ yr⁻¹ (90°S to 30°N), and the northern
2136 mid-latitudes (between -36 and -2 Tg CH₄ yr⁻¹). Satellite data provide stronger constraints on fluxes in tropical regions than
2137 surface data, due to a much larger spatial coverage. It is therefore not surprising that differences between these two types of
2138 observations are found in the tropical band, and consequently in the northern mid-latitudes to balance total emissions, thus
2139 affecting the north-south gradient of emissions. However, the regional patterns of these differences are not consistent
2140 through the different inverse systems. Indeed, some systems found higher emissions in the tropics when using GOSAT
2141 instead of surface observations, while others found the opposite. This difference between inversion systems may depend on
2142 whether or not a bias correction is applied to the satellite data based on surface observations, and also on the modelled
2143 horizontal and vertical transports, in the troposphere and in the stratosphere.

Supprimé: tropical emissions

Supprimé: [337-390]

Supprimé: [160-204]

2147 5.2.2 Latitudinal methane emissions per source category

2148 The analysis of the latitudinal CH₄ budget per source category (Fig. 8 and Table 6) can be performed both for bottom-up
2149 and top-down approaches but with limitations. Bottom-up estimates of natural and indirect anthropogenic emissions are
2150 based on assumptions as specified at the beginning of this section 5.2. For top-down estimates, as already noted, the
2151 partitioning of emissions per source category has to be considered with caution. Indeed, using only atmospheric
2152 CH₄ observations to constrain CH₄ emissions makes this partitioning largely dependent on prior emissions. However,
2153 differences in spatial patterns and seasonality of emissions can be utilised to constrain emissions from different categories
2154 by atmospheric methane observations (for those inversions solving for different sources categories, see Sect. 2.3).
2155 Agriculture and waste are the largest sources of CH₄ emissions in the tropics and southern hemisphere (140 [121-150] Tg
2156 CH₄ yr⁻¹ in the bottom-up budget and 150 [135-168] Tg CH₄ yr⁻¹ in the top-down budget, about 40% of total CH₄ emissions
2157 in this region) (Table 6). However, combined wetland and inland freshwater emissions are nearly as large with 151 [85-234]
2158 Tg CH₄ yr⁻¹ in the bottom-up budget and 128 [112-155] Tg CH₄ yr⁻¹ in the top-down budget (Table 6). Anthropogenic
2159 emissions dominate in the northern mid-latitudes, with the highest contribution from agriculture and waste emissions (40%
2160 of total emissions in the top-down budget), closely followed by fossil fuel emissions (32% of total emissions, top-down
2161 budget). Boreal regions are largely dominated by inland freshwater emissions (41% and 54% of total emissions, top-down
2162 and bottom-up budget, respectively) (Table 6).
2163 The largest discrepancies between the top-down and the bottom-up budgets are found in the mid-latitudes and boreal regions
2164 from the natural and indirect sources with bottom-up estimates twice as large as the top-down ones, especially in the inland
2165 freshwater category.
2166 The uncertainty for wetlands and inland freshwater emissions is larger in the bottom-up models than in the top-down models
2167 (mostly wetlands), while uncertainty in anthropogenic emissions is larger in the top-down models than in the bottom-up
2168 inventories. The large uncertainty in tropical inland freshwater emissions (mostly wetlands) of ±44% results from large
2169 regional differences between the bottom-up land-surface models. Although they are using the same forcings, their responses
2170 in terms of flux density show different sensitivities to temperature, water vapour pressure, precipitation, and radiation.

2171 5.2.3 Regional budget for total emissions

2172 The regional breakdown of emissions is provided for 18 continental regions (see map in Fig. S3 and Table S1 with the
2173 country aggregation in the supplementary materials).
2174 At the regional scale and, for the 2010-2019 decade (Table 7), total methane emissions are dominated by South East Asia
2175 with 63 [52-71] Tg CH₄ yr⁻¹, China with 57 [37-72] Tg CH₄ yr⁻¹, and South Asia with 52 [43-60] Tg CH₄ yr⁻¹ (top-down
2176 budget). These top three emitters contribute 30% of total global CH₄ emissions. The following high emitting regions are
2177 Brazil 47 [41-58] Tg CH₄ yr⁻¹, Equatorial Africa 47 [39-59] Tg CH₄ yr⁻¹, USA 38 [32-46] Tg CH₄ yr⁻¹, Southwest South
2178 America 38 [30-48] Tg CH₄ yr⁻¹, Russia 36 [27-45] Tg CH₄ yr⁻¹, Europe 31 [24-36] Tg CH₄ yr⁻¹, Middle East 31 [24-39] Tg

2179 CH₄ yr⁻¹, Northern Africa 25 [23-29] Tg CH₄ yr⁻¹, and Canada 20 [17-24] Tg CH₄ yr⁻¹. Other regions contribute less than
2180 20 Tg CH₄ yr⁻¹.

2181 **5.2.4 Regional budget per source category**

2182 **Natural and indirect anthropogenic emissions versus direct anthropogenic emissions.** In agreement with Stavert et al.
2183 (2021), natural and indirect anthropogenic emissions are dominated by Brazil, Canada, Russia, Equatorial Africa and
2184 Southeast Asia, contributing 126 Tg CH₄ yr⁻¹ in the bottom-up and 105 Tg CH₄ yr⁻¹ in the top-down budget (Table 7), i.e.,
2185 47% and 50% of the global natural and indirect anthropogenic emissions in these budgets, respectively. At regional scale
2186 also, the range of uncertainty in natural and indirect anthropogenic emissions are much larger in the bottom-up budget than
2187 in the top-down budget (Fig. S5). Except for 4 regions (Canada, Brazil, Northern South America, Southwest South America),
2188 direct anthropogenic emissions contribute more than half of the total regional emissions. Due to the large uncertainty and
2189 discrepancies in natural and indirect emissions estimates, the regional direct anthropogenic fractions may differ between the
2190 bottom-up and top-down budgets. However, in absolute values, the highest direct anthropogenic emitters are the same in
2191 the two budgets with China and South Asia being the top two by far, contributing 56 [51-66] Tg CH₄ yr⁻¹ and 45 [44-47] Tg
2192 CH₄ yr⁻¹, respectively (bottom-up values, Fig. 9 and Table 7). These two regions contribute 28% (26%) of the global direct
2193 anthropogenic emissions in the bottom-up (top-down) budget. The ranks of direct anthropogenic emitters are similar to those
2194 presented in the last budget (Stavert et al., 2021). Southeast Asia, United States of America, Middle East, Europe, Equatorial
2195 Africa, and Russia emit between 32 Tg CH₄ yr⁻¹ and 23 Tg CH₄ yr⁻¹ as direct anthropogenic emissions (bottom-up values,
2196 Fig 8). Brazil, Northern Africa, and Southwest South America emit between 10 CH₄ yr⁻¹ and 20 CH₄ yr⁻¹, while the rest of
2197 the regions emit less than 10 CH₄ yr⁻¹ direct anthropogenic emissions (Table 7 and Fig. S5).

2199 **Sectoral emissions.** The sectoral partitioning at the regional scale has been derived from both bottom-up and top-down
2200 approaches. However, the top-down budget has more limitations, as the sectoral partitioning is usually based on the prior
2201 fluxes fractions at the pixel scale, and assimilating only total methane observations does not allow to disentangle the different
2202 source sectors overlapping in a pixel grid. However, differences in spatial patterns and seasonality of emissions can still be
2203 constrained by atmospheric CH₄ observations for those inversions solving for different sources categories (see Sect. 2.3).
2204 Bottom-up approaches allow deeper sectorial splitting, especially in terms of direct anthropogenic emissions (Fig. 9). Table
2205 7, Fig. 9 and Fig. 10 present the estimations of CH₄ emissions on average over 2010-2019. Fig. 10 presents the budgets for
2206 three main categories (Combined wetland and inland freshwaters, Fossil fuels and Agriculture & Waste), a more detailed
2207 figure and table including the five categories is available in the supplementary material (Fig. S6 and Table S13 to S18).
2208 Values for each individual data-set for the decades 2000-2009, 2010-2019, and the last year 2020 are made available in a
2209 spreadsheet (see Data Availability).

2210 For most regions, “Combined wetland and inland freshwater emissions” are the most uncertain in the bottom-up budget,
 2211 and generally their range is larger than in the top-down budget. In the top-down budget [for 2010-2019 \(Table 7\)](#), this category
 2212 contributes the most to the regional emissions in Brazil 24 [20-33] Tg CH₄ yr⁻¹, Southeast Asia 24 [14-29] Tg CH₄ yr⁻¹
 2213 (though similar to their Agriculture and Waste emissions 24 [21-31] Tg CH₄ yr⁻¹), Equatorial Africa 22 [19-28] Tg CH₄ yr⁻¹,
 2214 Southwest South America 22 [14-33] Tg CH₄ yr⁻¹, Canada 12 [9-18] Tg CH₄ yr⁻¹, Northern South America 8 [6-10] Tg
 2215 CH₄ yr⁻¹, Southern Africa 7 [4-9] Tg CH₄ yr⁻¹. Agriculture and Waste emissions dominates in South Asia 39 [33-43] Tg CH₄
 2216 yr⁻¹, China 30 [13-37] Tg CH₄ yr⁻¹, Europe 19 [16-23] Tg CH₄ yr⁻¹, United States of America 13 [9-16] Tg CH₄ yr⁻¹, Northern
 2217 Africa 13 [12-14] Tg CH₄ yr⁻¹, Central America 9 [8-10] Tg CH₄ yr⁻¹, and Korea and Japan 3 [3-4] Tg CH₄ yr⁻¹. Fossil fuel
 2218 emissions dominate in the Middle East 18 [11-24] Tg CH₄ yr⁻¹ and Russia 14 [8-23] Tg CH₄ yr⁻¹ (close to their combined
 2219 wetland and inland freshwater emissions of 11 [8-13] Tg CH₄ yr⁻¹).
 2220 The four largest contributors to the Fossil Fuel sector remain China, the Middle East, Russia, and the United States of
 2221 America. Altogether they contribute 67 (64) Tg CH₄ yr⁻¹ in the bottom-up (top-down) budget, around 55% of the global
 2222 fossil fuel emissions. The bottom-up and top-down approaches generally agree in terms of ensemble mean, except for China
 2223 for which the top-down estimates suggest lower emissions than the inventories. While Chinese fossil fuel emissions occur
 2224 mainly through coal mining activity (88%), the Middle East, Russia and the USA extract mainly oil and gas (100%, 80%,
 2225 72%).
 2226 The three largest contributors to the Agriculture and Waste sector remain South Asia, China, and Southeast Asia. Together
 2227 they contribute 88 (92) Tg CH₄ yr⁻¹ in the bottom-up (top-down) budget, around 40% of the global agriculture and Waste
 2228 sector ([Table 7](#)). While the ensemble means tend to agree between bottom-up and top-down budgets, the uncertainty derived
 2229 from the top-down approaches is larger, especially for these three regions. CH₄ emissions due to rice cultivation originate
 2230 mostly from these same three regions (South East Asia, China and South Asia). Livestock management emissions occurs
 2231 mainly in South Asia 20 [18-22] Tg CH₄ yr⁻¹, Brazil 12 [11-13] Tg CH₄ yr⁻¹, China 11 [8-16] Tg CH₄ yr⁻¹, and Europe 11
 2232 [10-12] Tg CH₄ yr⁻¹ (bottom-up estimates, [Table 7](#)). The United States of America, Equatorial Africa, Northern Africa and
 2233 Southwest South America emit between 7 Tg CH₄ yr⁻¹ and 10 Tg CH₄ yr⁻¹ in this sub-sector. Other regions emit less than 4
 2234 Tg CH₄ yr⁻¹ in the livestock management sector. The Waste sector emissions are dominated by three regions: China 11 [6-
 2235 14] Tg CH₄ yr⁻¹, South Asia 9 [4-11] Tg CH₄ yr⁻¹, and Europe 8 [6-12] Tg CH₄ yr⁻¹ (bottom-up estimates, [Table 7](#)). These
 2236 three regions contribute around 40% of the global emissions of the Waste sector. It is worth noting that the uncertainty in
 2237 the inventory estimates at the regional scale is around 40% (from the min-max range of the estimate, not including the
 2238 uncertainty from each inventory).

2239 **6 Insights on the methane cycle from 2020-2022 during which there has been unprecedented high growth rates of**
2240 **methane emissions**

2241 The mean emissions estimate for the last year of the budget (2020) was 608 [581-627] Tg CH₄ yr⁻¹ (Top-down), with 65%
2242 of the emissions from direct anthropogenic sources. This is 65 Tg CH₄ yr⁻¹ higher (11%) than the mean emissions of the
2243 2000-2009 decade and 6% higher than 2010-2019. [In Jackson et al. \(2024\), we estimated that total methane emissions](#)
2244 [increased by around 20% between the early 2000s \(2000-2002\) and the late 2010s \(2018-2020\).](#) 2020 was a second highest
2245 year in terms of atmospheric CH₄ growth rate (+15.2 ppb/yr) since systematic measurements began in the late 1980s, coming
2246 in just behind the highest in 2021 at 17.97 ppb/yr. A few studies analysed the large growth rate increase between 2019 (+9.7
2247 ppb/yr) and 2020 (+15.2 ppb/yr) of +5.4 ppb/yr (corresponding to +14.4 ± 2.0 Tg CH₄ yr⁻¹) (Peng et al., 2022; Stevenson
2248 et al., 2022). Peng et al. (2022) estimated that the 2019-2020 growth rate change was almost equally due to an increase in
2249 wetland emissions (6.9 ± 2.1 Tg CH₄ yr⁻¹) and a decrease of the OH chemical loss (7.5 ± 0.8 Tg CH₄ yr⁻¹) due to reduced
2250 OH precursor emissions during the COVID lockdown (Laughner et al., 2021). The COVID19 lockdown resulted in
2251 decreased NO_x emissions and reduced fossil fuel related CH₄ emissions (Thorpe et al., 2023), leading to less OH production.
2252 At the global scale, Feng et al. (2023) calculated an emission increase of 27 Tg CH₄ yr⁻¹ between 2019 and 2020 considering
2253 constant OH, and a smaller increase of 21 Tg CH₄ yr⁻¹ when including a 1.4% decrease of OH. Increased emissions were
2254 mainly found in the northern tropics. Qu et al. (2022) also inferred a 31 Tg CH₄ yr⁻¹ increase of emissions, mostly in the
2255 tropics, half of it in Africa. [Furthermore, Niwa et al. \(2024\) suggested emission increases by 10–18 Tg CH₄ yr⁻¹ in 15°S–](#)
2256 [10°N and by 20 Tg CH₄ yr⁻¹ in 10–35°N from 2016–2019 to 2020–2022.](#) Such a result is compatible with wetland driven
2257 abnormal emissions during a consecutive 3-year La Nina event spanning from 2020 to 2022 (Zhang et al., 2023; Nisbet et
2258 al., 2023). The difference in terms of methodology and approaches between these three studies make it difficult to compare
2259 them quantitatively but provide a robust understanding on the possible causes. Importantly, all the studies indicate, in various
2260 proportions, increasing CH₄ emissions in the tropics and in the boreal region, potentially driven by microbial emission from
2261 wetlands due to wetter and warmer climate, and a significant contribution of reduced OH concentrations due to COVID
2262 lockdown.

2263 Based on our ensemble of data, we find that top-down approaches infer a much larger change in CH₄ emissions (median
2264 [Q1-Q3] at +23 [10-31] Tg CH₄ yr⁻¹) than bottom-up approaches (-1 [-5-3] Tg CH₄ yr⁻¹) between 2019 and 2020 (Fig. S7).
2265 Bottom-up approaches suggest a very small increase in wetland emissions (around +1 [0-3] Tg CH₄ yr⁻¹), while top-down
2266 approaches suggest on average a larger increase for wetlands of +8 [5-11] Tg CH₄ yr⁻¹, mainly in the tropics and mid-
2267 latitudes. It is worth noting that large uncertainties exist for a given year and that the interannual variability is much lower
2268 than the ensemble spread. While bottom-up approaches suggest almost constant fossil fuel emissions and slight increase in
2269 agriculture and waste (+3 Tg CH₄ yr⁻¹), top-down approaches tend to derive higher emissions changes (+6 Tg CH₄ yr⁻¹
2270 from the fossil fuel sector and +11 Tg CH₄ yr⁻¹ from agriculture and waste as the median over the ensemble). Biomass

Supprimé:

2272 burning emissions decreased using both approaches by about 5 Tg CH₄ yr⁻¹ in agreement with Peng et al. (2022). Some
2273 inversions were run with IAV of OH from Patra et al. (2021) and others with constant OH. However, the inferred OH IAV
2274 in 2019 and 2020 are rather low (0.3% and 0.15% on yearly average) in Patra et al. (2021), leading to a small impact in
2275 terms of emissions changes between 2019-2020, with +22 [9-31] (median [Q1-Q3]) based on the inversions with constant
2276 OH and 19 [7-28] based on the inversions with varying OH (Fig S8).
2277 This first analysis based on our ensemble shows how challenging it is to attribute CH₄ emissions changes to a specific sector
2278 or region between two years, because related uncertainties remain much larger than the targeted signal to explain. This calls
2279 again for further improvement of both approaches.
2280 NOAA estimates of 2021 and 2022 methane atmospheric growth rates 17.8.0±0.5 ppb/yr and 14.0±0.8 ppb/yr, respectively
2281 (Lan et al., 2024). They show a continuation of very high growth rates, challenging again our understanding of the methane
2282 budget. The very high values of CH₄ growth rate over 2020-2022 have also been accompanied by a sharp decline in the
2283 stable isotopic signal, δ¹³C_{CH₄}, which suggest that this recent increase of methane growth rate is at least partly explained by
2284 increased emissions from microbial sources such as those found in wetlands, inland waters, agriculture and waste systems
2285 (Nisbet et al., 2023; Michel et al., 2024). However, it is worth noting that almost all published top-down studies
2286 aforementioned include constraints only on CH₄, and do not discuss the consistency with the atmospheric isotopic signal.
2287 As of the time of submission of this manuscript, bottom-up estimates for anthropogenic emissions for 2021 and 2022 are
2288 only available from the EDGARv8 data set (https://edgar.jrc.ec.europa.eu/dataset_ghg80; EDGAR, 2023). This research
2289 inventory suggests that anthropogenic emissions continued to increase from 2020 (374 Tg CH₄ yr⁻¹) to 2021 (379 Tg CH₄
2290 yr⁻¹) and 2022 (386 Tg CH₄ yr⁻¹) with around 62% of the increase due to the fossil fuel sources, 23 % from the Waste
2291 sector, and 14% from the agriculture sector (Table S19). The bottom-up estimate of wetland emissions for 2021-2023,
2292 derived from a single wetland model, indicates positive anomalies of 26 Tg CH₄ yr⁻¹ in 2020, 23 Tg CH₄ yr⁻¹ in 2021, and
2293 21 Tg CH₄ yr⁻¹ 2022 relative to the 2000-2006 baseline ([https://earth.gov/ghgcenter/data-catalog/lpjwsl-wetlandch4-grid-](https://earth.gov/ghgcenter/data-catalog/lpjwsl-wetlandch4-grid-v1)
2294 [v1](https://earth.gov/ghgcenter/data-catalog/lpjwsl-wetlandch4-grid-v1); Zhang et al., 2023).

2295 **7 Future developments, missing elements, and remaining uncertainties**

2296 In this budget, robust features and uncertainties on sources and sinks estimated by bottom-up or top-down approaches have
2297 been highlighted as well as discrepancies between the two budgets. Limitations of the different approaches have also been
2298 highlighted. Four shortcomings of the CH₄ budget were already identified in Kirschke et al. (2013) and Saunio et al. (2016,
2299 2020) and are revisited below pointing to key research areas. Although much progress has been made, they are still relevant,
2300 and actions are needed. However, these actions fall into different timescales and actors. Here, we revisit the four
2301 shortcomings of the contemporary methane budget and discuss how each weakness has been addressed since Saunio et al.
2302 (2020). Each section ends by discussing remaining research needs with a list of suggestions, from higher to lower priority.

- Supprimé: records
- Mis en forme : Indice
- Mis en forme : Indice
- Supprimé: driven
- Mis en forme : Exposant
- Supprimé: and freshwater
- Mis en forme : Indice

2306

2307 1. Shortcoming 1: *Towards a decrease of the high uncertainty in the amount of methane emitted by wetland and inland*

2308 *water systems, and a weakened double counting issue.*

2309 This first shortcoming has probably received the largest interest in the last few years with significant improvements. First a

2310 community effort has been made based on more studies, documenting, or modelling more inland freshwater systems and

2311 synthesising emissions from the complex and heterogeneous ensemble of emitting areas: wetlands, ponds, lakes, reservoirs,

2312 streams, rivers, estuaries, and marine systems. The range of wetland and inland water emissions has been narrowed down

2313 with improved wetland extent and refined estimates for inland freshwater systems. Double counting between inland

2314 freshwater systems has been estimated for the first time and accounted for in this budget. All these improvements decreased

2315 the discrepancy between top-down and bottom-up estimate of combined wetland and inland freshwater emissions from

2316 156 Tg CH₄ yr⁻¹ in Saunio et al. (2020) down to 85 Tg CH₄ yr⁻¹ in this update for the 2000-2009 decade. Gridded maps

2317 for lakes, ponds, reservoirs, and streams and rivers freshwater emissions have been produced over the past years (Johnson

2318 et al., 2021, 2022; Rocher-Ros et al., 2023) making the spatial distribution of CH₄ sources almost complete for the first time

2319 and allowing better description of prior emissions in future top-down inversions.

2320 Next steps include on the short term from highest to lowest priority include:

2321 (i) integration of spatial distribution of inland waters in atmospheric inversion models to reach a full description of prior

2322 methane sources and sinks.

2323 (ii) refinement of double counting estimation and its possible reduction with more precise spatial and temporal distributions

2324 of the different systems contributing to inland freshwater emissions by using very high-resolution satellite data (down to

2325 metre resolutions) to properly separate them. The development of a dynamical global high-resolution (typically few metres)

2326 classification of saturated soils and inundated surfaces based on satellite data (visible and microwave), surface inventories,

2327 and expert knowledge.

2328 (iii) continuation of ongoing efforts to calibrate and evaluate land surface models for wetland emissions against in-situ

2329 observations such as FLUXNET-CH₄ (Knox et al., 2019; Delwiche et al., 2021) or BAWLD-CH₄ (Kuhn et al., 2021) for

2330 boreal regions and avoid dependence on top-down estimates. It is still critical to increase the limited number of tropical

2331 observations and to assimilate them in the inverse systems to help address the issue (e.g., Kallingal et al., 2023).

2332 (iv) continuation of ongoing efforts to develop a diversity of modelling approaches (among them process-based model or

2333 machine learning approaches) to estimate wetland and inland freshwater CH₄ emissions, including lateral fluxes, and

2334 reducing upscaling issues, as done by e.g. Zhuang et al. (2023) for lakes.

2335 (v) continuous integration of collected flux measurements such as in the FLUXNET-CH₄ activity (Knox et al., 2019;

2336 Delwiche et al., 2021) or in BAWLD-CH₄ data set (Kuhn et al., 2021) to provide global flux maps based on machine

2337 learning approaches or other approaches (Peltola et al., 2019, McNicol et al., 2023).

2338 Over the long run, developing measurement systems will help to improve estimates of the diversity of wetland and inland
2339 freshwater sources, and further reduce uncertainties:

- 2340 - More systematic measurements of CH₄ fluxes and their isotopic signatures from sites reflecting the diversity of
2341 environment of wetlands and inland waters, complemented with environmental meta-data (e.g., soil temperature
2342 and moisture, vegetation types, water temperature, acidity, nutrient concentrations, NPP, soil carbon density for
2343 wetlands, lake morphologies) will allow us to better understand and estimate the processes of production and
2344 transport to the atmosphere (diffusive, ebullitive, plants mediated..) and to better constrain methane fluxes and
2345 their isotopic signatures in the different modelling approaches (Glagolev et al., 2011; Turetsky et al., 2014).

2346

2347 2. Shortcoming 2: *Towards a better assessment of uncertainties for global methane sinks in top-down and bottom-up*
2348 *budgets.*

2349 The inverse systems used here have similar caveats than those described in Sauniois et al. (2016, 2020) (same OH field, same
2350 kind of proxy method to optimise it) leading to quite constrained atmospheric sink and therefore total global CH₄ sources.
2351 Although we have used the latest release of CCMI-2022 (Plummer et al., 2021) and CMIP6 simulations (Collins et al.,
2352 2017), the uncertainty of derived CH₄ chemical loss from the chemistry climate models remains at the same (large) level
2353 compared to the previous intercomparison project ACCMIP (Lamarque et al., 2013). The causes of uncertainties on the
2354 CH₄ loss and the differences between the different OH fields derived from Chemistry Transport Models (CTM) and Climate
2355 Chemistry Models (CCM) have been widely discussed (e.g., Nicely et al., 2017 ; Zhao et al., 2019, 2020a). These results
2356 emphasise the need to first assess, and then improve, atmospheric transport and chemistry models, especially vertically, and
2357 to integrate robust representation of OH fields in atmospheric models. Recently, numerous efforts based on satellite data
2358 have been made to constrain OH distribution, variability and trends (e.g. Anderson, 2023,2024; Pimlott et al. 2022; Zhao
2359 et al., 2023; Zhu et al., 2022). Finally, soil uptake estimates rely on very few studies, and interannual variations remain
2360 underconstrained.

2361 Next steps, in the short term, could include developments by the modelling community in:

- 2362 - Estimating the soil uptake with different land surface models (creating an ensemble) and discussing its variations
2363 over the past decade.
- 2364 - Assessing the impact of using updated and varying soil uptake estimates, especially considering a warmer climate
2365 in the top-down approach. Indeed, for top-down models resolving for the net flux of CH₄ at the surface integrating
2366 a larger estimate of soil uptake would allow larger emissions, and then reduce the uncertainty with the bottom-up
2367 estimates of total CH₄ sources.
- 2368 - Further studying the reactivity of the air parcels in the chemistry climate models and defining new diagnostics to
2369 assess modelled CH₄ lifetimes such as in Prather et al. (2023).

Supprimé: For

Supprimé: the latter, Zhao et al. (2023) have proposed a new approach based on OH precursor observations and a chemical box model to improve the 3D distributions of tropospheric OH radicals obtained from atmospheric chemistry models.

Supprimé: .

2376 - Developing benchmarking of CTM and CCM regarding simulated OH distribution and variability (as in Zhao et
2377 al. (2019) for example) to increase efforts to assess biases and improve atmospheric chemical schemes in CTM and
2378 CCM.

2379 - Developing methods to better constrain OH. Numerous have been proposed: satellite CH₄ observations (Zhang et
2380 al., 2018; Anderson et al., 2023; 2024) could afford this but strategy is needed (see Duncan et al., 2024 and
2381 references therein); using halogenated compounds beyond methyl chloroform (MCF), such as done in box models
2382 (Thompson et al., 2024) to derive a 3D dynamical OH. Such methods should be able to reach very low uncertainty
2383 for OH burden and trends (<2%) in order to really better constrain the CH₄ budget. Duncan et al. (2024) discuss
2384 the existing satellite-based methods and propose a strategy to constrain OH from space-based approaches.

2385 - Integrating the aforementioned different potential OH chemical fields, including also interannual variability, to
2386 assess the impact on the methane budget following Zhao et al. (2020).

2387 Over the long run, other parameters should be (better) integrated into top-down approaches, among them:

2388 - The magnitude of the CH₄ loss through oxidation by tropospheric Cl, a process debated in the recent literature.
2389 More modelling (e.g., Thanwerdas et al., 2022b) and instrumental studies should be devoted to reducing the
2390 uncertainty of this potential additional sink before integrating it in top-down models. This would be especially
2391 critical if inversions using ¹³C-CH₄ observations are included in GMB in the future.

2392

2393 3. *Shortcoming 3: Towards a better partitioning of methane sources and sinks by region and process using top-down*
2394 *models*

2395 In this work, we report inversions assimilating satellite data from GOSAT, which bring more constraints than provided by
2396 surface stations alone, especially over tropical continents. However, we still found that satellite- and surface-based
2397 inversions, and the different inversion systems do not consistently infer the same regional flux distribution.

2398 The estimates contributing to the Global Methane budget are further used in more specific studies focusing on the
2399 comparison of the estimates from bottom-up and top-down approaches at national (Deng et al., 2022) and regional scales,
2400 including efforts from the GCP-Regional Carbon Cycle Assessment and Processes (RECCAP2) (Petrescu et al., 2021; 2023;
2401 Tibrewal et al., 2024; Lauerwald et al., 2023b; and other RECCAP-2 publications to come, see
2402 <https://www.globalcarbonproject.org/reccap/publications.htm>).

2403 Next steps, in the short term, could integrate developments to be made by the top-down community:

2404 - Including GOSAT 2 retrievals (Noël et al., 2022; Imasu et al., 2023) for the GOSAT-based inversions and
2405 considering TROPOMI-based inversions (as done in Tsuruta et al. (2023), Shen et al. (2023), Chen et al. (2022),
2406 Qu et al. (2021), or Yu et al. (2023)) in the next releases once at least 8 years of data are available to provide a
2407 decadal estimate and biases are reduced for global scale use (Lorente et al., 2023; Balasu et al., 2023). Indeed,

Supprimé: strategy

Supprimé: constrained

Supprimé: Applying Zhao et al. (2023) recipe to several CTM used for top-down inversions in order to increase consistency between source and sink estimates in individual approaches.

Supprimé: ¶

Supprimé: Developing 3D inverse methods to optimise OH using CH₄ satellite data (Zhang et al., 2018) or

Supprimé: field or machine learning methods using satellite data to constrain OH (Anderson et al., 2023)

Supprimé: .

Mis en forme : Indice

Supprimé: -

Mis en forme : Français

Mis en forme : Français

Supprimé: and

Supprimé:)

Mis en forme : Français

Mis en forme : Français

Mis en forme : Français

Supprimé: X

Mis en forme : Français

Mis en forme : Français

Mis en forme : Français

Mis en forme : Français

Mis en forme : Français

2423 recent satellite developments have provided higher temporal and spatial resolutions of CH₄ observations in regions
 2424 with poor in-situ measurements (Figure S9, such as TROPOMI observations in North Africa).

- 2425 - Integrating the newly available updated gridded products for the different natural sources of CH₄ in their prior
 2426 fluxes (e.g. inland freshwaters) to reach a full spatial description of sources and sinks, and to be able to better
 2427 compare the top-down budget with the bottom-up budget.
- 2428 - Integration of the newly developed 4D variational inversion systems using isotopic species in the top-down budget
 2429 (Basu et al., 2022; Thanwerdas et al., 2024; Drinkwater et al. 2023; Mannisenaho et al., 2023).
- 2430 - Improving the availability of in-situ data at high temporal resolution for the scientific community, especially ones
 2431 covering poorly documented regions such as China (Liu et al., 2021b; Guo et al., 2020), India (Nomura et al., 2021;
 2432 Lin et al., 2015; Tiwari and Kumar, 2012) and Siberia (Sasakawa et al., 2010, 2017; Fujita et al., 2020; Winderlich
 2433 et al., 2010), which are not delivered so far to international databases, or only at poor temporal resolution.
- 2434 - Integrating the information from imagery satellites (e.g., TROPOMI, Carbon Mapper, Methane Sat, GHG Sat.) of
 2435 high to super-emitters to improve prior fluxes of anthropogenic emissions in terms of quantity and locations for
 2436 each covered sector.

2437 Over the long run, integrating more measurements and regional studies will help to improve the top-down systems, and
 2438 further reduce the uncertainties:

- 2439 - Extending the CH₄ surface networks to poorly observed regions (e.g., Tropics, China, India, high latitudes) and to
 2440 the vertical dimension: aircraft regular measurements (e.g., Filges et al., 2015; Brenninkmeijer et al., 2007; Paris
 2441 et al., 2010; Sweeney et al., 2015); Aircore campaigns (e.g., Andersen et al., 2018; Membrive et al., 2017) ; TCCON
 2442 observations (e.g., Wunch et al., 2011, 2019) remains critical to complement satellite data that do not observe well
 2443 in cloudy regions and at high latitudes, and also to evaluate and eventually correct satellite biases (Buchwitz et al.,
 2444 2016).
- 2445 - Extending and developing continuous isotopic measurements of CH₄ to help partitioning methane sources and to
 2446 be integrated in 4D variational isotopic inversions (e.g., Yacovitch et al., 2021).
- 2447 - Integrating global data from future satellite instruments with intrinsic low-bias, such as active LIDAR techniques
 2448 with MERLIN (Ehret et al., 2017), that are promising to overcome issues of systematic errors (Bousquet et al.,
 2449 2018) and should provide measurements over the Arctic, contrary to the existing and planned passive missions.
- 2450 - Other co-emitted species such as radiocarbon for fossil/non-fossil emissions (Lassey et al., 2007a, 2007b; Petrenko
 2451 et al., 2017), CO (e.g., Zheng et al., 2019) for biomass burning emissions, and ethane for fugitive emissions (e.g.,
 2452 Ramsden et al., 2022) could bring additional information for partitioning emissions.

2453

2454 4. Shortcoming 4: *Towards reducing uncertainties in the modelling of atmospheric transport in the models used in the*
 2455 *top-down budget*

2456 The TRANSCOM experiment synthesised in Patra et al. (2011) showed a large sensitivity of the representation of
2457 atmospheric transport on CH₄ abundances in the atmosphere. In particular, the modelled CH₄ budget appeared to depend
2458 strongly on the troposphere-stratosphere exchange rate and thus on the model vertical grid structure and circulation in the
2459 lower stratosphere. Also, regional changes in the CH₄ budget depend on the characteristics of the atmospheric transport
2460 models used in the inversion (Bruhwiler et al., 2017; Locatelli et al., 2015). This axis of research is demanding important
2461 development from the atmospheric modelling community. Waiting for future improvements (finer horizontal and vertical
2462 resolutions, more accurate physical parameterization, increase in computing resources...), assessing atmospheric transport
2463 error and the impact on the top-down budget remain crucial and mostly rely on the use of an ensemble of models.
2464 Methodology changes that could be integrated into the next methane budget releases include:

- 2465 - Evaluating more deeply the inversions provided against independent measurements such as aircraft regular
2466 campaigns available through for example the CH₄ GLOBALVIEWplus v6.0 ObsPack (Schuldt et al., 2023), the
2467 IAGOS data portal (<https://iagos.aeris-data.fr/download/>), the NIES portal
2468 (<https://db.cger.nies.go.jp/ged/en/datasetlist/index.html>) for CONTRAIL (e.g., Machida et al., 2008) and Siberian
2469 measurements (e.g., Sasakawa et al., 2017), the WDCGG data portal (<https://gaw.kishou.go.jp/>) for additional
2470 flights over three other Japanese airports and Orléans, France ; Aircore campaigns data set can be downloaded
2471 through the NOAA Global Monitoring Laboratory website (<https://gml.noaa.gov/ccgg/arc/?id=144>, Baier et al.,
2472 2021) and the French AirCore Program for atmospheric sampling (<https://aircore.aeris-data.fr>, Membrive et al.,
2473 2017); TCCON observations (<https://tcconda.org>; e.g., Wunch et al., 2011, 2019), and use this evaluation to
2474 weight the different models used in the CH₄ budget.

2475 Next steps, in the short term, could include some development to be addressed by the top-down community to reduce
2476 atmospheric transport errors:

- 2477 - Developing further methodologies to extract stratospheric partial column abundances from observations such as
2478 TCCON data (Saad et al., 2014; Wang et al., 2014), Aircore (e.g. Andersen et al., 2018; Membrive et al., 2017) or,
2479 ACE-FTS (De Mazière et al., 2018) or MIPAS (Glatthor et al., 2023) satellite data.
- 2480 - Combining SWIR and TIR measurements from space to better constrain the tropospheric column, from TROPOMI
2481 and IASI for example in the MethanePlus ESA project (<https://methaneplus.eu/#docs>, Buchwitz et al., 2023) or
2482 GOSAT (Kuze et al., 2020).
- 2483 - Porting transport models codes to run on Graphics processing Units (GPU) to achieve sub-degrees resolution global
2484 inversions (Chevallier et al., 2023).

2485 In the long run, developments within the dynamical core of the atmospheric transport models through the implementation
2486 of hexagonal-icosaedric grid with finer resolution (Dubos et al., 2015; Niwa et al., 2017, 2022; Lloret et al., 2023), and
2487 improvements in the simulated boundary layer dynamics or troposphere-stratosphere exchanges are promising to reduce
2488 atmospheric transport errors.

Supprimé: such as

Supprimé: hybrid vertical coordinates (Patra et al., 2018) or of

2491 **8 Conclusions**

2492 We have built an updated global methane budget by using and synthesising a large ensemble of published methods and new
2493 results using a consistent, transparent, and traceable approach, including atmospheric observations and inversions (top-down
2494 models), process-based models for land surface emissions and atmospheric chemistry, and inventories of anthropogenic
2495 emissions (bottom-up models and inventories). For the 2010-2019 decade, global CH₄ emissions are 575 Tg CH₄ yr⁻¹ (range
2496 of 553-586 Tg CH₄ yr⁻¹), as estimated by top-down inversions. About 65% of global emissions are anthropogenic (range of
2497 63-68%). Bottom-up models and inventories suggest larger global emissions (669 Tg CH₄ yr⁻¹ [512-849]) mostly because
2498 of larger and more uncertain natural emissions from inland freshwater systems, natural wetlands, and geological [seepage](#),
2499 and likely some unresolved double counting of these sources. It is also likely that some of the individual bottom-up emission
2500 estimates are too high, leading to larger global emissions from the bottom-up approach than the atmospheric constraints
2501 suggest. However, the important progress in this update is that for the first time, the bottom-up and top-down budgets agree
2502 within their uncertainty ranges. This is substantial progress toward defining more accurate global methane emissions.
2503 The latitudinal breakdown inferred from the top-down approach reveals a dominant role of tropical emissions (~64%)
2504 compared to mid (~32%) and high (~4%) northern latitudes (above 60°N) emissions.
2505 Our results, including an extended set of atmospheric inversions, are compared with the previous budget syntheses of
2506 Kirschke et al. (2013) and Saunio et al. (2016; 2020). They show overall good consistency when comparing the same
2507 decade (2000-2009) at the global and latitudinal scales. The magnitude and uncertainty of most natural or indirect
2508 anthropogenic sources have been revised and updated. In particular, this new budget benefits from large efforts and
2509 collaborations from the research community to provide improved estimates of the magnitude and uncertainty of the different
2510 freshwater sources and helps reduce the potential double counting at the global scale. Of note, newly available gridded
2511 datasets for lakes, ponds, reservoirs, streams, and rivers allow building latitudinal and regional estimates for all these sources
2512 for the first time in these estimates. In the next review, we hope to be able to reduce uncertainties in emissions from inland
2513 freshwater systems by better quantifying the emission factors of each contributing sub-systems (streams, rivers, lakes,
2514 ponds) and estimating double counting at regional scale or avoiding double counting by better defining the surface areas of
2515 each ecosystem. Another important priority for improvements is the uncertainty on the chemical loss of CH₄ which still
2516 needs to be better assessed in both the top-down and the bottom-up budgets. Building on the improvement of the points
2517 detailed in Sect. 7, our aim is to update this budget synthesis as a living review paper regularly (~every three or four years).
2518 Each update will produce a more recent decadal CH₄ budget, highlight changes in emissions and trends, and incorporate
2519 newly available data and model improvements.

2520
2521 It is still under debate why exactly there [is a](#) sustained increase of atmospheric CH₄ (more than +5 ppb yr⁻¹) since 2007
2522 (Nisbet et al., 2019; [Nisbet et al., 2023](#); Turner et al., 2019). Some likely explanations, already introduced by Saunio et al.
2523 (2017) and further investigated by Jackson et al. (2020; [2024](#)) and other studies, include, by decreasing order of certainty:

Supprimé: leaks

Supprimé: are

1) a positive contribution from microbial and fossil sources (e.g., Nisbet et al., 2019; Nisbet et al., 2023; Schwietzke et al., 2016; Jackson et al., 2020), a negative contribution from biomass burning emissions before 2014 (Giglio et al., 2013; Worden et al., 2017); 2) a negligible role of Arctic emission changes (e.g., Nisbet et al., 2019; Saunio et al., 2017); and 3) a tropical dominance of the increasing emissions (e.g., Saunio et al., 2017; Jackson et al., 2020; Wilson et al., 2021; Drinkwater et al., 2023). Although the accelerated atmospheric methane growth rate in 2020 (15.2 ppb/yr) has found some explanation with the impact of the world Pandemia in 2020, the sustained observed growth rates in 2021 (17.8 ppb/yr) and 2022 (14 ppb/yr) still challenge our understanding of the global methane cycle. While in Jackson et al. (2020, 2024), the increase in CH₄ emissions over the last two decades is almost attributed entirely to direct anthropogenic emissions, the uncertainty range from the GMB ensemble is large, and the contribution from natural emissions (wetlands) is still largely uncertain. Besides the decadal change in CH₄ emissions, large interannual variability can occur from these natural emissions. The recent high record of CH₄ growth rate highlights the potential of large variations from natural emissions from one year to another, in particular wetland emissions (e.g., Peng et al., 2022; Feng et al., 2023). These remain the challenges to be overcome in better quantifying global methane emissions.

Further investigation is needed in follow-up studies to (1) compare these results to the official UNFCCC declarations and to important assessment (as those of IEA) as done previously for example in Deng et al. (2022; 2024) or more specifically for fossil fuel emissions in Tibrewal et al. (2024) and (2) further discuss the trend and interannual variability of CH₄ sources and sinks at sectoral and regional scales as in Jackson et al. (2020, 2024), Stavert et al. (2021) or RECCAP-2 related publications (e.g., Petrescu et al., 2021; 2023; Lauerwald et al., 2023b), and discuss the compatibility of the budget against the atmospheric isotopic signal such as in Saunio et al. (2017). The next budgets will be critical to assess whether the Global Methane Pledge is successful and assess methane mitigation efforts.

The GCP will continue to support and coordinate the development of improved flux estimates for all budget components and new underlying science to support improved modelling, acquisition of observations, and data integration. At regular intervals (3-4 years), we will continue to bring all flux components together to produce an improved and updated global CH₄ budget, and provide a global benchmark for other CH₄ products and assessments.

9 Data availability

The data presented here are made available in the belief that their dissemination will lead to greater understanding and new scientific insights on the methane budget and changes to it, and help to reduce its uncertainties. For research projects, if the data used are essential to the work to be published, or if the conclusion or results largely depend on the data, co-authorship should be considered. Full contact details and information on how to cite the data are given in the accompanying database.

Supprimé: -

Mis en forme : Indice

Supprimé: The free availability of the data does not constitute permission for publication of the data.

2558 The accompanying database includes a netcdf file defining the regions used, an archive with the maps of prior fluxes used
2559 in the top-down activity, an archive with data corresponding to Fig. 3 and 5, and one Excel file organised in the following
2560 spreadsheets.

2561 The file Global_Methane_Budget_2000-2020_v1.0.xlsx includes (1) a summary, (2) the methane observed mixing ratio and
2562 growth rate from the four global networks (NOAA, AGAGE, CSIRO and UCI), (3) the evolution of global anthropogenic
2563 methane emissions (including biomass burning emissions) used to produce Fig. 2, (4) the global and latitudinal budgets over
2564 2000–2009 based on bottom-up approaches, (5) the global and latitudinal budgets over 2000–2009 based on top-down
2565 approaches, (6) the global and latitudinal budgets over 2010–2019 based on bottom-up approaches, (7) the global and
2566 latitudinal budgets over 2010–2019 based on top-down approaches, (8) the global and latitudinal budgets for year 2020
2567 based on bottom-up approaches, (9) the global and latitudinal budgets for year 2020 based on top-down approaches, and
2568 (10) the list of contributors to contact for further information on specific data.

2569 This database is available from ICOS Carbon Portal (<https://doi.org/10.18160/GKQ9-2RHT>, Martinez et al., 2024).

2570

2571 **Author contributions.**

2572 MS, AM, and JT gathered the bottom-up and top-down data sets and performed the post processing and analysis.

2573 MS, BP, PB, PeC, and RJ coordinated the global budget. MS, BP, PB, PeC, RJ, PP and PCi contributed to the update of the
2574 full text and all coauthors appended comments. AM, ED, and XL produced the figures. DJB, NG, PH, AI, AJ, TK, TL, XL,
2575 KMcD, JMe, JMu, SP, CP, WR, HT, YY, WZ, ZZ, Qing Z, Qian Z and Qianlai Z performed surface land model simulations
2576 to compute wetland emissions. GA, DB, SC, BRD, GE, MAH, GH, MSJ, RL, SN, GRR, JAR, EHS, PRa, PRc, and TSW
2577 provided data sets useful for natural emission estimates and/or contributed to text on bottom-up natural emissions. LHI, SJS,
2578 TNF, GRvW, and MC provided anthropogenic data sets and contributed to the text for this section. AM, JT, PP, DBc, RJ,
2579 YN, AS, AT, and BZ performed atmospheric inversions to compute top-down methane emission estimates for sources and
2580 sinks. EJD, XL, DRB, PBK, JM, RJP, MR, MS, DWo, and YYo are PI of atmospheric observations used in top-down
2581 inversions and/or contributed the text describing atmospheric methane observations. FD, MS, and JT contributed to the
2582 bottom-up chemical sink section by providing data sets, processing data and/or contributing to the text. FMF provided data
2583 for the soil sink.

2584

2585 **Competing interests.** At least one of the (co-)authors is a member of the editorial board of Earth System Science Data.

2586

2587 **Acknowledgements**

2588 This paper is the result of a collaborative international effort under the umbrella of the Global Carbon Project, a project of
2589 Future Earth and a research partner of the World Climate Research Programme (WCRP). We acknowledge all the people
2590 and institutions who provided the data used in the global methane budget as well as the institutions funding parts of this

Supprimé:

2592 effort (see Table A3). We are very grateful for the help provided by Alex Vermeulen in publishing the Global Methane
 2593 Budget dataset on the Integrated Carbon Observation System (ICOS) website. We acknowledge the modelling groups for
 2594 making their simulations available for this analysis, the joint WCRP Stratosphere-troposphere Processes And their Role in
 2595 Climate/International Global Atmospheric Chemistry (SPARC/IGAC) Chemistry-Climate Model Initiative (CCMI) for
 2596 organising and coordinating the model data analysis activity, and the British Atmospheric Data Centre (BADC) for
 2597 collecting and archiving the CCMI model output. We acknowledge the long-term support provided by the Commonwealth
 2598 Scientific and Industrial Research Organisation (CSIRO) and the National Environmental Science Program - Climate
 2599 Systems Hub to coordinate and support activities of the Global Carbon Project. We are grateful to the Emissions Database
 2600 for Global Atmospheric Research (EDGAR) team (M. Crippa, D. Guizzardi, F. Pagani, M. Banja, E. Schaaf, M. Muntean,
 2601 W. Becker, F. Monforti-Ferrario) for the work needed to publish the EDGAR greenhouse gas emission datasets used in this
 2602 work (<https://edgar.jrc.ec.europa.eu/>). We are particularly indebted to the dedicated station/instrumental operators/scientists
 2603 that have gathered the data and ensured their high quality.
 2604 We acknowledge more specifically Katherine Jensen for her contribution to the Surface Water Microwave Product Series
 2605 SWAMPS, Fortunat Joos for his contribution to simulations with the Land surface Processes and eXchanges model (LPX
 2606 Bern), Ray Langenfeld for his contribution to CSIRO network, Paul Miller for his contribution to simulations with the
 2607 Lund-Potsdam-Jena General Ecosystem Simulator (LPJ-GUESS), Peng Shushi for his contribution to simulations with the
 2608 Organising Carbon and Hydrology In Dynamic Ecosystems (ORCHIDEE) model, Shamil Maksyutov for his contribution
 2609 for simulations with the inverse model at the National Institute for Environmental Studies (NIES), Isobel Simpson for her
 2610 contribution to the University of California Irvine (UCI) network, Paul Steele for his former contribution to CSIRO
 2611 network, Ray Weiss for his contribution to the Advanced Global Atmospheric Gases Experiment (AGAGE) network,
 2612 Christine Widenmeyer for her contribution with the Fire INventory from the National Center for Atmospheric Research
 2613 (FINN) database, Xiaoming Xu for his contribution to simulations with the The Integrated Science Assessment Model
 2614 (ISAM), Yuanzhi Yao for his contribution to simulations with the Dynamic Land Ecosystem Model (DLEM), Diego
 2615 Guizzardi for his contribution to EDGAR, Maria Tenkanen for her contribution with the Carbon Tracker – Europe (CTE)
 2616 outputs, Giulia Conchedda for her contribution to the Food and Agriculture Organization (FAO) database. FAOSTAT data
 2617 collection, analysis, and dissemination is funded through FAO regular budget funds. The contribution of relevant experts in
 2618 member countries is gratefully acknowledged. We acknowledge Juha Hatakka from the Finnish Meteorological Institute
 2619 (FMI) for making methane measurements at the Pallas station and sharing the data with the community. We thank Ariana
 2620 Sutton-Grier and Lisamarie Windham-Myers for reviewing an earlier version of this manuscript. Any use of trade, firm, or
 2621 product names is for descriptive purposes only and does not imply endorsement by the US Government. We warmly thanks
 2622 the three anonymous reviewers for their time and their feedbacks that helped improving greatly the manuscript.
 2623
 2624

2625 **References**

2626 Abe, Y., Bignell, D. E. and Higashi, T., Eds.: Termites: Evolution, Sociality, Symbioses, Ecology, Springer Netherlands,

2627 Dordrecht., 2000.

2628 Aho, K.S., J.H. Fair, J.D. Hosen, E.D. Kyzivat, L.A. Logozzo, G. Rocher-Ros, L.C. Weber, B. Yoon, and P.A. Raymond:

2629 Distinct concentration-discharge dynamics in temperate streams and rivers: CO₂ exhibits chemostasis while CH₄

2630 exhibits source limitation due to temperature control, Limnology and Oceanography, 66(10): p. 3656-3668., 2021

2631 Allan, W., Lowe, D. C., Gomez, A. J., Struthers, H. and Brailsford, G. W.: Interannual variation of ¹³C in tropospheric

2632 methane: Implications for a possible atomic chlorine sink in the marine boundary layer, J. Geophys. Res.-Atmospheres,

2633 110(D11), doi:10.1029/2004JD005650, 2005.

2634 Allan, W., Struthers, H. and Lowe, D. C.: Methane carbon isotope effects caused by atomic chlorine in the marine

2635 boundary layer: Global model results compared with Southern Hemisphere measurements, J. Geophys. Res.-

2636 Atmospheres, 112(D4), D04306, doi:10.1029/2006jd007369, 2007.

2637 Allen, G. H., & Pavelsky, T. M.: Global extent of rivers and streams. Science, 361(6402), 585–588.

2638 <https://doi.org/10.1126/science.aat0636>, 2018

2639 Andersen, T., Scheeren, B., Peters, W. and Chen, H.: A UAV-based active AirCore system for measurements of

2640 greenhouse gases, Atmospheric Meas. Tech., 11(5), 2683–2699, doi:10.5194/amt-11-2683-2018, 2018.

2641 Anderson, D. C., Duncan, B. N., Fiore, A. M., Baublitz, C. B., Follette-Cook, M. B., Nicely, J. M., and Wolfe, G. M.:

2642 [Spatial and temporal variability in the hydroxyl \(OH\) radical: understanding the role of large-scale climate features](https://doi.org/10.5194/acp-21-6481-2021)

2643 [and their influence on OH through its dynamical and photochemical drivers, Atmos. Chem. Phys., 21, 6481–6508,](https://doi.org/10.5194/acp-21-6481-2021)

2644 [https://doi.org/10.5194/acp-21-6481-2021, 2021.](https://doi.org/10.5194/acp-21-6481-2021)

2645 Anderson, D. C., Duncan, B. N., Nicely, J. M., Liu, J., Strode, S. A., and Follette-Cook, M. B.: Technical note:

2646 Constraining the hydroxyl (OH) radical in the tropics with satellite observations of its drivers – first steps toward

2647 assessing the feasibility of a global observation strategy, Atmos. Chem. Phys., 23, 6319–6338,

2648 <https://doi.org/10.5194/acp-23-6319-2023>, 2023.

2649 Anderson, D. C., Duncan, B. N., Liu, J., Nicely, J. M., Strode, S. A., Follette-Cook, M. B., Souri, A. H., Ziemke, J. R.,

2650 Gonzales-Abad, G. and Ayazpour, Z.: Trends and interannual variability of the hydroxyl radical in the remote tropics

2651 during boreal autumn inferred from satellite proxy data. Geophysical Research Letters, 51, e2024GL108531,

2652 <https://doi.org/10.1029/2024GL108531>, 2024.

2653 André, J.-C., Boucher, O., Bousquet, P., Chanin, M.-L., Chappellaz, J. and Tardieu, B.: Le méthane : d'où vient-il et quel

2654 est son impact sur le climat ?, EDP Sciences, Académie des Sciences et Technologies, Paris., 2014.

2655 Aoki, S., Nakazawa, T., Murayama, S. and Kawaguchi, S.: Measurements of atmospheric methane at the Japanese

2656 Antarctic Station. Syowa, Tellus, 44B(4), 273–281, doi:10.1034/j.1600-0889.1992.t01-3-00005.x., 1992.

2657 Arora, V. K., Melton, J. R. and Plummer, D.: An assessment of natural methane fluxes simulated by the CLASS-CTEM

Supprimé: Allen, D. T., Torres, V. M., Thomas, J., Sullivan, D. W., Harrison, M., Hendler, A., Herndon, S. C., Kolb, C. E., Fraser, M. P., Hill, A. D., Lamb, B. K., Miskimins, J., Sawyer, R. F. and Seinfeld, J. H.: Measurements of methane emissions at natural gas production sites in the United States, Proc Natl Acad Sci USA, 110(44), 17,768-17,773, doi:10.1073/pnas.1304880110, 2013.

Supprimé: ¶

Supprimé: Alvarez, R. A., Zavala-Araiza, D., Lyon, D. R., Allen, D. T., Barkley, Z. R., Brandt, A. R., Davis, K. J., Herndon, S. C., Jacob, D. J., Karion, A., Kort, E. A., Lamb, B. K., Lauvaux, T., Maasakkers, J. D., Marchese, A. J., Omara, M., Pacala, S. W., Peischl, J., Robinson, A. L., Shepson, P. B., Sweeney, C., Townsend-Small, A., Wofsy, S. C. and Hamburg, S. P.: Assessment of methane emissions from the U.S. oil and gas supply chain, Science, 361(6398), 186–188, doi:10.1126/science.aar7204, 2018.

Supprimé: ¶

Mis en forme : Français

Code de champ modifié

Mis en forme : Français

Mis en forme : Français

Mis en forme : Français

model, Biogeosciences, 15(15), 4683–4709, doi:10.5194/bg-15-4683-2018, 2018.

Bader, W., Bovy, B., Conway, S., Strong, K., Smale, D., Turner, A. J., Blumenstock, T., Boone, C., Collaud Coen, M., Coulon, A., Garcia, O., Griffith, D. W. T., Hase, F., Hausmann, P., Jones, N., Krummel, P., Murata, I., Morino, I., Nakajima, H., O'Doherty, S., Paton-Walsh, C., Robinson, J., Sandrin, R., Schneider, M., Servais, C., Sussmann, R. and Mahieu, E.: The recent increase of atmospheric methane from 10 years of ground-based NDACC FTIR observations since 2005, *Atmospheric Chem. Phys.*, 17(3), 2255–2277, doi:10.5194/acp-17-2255-2017, 2017.

Baichich, P.: The Birds and Rice Connection, Bird Watch. Dig. [online] Available from: http://www.greatbirdingprojects.com/images/BWD_J-A_13_BIRDS_N_RICE.pdf, 2013.

Baier, B., Sweeney, C., Newberger, T., Higgs, J., Wolter, S., & NOAA Global Monitoring Laboratory : NOAA AirCore atmospheric sampling system profiles (Version 20230831) [Data set]. NOAA GML. <https://doi.org/10.15138/6AV0-MY81>, 2021

Balalus, N., Jacob, D. J., Lorente, A., Maasakkers, J. D., Parker, R. J., Boesch, H., Chen, Z., Kelp, M. M., Nesser, H., and Varon, D. J.: A blended TROPOMI+GOSAT satellite data product for atmospheric methane using machine learning to correct retrieval biases, *Atmos. Meas. Tech.*, 16, 3787–3807, <https://doi.org/10.5194/amt-16-3787-2023>, 2023.

Bansal, S., Van Der Berg, M.P., Fern, R.R., Jones, J.W., Lo, R., McKenna, O.P., Tangen, B.A., Zhang, Z., and Gleason, R.A.: Large increases in methane emissions expected from North America's largest wetland complex, *Sci. Adv.*, 9, eade1112, doi:10.1126/sciadv.ade1112, 2023.

Barba, J., Bradford, M. A., Brewer, P. E., Bruhn, D., Covey, K., van Haren, J., Megonigal, J. P., Mikkelsen, T. N., Pangala, S. R., Pihlatie, M., Poulter, B., Rivas-Ubach, A., Schadt, C. W., Terazawa, K., Warner, D. L., Zhang, Z. and Vargas, R.: Methane emissions from tree stems: a new frontier in the global carbon cycle, *New Phytol.*, 222(1), 18–28, doi:10.1111/nph.15582, 2019.

Barker, P. A., Allen, G., Gallagher, M., Pitt, J. R., Fisher, R. E., Bannan, T., Nisbet, E. G., Bauguitte, S. J.-B., Pasternak, D., Cliff, S., Schimpf, M. B., Mehra, A., Bower, K. N., Lee, J. D., Coe, H., and Percival, C. J.: Airborne measurements of fire emission factors for African biomass burning sampled during the MOYA campaign, *Atmos. Chem. Phys.*, 20, 15443–15459, <https://doi.org/10.5194/acp-20-15443-2020>, 2020.

Bastviken, D., Tranvik, L. J., Downing, J. A., Crill, P. M. and Enrich-Prast, A.: Freshwater Methane Emissions Offset the Continental Carbon Sink, *Science*, 331(6013), 50–50, doi:10.1126/science.1196808, 2011.

Bastviken, D., C.C. Treat, S.R. Pangala, V. Gauci, A. Enrich-Prast, M. Karlson, M. Gålfalk, M.B. Romano, and H.O. Sawakuchi, The importance of plants for methane emission at the ecosystem scale. *Aquatic Botany*, 184: p. 103596, 2023.

Basu, S., Lan, X., Dlugokencky, E., Michel, S., Schwietzke, S., Miller, J. B., Bruhwiler, L., Oh, Y., Tans, P. P., Apadula, F., Gatti, L. V., Jordan, A., Necki, J., Sasakawa, M., Morimoto, S., Di Iorio, T., Lee, H., Arduini, J., and Manca, G.: Estimating emissions of methane consistent with atmospheric measurements of methane and $\delta^{13}\text{C}$ of methane, *Atmos.*

Chem. Phys., 22, 15351–15377, <https://doi.org/10.5194/acp-22-15351-2022>, 2022.

Beaulieu, J.J., DelSontro, T. & Downing, J.A.: Eutrophication will increase methane emissions from lakes and impoundments during the 21st century. *Nat Commun* **10**, 1375, <https://doi.org/10.1038/s41467-019-09100-5>, 2019

Beck, H., Zimmermann, N., McVicar, T. *et al.* Present and future Köppen-Geiger climate classification maps at 1-km resolution. *Sci Data* **5**, 180214, doi.org/10.1038/sdata.2018.214, 2018

Beerling, D.J., Woodward, F.I., Vegetation and the Terrestrial Carbon Cycle: Modelling the First 400 Million Years. Cambridge University Press, Cambridge, 2001

Begum, M.S., M.J. Bogard, D.E. Butman, E. Chea, S. Kumar, X. Lu, O.K. Nayna, L. Ran, J.E. Richey, S.M. Tareq, D.T. Xuan, R. Yu, and J.-H. Park, Localized Pollution Impacts on Greenhouse Gas Dynamics in Three Anthropogenically Modified Asian River Systems. *Journal of Geophysical Research: Biogeosciences*, 126(5): p. e2020JG006124, 2021

Bergamaschi, P., Houweling, S., Segers, A., Krol, M., Frankenberg, C., Scheepmaker, R. A., Dlugokencky, E., Wofsy, S. C., Kort, E. A., Sweeney, C., Schuck, T., Brenninkmeijer, C., Chen, H., Beck, V. and Gerbig, C.: Atmospheric CH₄ in the first decade of the 21st century: Inverse modeling analysis using SCIAMACHY satellite retrievals and NOAA surface measurements, *J. Geophys. Res. Atmospheres*, 118(13), 7350–7369, [doi:10.1002/jgrd.50480](https://doi.org/10.1002/jgrd.50480), 2013.

Bergamaschi, P., DANILA, A. M., Weiss, R., Thompson, R. L., Brunner, D., Levin, I., meijer, Y., Chevallier, F., Janssens-Maenhout, G., Bovensmann, H., Crisp, D., Basu, S., Dlugokencky, E. J., Engelen, R., Gerbig, C., Günther, D., Hammer, S., Henne, S., Houweling, S., Karstens, U., Kort, E. A., Maione, M., Manning, A. J., Miller, J., Montzka, S., Pandey, S., Peters, W., Peylin, P., Pinty, B., Ramonet, M., Reimann, S., Röckmann, T., Schmidt, M., Strogies, M., Sussams, J., Tarasova, O., Van Aardenne, J., Vermeulen, A. and Vogel, F.: Atmospheric monitoring and inverse modelling for verification of greenhouse gas inventories, EUR - Scientific and Technical Research Reports, Publications Office of the European Union. [online] Available from: <https://ec.europa.eu/jrc/en/publication/euro-scientific-and-technical-research-reports/atmospheric-monitoring-and-inverse-modelling-verification-greenhouse-gas-inventories> (Accessed 17 March 2020a), 2018.

Best, A. I., Richardson, M. D., Boudreau, B. P., Judd, A. G., Leifer, I., Lyons, A. P., et al.: Shallow Seabed Methane Gas Could Pose Coastal hazard. *Eos Trans. AGU* **87** (22), 213–217. [doi:10.1029/2006EO220001](https://doi.org/10.1029/2006EO220001), 2006

Bian, L., Gao, Z., Sun, Y., Ding, M., Tang, J. and Schnell, R. C.: CH₄ Monitoring and Background Concentration at Zhongshan Station, Antarctica, *Atmospheric Clim. Sci.*, 6(1), 135–144, [doi:10.4236/acs.2016.61012](https://doi.org/10.4236/acs.2016.61012), 2015.

Bignell, D.E., Eggleton, P. Termites in ecosystems. In: Abe, T., Higashi, M. and Bignell, D.E. (Eds), *Termites: Evolution, Sociality, Symbioses, Ecology*. Kluwer, Dordrecht, Netherlands, 363–387, 2000.

Biskaborn, B.K., Smith, S.L., Noetzli, J. *et al.* Permafrost is warming at a global scale. *Nat Commun* **10**, 264, <https://doi.org/10.1038/s41467-018-08240-4>, 2019

Blake, D. R. and Rowland, F. S.: World-wide increase in tropospheric methane, 1978–1983, *J. Atmospheric Chem.*, 4, 43–62, 1986.

Mis en forme : Français

Mis en forme : Français

Mis en forme : Français

Code de champ modifié

Mis en forme : Français

Code de champ modifié

Mis en forme : Français

Mis en forme : Français

2740 Blake, D. R., Mayer, E. W., Tyler, S. C., Makide, Y., Montague, D. C. and Rowland, F. S.: Global Increase in Atmospheric
 2741 Methane Concentrations between 1978 and 1980, *Geophys. Res. Lett.*, 9(4), 477–480, 1982.
 2742 Bloom, A. A., Lee-Taylor, J., Madronich, S., Messenger, D. J., Palmer, P. I., Reay, D. S. and McLeod, A. R.: Global
 2743 methane emission estimates from ultraviolet irradiation of terrestrial plant foliage, *New Phytol.*, doi:10.1111/j.1469-
 2744 8137.2010.03259.x, 2010.
 2745 Bohn, T. J., Melton, J. R., Ito, A., Kleinen, T., Spahni, R., Stocker, B. D., Zhang, B., Zhu, X., Schroeder, R., Glagolev, M.
 2746 V., Maksyutov, S., Brovkin, V., Chen, G., Denisov, S. N., Eliseev, A. V., Gallego-Sala, A., McDonald, K. C., Rawlins,
 2747 M. A., Riley, W. J., Subin, Z. M., Tian, H., Zhuang, Q. and Kaplan, J. O.: WETCHIMP-WSL: Intercomparison of
 2748 wetland methane emissions models over West Siberia, *Biogeosciences*, 12(11), 3321–3349, doi:10.5194/bg-12-3321-
 2749 2015, 2015.
 2750 Bodmer, P., Vroom, R. J. E., Stepina, T., del Giorgio, P. A., Kosten, S.: Methane dynamics in vegetated habitats in inland
 2751 waters: quantification, regulation, and global significance, *Frontiers in Water*, 5, DOI=10.3389/frwa.2023.1332968,
 2752 2024
 2753 Borges, A. V. and Abril, G.: Carbon Dioxide and Methane Dynamics in Estuaries, in *Treatise on Estuarine and Coastal*
 2754 *Science*, vol. 5, pp. 119–161, Academic Press, Waltham. [online] Available from: doi:10.1016/B978-0-12-374711-
 2755 2.00504-0, 2011.
 2756 Borges, A., G. Abril, and S. Bouillon: Carbon dynamics and CO₂ and CH₄ outgassing in the Mekong delta,
 2757 *Biogeosciences*, 15: p. 1093-1114., 2018
 2758 Borges, A.V., F. Darchambeau, T. Lambert, C. Morana, G.H. Allen, E. Tambwe, A. Toengaho Sembaito, T. Mambo, J.
 2759 Nlandu Wabakhangazi, J.P. Descy, C.R. Teodoru, and S. Bouillon: Variations in dissolved greenhouse gases (CO₂,
 2760 CH₄, N₂O) in the Congo River network overwhelmingly driven by fluvial-wetland connectivity, *Biogeosciences*,
 2761 16(19): p. 3801-3834, 2019
 2762 Borges, A. V., Deirmendjian, L., Bouillon, S., Okello, W., Lambert, T., Roland, F.A. E., Razanamahandry, V. F. ,
 2763 Voarintsoa, N.R. G., Darchambeau, F., Kimirei, I. A. , Descy, J-P., Allen, G. H. and Morana, C.: Greenhouse gas
 2764 emissions from African lakes are no longer a blind spot. *Sci. Adv.* 8, eabi8716, DOI:10.1126/sciadv.abi8716, 2022
 2765 Bousquet, P., Ciais, P., Miller, J. B., Dlugokencky, E. J., Hauglustaine, D. A., Prigent, C., Van der Werf, G. R., Peylin, P.,
 2766 Brunke, E. G., Carouge, C., Langenfelds, R. L., Lathiere, J., Papa, F., Ramonet, M., Schmidt, M., Steele, L. P., Tyler,
 2767 S. C. and White, J.: Contribution of anthropogenic and natural sources to atmospheric methane variability, *Nature*,
 2768 443(7110), 439–443, 2006.
 2769 Bousquet, P., Pierangelo, C., Bacour, C., Marshall, J., Peylin, P., Ayar, P. V., Ehret, G., Bréon, F.-M., Chevallier, F.,
 2770 Crevoisier, C., Gibert, F., Rairoux, P., Kiemle, C., Armante, R., Bès, C., Cassé, V., Chinaud, J., Chomette, O.,
 2771 Delahaye, T., Edouard, D., Estève, F., Fix, A., Friker, A., Klonecki, A., Wirth, M., Alpers, M. and Millet, B.: Error
 2772 Budget of the Methane Remote Lidar mission and Its Impact on the Uncertainties of the Global Methane Budget, J.

2773 Geophys. Res. Atmospheres, 123(20), 11,766–11,785, doi:10.1029/2018JD028907, 2018.

2774 Brandt, A. R., Heath, G. A., Kort, E. A., O’Sullivan, F., Pétron, G., Jordaán, S. M., Tans, P., Wilcox, J., Gopstein, A. M.,
 2775 Arent, D., Wofsy, S., Brown, N. J., Bradley, R., Stucky, G. D., Eardley, D. and Harriss, R.: Methane Leaks from North
 2776 American Natural Gas Systems, *Science*, 343(6172), 733–735, doi:10.1126/science.1247045, 2014.

2777 Brasseur, G. P. and Solomon, S.: *Aeronomy of the Middle Atmosphere: Chemistry and Physics of the Stratosphere and*
 2778 *Mesosphere*, 3rd ed., Springer Netherlands., 2005.

2779 Brenninkmeijer C. A. M., Crutzen, P., Boumard, F., Dauer, T., Dix, B., Ebinghaus, R., Filippi, D., Fischer, H., Franke, H.,
 2780 Fries, U., Heintzenberg, J., Helleis, F., Hermann, M., Kock, H. H., Koeppel, C., Lelieveld, J., Leuenberger, M.,
 2781 Martinsson, B. G., Miemczyk, S., Moret, H. P., Nguyen, H. N., Nyfeler, P., Oram, D., O’Sullivan, D., Penkett, S., Platt,
 2782 U., Pupek, M., Ramonet, M., Randa, B., Reichelt, M., Rhee, T. S., Rohwer, J., Rosenfeld, K., Scharffe, D., Schlager,
 2783 H., Schumann, U., Slemr, F., Sprung, D., Stock, P., Thaler, R., Valentino, F., van Velthoven, P., Waibel, A., Wandel,
 2784 A., Waschitschek, K., Wiedensohler, A., Xueref-Remy, I., Zahn, A., Zech, U., and Ziereis, H.: Civil Aircraft for the
 2785 regular investigation of the atmosphere based on an instrumented container: The new CARIBIC system, *Atmos. Chem.*
 2786 *Phys.*, 7, 4953–4976, doi:10.5194/acp-7-4953-2007, 2007.

2787 Bruhwiler, L. M., Basu, S., Bergamaschi, P., Bousquet, P., Dlugokencky, E., Houweling, S., Ishizawa, M., Kim, H.-S.,
 2788 Locatelli, R., Maksyutov, S., Montzka, S., Pandey, S., Patra, P. K., Petron, G., Saunio, M., Sweeney, C., Schwietzke,
 2789 S., Tans, P. and Weatherhead, E. C.: U.S. CH₄ emissions from oil and gas production: Have recent large increases
 2790 been detected?, *J. Geophys. Res. Atmospheres*, 122(7), 4070–4083, doi:10.1002/2016JD026157, 2017.

2791 Brune, A.: Symbiotic digestion of lignocellulose in termite guts, *Nat Rev Microbiol* 12, 168–180,
 2792 doi.org/10.1038/nrmicro3182, 2014

2793 Buchwitz, M., de Beek, R., Burrows, J. P., Bovensmann, H., Warneke, T., Notholt, J., Meirink, J. F., Goede, A. P. H.,
 2794 Bergamaschi, P., Korner, S., Heimann, M. and Schulz, A.: Atmospheric methane and carbon dioxide from
 2795 SCIAMACHY satellite data: initial comparison with chemistry and transport models, *Atmospheric Chem. Phys.*, 5,
 2796 941–962, 2005a.

2797 Buchwitz, M., de Beek, R., Noel, S., Burrows, J. P., Bovensmann, H., Bremer, H., Bergamaschi, P., Korner, S. and
 2798 Heimann, M.: Carbon monoxide, methane and carbon dioxide columns retrieved from SCIAMACHY by WFM-
 2799 DOAS: year 2003 initial data set, *Atmospheric Chem. Phys.*, 5, 3313–3329, 2005b.

2800 Buchwitz, M., Dils, B., Boesch, H., Crevoisier, C., Detmers, R., Frankenberg, C., Hasekamp, O., Hewson, W., Laeng, A.,
 2801 Noel, S., Notholt, J., Parker, R., Reuter, M. and Schneising, O.: Product Validation and Intercomparison Report
 2802 (PVIR) for the Essential Climate Variable (ECV) Greenhouse Gases (GHG), ESA Climate Change Initiative (CCI),
 2803 report version 4, Feb 2016, http://www.esa-ghg-cci.org/?q=webfm_send/300, 2016.

2804 Buchwitz, M., Schneising, O., Vanselow, S., Houweling, S., van Peet, J., Siddans, R., Kerridge, B., Ventress, L., Knappett,
 2805 D., Crevoisier, C., Meilhac, N., Borsdorf, T., Lorente, A. and Aben, I.: Final Report of the Methane Plus ESA project,

2806 TN-D15/16-CH4PLUS, <https://methaneplus.eu/#docs>, Accessed on February 13 2024, 202
 2807 Butz, A., Guerlet, S., Hasekamp, O., Schepers, D., Galli, A., Aben, I., Frankenberg, C., Hartmann, J. M., Tran, H., Kuze,
 2808 A., Keppel-Aleks, G., Toon, G., Wunch, D., Wennberg, P., Deutscher, N., Griffith, D., Macatangay, R.,
 2809 Messerschmidt, J., Notholt, J. and Warneke, T.: Toward accurate CO₂ and CH₄ observations from GOSAT, *Geophys.*
 2810 *Res. Lett.*, 38(14), L14812, doi:10.1029/2011gl047888, 2011.
 2811 Cai, Z. C., Xing, G., Yan, X., Xu, H., Tsuruta, H., Yagi, K. and Minami, K.: Methane and nitrous oxide emissions from
 2812 rice paddy fields as affected by nitrous fertilizers and water management, *Plant Soil*, 196, 7–14, 1997.
 2813 Cael, B.B., J. Biggs, and D.A. Seekell, The size-distribution of earth’s lakes and ponds: Limits to power-law behavior.
 2814 *Frontiers in Environmental Science*, 10-, 2022
 2815 Call, M., D. T. Maher, I. R. Santos, and others.: Spatial and temporal variability of carbon dioxide and methane fluxes
 2816 over semi-diurnal and spring–neap–spring timescales in a mangrove creek. *Geochim. Cosmochim. Acta* **150**: 211–225.
 2817 doi:10.1016/j.gca.2014.11.023, 2015
 2818 Canadell, J.G., P.M.S. Monteiro, M.H. Costa, L. Cotrim da Cunha, P.M. Cox, A.V. Eliseev, S. Henson, M. Ishii, S. Jaccard,
 2819 C. Koven, A. Lohila, P.K. Patra, S. Piao, J. Rogelj, S. Syampungani, S. Zaehle, and K. Zickfeld: Global Carbon and
 2820 other Biogeochemical Cycles and Feedbacks. In *Climate Change 2021: The Physical Science Basis. Contribution of*
 2821 *Working Group I to the Sixth Assessment Report of the Intergovernmental Panel on Climate Change* [Masson-
 2822 Delmotte, V., P. Zhai, A. Pirani, S.L. Connors, C. Péan, S. Berger, N. Caud, Y. Chen, L. Goldfarb, M.I. Gomis, M.
 2823 Huang, K. Leitzell, E. Lonnoy, J.B.R. Matthews, T.K. Maycock, T. Waterfield, O. Yelekçi, R. Yu, and B. Zhou (eds.)].
 2824 Cambridge University Press, Cambridge, United Kingdom and New York, NY, USA, pp. 673–816, doi:
 2825 10.1017/9781009157896.007, 2021
 2826 Carlson, K. M., Gerber, J. S., Mueller, N. D., Herrero, M., MacDonald, G. K., Brauman, K. A., Havlik, P., O’Connell, C.
 2827 S., Johnson, J. A., Saatchi, S. and West, P. C.: Greenhouse gas emissions intensity of global croplands, *Nat. Clim.*
 2828 *Change*, 7(1), 63–68, doi:10.1038/nclimate3158, 2017.
 2829 Castelán-Ortega, O. A., Carlos Ku-Vera, J. and Estrada-Flores, J. G.: Modeling methane emissions and methane
 2830 inventories for cattle production systems in Mexico, *Atmósfera*, 27(2), 185–191, doi:10.1016/S0187-6236(14)71109-
 2831 9, 2014.
 2832 Cathles, L., Brown, L., Taam, M. and Hunter, A.: A commentary on “The greenhouse-gas footprint of natural gas in shale
 2833 formations” by R.W. Howarth, R. Santoro, and Anthony Ingraffea, *Clim. Change*, 113(2), 525–535,
 2834 doi:10.1007/s10584-011-0333-0, 2012.
 2835 Chandra, N., P. K. Patra, J. S. H. Bisht, A. Ito, T. Umezawa, S. Morimoto, S. Aoki, G. Janssens-Maenhout, R. Fujita, M.
 2836 Takigawa, S. Watanabe, N. Saitoh, J.G. Canadell, Emissions from the oil and gas sectors, coal mining and ruminant
 2837 farming drive methane growth over the past three decades, *J. Meteorol. Soc. Jpn.*, 99(2), doi:10.2151/jmsj.2021-015,
 2838 2021.

Supprimé: Caulton, D., Shepson, P. B., Santoro, R. L., Sparks, J. P., Howarth, R. W., Anthony R. Ingraffea, A. R., Cambaliza, M. O. L., Sweeney, C., Karion, A., Davis, K. J., Sturm, B. H., Montzka, S. A. and Miller, B. R.: Toward a better understanding and quantification of methane emissions from shale gas development, *Proc. Natl. Acad. Sci. USA*, 111(17), 6237–6242, doi:10.1073/pnas.1316546111, 2014.

Supprimé: ¶

Chandra, N., Patra, P.K., Fujita, R., Höglund-Isaksson, L., Umezawa, T., Goto, D., Morimoto, S., Vaughn, B. H., and Röckmann, T.: Methane emissions decreased in fossil fuel exploitation and sustainably increased in microbial source sectors during 1990–2020, *Comm. Earth Environ.*, 5, <https://doi.org/10.1038/s43247-024-01286-x>, 2024.

Chang, J., Peng, S., Ciais, P., Saunio, M., Dangal, S. R. S., Herrero, M., Havlik, P., Tian, H. and Bousquet, P.: Revisiting enteric methane emissions from domestic ruminants and their $\delta^{13}\text{C}$ CH₄ source signature, *Nat. Commun.*, 10(1), 1–14, doi:10.1038/s41467-019-11066-3, 2019.

Chang, J., Peng, S., Yin, Y., Ciais, P., Havlik, P., & Herrero, M.: The key role of production efficiency changes in livestock methane emission mitigation. *AGU Advances*, 2, e2021AV000391, <https://doi.org/10.1029/2021AV000391>, 2021.

Chappellaz, J., Blunier, T., Raynaud, D., Barnola, J. M., Schwander, J. and Stauffert, B.: Synchronous changes in atmospheric CH₄ and Greenland climate between 40 and 8 kyr BP, *Nature*, 366(6454), 443–445, doi:10.1038/366443a0, 1993.

Chen, H., Zhu, Q., Peng, C., Wu, N., Wang, Y., Fang, X., Jiang, H., Xiang, W., Chang, J., Deng, X. and Yu, G.: Methane emissions from rice paddies natural wetlands, lakes in China: Synthesis new estimate, *Glob. Change Biol.*, 19(1), 19–32, doi:10.1111/gcb.12034, 2013.

Chen, Y. H. and Prinn, R. G.: Estimation of atmospheric methane emissions between 1996 and 2001 using a three-dimensional global chemical transport model, *J. Geophys. Res.-Atmospheres*, 111(D10307), doi:10.1029/2005JD006058, 2006.

Chen, Z., Jacob, D. J., Nesser, H., Sulprizio, M. P., Lorente, A., Varon, D. J., Lu, X., Shen, L., Qu, Z., Penn, E., and Yu, X.: Methane emissions from China: a high-resolution inversion of TROPOMI satellite observations, *Atmos. Chem. Phys.*, 22, 10809–10826, <https://doi.org/10.5194/acp-22-10809-2022>, 2022.

Chen, Y., Hall, J., van Wees, D., Andela, N., Hantson, S., Giglio, L., van der Werf, G. R., Morton, D. C., and Randerson, J. T.: Multi-decadal trends and variability in burned area from the fifth version of the Global Fire Emissions Database (GFED5), *Earth Syst. Sci. Data*, 15, 5227–5259, <https://doi.org/10.5194/essd-15-5227-2023>, 2023.

Chevallier, F., Lloret, Z., Cozic, A., Takache, S., and Remaud, M.: Toward high-resolution global atmospheric inverse modeling using graphics accelerators. *Geophysical Research Letters*, 50(5), 1–9. <https://doi.org/10.1029/2022GL102135>, 2023.

Chiri, E., Greening, C., Lappan, R., Waite D. W., Jirapanjawat, T., Dong, X., Arndt, S. K., and Nauer, P. A.: Termite mounds contain soil-derived methanotroph communities kinetically adapted to elevated methane concentrations. *ISME J* 14, 2715–273, <https://doi.org/10.1038/s41396-020-0722-3>, 2020.

Chiri, E., Nauer, P. A., Lappan, R., Jirapanjawat, T., Waite, D. W., Handley, K. M., Hugenholtz, P., Cook, P. L. M., Arndt, S. K., and Greening, C.: Termite gas emissions select for hydrogenotrophic microbial communities in termite mounds. *Proceedings of the National Academy of Sciences of the United States of America*, 118(30), e2102625118, 2021.

Mis en forme : Anglais (E.U.)

<https://doi.org/10.1073/pnas.2102625118>, 2021
 Ciais, P., Sabine, C., Bala, G., Bopp, L., Brovkin, V., Canadell, J., Chhabra, A., DeFries, R., Galloway, J., Heimann, M., Jones, C., Le Quéré, C., Myneni, R. B., Piao, S. and Thornton, P.: Carbon and Other Biogeochemical Cycles, in In Climate Change 2013: The Physical Science Basis. Contribution of Working Group I to the Fifth Assessment Report of IPCC, edited by T. F. Stocker, D. Qin, G.-K. Plattner, M. Tignor, S. K. Allen, J. Boschung, A. Nauels, Y. Xia, V. Bex, and P. M. Midgley, Cambridge University Press, Cambridge., 2013.
 Cicerone, R. J. and Oremland, R. S.: Biogeochemical aspects of atmospheric methane, *Glob. Biogeochem. Cycles*, 2, 299–327, 1988.
 Cicerone, R. J. and Shetter, J. D.: Sources of atmospheric methane: Measurements in rice paddies and a discussion, *J. Geophys. Res.*, 86, 7203–7209, 1981.
 Collins, W. J., Lamarque, J. F., Schulz, M., Boucher, O., Eyring, V., Hegglin, M. I., Maycock, A., Myhre, G., Prather, M., Shindell, D. and Smith, S.J.: AerChemMIP: quantifying the effects of chemistry and aerosols in CMIP6. *Geoscientific Model Development* 10, 585–607. doi:10.5194/gmd-10-585-2017, 2017.
 Comer-Warner, S.A., P. Romeijn, D.C. Gooddy, S. Ullah, N. Kettridge, B. Marchant, D.M. Hannah, and S. Krause: Thermal sensitivity of CO₂ and CH₄ emissions varies with streambed sediment properties. *Nature Communications*, 9(1): p. 2803, 2018
 Conley, S., Franco, G., Faloona, I., Blake, D. R., Peischl, J. and Ryerson, T. B.: Methane emissions from the 2015 Aliso Canyon blowout in Los Angeles, CA, *Science*, 351(6279), 1317–1320, doi:10.1126/science.aaf2348, 2016.
 Conrad, R., Klose, M. and Claus, P.: Phosphate Inhibits Acetotrophic Methanogenesis on Rice Roots, *Appl. Environ. Microbiol.*, 66(2), 828–831, 2000.
 Covey, K. R. and Magonigal, J. P.: Methane production and emissions in trees and forests, *New Phytol.*, 222(1), 35–51, doi:10.1111/nph.15624, 2019.
 Covey, K. R., Wood, S. A., Warren, R. J., Lee, X. and Bradford, M. A.: Elevated methane concentrations in trees of an upland forest, *Geophys. Res. Lett.*, 39(15), doi:10.1029/2012gl052361, 2012.
 Covey, K. R., de Mesquita, C. P. B., Oberle, B., Maynard, D. S., Bettigole, C., Crowther, T. W., Duguid, M. C., Steven, B., Zanne, A. E., Lapin, M., Ashton, M. S., Oliver, C. D., Lee, X. and Bradford, M. A.: Greenhouse trace gases in deadwood, *Biogeochemistry*, 130(3), 215–226, doi:10.1007/s10533-016-0253-1, 2016.
 Crawford, J.T. and E.H. Stanley: Controls on methane concentrations and fluxes in streams draining human-dominated landscapes. *Ecological Applications*, 26(5): p. 1581-1591, 2016
 Crevoisier, C., Nobileau, D., Fiore, A. M., Armante, R., Chedin, A. and Scott, N. A.: Tropospheric methane in the tropics - first year from IASI hyperspectral infrared observations, *Atmospheric Chem. Phys.*, 9(17), 6337–6350, 2009.
 Crippa, M., Guizzardi, D., Solazzo, E., Muntean, M., Schaaf, E., Monforti-Ferrario, F., Banja, M., Olivier, J.G.J., Grassi, G., Rossi, S., Vignati, E., GHG emissions of all world countries - 2021 Report, EUR 30831 EN, Publications Office of

the European Union, Luxembourg, 2021, ISBN 978-92-76-41547-3, doi:10.2760/173513, JRC126363, 2021

Crippa, M., Guizzardi, D., Pagani, F., Banja, M., Muntean, M., Schaaf E., Becker, W., Monforti-Ferrario, F., Quadrelli, R., Risquez Martin, A., Taghavi-Moharamli, P., Köykkä, J., Grassi, G., Rossi, S., Brandao De Melo, J., Oom, D., Branco, A., San-Miguel, J., Vignati, E., GHG emissions of all world countries, Publications Office of the European Union, Luxembourg, 2023, doi:10.2760/953322, JRC134504, 2023

Crutzen, P. J., Aselmann, I. and Seiler, W.: Methane production by domestic animals, wild ruminants, other herbivorous fauna, and humans, *Tellus B*, 38B(3–4), 271–284, doi:10.1111/j.1600-0889.1986.tb00193.x, 1986.

Cucchi, M., Weedon, G. P., Amici, A., Bellouin, N., Lange, S., Müller Schmied, H., Hersbach, H. and Buontempo, C.: WFDE5: bias-adjusted ERA5 reanalysis data for impact studies. *Earth System Science Data*, 12, 2097–2120, 2020

Cunnold, D. M., Steele, L. P., Fraser, P. J., Simmonds, P. G., Prinn, R. G., Weiss, R. F., Porter, L. W., O'Doherty, S., Langenfelds, R. L., Krummel, P. B., Wang, H. J., Emmons, L., Tie, X. X. and Dlugokencky, E. J.: In situ measurements of atmospheric methane at GAGE/AGAGE sites during 1985-2000 and resulting source inferences, *J. Geophys. Res. - Atmospheres*, 107(D14), doi:10.1029/2001jd001226, 2002.

Curry, C. L.: Modeling the soil consumption of atmospheric methane at the global scale, *Glob. Biogeochem. Cycles*, 21(4), GB4012, doi:10.1029/2006gb002818, 2007.

Dalsøren, S. B., Isaksen, I. S. A., Li, L. and Richter, A.: Effect of emission changes in Southeast Asia on global hydroxyl and methane lifetime, *Tellus B*, 61(4), 588–601, doi:10.1111/j.1600-0889.2009.00429.x, 2009.

Darmenov, A. and da Silva, A.: The quick fire emissions dataset (QFED) - Documentation of versions 2.1, 2.2 and 2.4, Technical Report Series on Global Modeling and Data Assimilation, NASA Global Modeling and Assimilation Office., [online] Available from: <https://gmao.gsfc.nasa.gov/pubs/docs/Darmenov796.pdf> (Accessed 11 March 2020), 2015.

De Mazière, M., Vigouroux, C., Bernath, P. F., Baron, P., Blumenstock, T., Boone, C., Brogniez, C., Catoire, V., Coffey, M., Duchatelet, P., Griffith, D., Hannigan, J., Kasai, Y., Kramer, I., Jones, N., Mahieu, E., Manney, G. L., Piccolo, C., Randall, C., Robert, C., Senten, C., Strong, K., Taylor, J., Tétard, C., Walker, K. A., and Wood, S.: Validation of ACE-FTS v2.2 methane profiles from the upper troposphere to the lower mesosphere, *Atmos. Chem. Phys.*, 8, 2421–2435, <https://doi.org/10.5194/acp-8-2421-2008>, 2008.

Deemer, B. R., Harrison, J. A., Li, S., Beaulieu, J. J., DelSontro, T., Barros, N., Bezerra-Neto, J. F., Powers, S. M., dos Santos, M. A. and Vonk, J. A.: Greenhouse Gas Emissions from Reservoir Water Surfaces: A New Global Synthesis, *BioScience*, 66(11), 949–964, doi:10.1093/biosci/biw117, 2016.

Deemer, B.R. and M.A. Holgerson, Drivers of Methane Flux Differ Between Lakes and Reservoirs, Complicating Global Upscaling Efforts. *Journal of Geophysical Research: Biogeosciences* 126(4): p. e2019JG005600., 2021.

Defratyka, S. M., Paris, J.-D., Yver-Kwok, C., Fernandez, J. M., Korben, P., and Bousquet, P.: Mapping Urban Methane Sources in Paris, France, *Environmental Science & Technology*, 55, 8583–8591, 10.1021/acs.est.1c00859, 2021.

2946 DelSontro, T., Beaulieu, J. J. and Downing, J. A.: Greenhouse gas emissions from lakes and impoundments: Upscaling in
 2947 the face of global change, *Limnol. Oceanogr. Lett.*, 3(3), 64–75, doi:10.1002/lol2.10073, 2018.

2948 Delwiche, K. B., Knox, S. H., Malhotra, A., Fluet-Chouinard, E., McNicol, G., Feron, S., Ouyang, Z., Papale, D., Trotta,
 2949 C., Canfora, E., Cheah, Y.-W., Christianson, D., Alberto, Ma. C. R., Alekseychik, P., Aurela, M., Baldocchi, D.,
 2950 Bansal, S., Billesbach, D. P., Bohrer, G., Bracho, R., Buchmann, N., Campbell, D. I., Celis, G., Chen, J., Chen, W.,
 2951 Chu, H., Dalmagro, H. J., Dengel, S., Desai, A. R., Detto, M., Dolman, H., Eichelmann, E., Euskirchen, E., Famulari,
 2952 D., Fuchs, K., Goeckede, M., Gogo, S., Gondwe, M. J., Goodrich, J. P., Gottschalk, P., Graham, S. L., Heimann, M.,
 2953 Helbig, M., Helfter, C., Hemes, K. S., Hirano, T., Hollinger, D., Hörtnagl, L., Iwata, H., Jacotot, A., Jurasinski, G.,
 2954 Kang, M., Kasak, K., King, J., Klatt, J., Koebsch, F., Krauss, K. W., Lai, D. Y. F., Lohila, A., Mammarella, I., Belelli
 2955 Marchesini, L., Manca, G., Matthes, J. H., Maximov, T., Merbold, L., Mitra, B., Morin, T. H., Nemitz, E., Nilsson, M.
 2956 B., Niu, S., Oechel, W. C., Oikawa, P. Y., Ono, K., Peichl, M., Peltola, O., Reba, M. L., Richardson, A. D., Riley, W.,
 2957 Runkle, B. R. K., Ryu, Y., Sachs, T., Sakabe, A., Sanchez, C. R., Schuur, E. A., Schäfer, K. V. R., Sonnentag, O.,
 2958 Sparks, J. P., Stuart-Haëntjens, E., Sturtevant, C., Sullivan, R. C., Szutu, D. J., Thom, J. E., Torn, M. S., Tuittila, E.-
 2959 S., Turner, J., Ueyama, M., Valach, A. C., Vargas, R., Varlagin, A., Vazquez-Lule, A., Verfaillie, J. G., Vesala, T.,
 2960 Vourlitis, G. L., Ward, E. J., Wille, C., Wohlfahrt, G., Wong, G. X., Zhang, Z., Zona, D., Windham-Myers, L., Poulter,
 2961 B., and Jackson, R. B.: FLUXNET-CH4: a global, multi-ecosystem dataset and analysis of methane seasonality from
 2962 freshwater wetlands , *Earth Syst. Sci. Data*, 13, 3607–3689, <https://doi.org/10.5194/essd-13-3607-2021>, 2021.

2963 Deng, Z., Ciais, P., Tzompa-Sosa, Z. A., Saunois, M., Qiu, C., Tan, C., Sun, T., Ke, P., Cui, Y., Tanaka, K., Lin, X.,
 2964 Thompson, R. L., Tian, H., Yao, Y., Huang, Y., Lauerwald, R., Jain, A. K., Xu, X., Bastos, A., Sitch, S., Palmer, P. I.,
 2965 Lauvaux, T., d'Aspremont, A., Giron, C., Benoit, A., Poulter, B., Chang, J., Petrescu, A. M. R., Davis, S. J., Liu, Z.,
 2966 Grassi, G., Albergel, C., Tubiello, F. N., Perugini, L., Peters, W., and Chevallier, F.: Comparing national greenhouse
 2967 gas budgets reported in UNFCCC inventories against atmospheric inversions, *Earth Syst. Sci. Data*, 14, 1639–1675,
 2968 <https://doi.org/10.5194/essd-14-1639-2022>, 2022.

2969 [Deng, Z., Ciais, P., Hu, L., Martinez, A., Saunois, M., Thompson, R. L., Tibrewal, K., Peters, W., Byrne, B., Grassi, G.,](#)
 2970 [Palmer, P. I., Luijkx, I. T., Liu, Z., Liu, J., Fang, X., Wang, T., Tian, H., Tanaka, K., Bastos, A., Sitch, S., Poulter, B.,](#)
 2971 [Albergel, C., Tsuruta, A., Maksyutov, S., Janardanan, R., Niwa, Y., Zheng, B., Thanwerdas, J., Belikov, D., Segers,](#)
 2972 [A., and Chevallier, F.: Global Greenhouse Gas Reconciliation 2022, *Earth Syst. Sci. Data Discuss.* \[preprint\],](#)
 2973 [<https://doi.org/10.5194/essd-2024-103>, in review, 2024.](#)

2974 Denman, K. L., G. Brasseur, A. Chidthaisong, P. Ciais, P. M. Cox, R. E. Dickinson, D. Hauglustaine, C. Heinze, E.
 2975 Holland, D. Jacob, U. Lohmann, S Ramachandran, P. L. da Silva Dias, S. C. Wofsy and X. Zhang: Couplings Between
 2976 Changes in the Climate System and Biogeochemistry, Cambridge University Press, Cambridge, United Kingdom and
 2977 New York, NY, USA., 2007.

2978 [D'Imperio, L., B.-B. Li, J. M. Tiedje, Oh, Y., Christiansen, J.R., Kepfer-Rojas, S., Westergaard-Nielsen, A., Brandt, K.](#)

2979 [K., Holm P.E., Wang, P., Ambus, P., and Elberling, B.: Spatial Controls of Methane Uptake in Upland Soils Across](#)
 2980 [Climatic and Geological Regions in Greenland, Communications Earth & Environment, 4-46,](#)
 2981 <https://doi.org/10.1038/s43247-023-01143-3>, 2023.
 2982 Dirmeyer, P. A., Gao, X., Zhao, M., Guo, Z., Oki, T., and Hanasaki, N. GSWP-2: Multimodel analysis and impli-
 2983 cations for our perception of the land surface. Bulletin of the American Meteorological Society, 87(10):1381–1398, 2006.
 2984 Dlugokencky, E. J., Dutton, E. G., Novelli, P. C., Tans, P. P., Masarie, K. A., Lantz, K. O. and Madronich, S.: Changes in
 2985 CH₄ and CO growth rates after the eruption of Mt Pinatubo and their link with changes in tropical tropospheric UV
 2986 flux, Geophys. Res. Lett., 23(20), 2761–2764, 1996.
 2987 Dlugokencky, E. J., Myers, R. C., Lang, P. M., Masarie, K. A., Crotwell, A. M., Thoning, K. W., Hall, B. D., Elkins, J.
 2988 W. and Steele, L. P.: Conversion of NOAA atmospheric dry air CH₄ mole fractions to a gravimetrically prepared
 2989 standard scale, J Geophys Res, 110(D18306), doi:10.1029/2005JD006035., 2005.
 2990 Dlugokencky, E. J., Bruhwiler, L., White, J. W. C., Emmons, L. K., Novelli, P. C., Montzka, S. A., Masarie, K. A., Lang,
 2991 P. M., Crotwell, A. M., Miller, J. B. and Gatti, L. V.: Observational constraints on recent increases in the atmospheric
 2992 CH₄ burden, Geophys. Res. Lett., 36, 5 PP., doi:200910.1029/2009GL039780, 2009.
 2993 Dlugokencky, E. J., Nisbet, E. G., Fisher, R. and Lowry, D.: Global atmospheric methane: budget, changes and dangers,
 2994 Philos. Trans. R. Soc. - Math. Phys. Eng. Sci., 369(1943), 2058–2072, 2011.
 2995 Dong, B., Xi, Y., Cui, Y., and Peng, S.: Quantifying Methane Emissions from Aquaculture Ponds in China, Environ. Sci.
 2996 Technol., 57, 1576–1583, <https://doi.org/10.1021/acs.est.2c05218>, 2023.
 2997 Downing, J.: Emerging global role of small lakes and ponds: Little things mean a lot. Limnetica, 29: p. 9-24, 2010
 2998 Drinkwater, A., Palmer, P. I., Feng, L., Arnold, T., Lan, X., Michel, S. E., Parker, R., and Boesch, H.: Atmospheric data
 2999 support a multi-decadal shift in the global methane budget towards natural tropical emissions, Atmos. Chem. Phys.,
 3000 23, 8429–8452, <https://doi.org/10.5194/acp-23-8429-2023>, 2023.
 3001 Dubos, T., Dubey, S., Tort, M., Mittal, R., Meurdesoif, Y. and Hourdin, F.: DYNAMICO-1.0, an icosahedral hydrostatic
 3002 dynamical core designed for consistency and versatility, Geosci. Model Dev., 8(10), 3131–3150, doi:10.5194/gmd-8-
 3003 3131-2015, 2015.
 3004 Dueck, T. A., de Visser, R., Poorter, H., Persijn, S., A. Gorissen, A., W. de Visser, W., Schapendonk, A., Verhagen, J.,
 3005 Snel, J., Harren, F. J. M., Ngai, A. K. Y., Verstappen, F., Bouwmeester, H., Voesenek, L. A. C. J. and van der Werf,
 3006 A.: No evidence for substantial aerobic methane emission by terrestrial plants: a ¹³C-labelling approach, New Phytol.,
 3007 doi:10.1111/j.1469-8137.2007.02103.x, 2007.
 3008 [Duncan, B., Anderson, D., Fiore, A., Joiner, J., Krotkov, N., Li, C., Millet, D., Nicely, J., Oman, L., St. Clair, J., Shutter, J.,](#)
 3009 [Souri, A., Strode, S., Weir, B., Wolfe, G., Worden, H., and Zhu, Q.: Opinion: Beyond Global Means: Novel Space-Based](#)
 3010 [Approaches to Indirectly Constrain the Concentrations, Trends, and Variations of Tropospheric Hydroxyl Radical \(OH\),](#)
 3011 [EGUsphere \[preprint\], https://doi.org/10.5194/egusphere-2024-2331](#), 2024.

3012 Dutaur, L. and Verchot, L. V.: A global inventory of the soil CH₄ sink, Glob. Biogeochem Cycles, 21, GB4012,
3013 doi:10.1029/2006GB002734, 2007.

3014 Dyonisius, M. N., Petrenko, V. V., Smith, A. M., Hua, Q., Yang, B., Schmitt, J., Beck, J., Seth, B., Bock, M., Hmiel, B.,
3015 Vimont, I., Menking, J. A., Shackleton, S. A., Baggenstos, D., Bauska, T. K., Rhodes, R. H., Sperlich, P., Beaudette,
3016 R., Harth, C., Kalk, M., Brook, E.J., Fisher, H., Severinghaus, J.P., and Weiss, R. F.: Old carbon reservoirs were not
3017 important in the deglacial methane budget, Science, 367(6480), 907–910. <https://doi.org/10.1126/science.aax0504>,
3018 2020

3019 EDGAR (Emissions Database for Global Atmospheric Research) Community GHG Database (a collaboration between
3020 the European Commission, Joint Research Centre (JRC), the International Energy Agency (IEA), and comprising IEA-
3021 EDGAR CO₂, EDGAR CH₄, EDGAR N₂O, EDGAR F-GASES version 7.0, European Commission, JRC (Datasets),
3022 available at https://edgar.jrc.ec.europa.eu/dataset_ghg70#sources, 2022

3023 EDGAR (Emissions Database for Global Atmospheric Research) Community GHG Database, a collaboration between the
3024 European Commission, Joint Research Centre (JRC), the International Energy Agency (IEA), and comprising IEA-
3025 EDGAR CO₂, EDGAR CH₄, EDGAR N₂O, EDGAR F-GASES version 8.0, European Commission, JRC (Datasets),
3026 available at https://edgar.jrc.ec.europa.eu/dataset_ghg80, 2023

3027 Eggleton, P., Homathevi, R., Jones, D., MacDonald, J., Jeeva, D., Bignell, D., Davies, R., and Maryati, M.: Termite
3028 assemblages, forest disturbance and greenhouse gas fluxes in Sabah, East Malaysia, Philos. T. Roy. Soc. B, 354, 1791–
3029 1802, doi: 10.1098/rstb.1999.0521, 1999

3030 Ehhalt, D., Prather, M., Dentener, F., Derwent, R., Dlugokencky, E., Holland, E., Isaksen, I., Katima, J., Kirchhoff, V.,
3031 Matson, P., Midgley, P. and Wang, M.: Atmospheric chemistry and greenhouse gases. In: Climate Change 2001: The
3032 Scientific Basis. Contribution of Working Group I to the Third Assessment Report of the Intergovernmental Panel on
3033 Climate Change. [Houghton, J.T., et al. (eds.)]. Cambridge University Press, Cambridge, United Kingdom and New
3034 York, NY, USA, pp. 239-287, 2001.

3035 Ehhalt, D. H.: The atmospheric cycle of methane, Tellus, 26(1–2), 58–70, doi:10.1111/j.2153-3490.1974.tb01952.x, 1974.

3036 Ehret, G., Bousquet, P., Pierangelo, C., Alpers, M., Millet, B., Abshire, J. B., Bovensmann, H., Burrows, J. P., Chevallier,
3037 F., Ciais, P., Crevoisier, C., Fix, A., Flamant, P., Frankenberg, C., Gibert, F., Heim, B., Heimann, M., Houweling, S.,
3038 Hubberten, H. W., Jockel, P., Law, K., Low, A., Marshall, J., Agusti-Panareda, A., Payan, S., Prigent, C., Rairoux, P.,
3039 Sachs, T., Scholze, M. and Wirth, M.: MERLIN: A French-German Space Lidar Mission Dedicated to Atmospheric
3040 Methane, Remote Sens., 9(10), 2017.

3041 Etiope, G.: Natural Gas Seepage. The Earth's Hydrocarbon Degassing, Springer International Publishing., 2015.

3042 Etiope G.: Natural emissions of methane from geological seepage in Europe. Atmosph. Environment, 43, 1430-1443,
3043 doi:10.1016/j.atmosenv.2008.03.014., 2009

3044 Etiope, G. and Schwietzke, S.: Global geological methane emissions: an update of top-down and bottom-up estimates,

Supprimé: ¶

Supprimé: ¶

3047 Elem Sci Anth, 7(1), 47, doi:10.1525/elementa.383, 2019.

3048 Etiopie, G., Lassey, K. R., Klusman, R. W. and Boschi, E.: Reappraisal of the fossil methane budget and related emission
3049 from geologic sources, *Geophys. Res. Lett.*, 35(9), L09307, doi:10.1029/2008gl033623, 2008.

3050 Etiopie, G., Nakada, R., Tanaka, K. and Yoshida, N.: Gas seepage from Tokamachi mud volcanoes, onshore Niigata
3051 Basin (Japan): origin, post-genetic alterations and CH₄-CO₂ fluxes. *App. Geochem.*, 26, 348-359, 2011.

3052 Etiopie, G., Ciotoli, G., Schwietzke, S. and Schoell, M.: Gridded maps of geological methane emissions and their isotopic
3053 signature, *Earth Syst Sci Data*, 11(1), 1–22, doi:10.5194/essd-11-1-2019, 2019.

3054 EU-Landfill-Directive: <https://eur-lex.europa.eu/legal-content/EN/TXT/?uri=CELEX:31999L0031>, 1999.

3055 FAO: FAOSTAT Emissions Land Use database. Food and Agriculture Organization of the United Nations. Statistical
3056 Division., [online] Available from: <http://www.fao.org/faostat/en/#data/GL> (Accessed December 2022), 2022.

3057 Federici, S., Tubiello, F. N., Salvatore, M., Jacobs, H. and Schmidhuber, J.: New estimates of CO₂ forest emissions and
3058 removals: 1990–2015, *For. Ecol. Manag.*, 352, 89–98, doi:10.1016/j.foreco.2015.04.022, 2015.

3059 Feng, L., Braun, C., Arnold, S. R. and Gidden, M.: *iiasa/emissions_downscaling: Supplemental Data*,
3060 doi:10.5281/zenodo.2538194, 2019.

3061 Feng, L., Palmer, P. I., Parker, R. J., Lunt, M. F., and Bösch, H.: Methane emissions are predominantly responsible for
3062 record-breaking atmospheric methane growth rates in 2020 and 2021, *Atmos. Chem. Phys.*, 23, 4863–4880,
3063 <https://doi.org/10.5194/acp-23-4863-2023>, 2023.

3064 Fest, B. J., Hinko-Najera, N., Wardlaw, T., Griffith, D. W. T., Livesley, S. J., and Arndt, S. K.: Soil methane oxidation in
3065 both dry and wet temperate eucalypt forests shows a near-identical relationship with soil air-filled porosity,
3066 Biogeosciences, 14, 467–479, <https://doi.org/10.5194/bg-14-467-2017>, 2017.

3067 Filges, A., Gerbig, C., Chen, H., Franke, H., Klaus, C., and Jordan, A.: The IAGOS-core greenhouse gas package: a
3068 measurement system for continuous airborne observations of CO₂, CH₄, H₂O and CO, *Tellus B*, 68, 27989,
3069 <https://doi.org/10.3402/tellusb.v67.27989>, 2015.

3070 Fleischer, P., Orsi, T. H., Richardson, M. D., and Anderson, A. L. (2001). Distribution of free gas in marine sediments: a
3071 global overview. *Geo-Marine Lett.*, 21, 103–122, 2001.

3072 Flores, E., Rhoderick, G. C., Viallon, J., Moussay, P., Choteau, T., Gameson, L., Guenther, F. R. and Wielgosz, R. I.:
3073 Methane standards made in whole and synthetic air compared by cavity ring down spectroscopy and gas
3074 chromatography with flame ionization detection for atmospheric monitoring applications, *Anal. Chem.*, 87(6), 3272–
3075 3279, doi:10.1021/ac5043076, 2015.

3076 Fluet-Chouinard, E., Stocker, BD, Zhang, Z, Malhotra, A, Melton, JR, Poulter, B, Kaplan, JO, Goldewijk, KK, Siebert, S,
3077 Minayeva, T, Hugelius, G, Joosten, H, Barthelmes, A, Prigent, C, Aires, F, Hoyt, AM, Davidson, N, Finlayson, CM,
3078 Lehner, B, Jackson, RB, McIntyre, PB: Extensive global wetland loss over the past three centuries, *Nature*, 614(7947)
3079 281-286, doi:10.1038/s41586-022-05572-6, 2023

Mis en forme : Français

Forster, P., T. Storelvmo, K. Armour, W. Collins, J.-L. Dufresne, D. Frame, D.J. Lunt, T. Mauritsen, M.D. Palmer, M. Watanabe, M. Wild, and H. Zhang: The Earth's Energy Budget, Climate Feedbacks, and Climate Sensitivity. In Climate Change 2021: The Physical Science Basis. Contribution of Working Group I to the Sixth Assessment Report of the Intergovernmental Panel on Climate Change [Masson-Delmotte, V., P. Zhai, A. Pirani, S.L. Connors, C. Péan, S. Berger, N. Caud, Y. Chen, L. Goldfarb, M.I. Gomis, M. Huang, K. Leitzell, E. Lonnoy, J.B.R. Matthews, T.K. Maycock, T. Waterfield, O. Yelekçi, R. Yu, and B. Zhou (eds.)]. Cambridge University Press, Cambridge, United Kingdom and New York, NY, USA, pp. 923–1054, doi: [10.1017/9781009157896.009](https://doi.org/10.1017/9781009157896.009), 2021

Foschi M., Etiope G., Cartwright J.A.: Seismic evidence of extensive microbial gas migration and trapping in submarine marine hydrates (Rakhine Basin, Bay of Bengal). Mar. Petrol. Geol., 149, 106100, <https://doi.org/10.1016/j.marpetgeo.2023.106100>, 2023

[France, J. L., Lunt, M. F., Andrade, M., Moreno, I., Ganesan, A. L., Lachlan-Cope, T., Fisher, R. E., Lowry, D., Parker, R. J., Nisbet, E. G., and Jones, A. E.: Very large fluxes of methane measured above Bolivian seasonal wetlands, P. Natl. Acad. Sci. USA, 119, e2206345119, <https://doi.org/10.1073/pnas.2206345119>, 2022.](#)

Francey, R. J., Steele, L. P., Langenfelds, R. L. and Pak, B. C.: High precision long-term monitoring of radiatively active and related trace gases at surface sites and from aircraft in the southern hemisphere atmosphere, J. Atmospheric Sci., 56(2), 279–285, 1999.

Frankenberg, C., Meirink, J. F., van Weele, M., Platt, U. and Wagner, T.: Assessing methane emissions from global space-borne observations, Science, 308(5724), 1010–1014, 2005.

Fraser, P. J., Rasmussen, R. A., Creffield, J. W., French, J. R. and Khalil, M. A. K.: Termites and global methane – Another assessment, J. Atmospheric Chem., 4, 295–310, 1986.

Fraser, W. T., Blei, E., Fry, S. C., Newman, M. F., Reay, D. S., Smith, K. A. and McLeod, A. R.: Emission of methane, carbon monoxide, carbon dioxide and short-chain hydrocarbons from vegetation foliage under ultraviolet irradiation, Plant Cell Environ., 38(5), 980–989, doi:10.1111/pce.12489, 2015.

Fujita, R., Morimoto, S., Maksyutov, S., Kim, H.-S., Arshinov, M., Brailsford, G., Aoki, S. and Nakazawa, T.: Global and Regional CH₄ Emissions for 1995–2013 Derived From Atmospheric CH₄, δ¹³C-CH₄, and δD-CH₄ Observations and a 715 Chemical Transport Model. J. Geophys. Res. Atmos., 125: e2020JD032903. <https://doi.org/10.1029/2020JD032903>, 2020

Gauci, V., Figueiredo, V., Gedney, N., Pangala, S. R., Stauffer, T., Weedon, G., P. and Enrich-Prast A. Non-flooded riparian Amazon trees are a regionally significant methane source, *Phil. Trans. R. Soc. A*, 3802020044620200446 <http://doi.org/10.1098/rsta.2020.0446>, 2022.

[Gauci, V., Pangala, S.R., Shenkin, A., Barba, J., Bastviken, D., Figueiredo, V., Gomez, C., Enrich-Prast A., Sayer, E., s-Stauffer, T., Welch, B., Elias, D., McNamara, N., Allen, M. and Malhi Y.: Global atmospheric methane uptake by upland tree woody surfaces, Nature, 631, 796–800, <https://doi.org/10.1038/s41586-024-07592-w>, 2024](#)

Supprimé :

Supprimé :

Supprimé: 2021

3116 [Gedney, N., Huntinford, C., Comyn Platt, E. and Wiltshire, A. Significant feedbacks of wetland methane release on climate](#)
 3117 [change and the causes of their uncertainty. Env. Res. Letts. 14, 084027 doi:10.1088/1748-9326/ab2726, 2019.](#)
 3118 Gidden, M. J., Riahi, K., Smith, S. J., Fujimori, S., Luderer, G., Kriegler, E., Vuuren, D. P. van, Berg, M. van den, Feng,
 3119 L., Klein, D., Calvin, K., Doelman, J. C., Frank, S., Fricko, O., Harmsen, M., Hasegawa, T., Havlik, P., Hilaire, J.,
 3120 Hoesly, R., Horing, J., Popp, A., Stehfest, E. and Takahashi, K.: Global emissions pathways under different
 3121 socioeconomic scenarios for use in CMIP6: a dataset of harmonized emissions trajectories through the end of the
 3122 century, *Geosci. Model Dev.*, 12(4), 1443–1475, doi:10.5194/gmd-12-1443-2019, 2019.
 3123 Giglio, L., Randerson, J. T. and van der Werf, G. R.: Analysis of daily, monthly, and annual burned area using the fourth-
 3124 generation global fire emissions database (GFED4), *J. Geophys. Res. - Biogeosciences*, 118(1), 317–328,
 3125 doi:10.1002/jgrg.20042, 2013.
 3126 Glagolev, M., Kleptsova, I., Filippov, I., Maksyutov, S. and Machida, T.: Regional methane emission from West Siberia
 3127 mire landscapes, *Environ. Res. Lett.*, 6(4), 045214, doi:doi:10.1088/1748-9326/6/4/045214, 2011.
 3128 Glatthor, N., von Clarmann, T., Funke, B., Garcia-Comas, M., Grabowski, U., Höpfner, M., Kellmann, S., Kiefer, M.,
 3129 Laeng, A., Linden, A., Lopez-Puertas, M., and Stiller, G. P.: IMK/IAA MIPAS retrievals version 8: CH₄ and N₂O,
 3130 EGUsphere [preprint], <https://doi.org/10.5194/egusphere-2023-919>, 2023.
 3131 Global Methane Pledge, Global Methane Pledge website: Pledges, 1 September. [https://www.](https://www.globalmethanepledge.org/#pledges)
 3132 [globalmethanepledge.org/#pledges](https://www.globalmethanepledge.org/#pledges). Accessed 28 September 2023, 2023.
 3133 [Gorgolewski, A. S., Caspersen, J. P., Vantellingen, J., and Thomas, S. C.: Tree foliage is a methane sink in upland](#)
 3134 [temperate forests, *Ecosystems*, 26, 174–186, 2023.](#)
 3135 [Greinert, J., Artemov, Y., Egorov, V., De Batist, M., McGinnis, D.: 1300-m-high rising bubbles from mud volcanoes at](#)
 3136 [2080 m in the Black Sea: Hydroacoustic characteristics and temporal variability, *Earth and Planetary Science Letters*,
 3137 \[244, 1–2, <https://doi.org/10.1016/j.epsl.2006.02.011>, 2006\]\(#\)
 3138 Griffiths, K., A. Jeziorski, D. Antoniadis, M. Beaulieu, J.P. Smol, and I. Gregory-Eaves, Pervasive changes in algal
 3139 indicators since pre-industrial times: A paleolimnological study of changes in primary production and diatom
 3140 assemblages from ~200 Canadian lakes. *Science of The Total Environment*, 838: p. 155938., 2022.
 3141 Grinham, A., M. Dunbabin, D. Gale, and J. Udy, Quantification of ebullitive and diffusive methane release to atmosphere
 3142 from a water storage. *Atmospheric Environment*, 45\(39\): p. 7166-7173., 2011.
 3143 Gromov, S., Brenninkmeijer, C. A. M. and Jöckel, P.: A very limited role of tropospheric chlorine as a sink of the
 3144 greenhouse gas methane, *Atmospheric Chem. Phys.*, 18\(13\), 9831–9843, doi:10.5194/acp-18-9831-2018, 2018.
 3145 Guo, M., Fang, S., Liu, S., Liang, M., Wu, H., Yang, L., Li, Z., Liu, P., Zhang, F: Comparison of atmospheric CO₂, CH₄,
 3146 and CO at two stations in the Tibetan Plateau of China, *Earth Space Sci.*, 7, e2019EA001051, 2020
 3147 Gurney, K. R., Law, R. M., Denning, A. S., Rayner, P. J., Pak, B. C., Baker, D., Bousquet, P., Bruhwiler, L., Chen, Y. H.,
 3148 Ciais, P., Fung, I. Y., Heimann, M., John, J., Maki, T., Maksyutov, S., Peylin, P., Prather, M. and Taguchi, S.: Transcom](#)

Supprimé: 4

3150 3 inversion intercomparison: Model mean results for the estimation of seasonal carbon sources and sinks, Glob.
3151 Biogeochem. Cycles, 18(1), GB2010, doi:10.1029/2003gb002111, 2004.

3152 Harris, S. A., French, H. M., Heginbottom, J. A., Johnston, G. H., Ladanyi, B., Sego, D. C. and van Everdingen, R. O.:
3153 Glossary of permafrost and related ground-ice terms, National Research Council of Canada. Associate Committee on
3154 Geotechnical Research. Permafrost Subcommittee., 1988.

3155 Harris, I., Jones, P.D., Osborn, T.J. and Lister, D.H.: Updated high-resolution grids of monthly climatic observations – the
3156 CRU TS3.10 Dataset, Int. J. Climatol., 34: 623-642. <https://doi.org/10.1002/joc.3711>, 2014

3157 Harrison, J.A., Y.T. Prairie, S. Mercier-Blais, and C. Soued: Year-2020 Global Distribution and Pathways of Reservoir
3158 Methane and Carbon Dioxide Emissions According to the Greenhouse Gas From Reservoirs (G-res) Model. Global
3159 Biogeochemical Cycles 35(6): p. e2020GB006888, 2021.

3160 Heathcote, A. J., C. T. Filstrup, and J. A. Downing (2013): Watershed sediment losses to lakes accelerating despite
3161 agricultural soil conservation efforts, *PLoS One*, 8(1), e53554, doi:10.1371/journal.pone.0053554, 2013

3162 Heđěnc, P., Jiménez, J.J., Moradi, J. *et al.*: Global distribution of soil fauna functional groups and their estimated litter
3163 consumption across biomes. Sci Rep 12, 17362, <https://doi.org/10.1038/s41598-022-21563-z>, 2022

3164 [Hempson, G.P., Archibald, S. and Bond, W.J.: The consequences of replacing wildlife with livestock in Africa, Sci Rep,](https://doi.org/10.1038/s41598-017-17348-4)
3165 [7, 17196, https://doi.org/10.1038/s41598-017-17348-4, 2017](https://doi.org/10.1038/s41598-017-17348-4)

3166 [Hill, J., McSweeney, C., Wright, A.-D. G., Bishop-Hurley, G., and Kalantar-zadeh, K.: Measuring Methane Production](https://doi.org/10.1016/j.tibtech.2015.10.004)
3167 [from Ruminants, Trends in Biotechnology, Volume 34, Issue 1, doi:10.1016/j.tibtech.2015.10.004, 2016](https://doi.org/10.1016/j.tibtech.2015.10.004)

3168 Hmiel, B., Petrenko, V. V., Dyonisius, M. N., Buizert, C., Smith, A. M., Place, P. F., Harth, C., Beaudette, R., Hua, Q.,
3169 Yang, B., Vimont, I., Michel, S. E., Severinghaus, J. P., Etheridge, D., Bromley, T., Schmitt, J., Faïn, X., Weiss, R. F.
3170 and Dlugokencky, E.: Preindustrial 14 CH 4 indicates greater anthropogenic fossil CH 4 emissions, Nature, 578(7795),
3171 409–412, doi:10.1038/s41586-020-1991-8, 2020.

3172 Ho, J.C., A.M. Michalak, and N. Pahlevan: Widespread global increase in intense lake phytoplankton blooms since the
3173 1980s. Nature, 574(7780): p. 667-670, 2019

3174 Hoesly, R. M., Smith, S. J., Feng, L., Klimont, Z., Janssens-Maenhout, G., Pitkanen, T., Seibert, J. J., Vu, L., Andres, R.
3175 J., Bolt, R. M., Bond, T. C., Dawidowski, L., Kholod, N., Kurokawa, J. I., Li, M., Liu, L., Lu, Z., Moura, M. C. P.,
3176 O'Rourke, P. R. and Zhang, Q.: Historical (1750–2014) anthropogenic emissions of reactive gases and aerosols from
3177 the Community Emissions Data System (CEDS), Geosci Model Dev, 11(1), 369–408, doi:10.5194/gmd-11-369-2018,
3178 2018.

3179 Höglund-Isaksson, L.: Bottom-up simulations of methane and ethane emissions from global oil and gas systems 1980 to
3180 2012, Environ. Res. Lett., 12(2), 024007, doi:10.1088/1748-9326/aa583e, 2017.

3181 Höglund-Isaksson, L., Thomson, A., Kupiainen, K., Rao, S. and Janssens-Maenhout, G.: Anthropogenic methane sources,
3182 emissions and future projections, Chapter 5 in AMAP Assessment 2015: Methane as an Arctic Climate Forcer, p. 39-

3183 59, available at <http://www.amap.no/documents/doc/AMAP-Assessment-2015-Methane-as-an-Arctic-climate->
3184 [forcer/1285](http://www.amap.no/documents/doc/AMAP-Assessment-2015-Methane-as-an-Arctic-climate-), 2015.

3185 Höglund-Isaksson, L., Gómez-Sanabria, A., Klimont, Z., Rafaj, P., Schöpp, W.,: Technical potentials and costs for
3186 reducing global anthropogenic methane emissions in the 2050 timeframe -results from the GAINS model, Environ.
3187 Res. Comm. 2(2), <https://iopscience.iop.org/article/10.1088/2515-7620/ab7457> , 2020

3188 Holgerson, M. A. and Raymond, P. A.: Large contribution to inland water CO₂ and CH₄ emissions from very small
3189 ponds, Nat. Geosci., 9(3), 222–226, doi:10.1038/ngeo2654, 2016.

3190 Holmes, C. D., Prather, M. J., Søvde, O. A. and Myhre, G.: Future methane, hydroxyl, and their uncertainties: key climate
3191 and emission parameters for future predictions, Atmospheric Chem. Phys., 13(1), 285–302, doi:10.5194/acp-13-285-
3192 2013, 2013.

3193 Hopcroft, P.O. , P.J. Valdes & D.J. Beerling, (2011). Simulating idealised Dansgaard-Oeschger events and their potential
3194 influence on the global methane cycle, Quaternary Science Reviews, 30, 3258-3268,
3195 doi: 10.1016/j.quascirev.2011.08.01., 2011

3196 Hossaini, R., Chipperfield, M. P., Saiz-Lopez, A., Fernandez, R., Monks, S., Feng, W., Brauer, P. and Glasow, R. von: A
3197 global model of tropospheric chlorine chemistry: Organic versus inorganic sources and impact on methane oxidation,
3198 J. Geophys. Res. Atmospheres, 121(23), 14,271-14,297, doi:10.1002/2016JD025756, 2016.

3199 Houweling, S., Bergamaschi, P., Chevallier, F., Heimann, M., Kaminski, T., Krol, M., Michalak, A. M. and Patra, P.:
3200 Global inverse modeling of CH₄ sources and sinks: an overview of methods, Atmospheric Chem. Phys., 17(1), 235–
3201 256, doi:10.5194/acp-17-235-2017, 2017.

3202 M. Hovland, A.G. Judd, R.A. Burke: The global flux of methane from shallow submarine sediments, Chemosphere,
3203 Volume 26, Issues 1–4, Pages 559-578, doi:10.1016/0045-6535(93)90442-8., 1993

3204 Howarth, R. W.: Ideas and perspectives: is shale gas a major driver of recent increase in global atmospheric methane?,
3205 Biogeosciences, 16(15), 3033–3046, doi:10.5194/bg-16-3033-2019, 2019.

3206 Hu, H., Landgraf, J., Detmers, R., Borsdorff, T., Brugh, J. A. de, Aben, I., Butz, A. and Hasekamp, O.: Toward Global
3207 Mapping of Methane With TROPOMI: First Results and Intersatellite Comparison to GOSAT, Geophys. Res. Lett.,
3208 45(8), 3682–3689, doi:10.1002/2018GL077259, 2018.

3209 Hugelius, G., Tarnocai, C., Broll, G., Canadell, J. G., Kuhry, P., & Swanson, D. K.. The Northern Circumpolar Soil Carbon
3210 Database: spatially distributed datasets of soil coverage and soil carbon storage in the northern permafrost regions.
3211 *Earth System Science Data*, 5(1), 3–13. <https://doi.org/10.5194/essd-5-3-2013>, 2013

3212 Hugelius, G., Strauss, J., Zubrzycki, S., Harden, J. W., Schuur, E. A. G., Ping, C. L., Schirrmeister, L., Grosse, G.,
3213 Michaelson, G. J., Koven, C. D., O'Donnell, J. A., Elberling, B., Mishra, U., Camill, P., Yu, Z., Palmtag, J. and Kuhry,
3214 P.: Estimated stocks of circumpolar permafrost carbon with quantified uncertainty ranges and identified data gaps,
3215 Biogeosciences, 11(23), 6573–6593, doi:10.5194/bg-11-6573-2014, 2014.

3216 Hugelius, Gustaf, Loisel, J., Chadburn, S., Jackson, R. B., Jones, M., MacDonald, G., et al. : Large stocks of peatland
 3217 carbon and nitrogen are vulnerable to permafrost thaw. *Proceedings of the National Academy of Sciences*, 117(34),
 3218 20438–20446. <https://doi.org/10.1073/pnas.1916387117>, 2020

3219 Hugelius, G., Ramage, J.L., Burke, E.J., Chatterjee, A., Smallman, T.L., Aalto, T., Bastos, A., Biasi, C., Canadell, J.G.,
 3220 Chandra, N. and Chevallier, F., et al. Two decades of permafrost region CO₂, CH₄, and N₂O budgets suggest a small
 3221 net greenhouse gas source to the atmosphere. Preprint in ESS Open Archive. September 11, 2023. DOI:
 3222 10.22541/essoar.169444320.01914726/v1, 2023

3223 IEA, *Coal Information: Overview*, IEA, Paris <https://www.iea.org/reports/coal-information-overview>, License: CC BY
 3224 4.0, Accessed 17 January 2024, 2021

3225 IEA (2023), Energy Statistics Data Browser, IEA, Paris [https://www.iea.org/data-and-statistics/data-tools/energy-](https://www.iea.org/data-and-statistics/data-tools/energy-statistics-data-browser)
 3226 [statistics-data-browser](https://www.iea.org/data-and-statistics/data-tools/energy-statistics-data-browser), Accessed 17 January 2024, 2023a

3227 IEA, US natural gas production by source, 2013-2023, IEA, Paris [https://www.iea.org/data-and-statistics/charts/us-](https://www.iea.org/data-and-statistics/charts/us-natural-gas-production-by-source-2013-2023)
 3228 [natural-gas-production-by-source-2013-2023](https://www.iea.org/data-and-statistics/charts/us-natural-gas-production-by-source-2013-2023), IEA. Licence: CC BY 4.0, Accessed 17 January 2024, 2023b

3229 Imasu, R.; Matsunaga, T.; Nakajima, M.; Yoshida, Y.; Shiomi, K.; Morino, I.; Saitoh, N.; Niwa, Y.; Someya, Y.; Oishi,
 3230 Y.; et al. Greenhouse Gases Observing SATellite 2 (GOSAT-2): Mission Overview. *Prog. Earth Planet. Sci.*, 10, 33.,
 3231 2023,

3232 Inoue, M., Morino, I., Uchino, O., Nakatsuru, T., Yoshida, Y., Yokota, T., Wunch, D., Wennberg, P. O., Roehl, C. M.,
 3233 Griffith, D. W. T., Velazco, V. A., Deutscher, N. M., Warneke, T., Notholt, J., Robinson, J., Sherlock, V., Hase, F.,
 3234 Blumenstock, T., Rettinger, M., Sussmann, R., Kyrö, E., Kivi, R., Shiomi, K., Kawakami, S., Mazière, M. D., Arnold,
 3235 S. G., Feist, D. G., Barrow, E. A., Barney, J., Dubey, M., Schneider, M., Iraci, L. T., Podolske, J. R., Hillyard, P. W.,
 3236 Machida, T., Sawa, Y., Tsuboi, K., Matsueda, H., Sweeney, C., Tans, P. P., Andrews, A. E., Biraud, S. C., Fukuyama,
 3237 Y., Pittman, J. V., Kort, E. A. and Tanaka, T.: Bias corrections of GOSAT SWIR XCO₂ and XCH₄ with TCCON data
 3238 and their evaluation using aircraft measurement data, *Atmospheric Meas. Tech.*, 9(8), 3491–3512, doi:10.5194/amt-9-
 3239 3491-2016, 2016.

3240 IPCC: Good Practice Guidance and Uncertainty Management in National Greenhouse Gas Inventories. Intergovernmental
 3241 Panel on Climate Change, National Greenhouse Gas Inventories Programme. Montreal, IPCC-
 3242 XVI/Doc.10(1.IV.2000), May 2000., 2000.

3243 IPCC: Climate change 2001: The scientific basis. Contribution of working group I to the third assessment report of the
 3244 Intergovernmental Panel on Climate Change, Cambridge University Press, Cambridge, United Kingdom and New
 3245 York, NY, USA., 2001.

3246 IPCC: IPCC Guidelines for National Greenhouse Gas Inventories. The National Greenhouse Gas Inventories Programme,
 3247 Eggleston H.S., Buendia L., Miwa K., Ngara T. and Tanabe K. (eds). The Intergovernmental Panel on Climate Change,
 3248 IPCC TSU NGGIP, IGES. Institute for Global Environmental Strategy, Hayama, Kanagawa, Japan. Available online

at: http://www.ipcc-nggip.iges.or.jp/support/Primer_2006GLs.pdf, 2006.

IPCC: 2019 Refinement to the 2006 IPCC Guidelines for National Greenhouse Gas Inventories — IPCC. [online] Available from: <https://www.ipcc.ch/report/2019-refinement-to-the-2006-ipcc-guidelines-for-national-greenhouse-gas-inventories/> (Accessed 17 March 2020), 2019.

Ito, A. and Inatomi, M.: Use of a process-based model for assessing the methane budgets of global terrestrial ecosystems and evaluation of uncertainty, *Biogeosciences*, 9(2), 759–773, doi:10.5194/bg-9-759-2012, 2012.

Jacob, D. J., Varon, D. J., Cusworth, D. H., Dennison, P. E., Frankenberg, C., Gautam, R., Guanter, L., Kelley, J., McKeever, J., Ott, L. E., Poulter, B., Qu, Z., Thorpe, A. K., Worden, J. R., and Duren, R. M.: Quantifying methane emissions from the global scale down to point sources using satellite observations of atmospheric methane, *Atmos. Chem. Phys.*, 22, 9617–9646, <https://doi.org/10.5194/acp-22-9617-2022>, 2022.

Jackson, R. B., Down, A., Phillips, N. G., Ackley, R. C., Cook, C. W., Plata, D. L. and Zhao, K.: Natural gas pipeline leaks across Washington, D.C, *Environ. Sci. Technol.*, 48(3), 2051–2058, doi:10.1021/es404474x, 2014a.

Jackson, R. B., Sauniois, M., Bousquet, P., Canadell, J. G., Poulter, B., Stavert, A. R., Poulter, B., Bergamaschi, P., Niwa, Y., Segers, A., Tsuruta, A.: Increasing anthropogenic methane emissions arise equally from agricultural and fossil fuel sources, *Environmental Research Letters*, 15, 7, <https://doi.org/10.1088/1748-9326/ab9ed2>, 2020

Jackson, R. B., Sauniois, M., Martinez, A., Canadell, J. G., Yu, X., Li, M., Poulter, B., Raymind, P., Regnier, P., Davis, S.J., and Patra, P.: Human activities now fuel two-thirds of global methane emissions, *Environmental Research Letters*, 19, 101002, DOI:10.1088/1748-9326/ad6463, 2024

Jamali, H., Livesley, S.J., Dawes, T.Z. *et al.* Termite mound emissions of CH₄ and CO₂ are primarily determined by seasonal changes in termite biomass and behaviour. *Oecologia* 167, 525–534, doi.org/10.1007/s00442-011-1991-3, 2011

Janssens-Maenhout, G., Crippa, M., Guizzardi, D., Muntean, M., Schaaf, E., Dentener, F., Bergamaschi, P., Pagliari, V., Olivier, J., Peters, J., van Aardenne, J., Monni, S., Doering, U., Petrescu, R., Solazzo, E. and Oreggioni, G.: EDGAR v4.3.2 Global Atlas of the three major Greenhouse Gas Emissions for the period 1970-2012, *Earth Syst Sci Data Discuss*, 2019, 1–52, doi:10.5194/essd-2018-164, 2019.

JAXA: GOSAT-2: Greenhouse gases Observing SATellite-2@ibuki2_JAXA"IBUKI-2", [online] Available from: <https://global.jaxa.jp/projects/sat/gosat2/index.html> (Accessed 25 March 2020), 2019.

Jensen, K. and Mcdonald, K.: Surface Water Microwave Product Series Version 3: A Near-Real Time and 25-Year Historical Global Inundated Area Fraction Time Series From Active and Passive Microwave Remote Sensing, *IEEE Geosci. Remote Sens. Lett.*, 16(9), 1402–1406, doi:10.1109/LGRS.2019.2898779, 2019.

Jiang, Y., Groenigen, K. J. van, Huang, S., Hungate, B. A., Kessel, C. van, Hu, S., Zhang, J., Wu, L., Yan, X., Wang, L., Chen, J., Hang, X., Zhang, Y., Horwath, W. R., Ye, R., Linquist, B. A., Song, Z., Zheng, C., Deng, A. and Zhang, W.: Higher yields and lower methane emissions with new rice cultivars, *Glob. Change Biol.*, 23(11), 4728–4738,

Supprimé: Jackson, R. B., Vengosh, A., Carey, J. W., Davies, R. J., Darrah, T. H., O'Sullivan, F. and Pétron, G.: The Environmental Costs and Benefits of Fracking, *Annu. Rev. Environ. Resour.*, 39, 327–362, doi:10.1146/annurev-environ-031113-144051, 2014b.

Supprimé: ❌

Mis en forme : Français

doi:10.1111/gcb.13737, 2017.

Johnson, D. E., Phetteplace, H. W. and Seidl, A. F.: Methane, nitrous oxide and carbon dioxide emissions from ruminant livestock production systems, edited by J. Takahashi and B. A. Young, pp. 77–85, Elsevier, Amsterdam, The Netherlands., 2002.

Johnson, M.S., E. Matthews, J. Du, V. Genovese, and D. Bastviken, Methane Emission From Global Lakes: New Spatiotemporal Data and Observation-Driven Modeling of Methane Dynamics Indicates Lower Emissions, *Journal of Geophysical Research: Biogeosciences*, 127(7): p. e2022JG006793, 2022

Johnson, M. S., E. Matthews, D. Bastviken, B. Deemer, J. Du, and V. Genovese, Spatiotemporal methane emission from global reservoirs, *Journal of Geophysical Research: Biogeosciences*, 126, e2021JG006305, <https://doi.org/10.1029/2021JG006305>, 2021

Judd, A.G. (2004). Natural seabed seeps as sources of atmospheric methane, *Environ. Geol.*, 46, 988–996, 2004.

Jung, M., Reichstein, M., Margolis, H. A., Cescatti, A., Richardson, A. D., Arain, M. A., Arneth, A., Bernhofer, C., Bonal, D., Chen, J., Gianelle, D., Gobron, N., Kiely, G., Kutsch, W., Lasslop, G., Law, B. E., Lindroth, A., Merbold, L., Montagnani, L., Moors, E. J., Papale, D., Sottocornola, M., Vaccari, F., and Williams, C.: Global patterns of land-atmosphere fluxes of carbon dioxide, latent heat, and sensible heat derived from eddy covariance, satellite, and meteorological observations, *J. Geophys. Res.*, 116, G00J07, <https://doi.org/10.1029/2010jg001566>, 2011.

Kai, F. M., Tyler, S. C., Randerson, J. T. and Blake, D. R.: Reduced methane growth rate explained by decreased Northern Hemisphere microbial sources, *Nature*, 476(7359), 194–197, 2011.

Kaiser, J. W., Heil, A., Andreae, M. O., Benedetti, A., Chubarova, N., Jones, L., Morcrette, J. J., Razinger, M., Schultz, M. G., Suttie, M. and van der Werf, G. R.: Biomass burning emissions estimated with a global fire assimilation system based on observed fire radiative power, *Biogeosciences*, 9(1), 527–554, doi:10.5194/bg-9-527-2012, 2012.

Kallungal, J. T., Lindström, J., Miller, P. A., Rinne, J., Raivonen, M., and Scholze, M.: Optimising CH₄ simulations from the LPJ-GUESS model v4.1 using an adaptive MCMC algorithm, *Geosci. Model Dev. Discuss.* [preprint], <https://doi.org/10.5194/gmd-2022-302>, in review, 2023.

Karl, D., Beversdorf, L., Björkman, K. *et al.* Aerobic production of methane in the sea. *Nature Geosci* **1**, 473–478, <https://doi.org/10.1038/ngeo234>, 2008

Karlson, M., and Bastviken, D.: Multi-Source Mapping of Peatland Types Using Sentinel-1, Sentinel-2, and Terrain Derivatives—A Comparison Between Five High-Latitude Landscapes. *Journal of Geophysical Research: Biogeosciences* 128, e2022JG007195. <https://doi.org/10.1029/2022JG007195>, 2023

Keppler, F., Hamilton, J. T. G., Brass, M. and Rockmann, T.: Methane emissions from terrestrial plants under aerobic conditions, *Nature*, 439, 187–191, doi:10.1038/nature04420, 2006.

Kholod, N., Evans, M., Pilcher, R. C., Roshchanka, V., Ruiz, F., Côté, M. and Collings, R.: Global methane emissions from coal mining to continue growing even with declining coal production, *J. Clean. Prod.*, 256, 120489,

Supprimé: Karion, A., Sweeney, C., Pétron, G., Frost, G., Michael Hardesty, R., Kofler, J., Miller, B. R., Newberger, T., Wolter, S., Banta, R., Brewer, A., Dlugokencky, E., Lang, P., Montzka, S. A., Schnell, R., Tans, P., Trainer, M., Zamora, R. and Conley, S.: Methane emissions estimate from airborne measurements over a western United States natural gas field, *Geophys. Res. Lett.*, 40(16), 4393–4397, doi:10.1002/grl.50811, 2013.

Supprimé: 

doi:10.1016/j.jelepro.2020.120489, 2020.

Kim H., Global Soil Wetness Project Phase 3 Atmospheric Boundary Conditions (Experiment 1) [Data set]. Data Integration and Analysis System (DIAS)., <https://doi.org/10.20783/DIAS.501>, 2017

King, J.R., Warren, R.J., Bradford, M.A. Correction: Social Insects Dominate Eastern US Temperate Hardwood Forest Macroinvertebrate Communities in Warmer Regions. PLOS ONE 8(10): 10.1371/annotation/87285c86-f1df-4f8b-bc08-d64643d351f4, 2013.

Kirk, L. and MJ Cohen: River Corridor Sources Dominate CO₂ Emissions From a Lowland River Network. Journal of Geophysical Research, Biogeosciences, 128(1), e2022JG006954, 2023.

Kirschke, S., Bousquet, P., Ciais, P., Saunois, M., Canadell, J. G., Dlugokencky, E. J., Bergamaschi, P., Bergmann, D., Blake, D. R., Bruhwiler, L., Cameron-Smith, P., Castaldi, S., Chevallier, F., Feng, L., Fraser, A., Heimann, M., Hodson, E. L., Houweling, S., Josse, B., Fraser, P. J., Krummel, P. B., Lamarque, J. F., Langenfelds, R. L., Le Quere, C., Naik, V., O'Doherty, S., Palmer, P. I., Pison, I., Plummer, D., Poulter, B., Prinn, R. G., Rigby, M., Ringeval, B., Santini, M., Schmidt, M., Shindell, D. T., Simpson, I. J., Spahni, R., Steele, L. P., Strode, S. A., Sudo, K., Szopa, S., van der Werf, G. R., Voulgarakis, A., van Weele, M., Weiss, R. F., Williams, J. E. and Zeng, G.: Three decades of global methane sources and sinks, Nat. Geosci., 6(10), 813–823, doi:10.1038/ngeo1955, 2013.

Klauda, J. B. and Sandler, S. I.: Global distribution of methane hydrate in ocean sediment, Energy Fuels, 19(2), 459–470, 2005.

Kleinen, T., Brovkin, V. and Schuldt, R. J.: A dynamic model of wetland extent and peat accumulation: results for the Holocene, Biogeosciences, 9(1), 235–248, doi:10.5194/bg-9-235-2012, 2012.

Kleinen, T., Mikolajewicz, U., and Brovkin, V.: Terrestrial methane emissions from the Last Glacial Maximum to the preindustrial period, Clim. Past, 16, 575–595, doi:10.5194/cp-16-575-2020, 2020.

Kleinen, T., Gromov, S., Steil, B., and Brovkin, V.: Atmospheric methane underestimated in future climate projections, Environ. Res. Lett., 16, 094006, doi:10.1088/1748-9326/ac1814, 2021.

Kleinen, T., Gromov, S., Steil, B., and Brovkin, V.: Atmospheric methane since the last glacial maximum was driven by wetland sources, Clim. Past, 19, 1081–1099, doi:10.5194/cp-19-1081-2023, 2023

Knittel K and Boetius A : Anaerobic oxidation of methane: progress with an unknown process methane. Annu Rev Microbiol 63:311–334, 2009

Knox, S. H., Jackson, R. B., Poulter, B., McNicol, G., Fluet-Chouinard, E., Zhang, Z., Hugelius, G., Bousquet, P., Canadell, J. G., Saunois, M., Papale, D., Chu, H., Keenan, T. F., Baldocchi, D., Torn, M. S., Mammarella, I., Trotta, C., Aurela, M., Bohrer, G., Campbell, D. I., Cescatti, A., Chamberlain, S., Chen, J., Chen, W., Dengel, S., Desai, A. R., Euskirchen, E., Friborg, T., Gasbarra, D., Goded, I., Goeckede, M., Heimann, M., Helbig, M., Hirano, T., Hollinger, D. Y., Iwata, H., Kang, M., Klatt, J., Krauss, K. W., Kutzbach, L., Lohila, A., Mitra, B., Morin, T. H., Nilsson, M. B., Niu, S., Noormets, A., Oechel, W. C., Peichl, M., Peltola, O., Reba, M. L., Richardson, A. D., Runkle, B. R. K., Ryu,

3362 Y., Sachs, T., Schäfer, K. V. R., Schmid, H. P., Shurpali, N., Sonnentag, O., Tang, A. C. I., Ueyama, M., Vargas, R.,
 3363 Vesala, T., Ward, E. J., Windham-Myers, L., Wohlfahrt, G. and Zona, D.: FLUXNET-CH4 Synthesis Activity:
 3364 Objectives, Observations, and Future Directions, *Bull. Am. Meteorol. Soc.*, 100(12), 2607–2632, doi:10.1175/BAMS-
 3365 D-18-0268.1, 2019.
 3366 Knox, S. H., Bansal, S., McNicol, G., Schafer, K., Sturtevant, C., Ueyama, M., et al.: Identifying dominant environmental
 3367 predictors of freshwater wetland methane fluxes across diurnal to seasonal time scales. *Global Change Biology*,
 3368 27(15), 3582–3604. <https://doi.org/10.1111/gcb.15661>, 2021
 3369 Kretschmer, K., Biastoch, A., Rüpke, L. and Burwicz, E.: Modeling the fate of methane hydrates under global warming,
 3370 *Glob. Biogeochem Cycles*, 29(5), 610–625, doi:1002/2014GB005011, 2015.
 3371 Kuhn, M.A., Varner, R.K., Bastviken, D., Crill, P., MacIntyre, S., Turetsky, M., Walter Anthony, K., McGuire, A.D., and
 3372 Olefeldt, D. (2021). BAWLD-CH4: a comprehensive dataset of methane fluxes from boreal and arctic ecosystems.
 3373 *Earth Syst. Sci. Data* 13, 5151-5189. 10.5194/essd-13-5151-2021.
 3374 Kuze A, Kikuchi N, Kataoka F, Suto H, Shiomi K, Kondo Y. Detection of Methane Emission from a Local Source Using
 3375 GOSAT Target Observations. *Remote Sensing*, 12(2):267. <https://doi.org/10.3390/rs12020267>, 2020
 3376 Kyzivat, E.D., L.C. Smith, F. Garcia-Tigueros, C. Huang, C. Wang, T. Langhorst, J.V. Fayne, M.E. Harlan, Y. Ishitsuka,
 3377 D. Feng, W. Dolan, L.H. Pitcher, K.P. Wickland, M.M. Domblaser, R.G. Striegl, T.M. Pavelsky, D.E. Butman, and
 3378 C.J. Gleason, The Importance of Lake Emergent Aquatic Vegetation for Estimating Arctic-Boreal Methane Emissions.
 3379 *Journal of Geophysical Research: Biogeosciences* 127(6): p. e2021JG006635, 2022.
 3380 Lamarque, J. F., Shindell, D. T., Josse, B., Young, P. J., Cionni, I., Eyring, V., Bergmann, D., Cameron-Smith, P., Collins,
 3381 W. J., Doherty, R., Dalsoren, S., Faluvegi, G., Folberth, G., Ghan, S. J., Horowitz, L. W., Lee, Y. H., MacKenzie, I.
 3382 A., Nagashima, T., Naik, V., Plummer, D., Righi, M., Rumbold, S. T., Schulz, M., Skeie, R. B., Stevenson, D. S.,
 3383 Strode, S., Sudo, K., Szopa, S., Voulgarakis, A. and Zeng, G.: The Atmospheric Chemistry and Climate Model
 3384 Intercomparison Project (ACCMIP): overview and description of models, simulations and climate diagnostics, *Geosci.*
 3385 *Model Dev.*, 6(1), 179–206, doi:10.5194/gmd-6-179-2013, 2013.
 3386 Lamb, B. K., Edburg, S. L., Ferrara, T. W., Howard, T., Harrison, M. R., Kolb, C. E., Townsend-Small, A., Dyck, W.,
 3387 Possolo, A. and Whetstone, J. R.: Direct Measurements Show Decreasing Methane Emissions from Natural Gas Local
 3388 Distribution Systems in the United States, *Environ. Sci. Technol.*, 49(8), 5161–5169, doi:10.1021/es505116p, 2015.
 3389 Lan, X., K.W. Thoning, and E.J. Dlugokencky: Trends in globally-averaged CH4, N2O, and SF6 determined from NOAA
 3390 Global Monitoring Laboratory measurements. Version 2024-02, <https://doi.org/10.15138/P8XG-AA10>, 2024
 3391 Lange S., WFDE5 over land merged with ERA5 over the ocean (WSE5). V. 1.0. 2019. doi:10.5880/pik.2019.023, 2019
 3392 Laruelle, G. G., Dürr, H. H., Lauerwald, R., Hartmann, J., Slomp, C. P., Goossens, N. and Regnier, P. A. G.: Global multi-
 3393 scale segmentation of continental and coastal waters from the watersheds to the continental margins, *Hydrol. Earth*
 3394 *Syst. Sci.*, 17(5), 2029–2051, doi:10.5194/hess-17-2029-2013, 2013.

3395 [Laruelle, G.G., Rosentreter, J.A. and Regnier, P.: Extrapolation-Based Regionalized Re-evaluation of the Global Estuarine](#)
3396 [Surface Area. *Estuaries and Coasts*, 48, 34, <https://doi.org/10.1007/s12237-024-01463-3>, 2025](#)

3397 Lassey, K. R., Etheridge, D. M., Lowe, D. C., Smith, A. M. and Ferretti, D. F.: Centennial evolution of the atmospheric
3398 methane budget: what do the carbon isotopes tell us?, *Atmospheric Chem. Phys.*, 7(8), 2119–2139, 2007a.

3399 Lassey, K. R., Lowe, D. C. and Smith, A. M.: The atmospheric cycling of radiomethane and the “fossil fraction” of the
3400 methane source, *Atmospheric Chem. Phys.*, 7(8), 2141–2149, 2007b.

3401 Lauerwald, R., Allen, G.H., Deemer, B.R., Liu, S., Maavara, T., Raymond, P., Alcott, L., Bastviken, D., Hastie, A.,
3402 Holgerson, M.A., Johnson, M.S., Lehner, B., Lin, P., Marzadri, A., Ran, L., Tian, H., Yang, X., Yao, Y. and Regnier,
3403 P. Inland water greenhouse gas budgets for RECCAP2: 1. State-of- the-art of global scale assessments. *Global*
3404 *Biogeochemical Cycles*, 37, e2022GB007657. <https://doi.org/10.1029/2022GB007657>, 2023a.

3405 Lauerwald, R., Allen, G.H., Deemer, B.R., Liu, S., Maavara, T., Raymond, P., Alcott, L., Bastviken, D., Hastie, A.,
3406 Holgerson, M.A., Johnson, M.S., Lehner, B., Lin, P., Marzadri, A., Ran, L., Tian, H., Yang, X., Yao, Y. and Regnier,
3407 P. Inland water greenhouse gas budgets for RECCAP2: 2 Regionalization and homogenization of estimates following
3408 the RECCAP2 framework, *Global Biogeochemical Cycles*, 37, e2022GB007658. <https://doi.org/10.1029/2022GB007658>, 2023b.

3409

3410 Laughner, J. L., Neu, J. L., Schimel, D., Wennberg, P. O., Barsanti, K., Bowman, K. W., Chatterjee, A., Croes, B. E.,
3411 Fitzmaurice, H. L., Henze, D. K., Kim, J., Kort, E. A., Liu, Z., Miyazaki, K., Turner, A. J., Anenberg, S., Avise, J.,
3412 Cao, H., Crisp, D., de Gouw, J., Eldering, A., Fyfe, J. C., Goldberg, D. L., Gurney, K. R., Hasheminassab, S., Hopkins,
3413 F., Ivey, C. E., Jones, D. B. A., Liu, J., Lovenduski, N. S., Martin, R. V., McKinley, G. A., Ott, L., Poulter, B., Ru, M.,
3414 Sander, S. P., Swart, N., Yung, Y. L., and Zeng, Z.-C.: Societal shifts due to COVID-19 reveal large-scale complexities
3415 and feedbacks between atmospheric chemistry and climate change, *P. Natl. Acad. Sci. USA*, 118, e2109481118,
3416 <https://doi.org/10.1073/pnas.2109481118>, 2021.

3417 Lauvaux, T., Giron, C., Mazzolini, M., d’Aspremont, A., Duren, R., Cusworth, D., Shindell, D., and Ciais, P.: Global
3418 assessment of oil and gas methane ultra-emitters, *Science*, 375, 557–561, <https://doi.org/10.1126/science.abj4351>,
3419 2022.

3420 Lelieveld, J., Crutzen, P. J. and Dentener, F. J.: Changing concentration, lifetime and climate forcing of atmospheric
3421 methane, *Tellus Ser. B-Chem. Phys. Meteorol.*, 50(2), 128–150, doi:10.1034/j.1600-0889.1998.t01-1-00002.x, 1998.

3422 Lelieveld, J., Lechtenbohrer, S., Assonov, S. S., Brenninkmeijer, C. A. M., Dienst, C., Fishedick, M. and Hanke, T.:
3423 Greenhouse gases: Low methane leakage from gas pipelines, *Nature*, 434(7035), 841–842, doi:10.1038/434841a, 2005.

3424 Lenhart, K., Klintzsch, T., Langer, G., Nehrke, G., Bunge, M., Schnell, S. and Keppler, F.: Evidence for methane
3425 production by the marine algae *Emiliania huxleyi*, *Biogeosciences*, 13(10), 3163–3174, doi:10.5194/bg-13-3163-2016,
3426 2016.

3427 Lewan, M. D.: Comment on Ideas and perspectives: is shale gas a major driver of recent increase in global atmospheric

Supprimé: &

Supprimé: (2025).

methane? by Robert W. Howarth (2019), Biogeosciences Discuss., 1–10, doi:10.5194/bg-2019-419, 2020.

Li, C., Frolking, S., Xiao, X., Moore, B., Boles, S., Qiu, J., Huang, Y., Salas, W. and Sass, R.: Modeling impacts of farming management alternatives on CO₂, CH₄, and N₂O emissions: A case study for water management of rice agriculture of China, Glob. Biogeochem. Cycles, 19(3), doi:10.1029/2004gb002341, 2005.

Li T, Huang Y, Zhang W, Song C: CH4MODwetland: A biogeophysical model for simulating methane emissions from natural wetlands. Ecological Modelling 221: 666–680, 2010.

Li, Y., J. Shang, C. Zhang, W. Zhang, L. Niu, L. Wang, and H. Zhang, The role of freshwater eutrophication in greenhouse gas emissions: A review. Science of The Total Environment, 768: p. 144582., 2021

Li, H. Z., Seymour, S. P., MacKay, K., Wang, J. S., Warren, J., Guanter, L., Zavala-Araiza, D., Smith, M.L., and Xie, D.: Direct measurements of methane emissions from key facilities in Alberta's oil and gas supply chain, Science of The Total Environment, Volume 912, 169645, ISSN 0048-9697, doi:10.1016/j.scitotenv.2023.169645, 2024.

Lin, X., Indira, N. K., Ramonet, M., Delmotte, M., Ciais, P., Bhatt, B. C., Reddy, M. V., Angchuk, D., Balakrishnan, S., Jorphaal, S., Dorjai, T., Mahey, T. T., Patnaik, S., Begum, M., Brenninkmeijer, C., Durairaj, S., Kirubakaran, R., Schmidt, M., Swathi, P. S., Vinithkumar, N. V., Yver Kwok, C. and Gaur, V. K.: Long-lived atmospheric trace gases measurements in flask samples from three stations in India, Atmospheric Chem. Phys., 15(17), 9819–9849, doi:10.5194/acp-15-9819-2015, 2015.

Lin, P., Pan, M., Beck, H. E., Yang, Y., Yamazaki, D., Frasson, R., et al.: Global reconstruction of naturalized river flows at 2.94 million reaches. *Water Resources Research*, 55, 6499–6516. <https://doi.org/10.1029/2019WR025287>, 2019

Liu, Z., Guan, D., Wei, W., Davis, S. J., Ciais, P., Bai, J., Peng, S., Zhang, Q., Hubacek, K., Marland, G., Andres, R. J., Crawford-Brown, D., Lin, J., Zhao, H., Hong, C., Boden, T. A., Feng, K., Peters, G. P., Xi, F., Liu, J., Li, Y., Zhao, Y., Zeng, N. and He, K.: Reduced carbon emission estimates from fossil fuel combustion and cement production in China, *Nature*, 524(7565), 335–338, doi:10.1038/nature14677, 2015.

Liu, G., Peng, S., Lin, X., Ciais, P., Li, X., Xi, Y., Lu, Z., Chang, J., Saunio, M., Wu, Y., Patra, P., Chandra, N., Zeng, H., and Piao, S.: Recent Slowdown of Anthropogenic Methane Emissions in China Driven by Stabilized Coal Production, *Environ. Sci. Technol. Lett.*, 8, 739–746, <https://doi.org/10.1021/acs.estlett.1c00463>, 2021a.

Liu, S., Fang, S., Liu, P., Liang, M., Guo, M., and Feng, Z.: Measurement report: Changing characteristics of atmospheric CH₄ in the Tibetan Plateau: records from 1994 to 2019 at the Mount Waliguan station, *Atmos. Chem. Phys.*, 21, 393–413, <https://doi.org/10.5194/acp-21-393-2021>, 2021b

Liu, S., C. Kuhn, G. Amatulli, K. Aho, D.E. Butman, G.H. Allen, P. Lin, M. Pan, D. Yamazaki, C. Brinkerhoff, C. Gleason, X. Xia, and P.A. Raymond: The importance of hydrology in routing terrestrial carbon to the atmosphere via global streams and rivers. *Proceedings of the National Academy of Sciences*, 119(11): p. e2106322119, 2022.

3462 Lloret, Z., Chevallier, F., Cozic, A., Remaud, M., and Meurdesoif, Y.: Simulating the variations of carbon dioxide in the
 3463 global atmosphere on the hexagonal grid of DYNAMICO coupled with the LMDZ6 model, *Geosci. Model Dev.*
 3464 *Discuss.* [preprint], <https://doi.org/10.5194/gmd-2023-140>, in review, 2023.
 3465 Locatelli, R., Bousquet, P., Saunois, M., Chevallier, F. and Cressot, C.: Sensitivity of the recent methane budget to LMDz
 3466 sub-grid-scale physical parameterizations, *Atmospheric Chem. Phys.*, 15(17), 9765–9780, doi:10.5194/acp-15-9765-
 3467 2015, 2015.
 3468 Lohila, A., Aalto, T., Aurela, M., Hatakka, J., Tuovinen, J.-P., Kilkki, J., Penttilä, T., Vuorenmaa, J., Hänninen, P., Sutinen,
 3469 R., Viisanen, Y. and Laurila, T.: Large contribution of boreal upland forest soils to a catchment-scale CH₄ balance in
 3470 a wet year, *Geophys. Res. Lett.*, 43(6), 2946–2953, doi:10.1002/2016gl067718, 2016.
 3471 Lorente, A., Borsdorff, T., Martinez-Velarte, M. C., and Landgraf, J.: Accounting for surface reflectance spectral features
 3472 in TROPOMI methane retrievals, *Atmos. Meas. Tech.*, 16, 1597–1608, <https://doi.org/10.5194/amt-16-1597-2023>,
 3473 2023.
 3474 Lu, X., Jacob, D. J., Zhang, Y., Maasakkers, J. D., Sulprizio, M. P., Shen, L., Qu, Z., Scarpelli, T. R., Nesser, H., Yantosca,
 3475 R. M., Sheng, J., Andrews, A., Parker, R. J., Boesch, H., Bloom, A. A., and Ma, S.: Global methane budget and trend,
 3476 2010–2017: complementarity of inverse analyses using in situ (GLOBALVIEWplus CH₄ ObsPack) and satellite
 3477 (GOSAT) observations, *Atmos. Chem. Phys.*, 21, 4637–4657, <https://doi.org/10.5194/acp-21-4637-2021>, 2021
 3478 Lu, X., Jacob, D. J., Zhang, Y., Maasakkers, J. D., Zhang, Y., Qu, Z., Chen, Z., Sulprizio, M. P., Varon, D., Hmiel, H.,
 3479 Park, R. J., Boesch, H., and Fan, S.: Observation-derived 2010–2019 trends in methane emissions and intensities from
 3480 US oil and gas fields tied to activity metrics, *P. Natl. Acad. Sci. USA*, 120, e2217900120,
 3481 <https://doi.org/10.1073/pnas.2217900120>, 2023.
 3482 Maasakkers, J. D., Jacob, D. J., Sulprizio, M. P., Scarpelli, T. R., Nesser, H., Sheng, J.-X., Zhang, Y., Hersher, M., Bloom,
 3483 A. A., Bowman, K. W., Worden, J. R., Janssens-Maenhout, G., and Parker, R. J.: Global distribution of methane
 3484 emissions, emission trends, and OH concentrations and trends inferred from an inversion of GOSAT satellite data for
 3485 2010–2015, *Atmos. Chem. Phys.*, 19, 7859–7881, <https://doi.org/10.5194/acp-19-7859-2019>, 2019.
 3486 Maasakkers, J. D., Jacob, D. J., Sulprizio, M. P., Scarpelli, T. R., Nesser, H., Sheng, J., Zhang, Y., Lu, X., Bloom, A. A.,
 3487 Bowman, K. W., Worden, J. R., and Parker, R. J.: 2010–2015 North American methane emissions, sectoral
 3488 contributions, and trends: a high-resolution inversion of GOSAT observations of atmospheric methane, *Atmos. Chem.*
 3489 *Phys.*, 21, 4339–4356, <https://doi.org/10.5194/acp-21-4339-2021>, 2021.
 3490 Maavara, T., Lauerwald, R., Regnier, P. and Van Capellen P.: Global perturbation of organic carbon cycling by river
 3491 damming, *Nat Commun* 8, 153, <https://doi.org/10.1038/ncomms15347>, 2017.
 3492 Machacova, K., Borak, L., Agyei, T., Schindler, T., Soosaar, K., Mander, Ü., and Ah-Peng, C: Trees as net sinks for
 3493 methane (CH₄) and nitrous oxide (N₂O) in the lowland tropical rain forest on volcanic Réunion Island, *The New*
 3494 *phytologist*, 229(4), 1983–1994, <https://doi.org/10.1111/nph.17002>, 2021

Mis en forme : Indice

Mis en forme : Indice

3495 Machida, T., H. Matsueda, Y. Sawa, Y. Nakagawa, K. Hirotani, N. Kondo, K. Goto, N. Nakazawa, K. Ishikawa and T.
3496 Ogawa: Worldwide measurements of atmospheric CO₂ and other trace gas species using commercial airlines, *J. Atmos.*
3497 *Oceanic Technol.*, 25(10), 1744-1754, doi:10.1175/2008JTECHA1082.1, 2008

3498 Maksyutov, S., Oda, T., Saito, M., Janardanan, R., Belikov, D., Kaiser, J. W., Zhuravlev, R., Ganshin, A., Valsala, V. K.,
3499 Andrews, A., Chmura, L., Dlugokencky, E., Haszpra, L., Langenfelds, R. L., Machida, T., Nakazawa, T., Ramonet,
3500 M., Sweeney, C. and Worthy, D.: Technical note: A high-resolution inverse modelling technique for estimating surface
3501 CO₂ fluxes based on the NIES-TM & FLEXPART coupled transport model and its adjoint, *Atmospheric Chem.*
3502 *Phys. Discuss.*, 1–33, doi:10.5194/acp-2020-251, 2020.

3503 Malerba, M.E., T. de Kluyver, N. Wright, L. Schuster, and P.I. Macreadie: Methane emissions from agricultural ponds are
3504 underestimated in national greenhouse gas inventories. *Communications Earth & Environment*, 3(1): p. 306, 2022

3505 Maltby, J., L. Steinle, C. R. Löschner, H. W. Bange, M. A. Fischer, M. Schmidt, and T. Treude: Microbial methanogenesis
3506 in the sulfate-reducing zone of sediments in the Eckernförde Bay, SW Baltic Sea. *Biogeosciences* **15**: 137–157.
3507 doi:10.5194/bg-15-137-2018, 2018

3508 Manning, F. C. , Kho, L. K., Hill, T. C., Cornulier, T., and Teh, Y A: Carbon Emissions From Oil Palm Plantations on
3509 Peat Soil, *Front. For. Glob. Change, Sec. Tropical Forests*, Volume 2 , <https://doi.org/10.3389/ffgc.2019.0003>, 2019

3510 Mannisenaho V, Tsuruta A, Backman L, Houweling S, Segers A, Krol M, Saunio M, Poulter B, Zhang Z, Lan X, et al.
3511 Global Atmospheric $\delta^{13}\text{CH}_4$ and CH₄ Trends for 2000–2020 from the Atmospheric Transport Model TM5 Using CH₄
3512 from Carbon Tracker Europe–CH₄ Inversions. *Atmosphere*, 14(7):1121. <https://doi.org/10.3390/atmos14071121>, 2023

3513 van Marle, M. J. E., Kloster, S., Magi, B. I., Marlon, J. R., Daniau, A.-L., Field, R. D., Arneth, A., Forrest, M., Hantson,
3514 S., Kehrwald, N. M., Knorr, W., Lasslop, G., Li, F., Mangeon, S., Yue, C., Kaiser, J. W. and Werf, G. R. van der:
3515 Historic global biomass burning emissions for CMIP6 (BB4CMIP) based on merging satellite observations with
3516 proxies and fire models (1750–2015), *Geosci. Model Dev.*, 10(9), 3329–3357, doi:10.5194/gmd-10-3329-2017, 2017.

3517 Martinez, A., Saunio, M., Poulter B., Zhen, Z., Raymond, P., Regnier, P. Canadell, J. G., Jackson, R. B., Patra, P. K.,
3518 Bousquet, P., Ciais, P., Dlugokencky, E.J., Lan, X., Allen, G., Bastviken, D., Beerling, D. J., Belikov, D., Blake, D.,
3519 Castaldi, S., Crippa, M., Deemer, B.R., Dennison, F., Etiope, G., Gedney, N., Höglund-Isaksson, L., Holgersson, M.A.,
3520 Hopcroft, P. O. , Hugelius, G., Ito, A., Jain, A. K., Janardanan, R., Johnson, M. S., Kleinen, T., Krummel, P. B.,
3521 Lauerwald, R., Li, T., Liu, X., McDonald, K. C., Melton, J. R., Mühle, J., Müller, J., Murguía-Flores, F., Niwa, Y.,
3522 Noce, S., Pan, S., Parker, R. J., Peng, C., Ramonet, M., Riley, W. J., Rocher-Ros, G., Rosentreter, J. A., Sasakawa,
3523 M., Segers A. , Smith, S. J., Stanley, E. H., Thanwerdas, J., Tian, H., Tsuruta, A., Tubiello, F. N., Weber, T. S., van
3524 der Werf, G. R., Worthy, D. E. J., Xi, Y., Yoshida Y. , Zhang, W. , Zheng, B. , Zhu, Qing , Zhu, Qian, and Zhuang,
3525 Q.: *Supplemental data of the Global Carbon Project Methane Budget 2024* v1. [Data set],
3526 <https://doi.org/10.18160/GKQ9-2RHT>, 2024

3527 Matthews, E. and Fung, I.: Methane emission from natural wetlands: Global distribution, area, and environmental

characteristics of sources, *Glob. Biogeochem. Cycles*, 1(1), 61–86, doi:10.1029/GB001i001p00061, 1987.

Mazzini A., Etiope G. (2017). Mud volcanism: an updated review. *Earth Sci. Rev.*, 168, 81-112. <http://dx.doi.org/10.1016/j.earscirev.2017.03.001>, 2017

McCalley, C. K., Woodcroft, B. J., Hodgkins, S. B., Wehr, R. A., Kim, E.-H., Mondav, R., Crill, P. M., Chanton, J. P., Rich, V. I., Tyson, G. W. and Saleska, S. R.: Methane dynamics regulated by microbial community response to permafrost thaw, *Nature*, 514(7523), 478–481, doi:10.1038/nature13798, 2014.

McCarthy, M. C., Boering, K. A., Rice, A. L., Tyler, S. C., Connell, P. and Atlas, E.: Carbon and hydrogen isotopic compositions of stratospheric methane: 2. Two-dimensional model results and implications for kinetic isotope effects, *J. Geophys. Res. Atmospheres*, 108(D15), doi:10.1029/2002JD003183, 2003.

McGinnis, D. F., J. Greinert, Y. Artemov, S. E. Beaubien, and A. Wüest: Fate of rising methane bubbles in stratified waters: How much methane reaches the atmosphere?, *J. Geophys. Res.*, 111, C09007, doi:10.1029/2005JC003183, 2006

McGuire, A. D., Christensen, T. R., Heroult, A., Miller, P. A., Hayes, D., Euskirchen, E., Kimball, J. S., Yi, Y., Koven, C., Lafleur, P., Oechel, W., Peylin, P. and Williams, M.: An assessment of the carbon balance of Arctic tundra, *Comp. Obs. Process Models Atmospheric Inversions*, 9(Article), 3185–3204, doi:10.5194/bg-9-3185-2012, 2012.

McKain, K., Down, A., Raciti, S. M., Budney, J., Hutyrá, L. R., Floerchinger, C., Herndon, S. C., Nehr Korn, T., Zahniser, M. S., Jackson, R. B., Phillips, N. and Wofsy, S. C.: Methane emissions from natural gas infrastructure and use in the urban region of Boston, Massachusetts, *Proc. Natl. Acad. Sci.*, 112(7), 1941–1946, doi:10.1073/pnas.1416261112, 2015.

McNicol, G., Fluet-Chouinard, E., Ouyang, Z., Knox, S., Zhang, Z., Aalto, T., et al.: Upscaling wetland methane emissions from the FLUXNET-CH₄ eddy covariance network (UpCH₄ v1.0): Model development, network assessment, and budget comparison. *AGU Advances*, 4, e2023AV000956. <https://doi.org/10.1029/2023AV000956>, 2023

Meinshausen, M., Smith, S., Calvin, K., Daniel, J., Kainuma, M., Lamarque, J. F., Matsumoto, K., Montzka, S., Raper, S., Riahi, K., Thomson, A., Velders, G. and van Vuuren, D. P.: The RCP greenhouse gas concentrations and their extensions from 1765 to 2300, *Clim. Change*, 109(1), 213–241, doi:10.1007/s10584-011-0156-z, 2011.

Meinshausen, M., Vogel, E., Nauels, A., Lorbacher, K., Meinshausen, N., Etheridge, D. M., Fraser, P. J., Montzka, S. A., Rayner, P. J., Trudinger, C. M., Krummel, P. B., Beyerle, U., Canadell, J. G., Daniel, J. S., Enting, I. G., Law, R. M., Lunder, C. R., O'Doherty, S., Prinn, R. G., Reimann, S., Rubino, M., Velders, G. J. M., Vollmer, M. K., Wang, R. H. J., and Weiss, R.: Historical greenhouse gas concentrations for climate modelling (CMIP6), *Geosci. Model Dev.*, 10, 2057–2116, <https://doi.org/10.5194/gmd-10-2057-2017>, 2017.

Meinshausen, M., Nicholls, Z. R. J., Lewis, J., Gidden, M. J., Vogel, E., Freund, M., Beyerle, U., Gessner, C., Nauels, A., Bauer, N., Canadell, J. G., Daniel, J. S., John, A., Krummel, P. B., Luderer, G., Meinshausen, N., Montzka, S. A.,

Rayner, P. J., Reimann, S., Smith, S. J., van den Berg, M., Velders, G. J. M., Vollmer, M. K., and Wang, R. H. J.: The shared socio-economic pathway (SSP) greenhouse gas concentrations and their extensions to 2500, *Geosci. Model Dev.*, 13, 3571–3605, <https://doi.org/10.5194/gmd-13-3571-2020>, 2020.

Melton, J. R. and Arora, V. K.: Competition between plant functional types in the Canadian Terrestrial Ecosystem Model (CTEM) v. 2.0, *Geosci. Model Dev.*, 9(1), 323–361, doi:10.5194/gmd-9-323-2016, 2016.

Melton, J. R., Wania, R., Hodson, E. L., Poulter, B., Ringeval, B., Spahni, R., Bohn, T., Avis, C. A., Beerling, D. J., Chen, G., Eliseev, A. V., Denisov, S. N., Hopcroft, P. O., Lettenmaier, D. P., Riley, W. J., Singarayer, J. S., Subin, Z. M., Tian, H., Zürcher, S., Brovkin, V., van Bodegom, P. M., Kleinen, T., Yu, Z. C. and Kaplan, J. O.: Present state of global wetland extent and wetland methane modelling: conclusions from a model intercomparison project (WETCHIMP), *Biogeosciences*, 10(2), 753–788, doi:10.5194/bg-10-753-2013, 2013.

Membrive, O., Crevoisier, C., Sweeney, C., Danis, F., Hertzog, A., Engel, A., Bönisch, H. and Picon, L.: AirCore-HR: a high-resolution column sampling to enhance the vertical description of CH₄ and CO₂, *Atmospheric Meas. Tech.*, 10(6), 2163–2181, doi:10.5194/amt-10-2163-2017, 2017.

Messenger, M. L., Lehner, B., Grill, G., Nedeva, I. and Schmitt, O.: Estimating the volume and age of water stored in global lakes using a geo-statistical approach, *Nat. Commun.*, 7(1), 1–11, doi:10.1038/ncomms13603, 2016.

Michel, SE, Lan, X, Miller, J, Tans, P, Clark, JR, Schaefer, H, Sperlich, P, Brailsford, G, Morimoto, S, Moossen, H, Li, J.: Rapid shift in methane carbon isotopes suggests microbial emissions drove record high atmospheric methane growth in 2020-2022, *Proc Natl Acad Sci U S A*, 121(44):e2411212121, doi: 10.1073/pnas.2411212121, 2024.

Mijling, B., van der A, R. J. and Zhang, Q.: Regional nitrogen oxides emission trends in East Asia observed from space, *Atmospheric Chem. Phys.*, 13(23), 12003–12012, doi:10.5194/acp-13-12003-2013, 2013.

Milkov, A. V.: Molecular and stable isotope compositions of natural gas hydrates: A revised global dataset and basic interpretations in the context of geological settings, *Org. Geochem.*, 36(5), 681–702, 2005.

Minkinen, K. and Laine, J.: Vegetation heterogeneity and ditches create spatial variability in methane fluxes from peatlands drained for forestry, *Plant Soil*, 285(1), 289–304, doi:10.1007/s11104-006-9016-4, 2006.

Monforti Ferrario, Fabio; Crippa, Monica; Guizzardi, Diego; Muntean, Marilena; Schaaf, Edwin; Lo Vullo, Eleonora; Solazzo, Efisio; Olivier, Jos; Vignati, Elisabetta: EDGAR v6.0 Greenhouse Gas Emissions. European Commission, Joint Research Centre (JRC) [Dataset] PID: <http://data.europa.eu/89h/97a67d67-c62e-4826-b873-9d972c4f670b>, 2021

Montzka, S. A., Krol, M., Dlugokencky, E., Hall, B., Jockel, P. and Lelieveld, J.: Small Interannual Variability of Global Atmospheric Hydroxyl, *Science*, 331(6013), 67–69, 2011.

Morgenstern, O., Hegglin, M. I., Rozanov, E., O'Connor, F. M., Abraham, N. L., Akiyoshi, H., Archibald, A. T., Bekki, S., Butchart, N., Chipperfield, M. P., Deushi, M., Dhomse, S. S., Garcia, R. R., Hardiman, S. C., Horowitz, L. W., Jöckel, P., Josse, B., Kinnison, D., Lin, M., Mancini, E., Manyin, M. E., Marchand, M., Marécal, V., Michou, M., Oman, L. D., Pitari, G., Plummer, D. A., Revell, L. E., Saint-Martin, D., Schofield, R., Stenke, A., Stone, K., Sudo,

Supprimé: Moore, C. W., Zielinska, B., Pétron, G. and Jackson, R. B.: Air impacts of increased natural gas acquisition, processing, and use: a critical review, *Environ. Sci. Technol.*, 48, 8349–8359, doi:10.1021/es4053472, 2014.

Supprimé: ¶

3599 K., Tanaka, T. Y., Tilmes, S., Yamashita, Y., Yoshida, K., and Zeng, G.: Review of the global models used within
3600 phase 1 of the Chemistry–Climate Model Initiative (CCMI), *Geosci. Model Dev.*, 10, 639–671,
3601 <https://doi.org/10.5194/gmd-10-639-2017>, 2017.

3602 [Morgenstern, O., Stone, K. A., Schofield, R., Akiyoshi, H., Yamashita, Y., Kinnison, D. E., Garcia, R. R., Sudo, K.,](#)
3603 [Plummer, D. A., Scinocca, J., Oman, L. D., Manyin, M. E., Zeng, G., Rozanov, E., Stenke, A., Revell, L. E., Pitari,](#)
3604 [G., Mancini, E., Di Genova, G., Visioni, D., Dhomse, S. S., and Chipperfield, M. P.: Ozone sensitivity to varying](#)
3605 [greenhouse gases and ozone-depleting substances in CCMI-1 simulations, *Atmos. Chem. Phys.*, 18, 1091–1114,](#)
3606 <https://doi.org/10.5194/acp-18-1091-2018>, 2018.

3607 Morino, I., Uchino, O., Inoue, M., Yoshida, Y., Yokota, T., Wennberg, P. O., Toon, G. C., Wunch, D., Roehl, C. M.,
3608 Notholt, J., Warneke, T., Messerschmidt, J., Griffith, D. W. T., Deutscher, N. M., Sherlock, V., Connor, B., Robinson,
3609 J., Sussmann, R. and Rettinger, M.: Preliminary validation of column-averaged volume mixing ratios of carbon dioxide
3610 and methane retrieved from GOSAT short-wavelength infrared spectra, *Atmospheric Meas. Tech.*, 4(6), 1061–1076,
3611 2011.

3612 Murguía-Flores, F., Arndt, S., Ganesan, A. L., Murray-Tortarolo, G. and Hornibrook, E. R. C.: Soil Methanotrophy Model
3613 (MeMo v1.0): a process-based model to quantify global uptake of atmospheric methane by soil, *Geosci. Model Dev.*,
3614 11(6), 2009–2032, doi:10.5194/gmd-11-2009-2018, 2018.

3615 [Murguía-Flores, F., Ganesan, A. L., Arndt, S., and Hornibrook, E. R. C.: Global uptake of atmospheric methane by soil](#)
3616 [from 1900 to 2100, *Global Biogeochemical Cycles*, 35, e2020GB006774, <https://doi.org/10.1029/2020GB006774>,](#)
3617 [2021.](#)

3618 Myer, A., Myer, M.H., Trettin, C.C. and Forschler, B.T.: The fate of carbon utilized by the subterranean termite
3619 *Reticulitermes flavipes*. *Ecosphere* 12 (12):e03872, doi:10.1002/ecs2.3872, 2021

3620 Myhre, G., Shindell, D., Bréon, F.-M., Collins, W., Fuglestad, J., Huang, J., Koch, D., Lamarque, J.-F., Lee, D.,
3621 Mendoza, B., Nakajima, T., Robock, A., Stephens, G., Takemura, T. and Zhang, H.: Anthropogenic and Natural
3622 Radiative Forcing., in *Climate Change 2013: The Physical Science Basis. Contribution of Working Group I to the*
3623 *Fifth Assessment Report of the Intergovernmental Panel on Climate Change.*, edited by T. F. Stocker, D. D. Qin, G.-
3624 K. Plattner, M. Tignor, S. K. Allen, J. Boschung, A. Nauels, Y. Xia, V. Bex, and P. M. Midgley, Cambridge University
3625 Press, Cambridge, United Kingdom and New York, NY, USA., 2013.

3626 Naik, V., Voulgarakis, A., Fiore, A. M., Horowitz, L. W., Lamarque, J. F., Lin, M., Prather, M. J., Young, P. J., Bergmann,
3627 D., Cameron-Smith, P. J., Cionni, I., Collins, W. J., Dalsoren, S. B., Doherty, R., Eyring, V., Faluvegi, G., Folberth,
3628 G. A., Josse, B., Lee, Y. H., MacKenzie, I. A., Nagashima, T., van Noije, T. P. C., Plummer, D. A., Righi, M., Rumbold,
3629 S. T., Skeie, R., Shindell, D. T., Stevenson, D. S., Strode, S., Sudo, K., Szopa, S. and Zeng, G.: Preindustrial to present
3630 day changes in tropospheric hydroxyl radical and methane lifetime from the Atmospheric Chemistry and Climate
3631 Model Intercomparison Project (ACCMIP), *Atmospheric Chem. Phys.*, 13(10), 5277–5298, doi:10.5194/acp-13-5277-

2013, 2013.

Nakazawa, T., Machida, T., Tanaka, M., Fujii, Y., Aoki, S. and Watanabe, O.: Differences of the atmospheric CH₄ concentration between the Arctic and Antarctic regions in pre-industrial/pre-agricultural era, *Geophys. Res. Lett.*, 20(10), 943–946, doi:10.1029/93GL00776, 1993.

Natchimuthu, S., I. Sundgren, M. Gålfalk, L. Klemedtsson, P. Crill, Å. Danielsson, and D. Bastviken, Spatio-temporal variability of lake CH₄ fluxes and its influence on annual whole lake emission estimates. *Limnology and Oceanography*, 61(S1): p. S13-S26, 2016.

Nauer, P. A., Hutley, L. B., and Arndt, S. K.: Termite mounds mitigate half of termite methane emissions, *P. Natl. Acad. Sci. USA*, 115, 13306–13311, 2018.

Naus, S., Montzka, S. A., Patra, P. K., and Krol, M. C.: A three-dimensional-model inversion of methyl chloroform to constrain the atmospheric oxidative capacity, *Atmos. Chem. Phys.*, 21, 4809–4824, <https://doi.org/10.5194/acp-21-4809-2021>, 2021.

Nicely, J. M., Salawitch, R. J., Canty, T., Anderson, D. C., Arnold, S. R., Chipperfield, M. P., Emmons, L. K., Flemming, J., Huijnen, V., Kinnison, D. E., Lamarque, J.-F., Mao, J., Monks, S. A., Steenrod, S. D., Tilmes, S. and Turquety, S.: Quantifying the causes of differences in tropospheric OH within global models, *J. Geophys. Res. Atmospheres*, 122(3), 1983–2007, doi:10.1002/2016JD026239, 2017.

Nicely, J. M., Canty, T. P., Manyin, M., Oman, L. D., Salawitch, R. J., Steenrod, S. D., Strahan, S. E., and Strode, S. A.: Changes in Global Tropospheric OH Expected as a Result of Climate Change Over the Last Several Decades, *J. Geophys. Res.-Atmos.*, 123, 10774–10795, <https://doi.org/10.1029/2018JD028388>, 2018.

Nirmal Rajkumar, A., J. Barnes, R. Ramesh, R. Purvaja, and R.C. Upstill-Goddard, Methane and nitrous oxide fluxes in the polluted Adyar River and estuary, SE India. *Marine Pollution Bulletin*, 56(12): p. 2043-2051, 2008

Nisbet, R. E. R., Fisher, R., Nimmo, R. H., Bendall, D. S., Crill, P. M., Gallego-Sala, A. V., Hornibrook, E. R. C., Lopez-Juez, E., Lowry, D., Nisbet, P. B. R., Shuckburgh, E. F., Sriskantharajah, S., Howe, C. J. and Nisbet, E. G.: Emission of methane from plants, *Proc. R. Soc. B-Biol. Sci.*, 276(1660), 1347–1354, 2009.

Nisbet, E. G., Manning, M. R., Dlugokencky, E. J., Fisher, R. E., Lowry, D., Michel, S. E., Myhre, C. L., Platt, S. M., Allen, G., Bousquet, P., Brownlow, R., Cain, M., France, J. L., Hermansen, O., Hossaini, R., Jones, A. E., Levin, I., Manning, A. C., Myhre, G., Pyle, J. A., Vaughn, B., Warwick, N. J. and White, J. W. C.: Very strong atmospheric methane growth in the four years 2014-2017: Implications for the Paris Agreement, *Glob. Biogeochem. Cycles*, 0(ja), doi:10.1029/2018GB006009, 2019.

Nisbet, E. G., Fisher, R. E., Lowry, D., France, J. L., Allen, G., Bakkaloglu, S., Broderick, T.J., Cain, M., Coleman, M., Fernandez, J., Forster, G., Griffiths, P.T., Iverach, C.P., Keely, B.F.J., Manning, M.R., Nisbet-Jones, B.R., Pyle, J.A., Townsend-Samll, A., al-Shallan, A., Warwick, N. and Zazzeri, G.: Methane mitigation: methods to reduce emissions, on the path to the Paris agreement. *Reviews of Geophysics*, 58, e2019RG000675.

Supprimé: ¶

<https://doi.org/10.1029/2019RG000675>, 2020
 Nisbet, E. G., Manning, M. R., Dlugokencky, E. J., Michel, S. E., Lan, X., Röckmann, T., van der Denier Gon, H. A., Schmitt, J., Palmer, P. I., Dyonisius, M. N., Oh, Y., Fisher, R. E., Lowry, D., France, J. L., White, J. W. C., Brailsford, G., and Bromley, T.: Atmospheric methane: Comparison between methane's record in 2006–2022 and during glacial terminations, *Global Biogeochem. Cy.*, 37, e2023GB007875, <https://doi.org/10.1029/2023GB007875>, 2023.
 Nisbet, E.G.: Climate feedback on methane from wetlands, *Nat. Clim. Chang.*, 13, 421–422, <https://doi.org/10.1038/s41558-023-01634-3>, 2023.
 Niwa, Y., Fujii, Y., Sawa, Y., Iida, Y., Ito, A., Satoh, M., Imasu, R., Tsuboi, K., Matsueda, H. and Saigusa, N.: A 4D-Var inversion system based on the icosahedral grid model (NICAM-TM 4D-Var v1.0) – Part 2: Optimization scheme and identical twin experiment of atmospheric CO₂ inversion, *Geosci. Model Dev.*, 10(6), 2201–2219, doi:10.5194/gmd-10-2201-2017, 2017.
 Niwa, Y., Ishijima, K., Ito, A. and Iida, Y.: Toward a long-term atmospheric CO₂ inversion for elucidating natural carbon fluxes: technical notes of NISMON-CO₂ v2021.1. *Prog. Earth Planet Sci.* 9, 42, doi:10.1186/s40645-022-00502-6, 2022
 Niwa, Y., Tohjima, Y., Terao, Y., Saeki, T., Ito, A., Umezawa, T., Yamada, K., Sasakawa, M., Machida, T., Nakaoka, S.-I., Nara, H., Tanimoto, H., Mukai, H., Yoshida, Y., Morimoto, S., Takatsuji, S., Tsuboi, K., Sawa, Y., Matsueda, H., Ishijima, K., Fujita, R., Goto, D., Lan, X., Schuldt, K., Heliasz, M., Biermann, T., Chmura, L., Necki, J., and Xueref-Remy, I.: Multi-observational estimation of regional and sectoral emission contributions to the persistent high growth rate of atmospheric CH₄ for 2020–2022, *EGUsphere [preprint]*, <https://doi.org/10.5194/egusphere-2024-2457>, 2024.
 Noël, S., Reuter, M., Buchwitz, M., Borchardt, J., Hilker, M., Schneising, O., Bovensmann, H., Burrows, J. P., Di Noia, A., Parker, R. J., Suto, H., Yoshida, Y., Buschmann, M., Deutscher, N. M., Feist, D. G., Griffith, D. W. T., Hase, F., Kivi, R., Liu, C., Morino, I., Notholt, J., Oh, Y.-S., Ohyama, H., Petri, C., Pollard, D. F., Rettinger, M., Roehl, C., Rousogonous, C., Sha, M. K., Shiomi, K., Strong, K., Sussmann, R., Tê, Y., Velazco, V. A., Vrekoussis, M., and Warneke, T.: Retrieval of greenhouse gases from GOSAT and GOSAT-2 using the FOCAL algorithm, *Atmos. Meas. Tech.*, 15, 3401–3437, <https://doi.org/10.5194/amt-15-3401-2022>, 2022.
 Nomura, S., Naja, M., Ahmed, M. K., Mukai, H., Terao, Y., Machida, T., Sasakawa, M., and Patra, P. K.: Measurement report: Regional characteristics of seasonal and long-term variations in greenhouse gases at Nainital, India, and Comilla, Bangladesh, *Atmos. Chem. Phys.*, 21, 16427–16452, <https://doi.org/10.5194/acp-21-16427-2021>, 2021
 Obu, J., Westermann, S., Bartsch, A., Berdnikov, N., Christiansen, H. H., Dashtseren, A., Delaloye, R., Elberling, B., Etzelmüller, B., Kholodov, A., Khomutov, A., Kääb, A., Leibman, M. O., Lewkowicz, A. G., Panda, S. K., Romanovsky, V., Way, R. G., Westergaard-Nielsen, A., Wu, T., Yamkhin, J. and Zou, D.: Northern Hemisphere permafrost map based on TTOP modelling for 2000–2016 at 1 km² scale, *Earth-Sci. Rev.*, 193, 299–316, doi:10.1016/j.earscirev.2019.04.023, 2019.

Mis en forme : Français

Mis en forme : Français

Code de champ modifié

Mis en forme : Soulignement , Couleur de police : Bleu, Français

Mis en forme : Français

Supprimé: Nisbet, R. E. R., Fisher, R., Nimmo, R. H., Bendall, D. S., Crill, P. M., Gallego-Sala, A. V., Hornibrook, E. R. C., Lopez-Juez, E., Lowry, D., Nisbet, P. B. R., Shuckburgh, E. F., Sriskantharajah, S., Howe, C. J. and Nisbet, E. G.: Emission of methane from plants, *Proc. R. Soc. B-Biol. Sci.*, 276(1660), 1347–1354, 2009.

Supprimé: ¶

Ocko, I. B, Sun, T., Shindell, D., Oppenheimer, M., Hristov, A. N, Pacala, S. W, Mauzerall, D. L, Xu, Y. and Hamburg, S. P: Acting rapidly to deploy readily available methane mitigation measures by sector can immediately slow global warming, *Environ. Res. Lett.*, 16, 054042, doi :10.1088/1748-9326/abf9c8, 2021

Odelson, D.A. and Breznak, J. A. Volatile fatty acid production by the hindgut microbiota of xilophagus termites. *Applied and Environmental Microbiology*, 45, 1602-1613, 1983. doi: 10.1128/aem.45.5.1602-1613.1983.

Ollivier, Q. R., Maher, D. T., Pitfield, C. and Macreadie, P. I.: Punching above their weight: Large release of greenhouse gases from small agricultural dams, *Glob. Change Biol.*, 25(2), 721–732, doi:10.1111/gcb.14477, 2019.

Omara, M, Zavala-Araiza, D, Lyon, DR, Hmiel, B, Roberts, KA, Hamburg, SP: Methane emissions from US low production oil and natural gas well sites, *Nat Commun*, 13(1):2085, doi: 10.1038/s41467-022-29709-3, 2022

O'Neill, B. C., Tebaldi, C., Vuuren, D. P. van, Eyring, V., Friedlingstein, P., Hurtt, G., Knutti, R., Kriegler, E., Lamarque, J.-F., Lowe, J., Meehl, G. A., Moss, R., Riahi, K. and Sanderson, B. M.: The Scenario Model Intercomparison Project (ScenarioMIP) for CMIP6, *Geosci. Model Dev.*, 9(9), 3461–3482, doi:10.5194/gmd-9-3461-2016, 2016.

Oreggioni, G. D., F. Monforti Ferrario, M. Crippa, M. Muntean, E. Schaaf, D. Guizzardi, E. Solazzo, M. Duerr, M. Perry and E. Vignati: Climate change in a changing world: Socio-economic and technological transitions, regulatory frameworks and trends on global greenhouse gas emissions from EDGAR v.5.0, *Global Environmental Change*, doi:10.1016/j.gloenvcha.2021.10235, 2021

Oremland, R. S. Methanogenic activity in plankton samples and fish intestines: a mechanism for *in situ* methanogenesis in oceanic surface waters. *Limnol. Oceanogr.* **24**, 1136–1141, 1979.

O'Rourke, P. R, Smith, S. J., Mott, A., Ahsan, H., McDuffie, E. E., Crippa, M., Klimont, S., McDonald, B., Z., Wang, Nicholson, M. B, Feng, L., and Hoesly, R. M., CEDS v-2021-02-05 Emission Data 1975-2019 (Version Feb-05-2021). Zenodo. <http://doi.org/10.5281/zenodo.4509372>, 2021

Ovalle, A. R. C., C. E. Rezende, L. D. Lacerda, and C. A. R. Silva: Factors affecting the hydrochemistry of a mangrove tidal creek, Sepetiba Bay, Brazil. *Estuar. Coast. Shelf Sci.* 31: 639–650. doi:10.1016/0272-7714(90)90017-L, 1990

Pacala, S. W.: Verifying greenhouse gas emissions: Methods to support international climate agreements, National Academies Press., 2010

Pandey, S., Gautam, R., Houweling, S., Gon, H. D. van der, Sadavarte, P., Borsdorff, T., Hasekamp, O., Landgraf, J., Tol, P., Kempen, T. van, Hoogeveen, R., Hees, R. van, Hamburg, S. P., Maasakkers, J. D. and Aben, I.: Satellite observations reveal extreme methane leakage from a natural gas well blowout, *Proc. Natl. Acad. Sci.*, 116(52), 26376–26381, doi:10.1073/pnas.1908712116, 2019.

Pangala, S. R., Moore, S., Hornibrook, E. R. C. and Gauci, V.: Trees are major conduits for methane egress from tropical forested wetlands, *New Phytol.*, 197(2), 524–531, doi:10.1111/nph.12031, 2013.

Pangala, S. R., Hornibrook, E. R. C., Gowing, D. J. and Gauci, V.: The contribution of trees to ecosystem methane emissions in a temperate forested wetland, *Glob. Change Biol.*, 21(7), 2642–2654, doi:10.1111/gcb.12891, 2015.

Supprimé: Olivier, J. G. J. and Janssens-Maenhout, G.: Part III: Total Greenhouse Gas Emissions, of CO₂ Emissions from Fuel Combustion (2014 ed.), International Energy Agency, Paris, ISBN-978-92-64-21709-6., 2014.

Supprimé: 

Supprimé: <https://doi.org/>

3745 Pangala, S. R., Enrich-Prast, A., Basso, L. S., Peixoto, R. B., Bastviken, D., Hornibrook, E. R. C., Gatti, L. V., Marotta,
 3746 H., Calazans, L. S. B., Sakuragai, C. M., Bastos, W. R., Malm, O., Gloor, E., Miller, J. B. and Gauci, V.: Large
 3747 emissions from floodplain trees close the Amazon methane budget, *Nature*, 552(7684), 230–234,
 3748 doi:10.1038/nature24639, 2017.
 3749 Paris, J.-D., Ciais, P., Nedelec, P., Stohl, A., Belan, B. D., Arshinov, M. Y., Carouge, C., Golitsyn, G. S. and Granberg, I.
 3750 G.: New insights on the chemical composition of the Siberian air shed from the YAK AEROSIB aircraft campaigns,
 3751 *Bull. Am. Meteorol. Soc.*, 91(5), 625–641, doi:10.1175/2009BAMS2663.1., 2010.
 3752 Parker, R. J., Webb, A., Boesch, H., Somkuti, P., Barrio Guillo, R., Di Noia, A., Kalaitzi, N., Anand, J. S., Bergamaschi,
 3753 P., Chevallier, F., Palmer, P. I., Feng, L., Deutscher, N. M., Feist, D. G., Griffith, D. W. T., Hase, F., Kivi, R., Morino,
 3754 I., Notholt, J., Oh, Y.-S., Ohyama, H., Petri, C., Pollard, D. F., Roehl, C., Sha, M. K., Shiomi, K., Strong, K., Sussmann,
 3755 R., Té, Y., Velasco, V. A., Warneke, T., Wennberg, P. O., and Wunch, D.: A decade of GOSAT Proxy satellite CH4
 3756 observations, *Earth Syst. Sci. Data*, 12, 3383–3412, <https://doi.org/10.5194/essd-12-3383-2020>, 2020.
 3757 Parker, R. and Boesch, H. (2020): University of Leicester GOSAT Proxy XCH4 v9.0. Centre for Environmental Data
 3758 Analysis, 07 May 2020. <https://dx.doi.org/10.5285/18ef8247f52a4cb6a14013f8235cc1eb>, 2020
 3759 Parker, R. J., Wilson, C., Comyn-Platt, E., Hayman, G., Marthews, T. R., Bloom, A. A., Lunt, M. F., Gedney, N., Dadson,
 3760 S. J., McNorton, J., Humpage, N., Boesch, H., Chipperfield, M. P., Palmer, P. I., and Yamazaki, D.: Evaluation of
 3761 wetland CH4 in the Joint UK Land Environment Simulator (JULES) land surface model using satellite observations,
 3762 *Biogeosciences*, 19, 5779–5805, <https://doi.org/10.5194/bg-19-5779-2022>, 2022.
 3763 Pathak, H., Li, C. and Wassmann, R.: Greenhouse gas emissions from Indian rice fields: calibration and upscaling using
 3764 the DNDC model, *Biogeosciences*, 1(1), 1–11, 2005.
 3765 Patra, P. K., Houweling, S., Krol, M., Bousquet, P., Belikov, D., Bergmann, D., Bian, H., Cameron-Smith, P., Chipperfield,
 3766 M. P., Corbin, K., Fortems-Cheiney, A., Fraser, A., Gloor, E., Hess, P., Ito, A., Kawa, S. R., Law, R. M., Loh, Z.,
 3767 Maksyutov, S., Meng, L., Palmer, P. I., Prinn, R. G., Rigby, M., Saito, R. and Wilson, C.: TransCom model simulations
 3768 of CH4 and related species: linking transport, surface flux and chemical loss with CH4 variability in the troposphere
 3769 and lower stratosphere, *Atmospheric Chem. Phys.*, 11(24), 12,813–12,837, doi:10.5194/acp-11-12813-2011, 2011.
 3770 Patra, P. K., Krol, M. C., Montzka, S. A., Arnold, T., Atlas, E. L., Lintner, B. R., Stephens, B. B., Xiang, B., Elkins, J. W.,
 3771 Fraser, P. J., Ghosh, A., Hints, E. J., Hurst, D. F., Ishijima, K., Krummel, P. B., Miller, B. R., Miyazaki, K., Moore,
 3772 F. L., Mühle, J., O'Doherty, S., Prinn, R. G., Steele, L. P., Takigawa, M., Wang, H. J., Weiss, R. F., Wofsy, S. C. and
 3773 Young, D.: Observational evidence for interhemispheric hydroxyl-radical parity, *Nature*, 513(7517), 219–223,
 3774 doi:10.1038/nature13721, 2014.
 3775 Patra, P. K., Takigawa, M., Watanabe, S., Chandra, N., Ishijima, K. and Yamashita, Y.: Improved Chemical Tracer
 3776 Simulation by MIROC4.0-based Atmospheric Chemistry-Transport Model (MIROC4-ACTM), *SOLA*, 14(0), 91–96,
 3777 doi:10.2151/sola.2018-016, 2018.

3778 Patra, P. K., Krol, M. C., Prinn, R. G., Takigawa, M., Mühle, J., Montzka, S. A., Lal, S., Yamashita, Y., Naus, S., Chandra,
 3779 N., Weiss, R. F., Krummel, P. B., Fraser, P. J., O'Doherty, S., and Elkins, J. W.: Methyl Chloroform Continues to
 3780 Constrain the Hydroxyl (OH) Variability in the Troposphere, *J. Geophys. Res.-Atmos.*, 126, e2020JD033862,
 3781 <https://doi.org/10.1029/2020JD033862>, 2021.

3782 Paull, C. K., Brewer, P. G., Ussler, W., Peltzer, E. T., Rehder, G. and Clague, D.: An experiment demonstrating that marine
 3783 slumping is a mechanism to transfer methane from seafloor gas-hydrate deposits into the upper ocean and atmosphere,
 3784 *Geo-Mar. Lett.*, 22(4), 198–203, doi:10.1007/s00367-002-0113-y, 2002.

3785 Peacock, M., J. Audet, D. Bastviken, M.N. Futter, V. Gauci, A. Grinham, J.A. Harrison, M.S. Kent, S. Kosten, C.E.
 3786 Lovelock, A.J. Veraart, and C.D. Evans, Global importance of methane emissions from drainage ditches and canals.
 3787 *Environmental Research Letters*, 16(4): p. 044010., 2021

3788 Pekel, J.-F., Cottam, A., Gorelick, N. and Belward, A. S.: High-resolution mapping of global surface water and its long-
 3789 term changes, *Nature*, 540(7633), 418–422, doi:10.1038/nature20584, 2016.

3790 Peltola, O., Vesala, T., Gao, Y., Rätty, O., Alekseychik, P., Aurela, M., Chojnicki, B., Desai, A. R., Dolman, A. J.,
 3791 Euskirchen, E. S., Friborg, T., Göckede, M., Helbig, M., Humphreys, E., Jackson, R. B., Jocher, G., Joos, F., Klatt, J.,
 3792 Knox, S. H., Kowalska, N., Kutzbach, L., Lienert, S., Lohila, A., Mammarella, I., Nadeau, D. F., Nilsson, M. B.,
 3793 Oechel, W. C., Peichl, M., Pypker, T., Quinton, W., Rinne, J., Sachs, T., Samson, M., Schmid, H. P., Sonnentag, O.,
 3794 Wille, C., Zona, D. and Aalto, T.: Monthly gridded data product of northern wetland methane emissions based on
 3795 upscaling eddy covariance observations, *Earth Syst. Sci. Data*, 11(3), 1263–1289, doi:10.5194/essd-11-1263-2019,
 3796 2019.

3797 Peng, S. S., Piao, S. L., Bousquet, P., Ciais, P., Li, B. G., Lin, X., Tao, S., Wang, Z. P., Zhang, Y. and Zhou, F.: Inventory
 3798 of anthropogenic methane emissions in Mainland China from 1980 to 2010, *Atmospheric Chem. Phys. Discuss.*, 2016,
 3799 1–29, doi:10.5194/acp-2016-139, 2016.

3800 Peng, S., Lin, X., Thompson, R. L., Xi, Y., Liu, G., Hauglustaine, D., Lan, X., Poulter, B., Ramonet, M., Saunio, M.,
 3801 Yin, Y., Zhang, Z., Zheng, B., and Ciais, P.: Wetland emission and atmospheric sink changes explain methane growth
 3802 in 2020, *Nature*, 612, 477–482, <https://doi.org/10.1038/s41586-022-05447-w>, 2022.

3803 Pérez-Barbería, F. J.: Scaling methane emissions in ruminants and global estimates in wild populations, *Sci. Total*
 3804 *Environ.*, 579, 1572–1580, doi:10.1016/j.scitotenv.2016.11.175, 2017.

3805 Petersen, H. and Luxton, M. A comparative analysis of soil fauna populations and their role in decomposition processes.
 3806 *Oikos* 39: 287–388, doi.org/10.2307/3544689, 1982

3807 Petrenko, V. V., Smith, A. M., Schaefer, H., Riedel, K., Brook, E., Baggenstos, D., Harth, C., Hua, Q., Buizert, C., Schilt,
 3808 A., Fain, X., Mitchell, L., Bauska, T., Orsi, A., Weiss, R. F. and Severinghaus, J. P.: Minimal geological methane
 3809 emissions during the Younger Dryas–Preboreal abrupt warming event, *Nature*, 548, 443, doi:10.1038/nature23316
 3810 <https://www.nature.com/articles/nature23316#supplementary-information>, 2017.

Supprimé: Peischl, J., Ryerson, T. B., Aikin, K. C., de Gouw, J. A., Gilman, J. B., Holloway, J. S., Lerner, B. M., Nadkarni, R., Neuman, J. A., Nowak, J. B., Trainer, M., Warneke, C. and Parrish, D. D.: Quantifying atmospheric methane emissions from the Haynesville, Fayetteville, and northeastern Marcellus shale gas production regions, *J. Geophys. Res. Atmospheres*, 120(5), 2119–2139, doi:10.1002/2014jd022697, 2015.

Supprimé: 

3819 Petrescu, A. M. R., Qiu, C., Ciais, P., Thompson, R. L., Peylin, P., McGrath, M. M., Solazzo, E., Janssens-Maenhout, G.,
3820 Tubiello, F. N., Bergamaschi, P., Brunner, D., Peters, G. P., Höglund-Isaksson, L., Regnier, P., Lauerwald, R.,
3821 Bastviken, D., Tsuruta, A., Winiwarter, W., Patra, P. P., Kuhnert, M., Oreggioni, G. D., Crippa, M., Saunio, M.,
3822 Perugini, L., Markkanen, T., Aalto, T., Groot Zwaafink, C. C., Yao, Y., Wilson, C. C., Conchedda, G., Günther, D.,
3823 Leip, A., Smith, P., Haussaire, J. M., Leppänen, A., Manning, A. J., McNorton, J., Brockmann, P., & Dolman, A. J. H.
3824 A. The consolidated European synthesis of CH₄ and N₂O emissions for the European Union and United Kingdom:
3825 1990-2017. *Earth System Science Data*, 13(5), 2307-2362. doi:10.5194/essd-13-2307-2021, 2021.

3826 Petrescu, A. M. R., Qiu, C., McGrath, M. J., Peylin, P., Peters, G. P., Ciais, P., Thompson, R. L., Tsuruta, A., Brunner,
3827 D., Kuhnert, M., Matthews, B., Palmer, P. I., Tarasova, O., Regnier, P., Lauerwald, R., Bastviken, D., Höglund-
3828 Isaksson, L., Winiwarter, W., Etiope, G., Aalto, T., Balsamo, G., Bastrikov, V., Berchet, A., Brockmann, P., Ciotoli,
3829 G., Conchedda, G., Crippa, M., Dentener, F., Groot Zwaafink, C. D., Guizzardi, D., Günther, D., Haussaire, J.-M.,
3830 Houweling, S., Janssens-Maenhout, G., Kouyate, M., Leip, A., Leppänen, A., Lugato, E., Maisonnier, M., Manning,
3831 A. J., Markkanen, T., McNorton, J., Muntean, M., Oreggioni, G. D., Patra, P. K., Perugini, L., Pison, I., Raivonen, M.
3832 T., Saunio, M., Segers, A. J., Smith, P., Solazzo, E., Tian, H., Tubiello, F. N., Vesala, T., van der Werf, G. R., Wilson,
3833 C., and Zaehle, S.: The consolidated European synthesis of CH₄ and N₂O emissions for the European Union and United
3834 Kingdom: 1990–2019, *Earth Syst. Sci. Data*, 15, 1197–1268, <https://doi.org/10.5194/essd-15-1197-2023>, 2023.

3835 Phillips, N. G., Ackley, R., Crosson, E. R., Down, A., Hutyrá, L. R., Brondfield, M., Karr, J. D., Zhao, K. and Jackson, R.
3836 B.: Mapping urban pipeline leaks: Methane leaks across Boston, *Environ. Pollut.*, 173, 1–4,
3837 doi:10.1016/j.envpol.2012.11.003, 2013.

3838 Pimlott, M.A., Pope, R.J., Kerridge, B.J., Latter, B.G., Knappett, D.S., Heard, D.E., Ventress, L.J., Siddans, R., Feng, W.,
3839 and Chipperfield, M.P.: Investigating the global OH radical distribution using steady-state approximations and satellite
3840 data. *Atmos. Chem. Phys.*, 22, 10467–10488, doi:10.5194/acp-22-10467-2022, 2022

3841 Pison, I., Ringeval, B., Bousquet, P., Prigent, C. and Papa, F.: Stable atmospheric methane in the 2000s: key-role of
3842 emissions from natural wetlands, *Atmospheric Chem. Phys. Discuss.*, 13(4), 9017–9049, doi:10.5194/acpd-13-9017-
3843 2013, 2013.

3844 Pitz, S. and Megonigal, J. P.: Temperate forest methane sink diminished by tree emissions, *New Phytol.*, 214(4), 1432–
3845 1439, doi:10.1111/nph.14559, 2017.

3846 Platt, U., Allan, W. and Lowe, D.: Hemispheric average Cl atom concentration from ¹³C/¹²C ratios in atmospheric methane,
3847 *Atmos Chem Phys*, 4, 2393–2399, 2004.

3848 Plummer, D., Nagashima, T., Tilmes, S., Archibald, A., Chiodo, G., Fadnavis, S., Garny, H., Josse, B., Kim, J., Lamarque,
3849 J.-F., Morgenstern, O., Murray, L., Orbe, C., Tai, A., Chipperfield, M., Funke, B., Juckes, M., Kinnison, D., Kunze,
3850 M., Luo, B., Matthes, K., Newman, P. A., Pascoe, C. and Peter, T.: CCMI- 2022: a new set of Chemistry–Climate
3851 Model Initiative (CCMI) community simulations to update the assessment of models and support upcoming ozone

Supprimé: Pétron, G., Karion, A., Sweeney, C., Miller, B. R., Montzka, S. A., Frost, G. J., Trainer, M., Tans, P., Andrews, A., Kofler, J., Helmig, D., Guenther, D., Dlugokencky, E., Lang, P., Newberger, T., Wolter, S., Hall, B., Novelli, P., Brewer, A., Conley, S., Hardesty, M., Banta, R., White, A., Noone, D., Wolfe, D. and Schnell, R.: A new look at methane and nonmethane hydrocarbon emissions from oil and natural gas operations in the Colorado Denver-Julesburg Basin, *J. Geophys. Res. Atmospheres*, 119(11), 6836–6852, doi:10.1002/2013jd021272, 2014.

Supprimé: 

assessment activities. SPARC Newsletter 57, 22–30, 2021.

Pollard, D. F., Sherlock, V., Robinson, J., Deutscher, N. M., Connor, B. and Shiona, H.: The Total Carbon Column Observing Network site description for Lauder, New Zealand, *Earth Syst. Sci. Data*, 9(2), 977–992, doi:10.5194/essd-9-977-2017, 2017.

Portmann, F. T., Siebert, S. & Döll, P. : MIRCA2000 – Global monthly irrigated and rainfed crop areas around the year 2000: A new high-resolution data set for agricultural and hydrological modeling, *Global Biogeochemical Cycles*, 24, GB 1011, doi:10.1029/2008GB003435, 2010

Portmann, R. W., Daniel, J. S. and Ravishankara, A. R.: Stratospheric ozone depletion due to nitrous oxide: influences of other gases, *Philos. Trans. R. Soc. Lond. B Biol. Sci.*, 367(1593), 1256–1264, doi:10.1098/rstb.2011.0377, 2012.

Poulter, B., Bousquet, P., Canadell, J. G., Ciais, P., Peregon, A., Saunio, M., Arora, V. K., Beerling, D. J., Brovkin, V., Jones, C. D., Joos, F., Gedney, N., Ito, A., Kleinen, T., Koven, C. D., McDonald, K., Melton, J. R., Peng, C. H., Peng, S. S., Prigent, C., Schroeder, R., Riley, W. J., Saito, M., Spahni, R., Tian, H. Q., Taylor, L., Viovy, N., Wilton, D., Wiltshire, A., Xu, X. Y., Zhang, B. W., Zhang, Z. and Zhu, Q. A.: Global wetland contribution to 2000-2012 atmospheric methane growth rate dynamics, *Environ. Res. Lett.*, 12(9), doi:10.1088/1748-9326/aa8391, 2017.

Prairie, Y.T., J. Alm, J. Beaulieu, N. Barros, T. Battin, J. Cole, P. del Giorgio, T. DelSontro, F. Guérin, A. Harby, J. Harrison, S. Mercier-Blais, D. Serça, S. Sobek, and D. Vachon, *Greenhouse Gas Emissions from Freshwater Reservoirs: What Does the Atmosphere See?* *Ecosystems*, 21(5): p. 1058-1071, 2018

Prather, M. J., Holmes, C. D. and Hsu, J.: Reactive greenhouse gas scenarios: Systematic exploration of uncertainties and the role of atmospheric chemistry, *Geophys. Res. Lett.*, 39(9), L09803, doi:10.1029/2012gl051440, 2012.

Prather, M. J., Guo, H., and Zhu, X.: Deconstruction of tropospheric chemical reactivity using aircraft measurements: the Atmospheric Tomography Mission (ATom) data, *Earth Syst. Sci. Data*, 15, 3299–3349, <https://doi.org/10.5194/essd-15-3299-2023>, 2023.

Prinn, R. G., Weiss, R. F., Arduini, J., Arnold, T., DeWitt, H. L., Fraser, P. J., Ganesan, A. L., Gasore, J., Harth, C. M., Hermansen, O., Kim, J., Krummel, P. B., Li, S., Loh, Z. M., Lunder, C. R., Maione, M., Manning, A. J., Miller, B. R., Mitrevski, B., Mühle, J., O'Doherty, S., Park, S., Reimann, S., Rigby, M., Saito, T., Salameh, P. K., Schmidt, R., Simmonds, P. G., Steele, L. P., Vollmer, M. K., Wang, R. H., Yao, B., Yokouchi, Y., Young, D., and Zhou, L.: History of chemically and radiatively important atmospheric gases from the Advanced Global Atmospheric Gases Experiment (AGAGE), *Earth Syst. Sci. Data*, 10, 985–1018, <https://doi.org/10.5194/essd-10-985-2018>, 2018.

Prosperi, P., Bloise, M., Tubiello, F.N. *et al.* New estimates of greenhouse gas emissions from biomass burning and peat fires using MODIS Collection 6 burned areas. *Climatic Change* **161**, 415–432, <https://doi.org/10.1007/s10584-020-02654-0>, 2020

Purvaja, R., Ramesh, R., & Frenzel, P.: Plant-mediated methane emission from an Indian mangrove, *Global Change Biology*, 10, 1825–1834, 2004

Supprimé: ¶

Mis en forme : Français

Mis en forme : Français

Mis en forme : Français

Code de champ modifié

3896 Qin, B., Zhou, J., Elser, J.J., Gardner, W.S., Deng, J., and J.D. Brookes: Water depth underpins the relative roles and fates
3897 of nitrogen and phosphorus in lakes, *Environmental Science & Technology* 2020 54 (6), 3191-3198, DOI:
3898 10.1021/acs.est.9b05858, 2020.

3899 Qu, Z., Jacob, D. J., Shen, L., Lu, X., Zhang, Y., Scarpelli, T. R., Nesser, H., Sulprizio, M. P., Maasakkers, J. D., Bloom,
3900 A. A., Worden, J. R., Parker, R. J., and Delgado, A. L.: Global distribution of methane emissions: a comparative inverse
3901 analysis of observations from the TROPOMI and GOSAT satellite instruments, *Atmos. Chem. Phys.*, 21, 14159–
3902 14175, <https://doi.org/10.5194/acp-21-14159-2021>, 2021.

3903 Qu, Z., Jacob, D. J., Zhang, Y., Shen, L., Varon, D. J., Lu, X., Scarpelli, T., Bloom, A., Worden, J., and Parker, R. J.:
3904 Attribution of the 2020 surge in atmospheric methane by inverse analysis of GOSAT observations, *Environ. Res. Lett.*,
3905 17, 094003, <https://doi.org/10.1088/1748-9326/ac8754>, 2022.

3906 Randerson, J. T., Chen, Y., van der Werf, G. R., Rogers, B. M. and Morton, D. C.: Global burned area and biomass burning
3907 emissions from small fires, *J. Geophys. Res. Biogeosciences*, 117, G4, doi:10.1029/2012jg002128, 2012.

3908 Ramage, J.L., Kuhn, M., Virkkala, A.M., Voigt, C., Marushchak, M.E., Bastos, A., Biasi, C., Canadell, J.G., Ciais, P.,
3909 López-Blanco, E. Natali, S.M., et al.: The net GHG balance and budget of the permafrost region (2000-2020) from
3910 ecosystem flux upscaling. Preprint in ESS Open Archive. September 11, 2023. DOI:
3911 10.22541/essoar.169447408.86275712/v1, 2023

3912 Ramsden, A. E., Ganesan, A. L., Western, L. M., Rigby, M., Manning, A. J., Foulds, A., France, J. L., Barker, P., Levy,
3913 P., Say, D., Wisher, A., Arnold, T., Rennick, C., Stanley, K. M., Young, D., and O'Doherty, S.: Quantifying fossil fuel
3914 methane emissions using observations of atmospheric ethane and an uncertain emission ratio, *Atmos. Chem. Phys.*,
3915 22, 3911–3929, <https://doi.org/10.5194/acp-22-3911-2022>, 2022.

3916 Ray, N.E., Holgersson, M.A., Andersen, M.R., Bikše, J., Bortolotti, L.E., Futter, M., Kokorite, I., Law, A., McDonald, C.,
3917 Mesman, J.P., Peacock, M., Richardson, D.C., Arsénault, J., Bansal, S., Cawley, K., Kuhn, M., Shahabnia, A.R. and
3918 Smufer, F.: Spatial and temporal variability in summertime dissolved carbon dioxide and methane in temperate ponds
3919 and shallow lakes. *Limnol Oceanogr.*, 68: 1530-1545. <https://doi.org/10.1002/lno.12362>, 2023

3920 Regnier P., Arndt, S., Dale, A.W., LaRowe, D.E., Mogollon, J. and Van Cappellen, P. Advances in the biogeochemical
3921 modeling of anaerobic oxidation of methane (AOM). *Earth Science Reviews*. 106, 105-130, 2011;

3922 Ren, W. E. I., Tian, H., Xu, X., Liu, M., Lu, C., Chen, G., Melillo, J., Reilly, J. and Liu, J.: Spatial and temporal patterns
3923 of CO₂ and CH₄ fluxes in China's croplands in response to multifactor environmental changes, *Tellus B*, 63(2), 222–
3924 240, doi:10.1111/j.1600-0889.2010.00522.x, 2011.

3925 Repeta, D. J., Ferrón, S., Sosa, O. A., Johnson, C. G., Repeta, L. D., Acker, M., DeLong, E. F. and Karl, D. M.: Marine
3926 methane paradox explained by bacterial degradation of dissolved organic matter, *Nat. Geosci.*, 9(12), 884–887,
3927 doi:10.1038/ngeo2837, 2016.

Resplandy, L., Hogikyan, A., Müller, J.D., Najjar, R.G., Bange, H. W., Bianchi, D., Weber, T., Cai, W.-J., Doney, S. C., Fennel, K., Gehlen, M., Hauck, J., Lacroix, F., Landschützer, P., Le Quéré, C., Roobaert, A., Schwinger, J., Berthet, S., Bopp, L., Chau, T.T.T., Dai, M., Gruber, N., Ilyina, T., Kock, A., Manizza, M., Lachkar, Z., Laruelle, G. G., Liao, E., Lima, I. D., Nissen, C., Rödenbeck, C., Séférian, R., Toyama, K., Tsujino, H., and Regnier, P.: A synthesis of global coastal ocean greenhouse gas fluxes, *Global Biogeochemical Cycles*, 38, e2023GB007803, <https://doi.org/10.1029/2023GB007803>, 2024.

Riahi, K., van Vuuren, D. P., Kriegler, E., Edmonds, J., O'Neill, B. C., Fujimori, S., Bauer, N., Calvin, K., Dellink, R., Fricko, O., Lutz, W., Popp, A., Cuaserna, J. C., Kc, S., Leimbach, M., Jiang, L., Kram, T., Rao, S., Emmerling, J., Ebi, K., Hasegawa, T., Havlik, P., Humpenöder, F., Da Silva, L. A., Smith, S., Stehfest, E., Bosetti, V., Eom, J., Gernaat, D., Masui, T., Rogelj, J., Strefler, J., Drouet, L., Krey, V., Luderer, G., Harmsen, M., Takahashi, K., Baumstark, L., Doelman, J. C., Kainuma, M., Klimont, Z., Marangoni, G., Lotze-Campen, H., Obersteiner, M., Tabeau, A. and Tavoni, M.: The Shared Socioeconomic Pathways and their energy, land use, and greenhouse gas emissions implications: An overview, *Glob. Environ. Change*, 42, 153–168, doi:10.1016/j.gloenvcha.2016.05.009, 2017.

Rice, A. L., Butenhoff, C. L., Shearer, M. J., Teama, D., Rosenstiel, T. N. and Khalil, M. A. K.: Emissions of anaerobically produced methane by trees, *Geophys. Res. Lett.*, 37, L03807, doi:10.1029/2009GL041565, 2010.

Ridgwell, A. J., Marshall, S. J. and Gregson, K.: Consumption of atmospheric methane by soils: A process-based model, *Glob. Biogeochem. Cycles*, 13(1), 59–70, doi:10.1029/1998gb900004, 1999.

Riedel, T. P., Wolfe, G. M., Danas, K. T., Gilman, J. B., Kuster, W. C., Bon, D. M., Vlasenko, A., Li, S. M., Williams, E. J., Lerner, B. M., Veres, P. R., Roberts, J. M., Holloway, J. S., Lefer, B., Brown, S. S. and Thornton, J. A.: An MCM modeling study of nitryl chloride (ClNO₂) impacts on oxidation, ozone production and nitrogen oxide partitioning in polluted continental outflow, *Atmospheric Chem. Phys.*, 14(8), 3789–3800, doi:10.5194/acp-14-3789-2014, 2014.

Rigby, M., Montzka, S. A., Prinn, R. G., White, J. W. C., Young, D., O'Doherty, S., Lunt, M. F., Ganesan, A. L., Manning, A. J., Simmonds, P. G., Salameh, P. K., Harth, C. M., Mühle, J., Weiss, R. F., Fraser, P. J., Steele, L. P., Krummel, P. B., McCulloch, A. and Park, S.: Role of atmospheric oxidation in recent methane growth, *Proc. Natl. Acad. Sci.*, 114(21), 5373, 2017.

Riley, W. J., Subin, Z. M., Lawrence, D. M., Swenson, S. C., Torn, M. S., Meng, L., Mahowald, N. M. and Hess, P.: Barriers to predicting changes in global terrestrial methane fluxes: analyses using CLM4Me, a methane biogeochemistry model integrated in CESM, *Biogeosciences*, 8(7), 1925–1953, doi:10.5194/bg-8-1925-2011, 2011.

Ringeval, B., Friedlingstein, P., Koven, C., Ciais, P., de Noblet-Ducoudre, N., Decharme, B. and Cadule, P.: Climate-CH₄ feedback from wetlands and its interaction with the climate-CO₂ feedback, *Biogeosciences*, 8(8), 2137–2157, doi:10.5194/bg-8-2137-2011, 2011.

Robison, A.L., W.M. Wollheim, B. Turek, C. Bova, C. Snay, and R.K. Varner, Spatial and temporal heterogeneity of methane ebullition in lowland headwater streams and the impact on sampling design, *Limnology and Oceanography*,

66(12): p. 4063-4076, 2021

Rocher-Ros, G., Stanley, E.H., Loken, L.C., Casson, N.J., Raymond, P.A., Liu, S., Amatulli, G. and Sponseller, R.A., Global methane emissions from rivers and streams. *Nature*, pp.1-6.,621, 530–535, <https://doi.org/10.1038/s41586-023-06344-6>, 2023

Rosentreter, J. A., Maher, D. T., Erler, D. V., Murray, R. H. and Eyre, B. D.: Methane emissions partially offset “blue carbon” burial in mangroves, *Sci. Adv.*, 4(6), eaao4985, doi:10.1126/sciadv.aao4985, 2018.

Rosentreter, J. A., A. V Borges, B. R. Deemer, and others : Half of global methane emissions come from highly variable aquatic ecosystem sources. *Nat. Geosci.* **14**: 225–230. doi:10.1038/s41561-021-00715-2, 2021

Rosentreter, J.A., Laruelle, G.G., Bange, H.W., Bianchi, T.S., Busecke, J.J.M., Cai, W-J, Eyre, B.D., Forbrich, I., Kwon, E.Y., Mavara, T., Moosdorf, N., Van Dam, B. and Regnier, P. Coastal vegetation and estuaries are collectively a greenhouse gas sink. *Nature Climate Change*, 13, 579–587, doi: 10.1038/s41558-023-01682-9, 2023.

Rosentreter, J. A., Alcott, L., Maavara, T., Sun, X., Zhou, Y., Planavsky, N. J., and Raymond, P. A. : Revisiting the global methane cycle through expert opinion, *Earth's Future*, 12, e2023EF004234, <https://doi.org/10.1029/2023EF004234>, 2024

Rowlinson, M. J., Rap, A., Arnold, S. R., Pope, R. J., Chipperfield, M. P., McNorton, J., Forster, P., Gordon, H., Pringle, K. J., Feng, W., Kerridge, B. J., Latter, B. L., and Siddans, R.: Impact of El Niño–Southern Oscillation on the interannual variability of methane and tropospheric ozone, *Atmos. Chem. Phys.*, 19, 8669–8686, <https://doi.org/10.5194/acp-19-8669-2019>, 2019.

Ruppel, C. D., and J. D. Kessler (2017), The interaction of climate change and methane hydrates, *Rev. Geophys.*, 55, 126–168, doi:10.1002/2016RG000534, 2017

Saad, K. M., Wunch, D., Toon, G. C., Bernath, P., Boone, C., Connor, B., Deutscher, N. M., Griffith, D. W. T., Kivi, R., Notholt, J., Roehl, C., Schneider, M., Sherlock, V. and Wennberg, P. O.: Derivation of tropospheric methane from TCCON CH₄ and HF total column observations, *Atmospheric Meas. Technol.*, 7(9), 2907–2918, doi:10.5194/amt-7-2907-2014, 2014.

Sanderson, M. G.: Biomass of termites and their emissions of methane and carbon dioxide: A global database, *Glob. Biogeochem. Cycles*, 10(4), 543–557, doi:10.1029/96gb01893, 1996.

Sasakawa, M., Shimoyama, K., Machida, T., Tsuda, N., Suto, H., Arshinov, M., Davydov, D., Fofonov, A., Krasnov, O., Saeki, T., Koyama, Y. and Maksyutov, S.: Continuous measurements of methane from a tower network over Siberia, *Tellus B*, 62(5), 403–416, doi:10.1111/j.1600-0889.2010.00494.x, 2010.

Sasakawa, M., Machida, T., Ishijima, K., Arshinov, M., Patra, P. K., Ito, A., Aoki, S., and Petrov, V.: Temporal characteristics of CH₄ vertical profiles observed in the West Siberian Lowland over Surgut from 1993 to 2015 and Novosibirsk from 1997 to 2015. *Journal of Geophysical Research: Atmospheres*, 122, 11,261– 11,273. <https://doi.org/10.1002/2017JD026836>, 2017.

Supprimé: &

Supprimé: (2024).

Supprimé: .

Supprimé: .

Supprimé: Rosentreter, J.A., Alcott, L., Maavara, T., Sun, X., Zhou, Y., Planavsky, N., & Raymond, P. Revisiting the Global Methane Cycle Through Expert Opinion (submitted to Earth Future).

4002 Saunio, M., Bousquet, P., Poulter, B., Peregon, A., Ciais, P., Canadell, J. G., Dlugokencky, E. J., Etiope, G., Bastviken,
 4003 D., Houweling, S., Janssens-Maenhout, G., Tubiello, F. N., Castaldi, S., Jackson, R. B., Alexe, M., Arora, V. K.,
 4004 Beerling, D. J., Bergamaschi, P., Blake, D. R., Brailsford, G., Brovkin, V., Bruhwiler, L., Crevoisier, C., Crill, P.,
 4005 Covey, K., Curry, C., Frankenberg, C., Gedney, N., Höglund-Isaksson, L., Ishizawa, M., Ito, A., Joos, F., Kim, H. S.,
 4006 Kleinen, T., Krummel, P., Lamarque, J. F., Langenfelds, R., Locatelli, R., Machida, T., Maksyutov, S., McDonald, K.
 4007 C., Marshall, J., Melton, J. R., Morino, I., Naik, V., O'Doherty, S., Parmentier, F. J. W., Patra, P. K., Peng, C., Peng,
 4008 S., Peters, G. P., Pison, I., Prigent, C., Prinn, R., Ramonet, M., Riley, W. J., Saito, M., Santini, M., Schroeder, R.,
 4009 Simpson, I. J., Spahni, R., Steele, P., Takizawa, A., Thornton, B. F., Tian, H., Tohjima, Y., Viovy, N., Voulgarakis,
 4010 A., van Weele, M., van der Werf, G. R., Weiss, R., Wiedinmyer, C., Wilton, D. J., Wiltshire, A., Worthy, D., Wunch,
 4011 D., Xu, X., Yoshida, Y., Zhang, B., Zhang, Z. and Zhu, Q.: The global methane budget 2000–2012, *Earth Syst Sci*
 4012 *Data*, 8(2), 697–751, doi:10.5194/essd-8-697-2016, 2016.
 4013 Saunio, M., Bousquet, P., Poulter, B., Peregon, A., Ciais, P., Canadell, J. G., Dlugokencky, E. J., Etiope, G., Bastviken,
 4014 D., Houweling, S., Janssens-Maenhout, G., Tubiello, F. N., Castaldi, S., Jackson, R. B., Alexe, M., Arora, V. K.,
 4015 Beerling, D. J., Bergamaschi, P., Blake, D. R., Brailsford, G., Bruhwiler, L., Crevoisier, C., Crill, P., Covey, K.,
 4016 Frankenberg, C., Gedney, N., Höglund-Isaksson, L., Ishizawa, M., Ito, A., Joos, F., Kim, H. S., Kleinen, T., Krummel,
 4017 P., Lamarque, J. F., Langenfelds, R., Locatelli, R., Machida, T., Maksyutov, S., Melton, J. R., Morino, I., Naik, V.,
 4018 O'Doherty, S., Parmentier, F. J. W., Patra, P. K., Peng, C., Peng, S., Peters, G. P., Pison, I., Prinn, R., Ramonet, M.,
 4019 Riley, W. J., Saito, M., Santini, M., Schroeder, R., Simpson, I. J., Spahni, R., Takizawa, A., Thornton, B. F., Tian, H.,
 4020 Tohjima, Y., Viovy, N., Voulgarakis, A., Weiss, R., Wilton, D. J., Wiltshire, A., Worthy, D., Wunch, D., Xu, X.,
 4021 Yoshida, Y., Zhang, B., Zhang, Z. and Zhu, Q.: Variability and quasi-decadal changes in the methane budget over the
 4022 period 2000–2012, *Atmospheric Chem. Phys.*, 17(18), 11135–11161, doi:10.5194/acp-17-11135-2017, 2017.
 4023 Saunio, M., Stavert, A. R., Poulter, B., Bousquet, P., Canadell, J. G., Jackson, R. B., Raymond, P. A., Dlugokencky, E.
 4024 J., Houweling, S., Patra, P. K., Ciais, P., Arora, V. K., Bastviken, D., Bergamaschi, P., Blake, D. R., Brailsford, G.,
 4025 Bruhwiler, L., Carlson, K. M., Carrol, M., Castaldi, S., Chandra, N., Crevoisier, C., Crill, P. M., Covey, K., Curry, C.
 4026 L., Etiope, G., Frankenberg, C., Gedney, N., Hegglin, M. I., Höglund-Isaksson, L., Hugelius, G., Ishizawa, M., Ito, A.,
 4027 Janssens-Maenhout, G., Jensen, K. M., Joos, F., Kleinen, T., Krummel, P. B., Langenfelds, R. L., Laruelle, G. G., Liu,
 4028 L., Machida, T., Maksyutov, S., McDonald, K. C., McNorton, J., Miller, P. A., Melton, J. R., Morino, I., Müller, J.,
 4029 Murguia-Flores, F., Naik, V., Niwa, Y., Noce, S., O'Doherty, S., Parker, R. J., Peng, C., Peng, S., Peters, G. P., Prigent,
 4030 C., Prinn, R., Ramonet, M., Regnier, P., Riley, W. J., Rosentreter, J. A., Segers, A., Simpson, I. J., Shi, H., Smith, S.
 4031 J., Steele, L. P., Thornton, B. F., Tian, H., Tohjima, Y., Tubiello, F. N., Tsuruta, A., Viovy, N., Voulgarakis, A., Weber,
 4032 T. S., van Weele, M., van der Werf, G. R., Weiss, R. F., Worthy, D., Wunch, D., Yin, Y., Yoshida, Y., Zhang, W.,
 4033 Zhang, Z., Zhao, Y., Zheng, B., Zhu, Q., Zhu, Q., and Zhuang, Q.: The Global Methane Budget 2000–2017, *Earth*
 4034 *Syst. Sci. Data*, 12, 1561–1623, <https://doi.org/10.5194/essd-12-1561-2020>, 2020.

4035 Sayers, M.J., Grimm, A.G., Shuchman, R.A., Deines, A.M., Bunnell, D.B., Raymer, Z.B., Rogers, M.W., Woelmer, W.,
 4036 Bennion, D.H., Brooks, C.N., Whitley, M.A.A., Warner, D.M., and J. Mychek-Londer: A new method to generate a
 4037 high-resolution global distribution map of lake chlorophyll, *International Journal of Remote Sensing*, 36:7, 1942-1964,
 4038 DOI: [10.1080/01431161.2015.1029099](https://doi.org/10.1080/01431161.2015.1029099), 2015

4039 Schepers, D., Guerlet, S., Butz, A., Landgraf, J., Frankenberg, C., Hasekamp, O., Blavier, J. F., Deutscher, N. M., Griffith,
 4040 D. W. T., Hase, F., Kyro, E., Morino, I., Sherlock, V., Sussmann, R. and Aben, I.: Methane retrievals from Greenhouse
 4041 Gases Observing Satellite (GOSAT) shortwave infrared measurements: Performance comparison of proxy and physics
 4042 retrieval algorithms, *J. Geophys. Res. Atmospheres*, 117, D10, doi:10.1029/2012jd017549, 2012.

4043 Schmale O, Greinert J, Rehder G (2005) Methane emission from high-intensity marine gas seeps in the Black Sea into the
 4044 atmosphere. *Geophys Res Lett* 32:L07609. doi:10.1029/2004GL021138, 2005

4045 Schmid, M., Batist, M.D., Granin, N.G., Kapitanov, V.A., McGinnis, D.F., Mizandrontsev, I.B., Obzhairov, A.I., and
 4046 Wüest, A.. Sources and sinks of methane in Lake Baikal: A synthesis of measurements and modelling. *Limnol.*
 4047 *Oceanogr.*, 52(5), 1824–1837. doi: 10.4319/lo.2007.52.5.1824, 2007

4048 Schneising, O., Buchwitz, M., Reuter, M., Vanselow, S., Bovensmann, H., and Burrows, J. P.: Remote sensing of methane
 4049 leakage from natural gas and petroleum systems revisited, *Atmos. Chem. Phys.*, 20, 9169–9182,
 4050 <https://doi.org/10.5194/acp-20-9169-2020>, 2020.

4051 Schorn, S., S. Ahmerkamp, E. Bullock, and others. : Diverse methylophilic methanogenic archaea cause high methane
 4052 emissions from seagrass meadows. *Proc. Natl. Acad. Sci.* **119**: 1–12. doi:10.1073/pnas.2106628119, 2022

4053 Schuldt, K. N., Mund, J., Aalto, T., Arlyn Andrews, Apadula, F., Jgor Arduini, Arnold, S., Baier, B., Bani, L., Bartyzel,
 4054 J., Bergamaschi, P., Biermann, T., Biraud, S. C., Pierre-Eric Blanc, Boenisch, H., Brailsford, G., Brand, W. A.,
 4055 Brunner, D., Bui, T. P. V., ... Mirosław Zimnoch. : *Multi-laboratory compilation of atmospheric carbon dioxide data*
 4056 *for the period 1983-2022; obspack_ch4_1_GLOBALVIEWplus_v6.0_2023-12-01* [Data set]. NOAA Global
 4057 Monitoring Laboratory. <https://doi.org/10.25925/20231001>, 2023

4058 Schuur, E.A., Abbott, B.W., Commancin, R., Ermakovich, J., Euskirchen, E., Hugelius, G., Grosse, G., Jones, M., Koven,
 4059 C., Leshyk, V. and Lawrence, D. (2022) Permafrost and climate change: carbon cycle feedbacks from the warming
 4060 Arctic. *Annual Review of Environment and Resources*, 47, pp.343-371. [https://doi.org/10.1146/annurev-environ-](https://doi.org/10.1146/annurev-environ-012220-011847)
 4061 [012220-011847](https://doi.org/10.1146/annurev-environ-012220-011847), 2022

4062 Schwietzke, S., Sherwood, O. A., Bruhwiler, L. M. P., Miller, J. B., Etiope, G., Dlugokencky, E. J., Michel, S. E., Arling,
 4063 V. A., Vaughn, B. H., White, J. W. C. and Tans, P. P.: Upward revision of global fossil fuel methane emissions based
 4064 on isotope database, *Nature*, 538(7623), 88–91, doi:10.1038/nature19797, 2016.

4065 Segers, A., Steinke, T., and Houweling, S.: Description of the CH₄ Inversion Production Chain, CAMS (Copernicus
 4066 Atmospheric Monitoring Service) Report.. [online] Available from:
 4067 https://atmosphere.copernicus.eu/sites/default/files/2022-10/CAMS255_2021SC1_D55.5.2.1-

Supprimé: Schneising, O., Burrows, J. P., Dickerson, R. R.,
 Buchwitz, M., Reuter, M. and Bovensmann, H.: Remote sensing of
 fugitive methane emissions from oil and gas production in North
 American tight geologic formations, *Earths Future*, 2, 548–558,
 doi:10.1002/2014EF000265, 2014.

2021CH4_202206_production_chain_CH4_v1.pdf (Accessed 1 février 2024), 2022.

Shaw, J. T., Allen, G., Barker, P., Pitt, J. R., Pasternak, D., Bauguitte, S. J.-B., Lee, J., Boewer, K. N., Daly, M. C., Lunt, M. F., Ganesan, A. L., Vaughan, A. R., Chibesakunda, F., Lambakasa, M., Fisher, R. E., France, J. L., Lowry, D., Palmer, P. J., Metzger, S., Parker, R. J., Gedney, N., Bateson, P., Cain, M., Lorente, A., Borsdorff, T., and Nisbet, E. G.: Large methane emission fluxes observed from tropical wetlands in Zambia, *Global Biogeochem. Cy.*, **36**, e2021GB007261, <https://doi.org/10.1029/2021GB007261>, 2022.

Shen, L., Gautam, R., Omara, M., Zavala-Araiza, D., Maasakkers, J. D., Scarpelli, T. R., Lorente, A., Lyon, D., Sheng, J., Varon, D. J., Nesser, H., Qu, Z., Lu, X., Sulprizio, M. P., Hamburg, S. P., and Jacob, D. J.: Satellite quantification of oil and natural gas methane emissions in the US and Canada including contributions from individual basins, *Atmos. Chem. Phys.*, **22**, 11203–11215, <https://doi.org/10.5194/acp-22-11203-2022>, 2022.

Shen, L., Jacob, D.J., Gautam, R. et al. National quantifications of methane emissions from fuel exploitation using high resolution inversions of satellite observations. *Nat Commun* **14**, 4948 , <https://doi.org/10.1038/s41467-023-40671-6>, 2023

Sherwen, T., Schmidt, J. A., Evans, M. J., Carpenter, L. J., Großmann, K., Eastham, S. D., Jacob, D. J., Dix, B., Koenig, T. K., Sinreich, R., Ortega, I., Volkamer, R., Saiz-Lopez, A., Prados-Roman, C., Mahajan, A. S., and Ordóñez, C.: Global impacts of tropospheric halogens (Cl, Br, I) on oxidants and composition in GEOS-Chem, *Atmos. Chem. Phys.*, **16**, 12239–12271, <https://doi.org/10.5194/acp-16-12239-2016>, 2016.

Sherwin, E. D., Rutherford, J. S., Zhang, Z., Chen, Y., Wetherley, E. B., Yakovlev, P. V., Berman, E. S. F., Jones, B. B., Cusworth, D. H., Thorpe, A. K., Ayasse, A. K., Duren, R. M., and Brandt, A. R.: US oil and gas system emissions from nearly one million aerial site measurements, *Nature*, **627**(8003), 328–334, doi:10.1038/s41586-024-07117-5, 2024

Shindell, D., Sadavarte, P., Aben, I., Bredariol, TdO, Dreyfus, G., Höglund-Isaksson, L., Poulter, B., Sauniois, M., Schmidt, GA, Szopa, S., Rentz, K., Parsons, L., Qu, Z., Faluvegi, G and Maasakkers, JD. : The methane imperative, *Front Sci*, **2**:1349770, doi: 10.3389/fsci.2024.1349770, 2024

Shindell, D., Kuylenstierna, J. C. I., Vignati, E., van Dingenen, R., Amann, M., Klimont, Z., Anenberg, S. C., Muller, N., Janssens-Maenhout, G., Raes, F., Schwartz, J., Faluvegi, G., Pozzoli, L., Kupiainen, K., Höglund-Isaksson, L., Emberson, L., Streets, D., Ramanathan, V., Hicks, K., Oanh, N. T. K., Milly, G., Williams, M., Demkine, V. and Fowler, D.: Simultaneously Mitigating Near-Term Climate Change and Improving Human Health and Food Security, *Science*, **335**(6065), 183–189, doi:10.1126/science.1210026, 2012.

Shorter, J. H., Mcmanus, J. B., Kolb, C. E., Allwine, E. J., Lamb, B. K., Mosher, B. W., Harriss, R. C., Partchatka, U., Fischer, H., Harris, G. W., Crutzen, P. J. and Karbach, H.-J.: Methane emission measurements in urban areas in Eastern Germany, *J. Atmospheric Chem.*, **124**(2), 121–140, 1996.

Shu, S., Jain, A.K. and Khesghi, H.S.: Investigating Wetland and Nonwetland Soil Methane Emissions and Sinks Across

Mis en forme : Français

Mis en forme : Français

Code de champ modifié

Mis en forme : Français

Supprimé: ¶

the Contiguous United States Using a Land Surface Model. *Global Biogeochem. Cycles*, 34: e2019GB006251. <https://doi-org.insu.bib.cnrs.fr/10.1029/2019GB006251>, 2020

Simpson, I. J., Thurtell, G. W., Kidd, G. E., Lin, M., Demetriades-Shah, T. H., Flitcroft, I. D., Kanemasu, E. T., Nie, D., Bronson, K. F. and Neue, H. U.: Tunable diode laser measurements of methane fluxes from an irrigated rice paddy field in the Philippines, *J. Geophys. Res. Atmospheres*, 100(D4), 7283–7290, doi:10.1029/94jd03326, 1995.

Simpson, I. J., Sulbaek Andersen, M. P., Meinardi, S., Bruhwiler, L., Blake, N. J., Helmig, D., Rowland, F. S. and Blake, D. R.: Long-term decline of global atmospheric ethane concentrations and implications for methane, *Nature*, 488(7412), 490–494, doi:10.1038/nature11342, 2012.

Smith I.R., Grasby S.E., Lane L.S.: An investigation of gas seeps and aquatic chemistry in Fisherman Lake, southwest Northwest Territories. Geological Survey of Canada, Current Research 2005-A3, 8 p., 2005

Solomon EA, Kastner M, MacDonald IR, Leifer I: Considerable methane fluxes to the atmosphere from hydrocarbon seeps in the Gulf of Mexico. *Nat Geosci* 2:561–565, 2009

Spahni, R., Wania, R., Neef, L., van Weele, M., Pison, I., Bousquet, P., Frankenberg, C., Foster, P. N., Joos, F., Prentice, I. C. and van Velthoven, P.: Constraining global methane emissions and uptake by ecosystems, *Biogeosciences*, 8(6), 1643–1665, doi:10.5194/bg-8-1643-2011, 2011.

Stanley, E. H., Casson, N. J., Christel, S. T., Crawford, J. T., Loken, L. C. and Oliver, S. K.: The ecology of methane in streams and rivers: patterns, controls, and global significance, *Ecol. Monogr.*, doi:10.1890/15-1027, 2016.

Stanley, K. M., Grant, A., O'Doherty, S., Young, D., Manning, A. J., Stavert, A. R., Spain, T. G., Salameh, P. K., Harth, C. M., Simmonds, P. G., Sturges, W. T., Oram, D. E. and Derwent, R. G.: Greenhouse gas measurements from a UK network of tall towers: technical description and first results, *Atmospheric Meas. Tech.*, 11(3), 1437–1458, doi:10.5194/amt-11-1437-2018, 2018.

Stanley, E. H., Loken, L. C., Casson, N. J., Oliver, S. K., Sponseller, R. A., Wallin, M. B., Zhang, L., and Rocher-Ros, G.: GRiMeDB: the Global River Methane Database of concentrations and fluxes, *Earth Syst. Sci. Data*, 15, 2879–2926, <https://doi.org/10.5194/essd-15-2879-2023>, 2023.

Stavert, A. R., Sauniois, M., Canadell, J. G., Poulter, B., Jackson, R. B., Regnier, P., Lauerwald, R., Raymond, P. A., Allen, G. H., Patra, P. K., Bergamaschi, P., Bousquet, P., Chandra, N., Ciais, P., Gustafson, A., Ishizawa, M., Ito, A., Kleinen, T., Maksyutov, S., Joe McNorton, Joe R. Melton, Jurek Müller, Yosuke Niwa, Shushi Peng, William J. Riley, Arjo Segers, Hanqin Tian, Aki Tsuruta, Yi Yin, Zhen Zhang, Bo Zheng, Zhuang, Q. Regional trends and drivers of the global methane budget. *Global Change Biology*, 28, 182–200. <https://doi.org/10.1111/gcb.15901>, 2021

Steele, L. P., Fraser, P. J., Rasmussen, R. A., Khalil, M. A. K., Conway, T. J., Crawford, A. J., Gammon, R. H., Masarie, K. A. and Thoning, K. W.: The global distribution of methane in the troposphere, *J. Atmospheric Chem.*, 5, 125–171, 1987.

Stevenson, D. S., Zhao, A., Naik, V., O'Connor, F. M., Tilmes, S., Zeng, G., Murray, L. T., Collins, W. J., Griffiths, P. T., Shim, S., Horowitz, L. W., Sentman, L. T., and Emmons, L.: Trends in global tropospheric hydroxyl radical and methane lifetime since 1850 from AerChemMIP, *Atmos. Chem. Phys.*, **20**, 12905–12920, <https://doi.org/10.5194/acp-20-12905-2020>, 2020.

Stevenson, D. S., Derwent, R. G., Wild, O., and Collins, W. J.: COVID-19 lockdown emission reductions have the potential to explain over half of the coincident increase in global atmospheric methane, *Atmos. Chem. Phys.*, **22**, 14243–14252, <https://doi.org/10.5194/acp-22-14243-2022>, 2022.

Stocker, B. D., Spahn, R. and Joos, F.: DYPTOP: a cost-efficient TOPMODEL implementation to simulate sub-grid spatio-temporal dynamics of global wetlands and peatlands, *Geosci. Model Dev.*, **7**(6), 3089–3110, doi:10.5194/gmd-7-3089-2014, 2014.

Strauss, J., Abbott, B. W., Hugelius, G., Schuur, E., Treat, C., Fuchs, M., Schädel, C., Ulrich, M., Turetsky, M., Keuschnig, M. and Biasi, C. (2021) Chapter 9. Permafrost. In *FAO Recarbonizing global soils—A technical manual of recommended management practices: Volume 2—Hot spots and bright spots of soil organic carbon*, p.130, 2021

Strode, S. A., Wang, J. S., Manyin, M., Duncan, B., Hossaini, R., Keller, C. A., Michel, S. E., and White, J. W. C.: Strong sensitivity of the isotopic composition of methane to the plausible range of tropospheric chlorine, *Atmos. Chem. Phys.*, **20**, 8405–8419, <https://doi.org/10.5194/acp-20-8405-2020>, 2020.

Sugimoto, A., Inoue, T., Kitibutr, N., Abe, T: Methane oxidation by termite mounds estimate by the carbon isotope composition of methane. *Glob. Biogeochem. Cy.* **12**, 595-605. 1998.

Sweeney, C., Karion, A., Wolter, S., Newberger, T., Guenther, D., Higgs, J. A., Andrews, A. E., Lang, P. M., Neff, D., Dlugokencky, E., Miller, J. B., Montzka, S. A., Miller, B. R., Masarie, K. A., Biraud, S. C., Novelli, P. C., Crotwell, M., Crotwell, A. M., Thoning, K. and Tans, P. P.: Seasonal climatology of CO₂ across North America from aircraft measurements in the NOAA/ESRL Global Greenhouse Gas Reference Network, *J. Geophys. Res. Atmospheres*, **120**(10), 5155–5190, doi:10.1002/2014jd022591, 2015.

Szopa, S., V. Naik, B. Adhikary, P. Artaxo, T. Berntsen, W.D. Collins, S. Fuzzi, L. Gallardo, A. Kiendler-Scharr, Z. Klimont, H. Liao, N. Unger, and P. Zanis: Short-Lived Climate Forcers. In *Climate Change 2021: The Physical Science Basis. Contribution of Working Group I to the Sixth Assessment Report of the Intergovernmental Panel on Climate Change* [Masson-Delmotte, V., P. Zhai, A. Pirani, S.L. Connors, C. Péan, S. Berger, N. Caud, Y. Chen, L. Goldfarb, M.I. Gomis, M. Huang, K. Leitzell, E. Lonnoy, J.B.R. Matthews, T.K. Maycock, T. Waterfield, O. Yelekçi, R. Yu, and B. Zhou (eds.)]. Cambridge University Press, Cambridge, United Kingdom and New York, NY, USA, pp. 817–922, doi:10.1017/9781009157896.008., 2021

Tan, Z. and Zhuang, Q.: Methane emissions from pan-Arctic lakes during the 21st century: An analysis with process-based models of lake evolution and biogeochemistry, *J. Geophys. Res. Biogeosciences*, **120**(12), 2641–2653, doi:10.1002/2015JG003184, 2015.

Tans, P. and Zwellberg, C.: 17th WMO/IAEA Meeting on Carbon Dioxide, Other Greenhouse Gases and Related Tracers

Supprimé: 1

Measurement Techniques (GGMT-2013), GAW Report, WMO, Geneva. [online] Available from: https://library.wmo.int/index.php?lvl=notice_display&id=16373#.XnpBPW7jIq8, 2014.

Taranu, Z.E., I. Gregory-Eaves, P.R. Leavitt, L. Bunting, T. Buchaca, J. Catalan, I. Domaizon, P. Guilizzoni, A. Lami, S. McGowan, H. Moorhouse, G. Morabito, F.R. Pick, M.A. Stevenson, P.L. Thompson, and R.D. Vinebrooke: Acceleration of cyanobacterial dominance in north temperate-subarctic lakes during the Anthropocene. *Ecology Letters*, 18(4): p. 375-384., 2015

Taylor, P. G., Bilinski, T. M., Fancher, H. R. F., Cleveland, C. C., Nemergut, D. R., Weintraub, S. R., Wieder, W. R. and Townsend, A. R.: Palm oil wastewater methane emissions and bioenergy potential, *Nat. Clim. Change*, 4(3), 151–152, doi:10.1038/nclimate2154, 2014.

le Texier, H., Solomon, S. and Garcia, R. R.: The role of molecular hydrogen and methane oxidation in the water vapour budget of the stratosphere, *Q. J. R. Meteorol. Soc.*, 114(480), 281–295, doi:10.1002/qj.49711448002, 1988.

Thanverdas, J., Saunois, M., Berchet, A., Pison, I., Vaughn, B. H., Michel, S. E., and Bousquet, P.: Variational inverse modeling within the Community Inversion Framework v1.1 to assimilate $\delta^{13}\text{C}(\text{CH}_4)$ and CH_4 : a case study with model LMDz-SACS, *Geosci. Model Dev.*, 15, 4831–4851, <https://doi.org/10.5194/gmd-15-4831-2022>, 2022a.

Thanverdas, J., Saunois, M., Pison, I., Hauglustaine, D., Berchet, A., Baier, B., Sweeney, C., and Bousquet, P.: How do Cl concentrations matter for the simulation of CH_4 and $\delta^{13}\text{C}(\text{CH}_4)$ and estimation of the CH_4 budget through atmospheric inversions?, *Atmos. Chem. Phys.*, 22, 15489–15508, <https://doi.org/10.5194/acp-22-15489-2022>, 2022b.

Thanverdas, J., Saunois, M., Berchet, A., Pison, I., and Bousquet, P.: Investigation of the renewed methane growth post-2007 with high-resolution 3-D variational inverse modeling and isotopic constraints, *Atmos. Chem. Phys.*, 24, 2129–2167, <https://doi.org/10.5194/acp-24-2129-2024>, 2024.

Thompson, R. L., Montzka, S. A., Vollmer, M. K., Arduini, J., Crotwell, M., Krummel, P. B., Lunder, C., Mühle, J., O'Doherty, S., Prinn, R. G., Reimann, S., Vimont, I., Wang, H., Weiss, R. F., and Young, D.: Estimation of the atmospheric hydroxyl radical oxidative capacity using multiple hydrofluorocarbons (HFCs), *Atmos. Chem. Phys.*, 24, 1415–1427, <https://doi.org/10.5194/acp-24-1415-2024>, 2024.

Thoning, K. W., Tans, P. P. and Komhyr, W. D.: Atmospheric carbon dioxide at Mauna Loa Observatory. 2. Analysis of the NOAA GMCC data, 1974,1985, *J. Geophys. Res.*, 94(D6), 8549–8565, 1989.

Thorneloe, S. A., Barlaz, M. A., Peer, R., Huff, L. C., Davis, L. and Mangino, J.: Waste management, in *Atmospheric Methane: Its Role in the Global Environment*, edited by M. Khalil, pp. 234–262, Springer-Verlag, New York., 2000.

Thornton, B. F., Prytherch, J., Andersson, K., Brooks, I. M., Salisbury, D., Tjernström, M. and Crill, P. M.: Shipborne eddy covariance observations of methane fluxes constrain Arctic sea emissions, *Sci. Adv.*, 6(5), eaay7934, doi:10.1126/sciadv.aay7934, 2020.

Thornton B.F., Etiope G., Schwietzke S., Milkov A.V., Klusman R.W., Judd A., Oehler D.Z.: Conflicting estimates of natural geologic methane emissions. *Elem. Sci. Anth.*, 9, 1, doi:<https://doi.org/10.1525/elementa.2021.00031>, 2021

4207 Thornton, J. A., Kercher, J. P., Riedel, T. P., Wagner, N. L., Cozic, J., Holloway, J. S., Dubé, W. P., Wolfe, G. M., Quinn,
4208 P. K., Middlebrook, A. M., Alexander, B. and Brown, S. S.: A large atomic chlorine source inferred from mid-
4209 continental reactive nitrogen chemistry, *Nature*, 464(7286), 271–274, doi:10.1038/nature08905, 2010.

4210 Thorpe, A. K., Kort, E. A., Cusworth, D. H., Ayasse, A. K., Bue, B. D., Yadav, V., Thompson, D. R., Frankenberg, C.,
4211 Hermer, J., Falk, M., Green, R. O., Miller, C. E., and Duren, R. M.: Methane emissions decline from reduced oil,
4212 natural gas, and refinery production during COVID-19, *Environmental Research Communications*, 5, 021006, 2023

4213 Tian, H., Xu, X., Liu, M., Ren, W., Zhang, C., Chen, G. and Lu, C.: Spatial and temporal patterns of CH₄ and N₂O fluxes
4214 in terrestrial ecosystems of North America during 1979–2008: application of a global biogeochemistry model,
4215 *Biogeosciences*, 7(9), 2673–2694, doi:10.5194/bg-7-2673-2010, 2010.

4216 Tian, H., Xu, X., Lu, C., Liu, M., Ren, W., Chen, G., Melillo, J. and Liu, J.: Net exchanges of CO₂, CH₄, and N₂O between
4217 China's terrestrial ecosystems and the atmosphere and their contributions to global climate warming, *J. Geophys. Res.*
4218 *Biogeosciences*, 116, G2, doi:10.1029/2010jg001393, 2011.

4219 Tian, H., Chen, G., Lu, C., Xu, X., Ren, W., Zhang, B., Banger, K., Tao, B., Pan, S., Liu, M., Zhang, C., Bruhwiler, L.
4220 and Wofsy, S.: Global methane and nitrous oxide emissions from terrestrial ecosystems due to multiple environmental
4221 changes, *Ecosyst. Health Sustain.*, 1(1), 1–20, doi:10.1890/ehs14-0015.1, 2015.

4222 Tian, H., Lu, C., Ciais, P., Michalak, A. M., Canadell, J. G., Saikawa, E., Huntzinger, D. N., Gurney, K. R., Sitch, S.,
4223 Zhang, B., Yang, J., Bousquet, P., Bruhwiler, L., Chen, G., Dlugokencky, E., Friedlingstein, P., Melillo, J., Pan, S.,
4224 Poulter, B., Prinn, R., Saunio, M., Schwalm, C. R. and Wofsy, S. C.: The terrestrial biosphere as a net source of
4225 greenhouse gases to the atmosphere, *Nature*, 531(7593), 225–228, doi:10.1038/nature16946, 2016.

4226 Tian, H., Xu, R., Canadell, J. G., Thompson, R. L., Winiwarter, W., Suntharalingam, P., Davidson, E. A., Ciais, P.,
4227 Jackson, R. B., Janssens-Maenhout, G., Prather, M. J., Regnier, P., Pan, N., Pan, S., Peters, G. P., Shi, H., Tubiello, F.
4228 N., Zaehle, S., Zhou, F., Arneeth, A., Battaglia, G., Berthet, S., Bopp, L., Bouwman, A. F., Buitenhuis, E. T., Chang,
4229 J., Chipperfield, M. P., Dangal, S. R. S., Dlugokencky, E., Elkins, J. W., Eyre, B. D., Fu, B., Hall, B., Ito, A., Joos, F.,
4230 Krummel, P. B., Landolfi, A., Laruelle, G. G., Lauerwald, R., Li, W., Lienert, S., Maavara, T., MacLeod, M., Millet,
4231 D. B., Olin, S., Patra, P. K., Prinn, R. G., Raymond, P. A., Ruiz, D. J., van der Werf, G. R., Vuichard, N., Wang, J.,
4232 Weiss, R. F., Wells, K. C., Wilson, C., Yang, J., and Yao, Y.: A comprehensive quantification of global nitrous oxide
4233 sources and sinks, *Nature*, 586, 248–256, <https://doi.org/10.1038/s41586-020-2780-0>, 2020.

4234 Tian, H., Yao, Y., Li, Y., Shi, H., Pan, S., Najjar, R. G., et al. (2023). Increased terrestrial carbon export and CO₂ evasion
4235 from global inland waters since the preindustrial era. *Global Biogeochemical Cycles*, 37, e2023GB007776.
4236 <https://doi.org/10.1029/2023GB007776>, 2023

4237 Tibrewal, K., Ciais, P., Saunio, M., Martinez, A., Lin, X., Thanwerdas, J., Deng, Z., Chevallier, F., Giron, C., Albergel,
4238 C., Tanaka, K., Patra, P., Tsuruta, A., Zheng, B., Belikov, D., Niwa, Y., Janardanan, R., Maksyutov, S., Segers, A.,
4239 Tzompa-Sosa, Z. A., Bousquet, P., and Sciare, J.: Assessment of methane emissions from oil, gas and coal sectors

Mis en forme : Français

across inventories and atmospheric inversions, *Commun Earth Environ* 5, 26, <https://doi.org/10.1038/s43247-023-01190-w>, 2024

Tiwari, Y. K. and Kumar, K. R.: GHG observation programs in India, *Asian GAWgreenhouse Gases 3 Korea Meteorol. Adm. Chungnam South Korea*, 2012.

Tsuruta, A., Aalto, T., Backman, L., Hakkarainen, J., Laan-Luijckx, I. T. van der, Krol, M. C., Spahni, R., Houweling, S., Laine, M., Dlugokencky, E., Gomez-Pelaez, A. J., Schoot, M. van der, Langenfelds, R., Ellul, R., Arduini, J., Apadula, F., Gerbig, C., Feist, D. G., Kivi, R., Yoshida, Y. and Peters, W.: Global methane emission estimates for 2000–2012 from CarbonTracker Europe-CH₄ v1.0, *Geosci. Model Dev.*, 10(3), 1261–1289, doi:10.5194/gmd-10-1261-2017, 2017.

Tsuruta, A.; Kivimäki, E.; Lindqvist, H.; Karppinen, T.; Backman, L.; Hakkarainen, J.; Schneising, O.; Buchwitz, M.; Lan, X.; Kivi, R.; et al. CH₄ Fluxes Derived from Assimilation of TROPOMI XCH₄ in CarbonTracker Europe-CH₄: Evaluation of Seasonality and Spatial Distribution in the Northern High Latitudes. *Remote Sens.* 2023, 15, 1620. <https://doi.org/10.3390/rs15061620>, 2023

Tubiello, F. N.: Greenhouse Gas Emissions Due to Agriculture, in *Elsevier Encyclopedia of Food Systems.*, 2019.

Tubiello, F. N., Salvatore, M., Rossi, S., Ferrara, A., Fitton, N. and Smith, P.: The FAOSTAT database of greenhouse gas emissions from agriculture, *Environ. Res. Lett.*, 8(1), 015009, doi:10.1088/1748-9326/8/1/015009, 2013.

Tubiello, F. N., Karl, K., Flammini, A., Gütschow, J., Obli-Laryea, G., Conchedda, G., Pan, X., Qi, S. Y., Halldórudóttir Heiðarsdóttir, H., Wanner, N., Quadrelli, R., Rocha Souza, L., Benoit, P., Hayek, M., Sandalow, D., Mencos Contreras, E., Rosenzweig, C., Rosero Moncayo, J., Conforti, P., and Torero, M.: Pre- and post-production processes increasingly dominate greenhouse gas emissions from agri-food systems, *Earth Syst. Sci. Data*, 14, 1795–1809, <https://doi.org/10.5194/essd-14-1795-2022>, 2022.

Turetsky, M. R., Kotowska, A., Bubier, J., Dise, N. B., Crill, P., Hornibrook, E. R. C., Minkinen, K., Moore, T. R., Myers-Smith, I. H., Nykänen, H., Olefeldt, D., Rinne, J., Saarnio, S., Shurpali, N., Tuittila, E.-S., Waddington, J. M., White, J. R., Wickland, K. P. and Wilkening, M.: A synthesis of methane emissions from 71 northern, temperate, and subtropical wetlands, *Glob. Change Biol.*, 20(7), 2183–2197, doi:10.1111/gcb.12580, 2014.

Turetsky, M. R., Abbott, B. W., Jones, M. C., Anthony, K. W., Olefeldt, D., Schuur, E. A. G., et al.: Carbon release through abrupt permafrost thaw. *Nature Geoscience*, 13(2), 138–143. <https://doi.org/10.1038/s41561-019-0526-0>, 2020

Turner, A. J., Fung, I., Naik, V., Horowitz, L. W. and Cohen, R. C.: Modulation of hydroxyl variability by ENSO in the absence of external forcing, *Proc. Natl. Acad. Sci.*, 115(36), 8931–8936, doi:10.1073/pnas.1807532115, 2018.

Turner, A. J., Frankenberg, C. and Kort, E. A.: Interpreting contemporary trends in atmospheric methane, *Proc. Natl. Acad. Sci.*, 116(8), 2805, doi:10.1073/pnas.1814297116, 2019.

UNEP, United Nations Environment Programme and Climate and Clean Air Coalition. Global Methane Assessment:

4273 Benefits and Costs of Mitigating Methane Emissions. Nairobi: United Nations Environment Programme., 2021

4274 UNEP, United Nations Environment Programme/Climate and Clean Air Coalition. Global Methane Assessment: 2030

4275 Baseline Report. Nairobi, 2022.

4276 USEPA: Greenhouse Gas Emissions Estimation Methodologies for Biogenic Emissions from Selected Source Categories:

4277 Solid Waste Disposal Wastewater Treatment Ethanol Fermentation, Measurement Policy Group, US EPA. [online]

4278 Available from: https://www3.epa.gov/ttnchie1/efpac/ghg/GHG_Biogenic_Report_draft_Dec1410.pdf (Accessed 11

4279 March 2020a), 2010a.

4280 USEPA: Office of Atmospheric Programs (6207J), Methane and Nitrous Oxide Emissions From Natural Sources, U.S.

4281 Environmental Protection Agency, EPA 430-R-10-001. Available online at <http://nepis.epa.gov/>, Washington, DC

4282 20460., 2010b.

4283 USEPA: Draft: Global Anthropogenic Non-CO₂ Greenhouse Gas Emissions: 1990-2030. EPA 430-R-03-002, United

4284 States Environmental Protection Agency, Washington D.C., 2011.

4285 USEPA: Global Anthropogenic Non-CO₂ Greenhouse Gas Emissions 1990-2030, EPA 430-R-12-006, US Environmental

4286 Protection Agency, Washington DC., 2012.

4287 USEPA: Draft Inventory of U.S. Greenhouse gas Emissions and Sinks: 1990-2014. EPA 430-R-16-002. February 2016.

4288 U.S. Environmental protection Agency, Washington, DC, USA., 2016.

4289 USEPA: Global Non-CO₂ Greenhouse Gas Emission Projections & Mitigation Potential: 2015-2050, EPA-430-R-19-010,

4290 U.S. Environmental protection Agency, Washington, DC, USA., 2019

4291 Valentine, D. W., Holland, E. A. and Schimel, D. S.: Ecosystem and physiological controls over methane production in

4292 northern wetlands, *J. Geophys. Res.*, 99(D1), 1563–1571, 1994.

4293 Vardag, S. N., Hammer, S., O'Doherty, S., Spain, T. G., Wastine, B., Jordan, A. and Levin, I.: Comparisons of continuous

4294 atmospheric CH₄, CO₂ and N₂O measurements – results from a travelling instrument campaign at Mace Head,

4295 *Atmospheric Chem. Phys.*, 14(16), 8403–8418, doi:10.5194/acp-14-8403-2014, 2014.

4296 [Varon, D. J., Jacob, D. J., Hmiel, B., Gautam, R., Lyon, D. R., Omara, M., Sulprizio, M., Shen, L., Pendergrass, D., Nesser,](#)

4297 [H., Qu, Z., Barkley, Z. R., Miles, N. L., Richardson, S. J., Davis, K. J., Pandey, S., Lu, X., Lorente, A., Borsdorff, T.,](#)

4298 [Maasackers, J. D., and Aben, I.: Continuous weekly monitoring of methane emissions from the Permian Basin by](#)

4299 [inversion of TROPOMI satellite observations, *Atmos. Chem. Phys.*, 23, 7503–7520, \[https://doi.org/10.5194/acp-23-\]\(https://doi.org/10.5194/acp-23-7503-2023\)](#)

4300 [7503-2023, 2023.](#)

4301 VODCA2GPP – a new, global, long-term (1988–2020) gross primary production dataset from microwave remote sensing,

4302 *Earth Syst. Sci. Data*, 14, 1063–1085, <https://doi.org/10.5194/essd-14-1063-2022>, 2022.

4303 Voulgarakis, A., Naik, V., Lamarque, J. F., Shindell, D. T., Young, P. J., Prather, M. J., Wild,

4304 O., Field, R. D., Bergmann, D., Cameron-Smith, P., Cionni, I., Collins, W. J., Dalsøren,

4305 S. B., Doherty, R. M., Eyring, V., Faluvegi, G., Folberth, G. A., Horowitz, L. W., Josse, B.,

Supprimé: 4

MacKenzie, I. A., Nagashima, T., Plummer, D. A., Righi, M., Rumbold, S. T., Stevenson, D. S., Strode, S. A., Sudo, K., Szopa, S. and Zeng, G.: Analysis of present day and future OH and methane lifetime in the ACCMIP simulations, *Atmospheric Chem. Phys.*, 13(5), 2563–2587, doi:10.5194/acp-13-2563-2013, 2013.

Voulgarakis, A., Marlier, M. E., Faluvegi, G., Shindell, D. T., Tsigaridis, K. and Mangeon, S.: Interannual variability of tropospheric trace gases and aerosols: The role of biomass burning emissions, *J. Geophys. Res. Atmospheres*, 120(14), 7157–7173, doi:10.1002/2014jd022926, 2015.

Wallmann, K., Pinero, E., Burwicz, E., Haeckel, M., Hensen, C., Dale, A. and Ruepke, L.: The Global Inventory of Methane Hydrate in Marine Sediments: A Theoretical Approach, *Energies*, 5(7), 2449, 2012.

Walter Anthony, K.M., Anthony, P., Grosse, G. and Chanton, J.: Geologic methane seeps along boundaries of Arctic permafrost thaw and melting glaciers. *Nature Geoscience*, 5(6), pp.419-426., DOI: 10.1038/ngeo1480, 2012

Wang, F., Maksyutov, S., Tsuruta, A., Janardanan, R., Ito, A., Sasakawa, M., Machida, T., Morino, I., Yoshida, Y., Kaiser, J. W., Janssens-Maenhout, G., Dlugokencky, E. J., Mammarella, I., Lavric, J. V. and Matsunaga, T.: Methane Emission Estimates by the Global High-Resolution Inverse Model Using National Inventories, *Remote Sens.*, 11(21), 2489, doi:10.3390/rs11212489, 2019a.

Wang, G., X. Xia, S. Liu, L. Zhang, S. Zhang, J. Wang, N. Xi, and Q. Zhang, Intense methane ebullition from urban inland waters and its significant contribution to greenhouse gas emissions. *Water Research*, 189: p. 116654, 2021a

Wang, X., Jacob, D. J., Eastham, S. D., Sulprizio, M. P., Zhu, L., Chen, Q., Alexander, B., Sherwen, T., Evans, M. J., Lee, B. H., Haskins, J. D., Lopez-Hilfiker, F. D., Thornton, J. A., Huey, G. L. and Liao, H.: The role of chlorine in global tropospheric chemistry, *Atmospheric Chem. Phys.*, 19(6), 3981–4003, doi:10.5194/acp-19-3981-2019, 2019b.

Wang, X., Jacob, D. J., Downs, W., Zhai, S., Zhu, L., Shah, V., Holmes, C. D., Sherwen, T., Alexander, B., Evans, M. J., Eastham, S. D., Neuman, J. A., Veres, P. R., Koenig, T. K., Volkamer, R., Huey, L. G., Bannan, T. J., Percival, C. J., Lee, B. H., and Thornton, J. A.: Global tropospheric halogen (Cl, Br, I) chemistry and its impact on oxidants, *Atmos. Chem. Phys.*, 21, 13973–13996, <https://doi.org/10.5194/acp-21-13973-2021>, 2021b.

Wang, Z., Deutscher, N. M., Warneke, T., Notholt, J., Dils, B., Griffith, D. W. T., Schmidt, M., Ramonet, M. and Gerbig, C.: Retrieval of tropospheric column-averaged CH₄ mole fraction by solar absorption FTIR-spectrometry using N₂O as a proxy, *Atmospheric Meas. Tech.*, 7(10), 3295–3305, doi:10.5194/amt-7-3295-2014, 2014.

Wang, Z.-P., Gu, Q., Deng, F.-D., Huang, J.-H., Megonigal, J. P., Yu, Q., Lü, X.-T., Li, L.-H., Chang, S., Zhang, Y.-H., Feng, J.-C. and Han, X.-G.: Methane emissions from the trunks of living trees on upland soils, *New Phytol.*, 211(2), 429–439, doi:10.1111/nph.13909, 2016.

Wania, R., I. Ross and I. C. Prentice: Implementation and evaluation of a new methane model within a dynamic global vegetation model: LPJ-WHyMe v1.3, *Geosci. Model Dev. Discuss.*, 3, 1–59, 2010.

Wania, R., Melton, J. R., Hodson, E. L., Poulter, B., Ringeval, B., Spahni, R., Bohn, T., Avis, C. A., Chen, G., Eliseev, A.

4340 V., Hopcroft, P. O., Riley, W. J., Subin, Z. M., Tian, H., van Bodegom, P. M., Kleinen, T., Yu, Z. C., Singarayer, J.
 4341 S., Zurcher, S., Lettenmaier, D. P., Beerling, D. J., Denisov, S. N., Prigent, C., Papa, F. and Kaplan, J. O.: Present state
 4342 of global wetland extent and wetland methane modelling: Methodology of a model inter-comparison project
 4343 (WETCHIMP), *Geosci. Model Dev.*, 6(3), 617–641, 2013.
 4344 Wassmann, R., Lantin, R. S., Neue, H. U., Buendia, L. V., Corton, T. M. and Lu, Y.: Characterization of methane emissions
 4345 in Asia III: Mitigation options and future research needs, *Nutr. Cycl. Agroecosystems*, 58, 23–36, 2000.
 4346 Weber, T., Wiseman, N. A. and Kock, A.: Global ocean methane emissions dominated by shallow coastal waters, *Nat.*
 4347 *Commun.*, 10(1), 1–10, doi:10.1038/s41467-019-12541-7, 2019.
 4348 Wells, N. S., J. J. Chen, D. T. Maher, P. Huang, D. V. Erler, M. Hipsey, and B. D. Eyre: Changing sediment and surface
 4349 water processes increase CH₄ emissions from human-impacted estuaries. *Geochim. Cosmochim. Acta* **280**: 130–147.
 4350 doi:10.1016/j.gca.2020.04.020, 2020
 4351 van der Werf, G. R., Randerson, J. T., Giglio, L., Collatz, G. J., Mu, M., Kasibhatla, P. S., Morton, D. C., DeFries, R. S.,
 4352 Jin, Y. and van Leeuwen, T. T.: Global fire emissions and the contribution of deforestation, savanna, forest,
 4353 agricultural, and peat fires (1997-2009), *Atmospheric Chem. Phys.*, 10(23), 11,707-11,735, 2010.
 4354 van der Werf, G. R., Randerson, J. T., Giglio, L., Leeuwen, T. T. van, Chen, Y., Rogers, B. M., Mu, M., Marle, M. J. E.
 4355 van, Morton, D. C., Collatz, G. J., Yokelson, R. J. and Kasibhatla, P. S.: Global fire emissions estimates during 1997–
 4356 2016, *Earth Syst. Sci. Data*, 9(2), 697–720, doi:10.5194/essd-9-697-2017, 2017.
 4357 Westbrook, G. K., Thatcher, K. E., Rohling, E. J., Piotrowski, A. M., Pálíke, H., Osborne, A. H., Nisbet, E. G., Minshull,
 4358 T. A., Lanoisellé, M., James, R. H., Hühnerbach, V., Green, D., Fisher, R. E., Crocker, A. J., Chabert, A., Bolton, C.,
 4359 Beszczyńska-Möller, A., Berndt, C., and Aquilina, A.: Escape of methane gas from the seabed along the West
 4360 Spitsbergen continental margin, *Geophys. Res. Lett.*, 36, L15608, <https://doi.org/10.1029/2009GL039191>, 2009.
 4361 Whalen, S. C.: Biogeochemistry of Methane Exchange between Natural Wetlands and the Atmosphere, *Environ. Eng.*
 4362 *Sci.*, 22(1), 73–94, doi:10.1089/ees.2005.22.73, 2005.
 4363 Wiedinmyer, C., Kimura, Y., McDonald-Buller, E. C., Emmons, L. K., Buchholz, R. R., Tang, W., Seto, K., Joseph, M.
 4364 B., Barsanti, K. C., Carlton, A. G., and Yokelson, R.: The Fire Inventory from NCAR version 2.5: an updated global
 4365 fire emissions model for climate and chemistry applications, *EGUsphere* [preprint], [https://doi.org/10.5194/egusphere-](https://doi.org/10.5194/egusphere-2023-124)
 4366 2023-124, 2023.
 4367 Wik, M., Thornton, B. F., Bastviken, D., Uhlbäck, J. and Crill, P. M.: Biased sampling of methane release from northern
 4368 lakes: A problem for extrapolation, *Geophys. Res. Lett.*, 43(3), 1256–1262, doi:10.1002/2015gl066501, 2016a.
 4369 Wik, M., Varner, R. K., Anthony, K. W., MacIntyre, S. and Bastviken, D.: Climate-sensitive northern lakes and ponds are
 4370 critical components of methane release, *Nat. Geosci.*, 9(2), 99–105, doi:10.1038/ngeo2578, 2016b.
 4371 Wild, B., Teubner, I., Moesinger, L., Zotta, R.-M., Forkel, M., van der Schalie, R., Sitch, S., and Dorigo, W.:
 4372 VODCA2GPP – a new, global, long-term (1988–2020) gross primary production dataset from microwave remote

sensing, *Earth Syst. Sci. Data*, 14, 1063–1085, <https://doi.org/10.5194/essd-14-1063-2022>, 2022.

Williams, J. P., Omara, M., Himmelberger, A., Zavala-Araiza, D., MacKay, K., Benmergui, J., Sargent, M., Wofsy, S. C., Hamburg, S. P., and Gautam, R.: Small emission sources disproportionately account for a large majority of total methane emissions from the US oil and gas sector, *EGUsphere* [preprint], <https://doi.org/10.5194/egusphere-2024-1402>, 2024.

Winderlich, J., Chen, H., Gerbig, C., Seifert, T., Kolle, O., Lavrič, J. V., Kaiser, C., Höfer, A. and Heimann, M.: Continuous low-maintenance CO₂/CH₄/H₂O measurements at the Zotino Tall Tower Observatory (ZOTTO) in Central Siberia, *Atmospheric Meas. Tech.*, 3(4), 1113–1128, doi:10.5194/amt-3-1113-2010, 2010.

Wilson, C., Chipperfield, M. P., Gloor, M., Parker, R. J., Boesch, H., McNorton, J., Gatti, L. V., Miller, J. B., Basso, L. S., and Monks, S. A.: Large and increasing methane emissions from eastern Amazonia derived from satellite data, 2010–2018, *Atmos. Chem. Phys.*, 21, 10643–10669, <https://doi.org/10.5194/acp-21-10643-2021>, 2021.

Wood, T.G. and Sands, W.A. The role of termites in ecosystems. In: Brian, M.V. (Ed.), *Production Ecology of Ants and Termites*. Cambridge University Press, Cambridge, UK, 245–292, 1978.

Woodward G, Perkins D.M., and Brown L. E.: Climate change and freshwater ecosystems: impacts across multiple levels of organization, *Philos Trans R Soc Lond B Biol Sci.* ,365(1549), 2093–106, doi: 10.1098/rstb.2010.0055, 2010

Woodward, G., Gessner, M. O., Giller, P. S., Gulis, V., Hladysz, S., Lecerf, A., Malmqvist, B., McKie, B. G., Tiegs, S. D., Cariss, H., Dobson, M., Eloegi, A., Ferreira, V., Graça, M. A. S., Fleituch, T., Lacoursière, J. O., Nistorescu, M., Pozo, J., Risnoveanu, G., Schindler, M., Vadineanu, A., Vought, L. B.-M. and Chauvet, E.: Continental-Scale Effects of Nutrient Pollution on Stream Ecosystem Functioning, *Science*, 336(6087), 1438–1440, doi:10.1126/science.1219534, 2012.

Woolway RI, Jones ID, Maberly SC, French JR, Livingstone DM, Monteith DT, et al.: Diel Surface Temperature Range Scales with Lake Size, *PLoS ONE* 11(3): e0152466, [doi:10.1371/journal.pone.0152466](https://doi.org/10.1371/journal.pone.0152466), 2016

Worden, J. R., Bloom, A. A., Pandey, S., Jiang, Z., Worden, H. M., Walker, T. W., Houweling, S. and Röckmann, T.: Reduced biomass burning emissions reconcile conflicting estimates of the post-2006 atmospheric methane budget, *Nat. Commun.*, 8(1), 2227, doi:10.1038/s41467-017-02246-0, 2017.

Wu, Z., Li, J., Sun, Y. *et al.* : Imbalance of global nutrient cycles exacerbated by the greater retention of phosphorus over nitrogen in lakes. *Nat. Geosci.* 15, 464–468, <https://doi.org/10.1038/s41561-022-00958-7>, 2022

Wuebbles, D. J. and Hayhoe, K.: Atmospheric methane and global change, *Earth-Sci. Rev.*, 57(3–4), 177–210, 2002.

Wunch, D., Toon, G. C., Blavier, J.-F. L., Washenfelder, R. A., Notholt, J., Connor, B. J., Griffith, D. W. T., Sherlock, V. and Wennberg, P. O.: The Total Carbon Column Observing Network, *Philos. Trans. R. Soc. A*, 369(1943), doi:10.1098/rsta.2010.0240, 2011.

Wunch, D., Toon, G. C., Hedelius, J. K., Vizenor, N., Roehl, C. M., Saad, K. M., Blavier, J.-F. L., Blake, D. R. and Wennberg, P. O.: Quantifying the loss of processed natural gas within California’s South Coast Air Basin using long-

4439 [Phys., 23, 3325–3346, https://doi.org/10.5194/acp-23-3325-2023, 2023.](https://doi.org/10.5194/acp-23-3325-2023)

4440 Yuan, J., J. Xiang, D. Liu, and others: Rapid growth in greenhouse gas emissions from the adoption of industrial-scale

4441 aquaculture. *Nat. Clim. Chang.* 9: 318–322. doi:10.1038/s41558-019-0425-9, 2019

4442 Yver Kwok, C. E., Müller, D., Caldow, C., Lebègue, B., Münster, J. G., Rella, C. W., Scheutz, C., Schmidt, M., Ramonet,

4443 M., Warneke, T., Broquet, G. and Ciais, P.: Methane emission estimates using chamber and tracer release experiments

4444 for a municipal waste water treatment plant, *Atmospheric Meas. Tech.*, 8(7), 2853–2867, doi:10.5194/amt-8-2853-

4445 2015, 2015.

4446 [Zhang, Magnitude, spatio-temporal variability and environmental controls of methane emissions from global rice fields:](#)

4447 [Implications for water management and climate mitigation, *Glob. Change Biol.*, 2016.](#)

4448 Zhang, B. and Chen, G. Q.: China’s CH₄ and CO₂ Emissions: Bottom-Up Estimation and Comparative Analysis, *Ecol.*

4449 *Indic.*, 47, 112–122, doi:10.1016/j.ecolind.2014.01.022, 2014.

4450 Zhang, L., X. Xia, S. Liu, S. Zhang, S. Li, J. Wang, G. Wang, H. Gao, Z. Zhang, Q. Wang, W. Wen, R. Liu, Z. Yang, E.H.

4451 Stanley, and P.A. Raymond: Significant methane ebullition from alpine permafrost rivers on the East Qinghai–Tibet

4452 Plateau. *Nature Geoscience*, 13(5): p. 349-354, 2020

4453 Zhang, L., H. Tian, H. Shi, S. Pan, J. Chang, S. R. S. Dungal, X. Qin, S. Wang, F. N. Tubiello, J. G. Canadell, R. B.

4454 Jackson: A 130-year global inventory of methane emissions from livestock: Trends, patterns, and drivers, *Global*

4455 *Change Biology*, 28 (17), 5142-5158. <https://doi.org/10.1111/gcb.16280>, 2022

4456 [Zhang, P., Zhang, Y., Liang, R., Chen, W., and Xie, X.: Evaluation of the stratospheric contribution to the inter-annual](#)

4457 [variabilities of tropospheric methane growth rates, *Geophysical Research Letters*, 50,](#)

4458 [e2023GL103350,https://doi.org/10.1029/2023GL103350, 2023.](#)

4459 Zhang, Y., Xiao, X., Wu, X., Zhou, S., Zhang, G., Qin, Y., and Dong, J.: A global moderate resolution dataset of gross

4460 primary production of vegetation for 2000–2016, *Sci. Data*, 4, 1–13, <https://doi.org/10.1038/sdata.2017.165>, 2017.

4461 Zhang, Y., Jacob, D. J., Maasakkers, J. D., Sulprizio, M. P., Sheng, J.-X., Gautam, R., and Worden, J.: Monitoring global

4462 tropospheric OH concentrations using satellite observations of atmospheric methane, *Atmos. Chem. Phys.*, 18, 15959–

4463 15973, <https://doi.org/10.5194/acp-18-15959-2018>, 2018.

4464 [Zhang, Y., Gautam, R., Pandey, S., Omara, M., Maasakkers, J. D., Sadavarte, P., Lyon, D., Nesser, H., Sulprizio, M. P.,](#)

4465 [Varon, D. J., Zhang, R., Houweling, S., Zavala-Araiza, D., Alvarez, R. A., Lorente, A., Hamburg, S. P., Aben, I., and](#)

4466 [Jacob, D. J.: Quantifying Methane Emissions from the Largest Oil-Producing Basin in the United States from Space,](#)

4467 [Sci. Adv., 6, eaaz5120, <https://doi.org/10.1126/sciadv.aaz5120>, 2020.](#)

4468 Zhang, Z., Zimmermann, N. E., Kaplan, J. O. and Poulter, B.: Modeling spatiotemporal dynamics of global wetlands:

4469 comprehensive evaluation of a new sub-grid TOPMODEL parameterization and uncertainties, *Biogeosciences*, 13(5),

4470 1387–1408, doi:10.5194/bg-13-1387-2016, 2016.

Supprimé: Zavala-Araiza, D., Lyon, D. R., Alvarez, R. A., Davis, K. J., Harriss, R., Herndon, S. C., Karion, A., Kort, E. A., Lamb, B. K., Lan, X., Marchese, A. J., Pacala, S. W., Robinson, A. L., Shepson, P. B., Sweeney, C., Talbot, R., Townsend-Small, A., Yacovitch, T. I., Zimmerle, D. J. and Hamburg, S. P.: Reconciling divergent estimates of oil and gas methane emissions, *Proc. Natl. Acad. Sci. USA*, 112, 15597–15602, doi:10.1073/pnas.1522126112, 2015.

Supprimé: 

Supprimé: :

4481 [Zhang, Z., Fluet-Chouinard, E., Jensen, K., McDonald, K., Hugelius, G., Gumbrecht, T., et al. Development of the global](#)
4482 [dataset of Wetland Area and Dynamics for Methane Modeling \(WAD2M\), Earth System Science Data, 13\(5\), 2001–](#)
4483 [2023. <https://doi.org/10.5194/essd-13-2001-2021>, 2021a.](#)

4484 [Zhang, Z., Poulter, B., Knox, S., Stavert, A., McNicol, G., Fluet-Chouinard, E., Feinberg, A., Zhao, Y., Bousquet, P.,](#)
4485 [Canadell, J. G., Ganesan, A., Hugelius, G., Hurtt, G., Jackson, R. B., Patra, P. K., Saunio, M., Höglund-Isaksson, L.,](#)
4486 [Huang, C., Chatterjee, A., and Li, X.: Anthropogenic emission is the main contributor to the rise of atmospheric](#)
4487 [methane during 1993-2017, National science review, 9\(5\), nwab200, doi:10.1093/nsr/nwab200, 2021b](#)

4488 Zhang, Z., Poulter, B., Feldman, A.F., Ying, Q., Ciais, P., Peng, S. and Li, X.: Recent intensification of wetland methane
4489 feedback, Nat. Clim. Chang. 13, 430–433, <https://doi.org/10.1038/s41558-023-01629-0>, 2023

4490 [Zhang, Z., Poulter, B., Melton, J. R., Riley, W. J., Allen, G. H., Beerling, D. J., Bousquet, P., Canadell, J. G., Fluet-](#)
4491 [Chouinard, E., Ciais, P., Gedney, N., Hoppercroft, P. O., Ito, A., Jackson, R. B., Jain, A. K., Jensen, K., Joos, F., Kleinen,](#)
4492 [T., Knox, S., Li, T., Li, X., Liu, X., McDonald, K., McNicol, G., Miller, P. A., Müller, J., Patra, P. K., Peng, C., Peng,](#)
4493 [S., Qin, Z., Riggs, R. M., Saunio, M., Sun, Q., Tian, H., Xu, X., Yao, Y., Yi, X., Zhang, W., Zhu, Q., Zhu, Q., and](#)
4494 [Zhuang, Q.: Ensemble estimates of global wetland methane emissions over 2000–2020, EGU sphere \[preprint\],](#)
4495 <https://doi.org/10.5194/egusphere-2024-1584>, 2024.

4496 [Zhao, J., M. Zhang, W. Xiao, L. Jia, X. Zhang, J. Wang, Z. Zhang, Y. Xie, Y. Pu, S. Liu, Z. Feng, and X. Lee: Large](#)
4497 [methane emission from freshwater aquaculture ponds revealed by long-term eddy covariance observation. Agricultural](#)
4498 [and Forest Meteorology, 308-309: p. 108600, 2021](#)

4499 Zhao, Y., Saunio, M., Bousquet, P., Lin, X., Berchet, A., Hegglin, M. I., Canadell, J. G., Jackson, R. B., Hauglustaine,
4500 D. A., Szopa, S., Stavert, A. R., Abraham, N. L., Archibald, A. T., Bekki, S., Deushi, M., Jöckel, P., Josse, B., Kinnison,
4501 D., Kirner, O., Marécal, V., O'Connor, F. M., Plummer, D. A., Revell, L. E., Rozanov, E., Stenke, A., Strode, S.,
4502 Tilmes, S., Dlugokencky, E. J. and Zheng, B.: Inter-model comparison of global hydroxyl radical (OH) distributions
4503 and their impact on atmospheric methane over the 2000–2016 period, Atmospheric Chem. Phys., 19(21), 13701–
4504 13723, doi:10.5194/acp-19-13701-2019, 2019.

4505 [Zhao, Y., Saunio, M., Bousquet, P., Lin, X., Berchet, A., Hegglin, M. I., Canadell, J. G., Jackson, R. B., Dlugokencky,](#)
4506 [E. J., Langenfelds, R. L., Ramonet, M., Worthy, D., and Zheng, B.: Influences of hydroxyl radicals \(OH\) on top-down](#)
4507 [estimates of the global and regional methane budgets, Atmos. Chem. Phys., 20, 9525–9546,](#)
4508 <https://doi.org/10.5194/acp-20-9525-2020>, 2020a.

4509 [Zhao, Y., Saunio, M., Bousquet, P., Lin, X., Berchet, A., Hegglin, M. I., Canadell, J. G., Jackson, R. B., Deushi, M.,](#)
4510 [Jöckel, P., Kinnison, D., Kirner, O., Strode, S., Tilmes, S., Dlugokencky, E. J., and Zheng, B.: On the role of trend and](#)
4511 [variability in the hydroxyl radical \(OH\) in the global methane budget, Atmos. Chem. Phys., 20, 13011–13022,](#)
4512 <https://doi.org/10.5194/acp-20-13011-2020>, 2020b.

4513 Zhao, Y., Saunio, M., Bousquet, P., Lin, X., Hegglin, M. I., Canadell, J. G., Jackson, R. B., and Zheng, B.: Reconciling

Supprimé: Zhang, Z., Poulter, B., Melton, J., Riley, W., Allen, G., Beerling D., Bousquet P., Canadell, J., Fluet-Chouinard E., Ciais, P., Gedney, N., Hoppercroft, P., Ito, A., Jackson, R., Jain, A., Jensen, K., Joos, F., Kleinen, T., Knox, S., Li, T., Li, X., Liu, X., McDonald, K., McNicol, G., Miller, P., Müller, J., Patra, P., Prigent, C., Peng, C., Peng, S., Qin, Z., Riggs, R., Saunio, M., Sun Q., Tian, H., Xu, X., Yao Y., Yi, X., Zhang, W., Zhu, Q., Zhu, Q., and Zhuang, Q.: Ensemble estimates of global wetland methane emissions over 2000-2020. Global Change Biology, in review.

Supprimé: 

Supprimé: e

Supprimé: Zhao, Y., Saunio, M., Bousquet, P., Lin, X., Berchet, A., Hegglin, M. I., Canadell, J. G., Jackson, R. B., Dlugokencky, E. J., Langenfelds, R. L., Ramonet, M., Worthy, D. and Zheng, B.: Influences of hydroxyl radicals (OH) on top-down estimates of the global and regional methane budgets, Atmospheric Chem. Phys. Discuss., 1–45, doi:10.5194/acp-2019-1208, 2020.

the bottom-up and top-down estimates of the methane chemical sink using multiple observations, *Atmos. Chem. Phys.*, 23, 789–807, <https://doi.org/10.5194/acp-23-789-2023>, 2023.

Zheng, B., Chevallier, F., Ciais, P., Yin, Y. and Wang, Y.: On the Role of the Flaming to Smoldering Transition in the Seasonal Cycle of African Fire Emissions, *Geophys. Res. Lett.*, 45(21), 11,998–12,007, doi:10.1029/2018GL079092, 2018a.

Zheng, B., Chevallier, F., Ciais, P., Yin, Y., Deeter, M. N., Worden, H. M., Wang, Y., Zhang, Q. and He, K.: Rapid decline in carbon monoxide emissions and export from East Asia between years 2005 and 2016, *Environ. Res. Lett.*, 13(4), 044007, doi:10.1088/1748-9326/aab2b3, 2018b.

Zheng, B., Chevallier, F., Yin, Y., Ciais, P., Fortems-Cheiney, A., Deeter, M. N., Parker, R. J., Wang, Y., Worden, H. M., and Zhao, Y.: Global atmospheric carbon monoxide budget 2000–2017 inferred from multi-species atmospheric inversions, *Earth Syst. Sci. Data*, 11, 1411–1436, doi: 10.5194/essd-11-1411-2019, 2019.

Zheng, B., Ciais, P., Chevallier, F., Yang, H., Canadell, J. G., Chen, Y., van der Velde, I. R., Aben, I., Chuvieco, E., Davis, S. J., Deeter, M., Hong, C., Kong, Y., Li, H., Li, H., Lin, X., He, K., and Zhang, Q.: Record-high CO₂ emissions from boreal fires in 2021, *Science*, 379, 912–917, doi: 10.1126/science.ade0805, 2023.

Zhu, Q., Liu, J., Peng, C., Chen, H., Fang, X., Jiang, H., Yang, G., Zhu, D., Wang, W. and Zhou, X.: Modelling methane emissions from natural wetlands by development and application of the TRIPLEX-GHG model, *Geosci. Model Dev.*, 7(3), 981–999, doi:10.5194/gmd-7-981-2014, 2014.

Zhu, Q., Peng, C., Chen, H., Fang, X., Liu, J., Jiang, H., Yang, Y. and Yang, G.: Estimating global natural wetland methane emissions using process modelling: spatio-temporal patterns and contributions to atmospheric methane fluctuations, *Glob. Ecol. Biogeogr.*, 24, 959–972, 2015.

[Zhu, Q., Laughner, J.L., Cohen, R.C.: Combining Machine Learning and Satellite Observations to Predict Spatial and Temporal Variation of near Surface OH in North American Cities, *Environ. Sci. Technol.*, 56, 11, doi:10.1021/acs.est.1c05636, 2022](#)

Zhu, Y., K.J. Purdy, Ö. Eyice, L. Shen, S.F. Harpenslager, G. Yvon-Durocher, A.J. Dumbrell, and M. Trimmer: Disproportionate increase in freshwater methane emissions induced by experimental warming. *Nature Climate Change*, 10(7): p. 685–690., 2020

Zhuang, Q., Melillo, J. M., Kicklighter, D. W., Prinn, R. G., McGuire, A. D., Steudler, P. A., Felzer, B. S. and Hu, S.: Methane fluxes between terrestrial ecosystems and the atmosphere at northern high latitudes during the past century: A retrospective analysis with a process-based biogeochemistry model, *Glob. Biogeochem Cycles*, 18(3), GB3010, doi:10.1029/2004gb002239, 2004.

Zhuang, Q., Chen, M., Xu, K., Tang, J., Saikawa, E., Lu, Y., Melillo, J. M., Prinn, R. G. and McGuire, A. D.: Response of global soil consumption of atmospheric methane to changes in atmospheric climate and nitrogen deposition, *Glob. Biogeochem. Cycles*, 27(3), 650–663, doi:10.1002/gbc.20057, 2013.

4564 Zhuang, Q., M. Guo, J.M. Melack, X. Lan, Z. Tan, Y. Oh, and L.R. Leung: Current and Future Global Lake Methane
4565 Emissions: A Process-Based Modeling Analysis. *Journal of Geophysical Research: Biogeosciences*, 128(3): p.
4566 e2022JG007137, 2023

57 **Table 1: Bottom-up (BU) models and inventories for anthropogenic and biomass burning used in this study. *Due to its limited**
58 **sectoral breakdown this dataset was not used in Table 3.**

B-U models and inventories	Contribution	Time period (resolution)	Gridded	References	
CEDS (country based)	Fossil fuels, Agriculture and waste, Biofuel	1970-2019 (yearly)	no	Hoesly et al. (2018)	
CEDS (gridded)*	Fossil fuels, Agriculture and waste, Biofuel	1970-2020 (monthly)	0.5x0.5°	Hoesly et al. (2018) O'Rourke et al (2021)	Mis en forme : Français
EDGARv6	Fossil fuels, Agriculture and waste, Biofuel	1990-2018^ (yearly, monthly for some sectors)	0.1x0.1°	Oreggioni et al. (2021), Crippa et al. (2021)	Mis en forme : Français
EDGARv7	Fossil fuels, Agriculture and waste, Biofuel	1990-2021 (yearly)	0.1x0.1°	Crippa et al. (2023)	
IIASA GAINS v4.0	Fossil fuels, Agriculture and waste, Biofuel	1990-2020 (yearly)	0.5x0.5°	Höglund-Isaksson et al., (2020)	
USEPA	Fossil fuels, Agriculture and waste, Biofuel, Biomass Burning	1990-2030 (10-yr interval, interpolated to yearly)	no	USEPA (2019)	
FAO-CH4	Agriculture, Biomass Burning	1961-2020 1990-2020 (Yearly)	no	Federici et al. (2015) ; Tubiello et al. (2013); Tubiello (2019)	Mis en forme : Français
FINNv2.5	Biomass burning	2002-2020 (daily)	1km resolution	Wiedinmyer et al. (2023)	
GFASv1.3	Biomass burning	2003-2020 (daily)	0.1x0.1°	Kaiser et al. (2012)	
GFEDv4.1s	Biomass burning	1997-2020 (monthly)	0.25x0.25°	Giglio et al. (2013); van der Werf et al (2017)	Mis en forme : Français
QFEDv2.5	Biomass burning	2000-2020 (daily)	0.1x0.1°	Darmenov and da Silva (2015)	

59
60

1
2
3
Table 2: Biogeochemical models that computed wetland emissions used in this study. Model runs were performed with two climate inputs, CRU and GSWP3-W5E5. Models were run with prognostic (using their own calculation of wetland areas) and/or diagnostic (using WAD2M (Zhang et al., 2021b)) wetland surface areas (see Sect 3.2.1).

Model	Institution	Prognostic		Diagnostic		References
		CRU	GSWP3-W5E5	CRU	GSWP3-W5E5	
CH4MOD _{wetland}	Institute of Atmospheric Physics, CAS	n	n	y	y	Li et al. (2010)
CLASSIC	Environment and Climate Change Canada	y	y*	y	y*	Arora et al. (2018); Melton and Arora (2016)
DLEM	Boston College	y	y	y	y	Tian et al. (2015, 2023)
ELM-ECA	Lawrence Berkeley National Laboratory	y	y	y	y	Riley et al. (2011)
ISAM	University of Illinois, Urbana-Champaign	y	y	y	y	Shu et al. (2020) Xu et al. (2021)
JSBACH	MPI	y	y	y	y	Kleinen et al. (2020, 2021, 2023)
JULES	UKMO	y	y	y	y	Gedney et al. (2019)
LPJ-GUESS	Lund University	n	n	y	y	McGuire et al. (2012)
LPJ-MPI	MPI	y	y	y	y	Kleinen et al. (2012)
LPJ-WSL	NASA GSFC	y	y	y	y	Zhang et al. (2016)
LPX-Bern	University of Bern	y	y	y	y	Spahni et al. (2011), Stocker et al. (2014)
ORCHIDEE	LSCE	y	y	y	y	Ringeval et al. (2011)

Mis en forme : Français

Mis en forme : Français

SDGVM	University of Birmingham/ University of Sheffield	y	y	y	y	Beerling & Woodward (2001), Hopcroft et al. (2011, 2020)
TEM-MDM	Purdue University	n	n	y	y	Zhuang et al. (2004)
TRIPLEX-GHG	UQAM	n	n	y	y	Zhu et al. (2014, 2015)
VISIT	NIES	y	y	y	y	Ito and Inatomi (2012)

¹⁴ *CLASSIC uses GSWP3-W5E version 2 that covers the time period till 2016. All other models use GSWP-W5E5 version 3.

15 Table 3: Global methane emissions by source type in Tg CH₄ yr⁻¹ from Saunois et al. (2020) (left column pair) and from this work
 16 using bottom-up and top-down approaches. Because top-down models cannot fully separate individual processes, only five categories
 17 of emissions are provided (see text). Uncertainties are reported as [min-max] range of reported studies. The mean, minimum and
 18 maximum values are calculated while discarding outliers, for each category of source and sink. As a result, discrepancies may occur
 19 when comparing the sum of categories and their corresponding total due to differences in outlier detections. Differences of 1 Tg CH₄
 20 yr⁻¹ in the totals can also occur due to rounding errors. Compared to Saunois et al. (2020), emissions are split between “direct
 21 anthropogenic” emissions and “natural and indirect anthropogenic” sources. We also propose an estimate of the double-counting
 22 between bottom-up wetland and inland freshwater ecosystems emissions.

	Saunois et al. (2020)		This work					
Period of time	2000-2009		2000-2009		2010-2019		2020	
Approaches	bottom-up	top-down	bottom-up	top-down	bottom-up	top-down	bottom-up	top-down
NATURAL & indirect anthropogenic SOURCES								
Combined wetlands and inland freshwaters	306 [229-391]	180 [153-196]	242 [156-355]	158 [145-172]	248 [159-369]	165 [145-214]	251 [171-364]	175 [151-229]
Wetlands	147 [102-179]	180 [153-196]	153 [116-189] (***)	158 [145-172]	159 [119-203] (***)	165 [145-214]	161 [131-198] (***)	175 [151-229]
Inland freshwaters ^a	159 [117-212]		112 [49-202]		112 [49-202]		112 [49-202]	
Double counting ^b	NA		-23 [-9 - -36]		-23 [-9 - -36]		-23 [-9 - -36]	
Other natural sources	63 [26-94]	35 [21-47]	63 [24-93]	44 [40-46]	63 [24-93]	43 [40-46]	63 [24-93]	44 [40-47]
Land sources	50 [17-72]		51 [18-73]					
Geological (onshore)	38 [13-53]		38 [13-53]					
Wild animals	2 [1-3]		2 [1-3]					
Termites	9 [3-15]		10 [4-16]					
Wildfires	(**)		(**)					
Permafrost soils (direct)	1 [0-1]		1 [0-1]					
Vegetation	(*)		(*)					
Coastal and Oceanic sources ^c	13 [9-22]		12 [6-20]					
Biogenic	6 [4-10]		5 [3-10]					
Geological (offshore)	7 [5-12]		7 [5-12]					
TOTAL NATURAL & INDIRECT SOURCES	369 [245-485]	215 [176-243]	305 [180-448]	204 [189-223]	311 [183-462]	206 [188-225]	314 [195-457]	216 [193-241]
DIRECT ANTHROPOGENIC SOURCES								
Agriculture and waste	192 [178-206]	202 [198-219]	194 [181-208]	210 [197-223]	211 [195-231]	228 [213-242]	211 [204-216]	245 [232-259]
Agriculture	132 [NA]		134 [125-142]		143 [132-155]		147 [143-149]	
Enteric ferm. & manure	104 [93-109]		104 [100 -110]		112 [107 -118]		117 [114 -124]	
Rice cultivation	28 [23-34]		30 [24-34]		32 [25-37]		32 [29-37]	
Landfills and waste	60 [55-63]		61 [52-71]		69 [56-80]		71 [60-84]	
Fossil fuels	110 [94-129]	101 [71-151]	105 [97-123] (****)	105 [88-115]	120 [117-125] (****)	115 [100-124]	128 [120-133] (****)	122 [101-133]
Coal mining	32 [24-42]							

	Saunois et al. (2020)		This work					
Period of time	2000-2009		2000-2009		2010-2019		2020	
Oil & Gas	73 [60-85]		30 [26-32]		40 [37-44]		41 [38-43]	
Industry	2 [0-6]		65 [63-71]		67 [57-74]		74 [67-80]	
Transport	4 [1-11]		4 [1-8]		5 [1-9]		5 [1-8]	
			3 [1-8]		2 [1-3]		2 [1-3]	
Biomass & biof. burn.	31 [26-46]	29 [23-35]	30 [22-44]	26 [22-29]	28 [21-39]	27 [26-27]	27 [20-41]	26 [22-27]
Biomass burning	19 [15-32]		19 [14-29]		17 [12-24]		17 [13-27]	
Biofuel burning	12 [9-14]		11 [8-14]		11 [8-14]		10 [7-14]	
TOTAL DIRECT ANTHROPOGENIC SOURCES	334 ^d [321-358]	332 [312-347]	333 ^d [305-365]	341 [319-355]	358 ^d [329-387]	369 [350-391]	372 ^d [345-409]	392 [368-409]
SINKS								
Total chemical loss	595 [489-749]	505 [459-516]	585 [481-716]	504 ^e [496-511]	602 [496-747]	521 ^a [485-532]	602 [496-747]	538 ^e [503-554]
Tropospheric OH	553 [476-677]		546 [446-663]		563 [462-663]		563 [462-663]	
Stratospheric loss	31 [12-37]		27 [27-51]		27 [28-43]		27 [28-43]	
Tropospheric Cl	11 [1-35]		6 [1-13]		6 [1-13]		6 [1-13]	
Soil uptake	30 [11-49]	34 [27-41]	30 [11-49]	34 [34-34]	31 [11-49]	35 [35-35]	31 [11-49]	36 [35-36]
TOTAL SINKS	625 [500-798]	540 [486-556]	615 [492-765]	538 [530-545] ^e	633 [507-796]	554 [520-567] ^e	633 [507-796]	575 [566-589] ^e
SOURCES – SINKS IMBALANCE								
TOTAL SOURCES	703 [566-842]	547 [524-560]	638 [485-813]	543 [526-558]	669 [512-849]	575 [553-586]	685 [540-865]	608 [581-627]
TOTAL SINKS	625 [500-798]	540 [486-556]	615 [492-765]	538 [530-545] ^e	633 [507-796]	554 [550-567] ^e	633 [507-796]	575 [566-589] ^e
IMBALANCE	78	3 [-10-38]	23	5 [-4-13] ^e	36	21 [19-33] ^e	52	32 [15-38] ^e
ATMOSPHERIC GROWTH ^f		5.8 [4.9-6.6] ^f		6.1 [5.2-6.9] ^f		20.9 [20.1-21.7] ^f		41.8 [40.7-42.9] ^f

Supprimé: 34

Supprimé: 10

Supprimé: 35

Supprimé: 10-51

Supprimé: 35

Supprimé: 10-51

(*) uncertain but likely small for upland forest and aerobic emissions, potentially large for forested wetland, but likely included elsewhere

(**) We stop reporting this value to avoid potential double counting with satellite-based products of biomass burning (see Sect. 3.1.5)

(***) Here the numbers are from prognostic runs. To ensure a fair comparison with previous budgets (Saunois et al., 2020), the numbers are 163[117-195] for 2000-2009 from diagnostic runs with CRU/CRU-JRA-55 climate inputs (see Sect. 3.2.1).

(****) Up to 8 Tg of additional emissions could account for ultra emitters (Lauvaux et al., 2022), as in Tibrewal et al. (2024), that are fully or partly missed in regular anthropogenic inventories

a: Freshwater includes lakes, ponds, reservoirs, streams and rivers, part of it is due to anthropogenic disturbances estimated in Sect.3.2.2

b: The double counting estimate is discussed in Sect. 3.2.2

c: includes flux from hydrates considered at 0 for this study, includes estuaries

d: Total anthropogenic emissions are based on estimates of full anthropogenic inventory and not on the sum of “Agriculture and Waste”, “Fossil fuels” and “Biofuel and biomass burning” categories (see Sect. 3.1.2)

e: Some inversions did not provide the chemical sink. These values are derived from a subset of the inversion ensemble.

f: Atmospheric growth rates are given in the same unit Tg CH₄ yr⁻¹, based on the conversion factor of 2.75 Tg CH₄ ppb⁻¹ given by Prather et al. (2012) and the atmospheric growth rates provided in the text in ppb yr⁻¹.

2 Table 4: Top-down studies used here with their contribution to the decadal and yearly estimates noted. For decadal means, top down
3 studies must provide at least 8 years of data over the decade to contribute to the estimate. Details on each inverse system and inversions
4 are provided in Table S8 to S11 in the Supplementary Material.

Model	Institution	Observation used	Time period	Number of inversions	2000-2009	2010-2019	2020	References
Carbon Tracker-Europe CH ₄	FMI	Surface stations	2000-2020	4	y	y	y	Tsuruta et al. (2017)
LMDz-CIF	LSCE/CE A	Surface stations	2000-2020	4	y	y	y	Thanwerdas et al. (2022a)
LMDz-PYVAR	LSCE/CE A/THU	GOSAT Leicester v9.0	2010-2020	4	n	y	y	Zheng et al. (2018a, 2018b, 2019)
MIROC4-ACTM	JAMSTEC	Surface stations	2000-2020	5	y	y	y	Patra et al. (2018); Chandra et al. (2021)
NISMON-CH ₄	NIES/MRI	Surface stations	2000-2020	2	y	y	y	Niwa et al. (2022, 2024)
NIES-TM-FLEXPART (NTFVAR)	NIES	Surface stations	2000-2020	2	y	y	y	Maksyutov et al. (2020); Wang et al. (2019a)
NIES-TM-FLEXPART (NTFVAR)	NIES	GOSAT NIES L2 v02.95	2010-2020	1	n	y	y	Maksyutov et al. (2020); Wang et al. (2019a)
TM5-CAMS	TNO/VU	Surface stations	2000-2020	1	y	y	y	Segers et al. (2022)
TM5-CAMS	TNO/VU	GOSAT ESA/CCI v2.3.8 (combined with surface observations)	2010-2020	1	n	y	y	Segers et al. (2022)
Total number of runs				24	18	24	24	

Mis en forme : Français

Mis en forme : Français

Supprimé: 2022

Mis en forme : Français

Mis en forme : Français

Table 5: Global and latitudinal total methane emissions in Tg CH₄ yr⁻¹, as decadal means (2000-2009 and 2010-2019) and for the year 2020 from this work using bottom-up and top-down approaches. Global and latitudinal emissions for 2000-2009 are also compared with Saunois et al. (2016, 2020) for top-down and bottom-up approaches when available. Uncertainties are reported as [min-max] range. The mean, minimum and maximum values are calculated while discarding outliers, for each category of source and sink. As a result, discrepancies may occur when comparing the sum of categories and their corresponding total due to differences in outlier detections. Differences of 1 Tg CH₄ yr⁻¹ in the totals can also occur due to rounding errors. For the latitudinal breakdown, bottom-up anthropogenic estimates are based only on the gridded products (see Table 1). As a result, the total from the latitudinal breakdown (line called “This work (gridded BU products only)”) is slightly different from the values provided in Table 3 and recalled in the line “This work (all BU products)”. BU stands for bottom-up.

Period	2000-2009		2010-2019		2020	
Approach	Bottom-up	Top-down	Bottom-up	Top-down	Bottom-up	Top-down
Global						
This work (all BU products)	638 [485-813]	543 [526-558]	669 [512-849]	575 [553-586]	685 [540-865]	608 [581-627]
This work (gridded BU products only)	642 [501-809]		676 [526-845]		691 [565-862]	
<i>S2020</i>	703 [566-842]	547 [524-560]	-	-	-	-
<i>S2016</i>	719[583-861]	552[535-566]	-	-	-	-
90°S-30°N						
This work	367 [254-487]	337 [311-361]	388 [275-503]	364 [337-390]	395 [292-521]	386 [353-425]
<i>S2020</i>	408 [322-532]	346 [320-379]	-	-	-	-
<i>S2016</i>	-	356 [334-381]	-	-	-	-
30°N-60°N						
This work	234 [169-335]	182 [162-197]	250 [184-345]	187 [160-204]	256 [186-356]	197 [170-215]
<i>S2020</i>	252 [202-342]	178 [159-199]	-	-	-	-
<i>S2016</i>	-	176[159-195]	-	-	-	-
60°N-90°N						
This work	42 [22-79]	26 [22-33]	38[17-73]	24 [18-29]	39 [17-74]	25 [20-32]
<i>S2020</i>	42 [28-70]	23 [17- 32]	-	-	-	-
<i>S2016</i>	-	20 [15-25]	-	-	-	-

27
 28 **Table 6: Latitudinal methane emissions in Tg CH₄ yr⁻¹ for the last decade 2010-2019, based on top-down and bottom-up approaches.**
 29 **Uncertainties are reported as [min-max] range of reported studies. The mean, minimum, and maximum values are calculated while**
 30 **discarding outliers, for each category of source and sink. As a result, discrepancies may occur when comparing the sum of categories**
 31 **and their corresponding total due to differences in outlier detections. Differences of 1 Tg CH₄ yr⁻¹ in the totals can also occur due to**
 32 **rounding errors. For bottom-up approaches, natural and indirect anthropogenic sources are estimated based on available gridded**
 33 **data sets (see text Sect 5.2). As some emissions are missing gridded products (wild animals, permafrost, and hydrates), discrepancies**
 34 **may occur in terms of totals proposed in Table 3. Bottom-up direct anthropogenic estimates are based only on the gridded products**
 35 **(see Table 1).**

36

Latitudinal band	90°S- 30°N		30°N-60°N		60°-90°N	
Approach	Bottom-up	Top-Down	Bottom-up	Top-Down	Bottom-up	Top-Down
Natural and indirect anthropogenic Sources	178 [95-276]	148 [133-164]	100 [43-188]	42 [36-50]	28 [9-53]	14 [10-21]
Combined wetland and Inland freshwaters	151 [85-234]	128 [112-155]	73 [32-147]	27 [20-42]	24 [9-53]	9 [7-17]
Other natural	27 [11-42]	22 [20-29]	27 [10-41]	19 [16-22]	4 [2-6]	3 [1-5]
Anthropogenic direct sources	210 [180-227]	215 [191-238]	151 [142-157]	144 [121-162]	10 [6-14]	10 [6-16]
Agriculture & Waste	140 [121-150]	150 [135-168]	81 [77-84]	77 [56-88]	1 [1-2]	2 [2-2]
Fossil Fuels	52 [44-65]	46 [36-62]	65 [61-71]	61 [50-69]	7 [4-10]	7 [3-13]
Biomass & biofuel burning	22 [18-30]	19 [16-21]	7 [4-10]	6 [2-7]	1 [0-1]	1 [1-2]
Sum of sources	388 [275-503]	364 [337-390]	250 [184-345]	187 [160-204]	38 [7-73]	24 [18- 29]

37
 38
 39

i40 Table 7: Regional methane emissions (regions ranked by continent) in Tg CH₄ yr⁻¹ for the last decade 2010-2019, based on top-down
 i41 and bottom-up approaches. Uncertainties are reported as [min-max] range of reported studies. Differences of 1 Tg CH₄ yr⁻¹ in the
 i42 totals can occur due to rounding errors. For bottom-up approaches, natural and indirect anthropogenic sources are estimated based
 i43 on available gridded data sets (see text Sect 5.2). As some emissions are missing gridded products (wild animals, permafrost, and
 i44 hydrates), discrepancies may occur in terms of totals proposed in Table 3. Bottom-up direct anthropogenic estimates are based on
 i45 all products (gridded and per country).
 i46

Region	Total emissions		Natural and indirect anthropogenic emissions		Direct anthropogenic emissions	
	Bottom-up	Top-down	Bottom-up	Top-down	Bottom-up	Top-down
USA	49 [27-77]	38 [32-46]	24 [7-43]	12 [7-22]	26 [19-34]	25 [16-31]
Canada	38 [14-71]	20 [17-24]	32 [11-63]	14 [11-22]	6 [3-8]	7[5-9]
Central America	18 [10-28]	17 [14-19]	8 [3-17]	5 [2-6]	10 [8-12]	12 [11-13]
Northern South America	19 [9-35]	16 [13-20]	10 [3-17]	9 [7-11]	9 [6-17]	7 [6-8]
Brazil	51 [26-79]	47 [41-58]	32 [11-57]	26 [22-36]	19 [16-22]	21 [17-26]
Southwest South America	34 [16-51]	38 [30-48]	21 [6-35]	24 [16-34]	13 [10-16]	14 [12-17]
Europe	42 [29-57]	31 [24-36]	17 [6-30]	7 [5-9]	25 [22-27]	24 [20-31]
Northern Africa	24 [18-33]	25 [23-29]	7 [2-13]	6 [6-8]	18 [16-20]	19 [17-21]
Equatorial Africa	47 [28-83]	47 [39-59]	23 [10-49]	24 [20-30]	24 [19-34]	23 [19-29]
Southern Africa	21 [5-43]	19 [16-24]	11 [2-29]	8 [7-10]	10 [3-14]	11 [10-12]
Russia	48 [24-83]	36 [27-45]	25 [9-47]	14 [11-18]	23 [15-36]	21 [14-29]
Central Asia	15 [6-29]	10 [8-13]	8 [2-19]	1 [0-2]	8 [4-10]	9 [7-11]
Middle East	35 [21-47]	31 [24-39]	9 [3-15]	4 [1-6]	26 [18-31]	28 [20-34]
China	71 [55-99]	57 [37-72]	15 [4-33]	4 [3-7]	57 [51-66]	53 [34-66]
Korean-Japan	6 [4-12]	5 [4-6]	3 [1-7]	1 [1-1]	4 [3-5]	4 [3-5]
South Asia	58 [49-72]	52 [43-60]	13 [5-25]	6 [5-6]	45 [44-47]	45[37-49]
Southeast Asia	64 [42-93]	63 [52-71]	32 [19-54]	27 [20-34]	32 [23-39]	35 [31-46]
Australasia	16 [9-26]	13 [10-17]	10 [4-19]	6 [4-7]	7 [6-7]	7 [6-7]

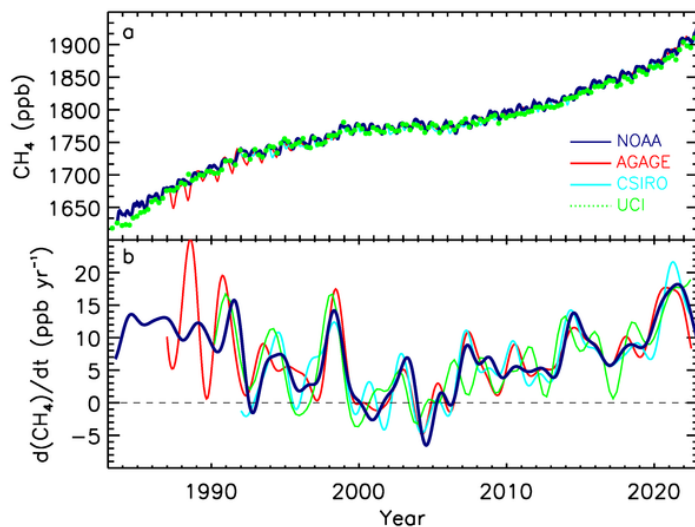


Figure 1: Globally averaged atmospheric CH_4 concentrations (ppb) (a) and annual growth rates G_{ATM} (ppb yr^{-1}) (b) between 1983 and 2022, from four measurement programs, National Oceanic and Atmospheric Administration (NOAA), Advanced Global Atmospheric Gases Experiment (AGAGE), Commonwealth Scientific and Industrial Research Organisation (CSIRO), and University of California, Irvine (UCI). Detailed descriptions of methods are given in the supplementary material of Kirschke et al. (2013).

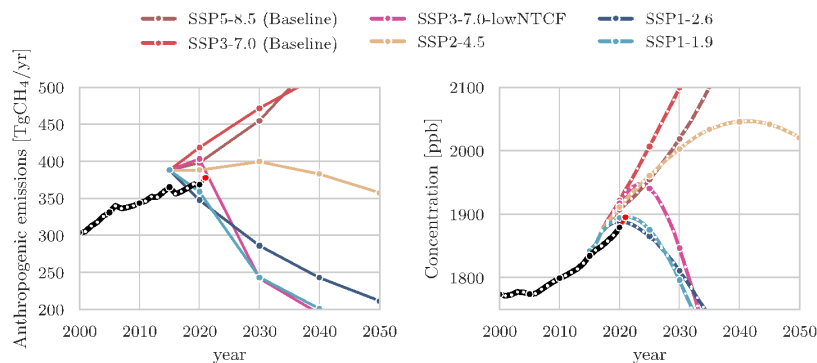
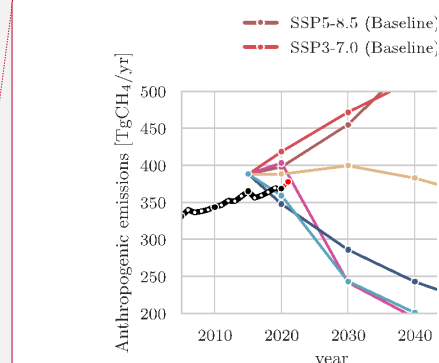


Figure 2: Left: Global anthropogenic methane emissions (including biomass burning) over 2005–2050 from historical inventories (black line and grey shaded area) and future projections (colored lines) (in Tg CH₄ yr⁻¹) from selected scenarios harmonized with historical emissions (CEDS) for CMIP6 activities (Gidden et al., 2019). Historical mean emissions correspond to the average of anthropogenic inventories listed in Table 1 added to the GFEDv4.1s (van der Werf et al., 2017) biomass burning historical emissions. Right: Global atmospheric methane concentrations for NOAA surface site observations (black) and projections based on SSPs (Riahi et al., 2017) with concentrations estimated using MAGICC (Meinshausen et al., 2017, 2020). Red dots show the last year available (2022 for observations).



Supprimé:

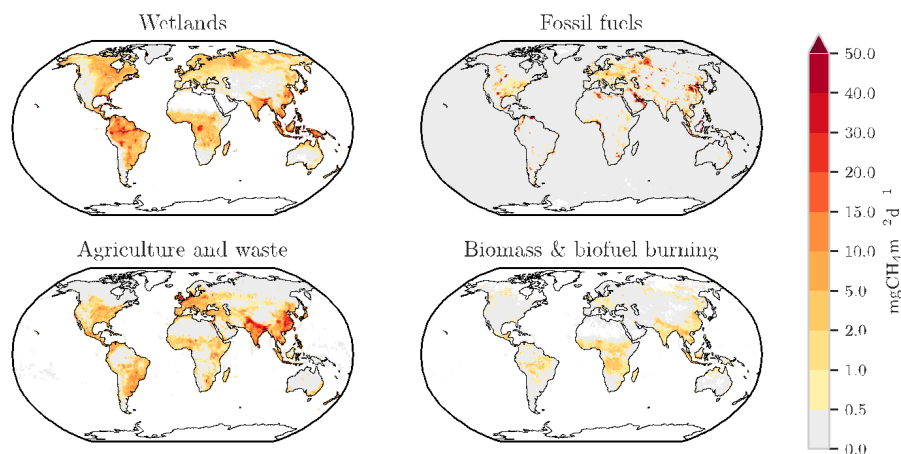
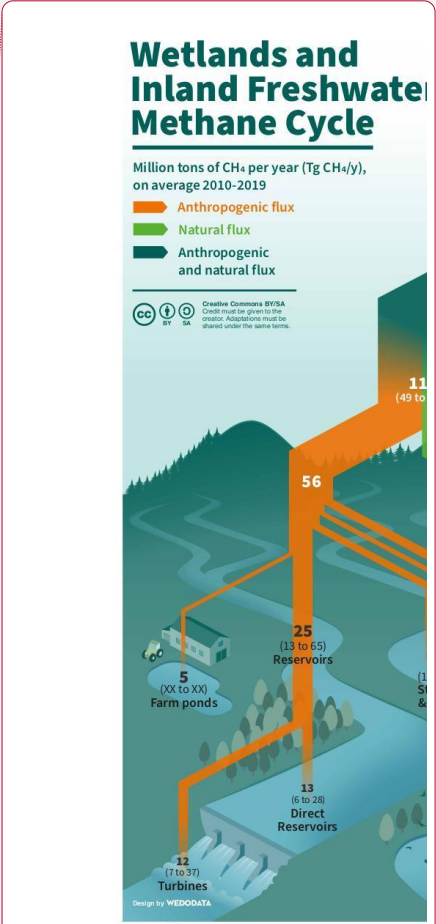
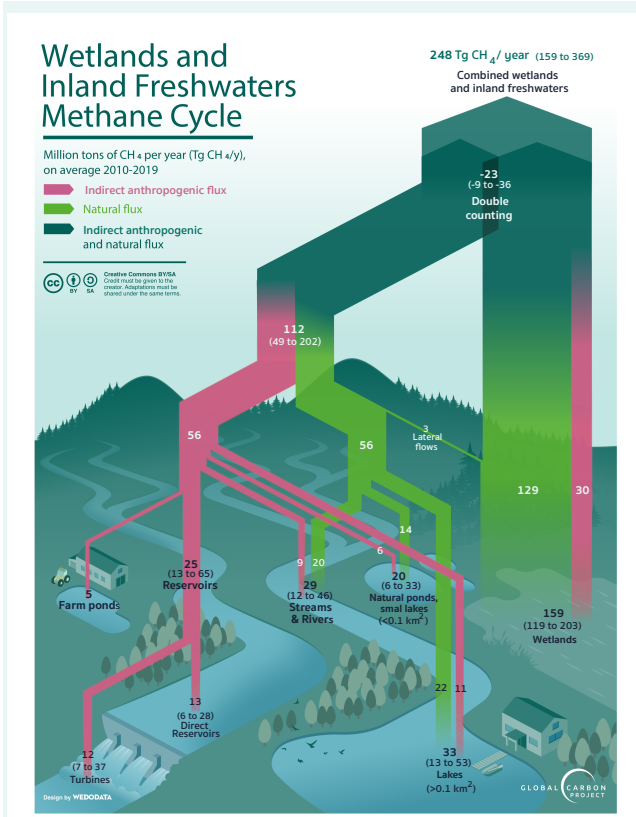


Figure 3: Methane emissions from four source categories: natural wetlands (excluding lakes, ponds, and rivers), biomass and biofuel burning, agriculture and waste, and fossil fuels for the 2010-2019 decade in $\text{mg CH}_4 \text{ m}^{-2} \text{ day}^{-1}$. The wetland emission map represents the mean daily emission average over the 16 biogeochemical models listed in Table 2 and over the 2010-2019 decade. Fossil fuel and Agriculture and Waste emission maps are derived from the mean estimates of gridded CEDS, EGDARv6, EDGARv7 and GAINS models. The biomass and biofuel burning map results from the mean of the biomass burning inventories listed in Table 1 added to the mean of the biofuel estimate from CEDS (O'Rourke et al., 2021), EDGARv6 (Crippa et al., 2021), EDGARv7 (Crippa et al., 2023) and GAINS (Höglund-Isaksson et al., (2020)) models.



Supprimé:
Supprimé:
Supprimé: orange
Supprimé: However, t

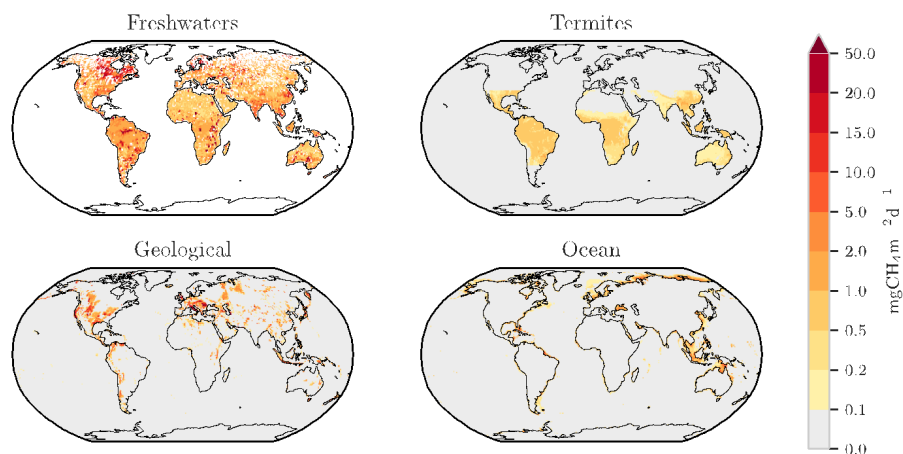


Figure 5: Methane emissions ($\text{mg CH}_4 \text{m}^{-2} \text{day}^{-1}$) from four natural and indirect anthropogenic sources: inland freshwaters (includes lakes, ponds (Johnson et al., 2022.), reservoirs (Johnson et al., 2021) and stream and rivers (Rocher-Ros et al., 2023) with a global total scaled to 89 Tg yr^{-1}), geological (Etiope et al., 2019), termites (this study) and oceans (Weber et al., 2019).

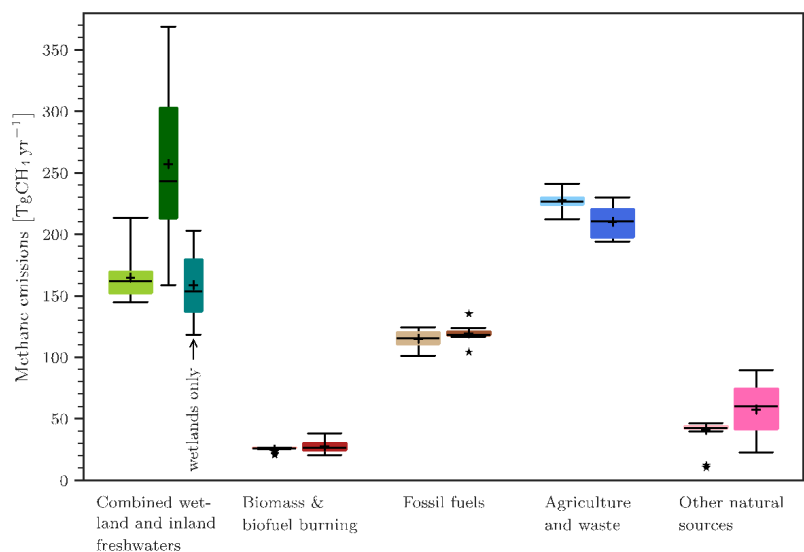


Figure 6: Methane global emissions from five broad categories (see Sect. 2.3) for the 2010-2019 decade for top-down inversion models (left light coloured boxplots) in Tg CH₄ yr⁻¹ and for bottom-up models and inventories (right dark coloured boxplots). For combined wetland and inland freshwaters three estimates are given: left = top-down estimates, middle = bottom-up estimates, right = bottom-up estimates for wetlands only. Median value, first and third quartiles are presented in the boxes. The whiskers represent the minimum and maximum values when suspected outliers are removed (see Sect. 2.2). Suspected outliers are marked with stars. Bottom-up quartiles are not available for bottom-up estimates, except for wetland emissions. Mean values are represented with “+” symbols, these are the values reported in Table 3.

'04

'05

'06

'07

'08

'09

'10

'11

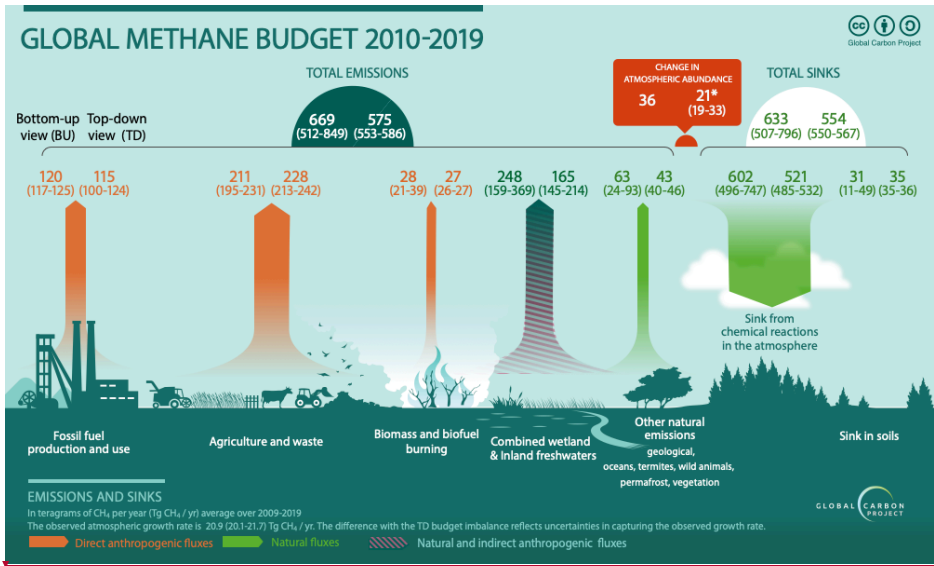
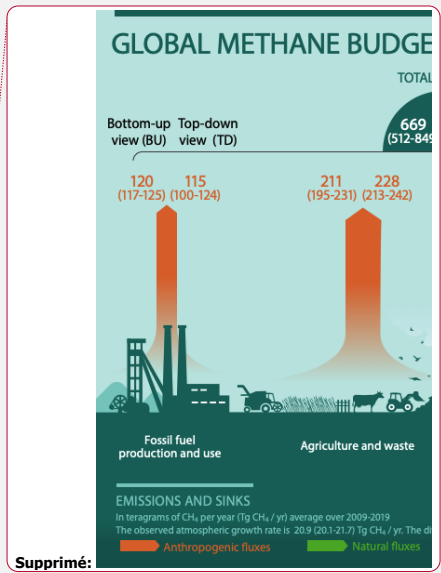
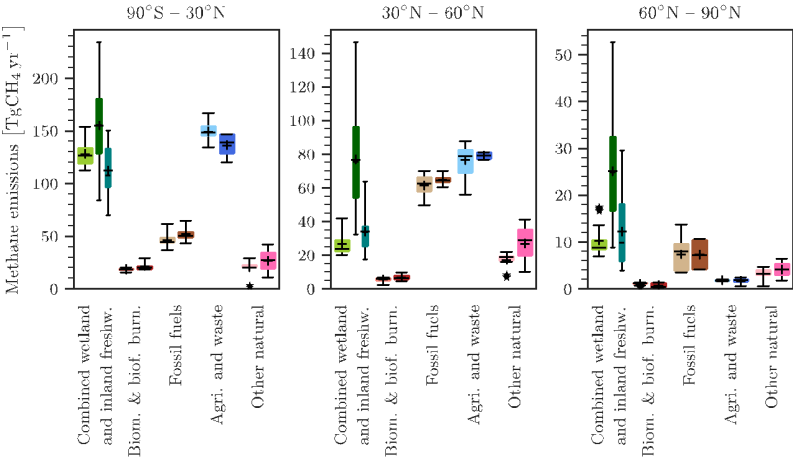


Figure 7: Global Methane Budget for the 2010-2019 decade. Both bottom-up (left) and top-down (right) estimates are provided for each emission and sink category in Tg CH₄ yr⁻¹, as well as for total emissions and total sinks. Combined wetland and inland freshwaters are depicted as natural and indirect anthropogenic sources (darker green and pink hatches) to recall Figure 4 (Sect. 3.2.2).



- Supprimé:** Biomass and biofuel burning emissions are depicted here as both natural and anthropogenic emissions while they are fully included in anthropogenic emissions in the budget tables and text (Sect. 3.1.5).
- Supprimé:** fully
- Supprimé:** while part has been attributed
- Supprimé:** component
- Supprimé:** and Figure 4

21



22

23 **Figure 8: Methane latitudinal emissions from five broad categories (see Sect. 2.3) for the 2010-2019 decade for top-down inversion**
24 **models (left light coloured boxplots) in Tg CH₄ yr⁻¹ and for bottom-up models and inventories (right dark coloured boxplots). For**
25 **combined wetland and inland freshwaters three estimates are given: left = top-down estimates, middle = bottom-up estimates, right**
26 **= bottom-up estimates for wetlands only. Median value, first and third quartiles are presented in the boxes. The whiskers represent**
27 **the minimum and maximum values when suspected outliers are removed (see Sect. 2.2). Suspected outliers are marked with stars.**
28 **Bottom-up quartiles are not available for bottom-up estimates, except wetland emissions. Mean values are represented with “+”**
29 **symbols, these are the values reported in Table 6.**

30

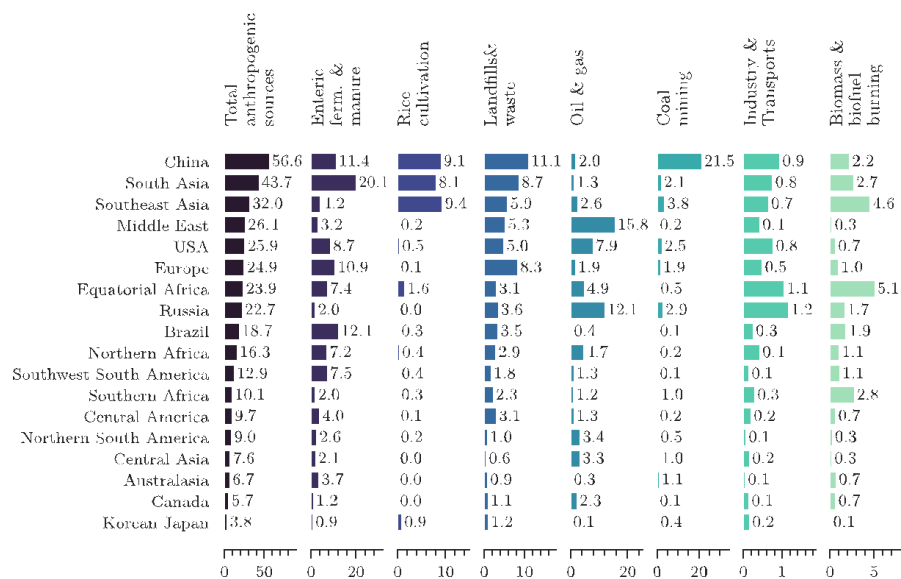


Figure 9: Regional anthropogenic emissions for the 2010-2019 decade from bottom-up estimates in Tg CH₄ yr⁻¹. Regions are ranked by their total anthropogenic emissions. Note that each category has its own emission scale.

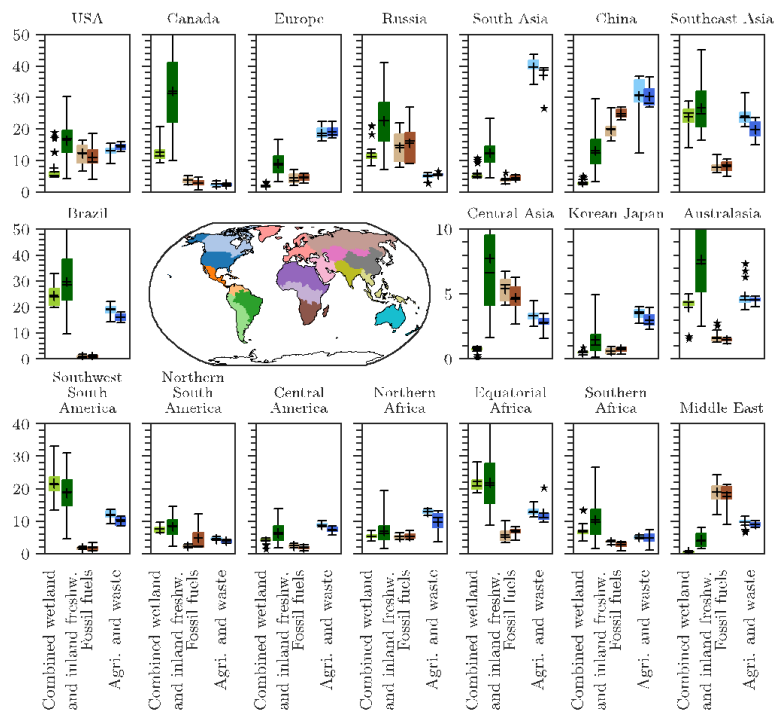


Figure 10: Regional emissions for three broad main emissions categories for the 2010-2019 decade: Combined wetland and inland freshwaters, fossil fuel and agriculture & waste from top-down estimates (left box-plots- and bottom-up estimates (right boxplots). The inner map shows the region's distribution (see also Supplementary material, Table S1 and Fig. S3). More categories are presented in the Supplementary Material in Figure S6.

40 **Table A1.** Comparison of terminologies used in this study and previous reports for methane sources.

GCP terminology (This study)		IPCC AR6 (Canadell et al., 2021)	National GHG inventories (used by UNFCCC according to IPCC (2006) and IPCC (2019))	IPCC (2006, 2019) Source sector numbering
<i>Anthropogenic Sources</i>				
Fossil fuels	Coal Mining	Coal Mining	Fugitive emissions from Fuels / Solid fuels	1B1
	Oil and gas	Oil and gas	Fugitive emissions from Fuels / Oil and natural gas	1B2
	Transport	Transport	Transport	1A3
	Industry	Industry	Mineral, chemical, metal industry and others	2A, 2B, 2C, 2D, 2E
			Energy/fuel Combustion activities	1A except 1A3 + 1B3
Agriculture	Enteric fermentation and manure management	Enteric fermentation and manure management	Livestock	3A
	Rice cultivation	Rice cultivation	Rice cultivation	3C7
Waste	Landfills and waste	Landfills and waste	Waste	4
Biofuel and biomass burning	Biofuel burning	Biofuel burning	Biofuel burning	1A4b
	Biomass burning	Biomass burning	Biomass burning	3C1
<i>Natural and indirect sources</i>				
Wetlands	Wetlands	Wetlands	--	--
Inland freshwaters	Reservoirs	included in Inland freshwaters	Land (incl Reservoirs)	in 3B
	Lakes, ponds, and rivers	incl in Inland freshwaters	only canal, ditches and ponds for human uses	in 3B
Other natural sources	Oceans	Oceans	--	--
	Termites	Termites	--	--

'41
'42

	Geological sources	Geological sources	--	--
--	--------------------	--------------------	----	----

'43 **Table A2.** Summary of methodological changes since the previous budget (Saunois et al., 2020). No significant changes have been
 '44 applied to the vegetation (Sect. 3.2.8), wild animal (Sect. 3.2.5) and terrestrial permafrost and hydrates (Sect 3.2.7) estimates, though
 '45 literature has been expanded and/or updated.
 '46

	Saunois et al. (2020)	This study
Regions definition (Table S1, Fig S3)	18 continental regions + ocean	same regions except the last region including only Australia and New-Zealand and called Australasia
Anthropogenic global inventories (See Table 1, Sect 3.1.1)	CEDS, EDGARv4.3.2, USEPA (2012), FAO and GAINS ECLIPSE v6	CEDS, EDGARv6 and v7, USEPA (2019), FAO, IIASA GAINS v4 Add estimate of ultra emitters from Lauvaux et al. (2022)
Biomass burning data sets	FINNv1.5, GFASv1.3, GFEDv4.1s, QFEDv2.5	FINNv2.5, GFASv1.3, GFEDv4.1s, QFEDv2.5
Estimate of wetland emissions (See Tables 2 and S3 and Section 3.2.1)	13 land surface models involved, runs with either prescribed areas or based on Hydrological scheme, single meteorological forcing	16 land surface models involved, runs with either prescribed areas or based on Hydrological scheme, two sets of meteorological forcings
Estimate of reservoirs emissions (Sect.3.2.2)	based on Deemer et al. (2016)	based on Johnson et al. (2021), Rosentreter et al. (2021) and Harrison et al. (2021)
Estimate of lakes and ponds emissions (Sect.3.2.2)	based on Bastviken et al. (2011), Wik et al. (2016b) and Tan and Zhuang (2015)	lakes > .1km2 : based on Rosentreter et al. (2021), Zhuang et al. (2023) and Johnson et al. (2022) lakes and ponds < 0.1 km2 : based on Rosentreter et al. (2021), and Johnson et al. (2022)
Estimates of stream and river emissions (Sect.3.2.2)	From Stanley et al. (2016)	based on Rosentreter et al. (2021) and Rocher-Ros et al. (2023)
Estimates of the anthropogenic perturbation component of inland freshwater emissions (Sect.3.2.2)	- -	based on several individual studies on the effect of eutrophication on emissions from lakes, and ponds (See text in Sect. 3.2.2)
Estimate of the double counting in the aquatic systems (Sect.3.2.2)	--	due to the accounting of small lakes and ponds (<0.1km2) in the vegetated wetlands areas used in land surface models and to lateral transport from vegetated wetland to rivers.

Mis en forme : Français

Mis en forme : Français

Geological sources (Sect 3.2.3) - onshore and offshore	based on Etiope and Schwietzke et al. (2019)	same as in Saunio et al. (2020)
Termite emissions (Sect. 3.2.4)	GPP : Zhang et al. (2017) termite biomass: Jung et al. (2011) EF : Kirshke et al. (2013) and Fraser et al., 1986)	GPP: Wild et al. (2022) termite biomass: based on different studies depending on regions (see text) EF: Sugimoto et al. (1998) Applied a correction factor for mound from Nauer et al. (2018)
Oceanic sources (Sect 3.2.6)	modern biogenic: based on Wuebbles and Hayhoe (2002), Laruelle et al. (2013) and Rosentreter et al. (2018); geological: based on Etiope (2019)	modern biogenic: based on Rosentreter et al. (2021;2023) and Laruelle et al. (2025) geological: based on Etiope (2019)
Tropospheric OH oxidation (Sect 3.3.2) and stratospheric loss (Sect 3.3.3) (See Supplementary Table S4)	based on results from 11 models contributing to the Chemistry Climate Model Initiative (Morgenstern et al., 2017)	based on results from 11 models contributing to the Chemistry Climate Model Initiative 2022 (Plummer et al., 2021) and the CMIP6 simulations (Collins et al., 2017)
Tropospheric reaction with Cl	based on Hossaini et al. (2016), Wang et al. (2019b) and Gromov (2018)	based on Hossaini et al (2016), Sherwenn et al. (2016), Wang et al (2019b, 2021b) and Gromov (2018)
Soil uptake (See Table S6)	based on Tian et al. (2016)	based on VISIT, JSBACH en MeMo surface models.
Estimates through top-down approaches (See table S7 and S8 to S11)	9 inverse systems contributing, prior fluxes based on EDGARv4.2 or v4.3.2 for most inversions. Most inversion used constant OH.	7 inverse systems contributing, runs with constant and varying OH, prior fluxes based on either EDGARv6 or GAINS

Mis en forme : Français

Supprimé:

Supprimé: 23

Mis en forme : Français

'50 **Table A3.** Funding supporting the production of the various components of the global methane budget in addition to the authors'
'51 supporting institutions (see also acknowledgements).
'52

Funder and grant number (where relevant)	Authors/Simulations/Observations
Director, Office of Science, Office of Biological and Environmental Research of the US Department of Energy under Contract No. DE-AC02-05CH11231 to Lawrence Berkeley National Laboratory as part of the RUBISCO Scientific Focus Area.	WJR, QZ, E3SM/ELM simulations
Funded by NASA's Interdisciplinary Research in Earth Science (IDS) Program and the NASA Terrestrial Ecology and Tropospheric Composition Programs	MSJ; lake and reservoir bottom-up methane emission data sets
Funded by Agence National de la Recherche through the project Advanced Methane Budget through Multi-constraints and Multi-data streams Modelling (AMB-M ³) - (ANR-21-CE01-0030)	AM, MS
The Environment Research and Technology Development Fund (JPMEERF21S20800) of the Environmental Restoration and Conservation Agency provided by Ministry of the Environment of Japan	YN, NISMON-CH ₄
Funded by the German Federal Ministry of Education and Research (BMBF) via the "PalMod" project, grant No. 01LP1921A	TK; CH ₄ emission modelling with JSBACH and LPJ-MPI
Funded by the Swedish Research Council VR (2020-05338) and Swedish National Space Agency (209/19)	WZ; LPJ-GUESS simulations
Funded by BELSPO (project FedTwin ReCAP), EU Horizon 2020 project ESM2025 (nr. 101003536) and FRNS PDR project CH4-lake (T.0191.23)	PR; inland water, coastal and oceanic CH ₄ emission synthesis
EU H2020 (725546 ERC METLAKE and 101015825 TRIAGE) , Swedish Research Councils VR (2022-03841) and Formas (2018-01794)	DB; inland waters - data and bottom up estimation.
Supported by the Newton Fund through the Met Office Climate Science for Service Partnership Brazil (CSSP Brazil)	NG; JULES simulations
Funded by United Nations Environment Programme, Stanford University DTIE21-EN3143	RBJ; inversions and general budget support
the Joint Fund for Regional Innovation and Development of the National Natural Science Foundation (Grant No. U22A20570); the Natural Sciences and Engineering Research Council of Canada (NSERC, #371706)	Changhui Peng/TRIPLEX-GHG
Computing Resources	
LSCE computing resources	Marielle Saunois, Philippe Bousquet, Joël Thanwerdas and Adrien Martinez
NASA High-End Computing (HEC) Program through the NASA Advanced Supercomputing (NAS) Division at NASA Ames Research Center	Matthew S. Johnson (MSJ)
Deutsches Klimarechenzentrum (DKRZ), Hamburg, Germany	Thomas Kleinen (TK)

Mis en forme : Français

ALICE High Performance Computing Facility at the University of Leicester	GOSAT retrievals
FUJITSU PRIMERGY CX2550M5 at MRI and NEC SX-Aurora TSUBASA at NIES	Yosuke Niwa (YN)
Support for atmospheric observations	
Australian Antarctic Division	CSIRO flask network
Australian Institute of Marine Science	CSIRO flask network
Bureau of Meteorology (Australia)	Kennaook/Cape Grim AGAGE, CSIRO flask network
Commonwealth Scientific and Industrial Research Organisation (CSIRO, Australia)	Kennaook/Cape Grim AGAGE, CSIRO flask network
Department of Climate Change, Energy, the Environment and Water (DCCEEW, Australia)	Kennaook/Cape Grim AGAGE
Meteorological Service of Canada	CSIRO flask network
NASA: grants NAG5-12669, NNX07AE89G, NNX11AF17G, NNX16AC98G and 80NSSC21K1369 to MIT with subawards to the University of Bristol (for Barbados and Mace Head) and CSIRO (for Kennaook/Cape Grim); grants NAG5-4023, NNX07AE87G, NNX07AF09G, NNX11AF15G, NNX11AF16G, NNX16AC96G, NNX16AC97G, 80NSSC21K1210 and 80NSSC21K1201 to SIO.	AGAGE calibrations and measurements at SIO, La Jolla and AGAGE station operations at Trinidad Head, Mace Head, Barbados, American Samoa, and Kennaook/Cape Grim
National Oceanic and Atmospheric Administration (NOAA, USA) contract RA133R15CN0008 to the University of Bristol	Barbados
NOAA USA	CSIRO flask network
Refrigerant Reclaim Australia	Kennaook/Cape Grim AGAGE
UK Department for Business, Energy & Industrial Strategy (BEIS) contract TRN1537/06/2018 and TRN 5488/11/2021 to the University of Bristol	Mace Head
National Oceanic and Atmospheric Administration (NOAA, USA)	Cape Matatula
Japanese Ministry of Environment	GOSAT data, Robert Parker
Japanese Aerospace Exploration Agency, National Institute for Environmental Studies	GOSAT data, Robert Parker
UKRI UK: grants NE/W004895/1, NE/R016518/1, NE/X019071/1 and MR/X033139/1	GOSAT data, Robert Parker
The Swedish Research Council VR (2022-04839), European Space Agency projects AMPAC-Net and CCI+ permafrost, European Union's Horizon 2020 Research and Innovation Programme to the Nunataryuk project (no. 773421)	Permafrost region, Gustaf Hugelius

Supprimé: NERC

Supprimé: and